ULB FACULTÉ DE MÉDECINE

UNIVERSITÉ LIBRE DE BRUXELLES

DEFINING THE MOLECULAR AND CELLULAR MECHANISMS UNDERLYING WOUND REPAIR AND POST-NATAL GROWTH IN THE MOUSE EPIDERMIS

Thesis submitted by Sophie DEKONINCK
in fulfilment of the requirements
of the PhD Degree in Biomedical and Pharmaceutical Sciences
(« Docteur en Sciences Biomédicales et Pharmaceutiques »)
Academic year 2019-2020

Supervisor: Professor Cédric BLANPAIN

Laboratory of Stem Cells and Cancer

Thesis jury:

Jean-Pierre BRION (Université libre de Bruxelles, Chair)
Cédric BLANPAIN (Université libre de Bruxelles, Secretary)
Denis FRANCHIMONT (Université libre de Bruxelles)
Marc PARMENTIER (Université libre de Bruxelles)
Bertrand RICHERT (Université libre de Bruxelles)
Shalev ITZKOVITZ (Weizman Institute of Science, Israël)
Kim Bak JENSEN (University of Copenhaguen, Denmark)

erc European Research Council

REMERCIEMENTS

JE REMERCIE **CÉDRIC BLANPAIN** DE M'AVOIR ACCUEILLIE DANS SON LABORATOIRE, DE M'AVOIR ACCORDÉ SA CONFIANCE ET SON SOUTIEN TOUT AU LONG DE CETTE THÈSE DE DOCTORAT. JE LE REMERCIE DE M'AVOIR APPRIS COMMENT MENER UN PROJET DE RECHERCHE.

MERCI À **TOUS MES COLLÈGUES ET EX-COLLÈGUES** QUI M'ONT AIDÉ À MENER CE PROJET À BIEN ET QUI M'ONT SURTOUT APPRIS À OUVRIR LES YEUX SUR LE MONDE, LA VIE, LA DIVERSITÉ DE CULTURES QUI PEUPLE NOTRE PLANÈTE. GRÂCE À EUX, UNE JOURNÉE AU LABORATOIRE ÉTAIT UN VÉRITABLE TOUR DU MONDE. DE PAR LEUR MOTIVATION SANS LIMITE ILS M'ONT OFFERT L'ÉNERGIE NÉCESSAIRE POUR MENER À TERME CE PROJET ET ILS M'ONT TANT APPRIS, SCIENTIFIQUEMENT ET HUMAINEMENT. JE NE LES CITERAI PAS TOUS ICI, MAIS JE N'OUBLIE AUCUN D'ENTRE EUX, MÊME CEUX DONT LE PASSAGE FUT PLUS BREF QUE D'AUTRES. JE REMERCIE PARTICULIÈREMENT **GUILHEM** POUR M'AVOIR MISE SUR LES RAIL DE LA RECHERCHE. MERCI À **MARIELLE**, **ADRIANA**, **PEGGY, BENJAMIN B** ET **GAELLE L** POUR M'AVOIR COMMUNIQUÉ LEUR RIGUEUR SCIENTIFIQUE ET LEUR ÉNERGIE INTARISSABLE. MERCI À TOUS CEUX QUI ONT TOUJOURS ÉTÉ PARTANTS POUR ME DONNER UN COUP DE MAIN OU ME FORCER À PRENDRE UNE PAUSE ET À BOIRE UN VERRE SUR LE BALCON (ILS SE RECONNAÎTRONT). MERCI À **EDOUARD ET ALEJANDRO** POUR LEUR DISPONIBILITÉ ET LEUR CONTRIBUTION DANS L'ABOUTISSEMENT DE CE PROJET. MERCI À **SANDRINE**, **CHARLOTTE** ET **SOUHIR** POUR LEUR AIDE TECHNIQUE ET LEUR CONSEILS. ET, BIEN SÛR, UN IMMENSE MERCI À **MARIACELESTE** QUI M'A GUIDÉ, ÉPAULÉ ET COMPLÉTÉ DURANT TOUTES CES ANNÉES ET SANS QUI CE TRAVAIL N'AURAIT PAS PU ABOUTIR.

MERCI À **JEAN-MARIE** ET **MICHIEL**, GRÂCE À QUI LA MICROSCOPIE CONFOCALE N'A (PRESQUE) PLUS DE SECRET POUR MOI. MERCI À **CHRISTINE**, POUR LES TRIS EN DERNIÈRE MINUTE. MERCI À TOUTE L'ÉQUIPE DES **ANIMALIERS**.

MERCI À TOUTE MA FAMILLE, **PAPA**, **MAMAN**, **MANON**, **NATH & MAX, MAX & STEPH** AINSI QUE TOUTE MA **BELLE FAMILLE**, POUR LEUR SOUTIENT, LEUR PRÉSENCE, LEUR BONNE HUMEUR ET LEUR INTÉRÊT POUR MON SUJET DE RECHERCHE.

MERCI À TOUS MES AMIS POUR LEURS MOTS D'ENCOURAGEMENTS ET LEUR SOUCIS DE SAVOIR COMMENT AVANCE MON PROJET. UN MERCI PARTICULIER À **LAUREEN**, POUR NOS SÉANCES D'ÉCRITURES.

ENFIN, MES REMERCIEMENTS LES PLUS IMPORTANTS VONT À MON COMPAGNON. MERCI À **BASTIEN** POUR SON SOUTIEN, POUR SA PATIENCE INFINIE ET POUR ME RAPPELER SANS CESSE OÙ PLACER MES LIMITES, QUI JE SUIS ET QUEL EST MON BUT DANS LA VIE.

Résumé

L'épiderme est la première barrière de protection des organismes vivants contre des attaques extérieures. Il est constamment renouvelé au cours de la vie, via un processus appelé « homeostasie », qui assure que chaque cellule perdue à sa surface soit remplacée par de nouvelles. Des études récentes ont montré que cet équilibre était assuré par une hiérarchie de cellules souches (CS) et de progéniteurs qui réalisent 3 types de divisions cellulaires, chaque type de division ayant une probabilité fixe. Bien que l'épiderme ait été intensivement étudié durant l'homeostasie, peu de choses sont connues concernant la dynamique cellulaire prenant place lors de phénomènes où l'épiderme doit grandir. Ces probabilités de division sont-elles immuables ou peuvent-elles au contraire changer ? Dans ce projet, nous nous sommes intéressés à deux conditions d'expansion de l'épiderme : la croissance post-natale et la cicatrisation des plaies.

En utilisant l'épiderme de la queue de souris comme modèle, nous montrons que la ré-épithélialisation d'une plaie est réalisée via la formation de deux compartiments cellulaires transitoires distincts spatialement et du point de vue moléculaire : un front de migration et un centre prolifératif. Nous montrons que les cellules du front de migration ont une signature transcriptionnelle spécifique qui est indépendante de leur état de quiescence et proposons de nouveaux marqueurs non décrits auparavant. En utilisant la technique du « lineage tracing », couplée à une analyse clonale et à de la modélisation mathématique, nous mettons en évidence la dynamique de prolifération des CS et des progéniteurs lors de la cicatrisation. Nous montrons que différentes populations de cellules résidant dans des compartiments différents, l'infundibulum du follicule pileux et l'épiderme interfolliculaire, acquièrent une dynamique similaire et ré-activent leur CS tandis que les progéniteurs augmentent leur taux de prolifération sans changer leur probabilité de division. Cette dynamique de prolifération similaire dans deux compartiments de l'épiderme suggère que les probabilités de divisions ne sont pas dictées par la cellule d'origine.

De façon intéressante, la dynamique cellulaire est par contre différente durant la croissance post-natale. En utilisant le lineage tracing, l'analyse clonale et des analyses transcriptionnelles sur cellule unique, nous démontrons que l'épiderme post-natal est composé d'une population homogène de progéniteurs équipotents qui présentent un constant déséquilibre envers des divisions d'auto-renouvèlement et un taux de prolifération décroissant, assurant une croissance harmonieuse de l'épiderme. En revanche, les cellules basales de l'épiderme adulte montrent une plus grande hétérogénéité moléculaire et cet hétérogénéité est acquise progressivement à la fin de la croissance. Enfin, en couplant des mesures *in vivo* et des expériences de micro-patterning *in vitro*, nous montrons que l'orientation de la division cellulaire des progéniteurs équipotents est localement influencée par l'alignement des fibres de collagène du derme sous-jacent. Ces données suggèrent que la spécification des CS survient tardivement au cours du développement post-natal et que la dynamique de prolifération n'est pas immuable et pourraient donc être influencée par des facteurs extrinsèques.

Abstract

The epidermis is the first barrier of protection of living organisms against external attacks. It is constantly renewed throughout life, through a process called "homeostasis", which ensures that every cell lost on its surface is replaced by new ones. Recent studies have shown that this balance is ensured by a hierarchy of stem cells (SC) and progenitors that perform 3 types of cell divisions, each having a fixed probability. Although the epidermis has been extensively studied during homeostasis, little is known about the cellular dynamics taking place when the epidermis must expand its surface. Are these probabilities of division immutable or can they change? In this project, we focused on two conditions of epidermal expansion: post-natal growth and wound healing.

Using the mouse tail epidermis as a model, we show that the re-epithelialization after a wound is achieved via the formation of two transient compartments that are spatially and molecularly distinct : a leading edge and a proliferative hub. We show that the leading edge cells have a specific transcriptional signature that is independent of their quiescent state and we propose new markers not previously described. Using the technique of "lineage tracing", coupled with clonal analysis and mathematical modeling, we highlight the proliferation dynamics of SCs and progenitors during healing. We show that different populations of cells residing in different compartments, the hair follicle infundibulum and the interfollicular epidermis, acquire a similar dynamics and re-activate their SC while the progenitors increase their rate of proliferation without changing their division probabilities. This similar proliferation dynamics in two compartments of the epidermis suggests that division probabilities are not dictated by the cell of origin.

Interestingly, cell dynamics is different during postnatal growth. Using lineage tracing, clonal analysis and single-cell transcriptional analysis, we demonstrate that the post-natal epidermis is composed of a homogeneous population of equipotent progenitors which ensure a harmonious tissue growth through a constant imbalance towards self-renewing divisions and an ever decreasing proliferation rate. On the other hand, we show that basal cells in the adult epidermis display a greater molecular heterogeneity and that this heterogeneity is acquired progressively at the end of growth. Finally, by coupling *in vivo* measurements and *in vitro* micro-patterning experiments, we show that the orientation of cell division of equipotent progenitors is locally influenced by the alignment of the collagen fibers of the underlying dermis. These data suggest that SC specification occurs late in postnatal development and that proliferation dynamics are not immutable and could therefore be influenced by extrinsic factors.

LIST OF RECURRENTS ABBREVIATIONS

AFM	Atomic Force Microscopy
AJ	Adherens Junctions
AP-1	Activator Protein 1
ATAC-seq	Assay for Transposase Accessible Chromatin with highthroughput sequencing
BCC	BasoCellular Carcinoma
BrdU	Bromo deoxyuridine
BM	Basement membrane
Chip-seq	Chromatin ImmunoPrecipitation followed by sequencing
CP	Committed Progenitors
DETC	Dendritic Epidermal γδ T cells
DP	Developmental Progenitors
DWAT	Dermal White Adipose tissue
EB	Epidermolysis Bullosa
ECM	Extracellular Matrix
EdU	5-ethynyl-2'-deoxyuridine
EGF	Epidermal Growth Factor
EPU	Epidermal Proliferative Unit
FA	Focal Adhesion
Fil	Filaggrin
FZD	Frizzeled
GC	Glucocorticoid
GOF	Gain of Function
hESC	Human Embryonic Stem Cells
HF	Hair Follicle
IFE	Interfollicular Epidermis
ifgMosaic	Induced, Fluorescent and Genetic Mosaic (genetic construct)
Inv	Involucrin
Itgα5	Integrin α5
Itgβ4	Integrin β4
JEB	Junctionnal Epidermolysis Bullosa
K1	Keratin 1
K10	Keratin 10
K14	Keratin 14
K5	Keratin 5
Lam5	Laminin 5
LE	Leading Edge
LOF	Loss of function
Lor	Loricrin
MAPK	Mitogen Activated Protein Kinase
MMP	Matrix MetalloProteinase
NICD	Notch Intra-Cellular Domain
SC	Stem Cells
SG	Sebaceous gland
Smo	Smothened
Sostdc1	Sclerostin Domain Containing-1
TA	Transit-Amplifying (cells)
TAM	Tamoxifen
TF	Transcription Factor

TJ	Tight Junctions
β-cat	β-catenin

1 TABLE OF CONTENTS

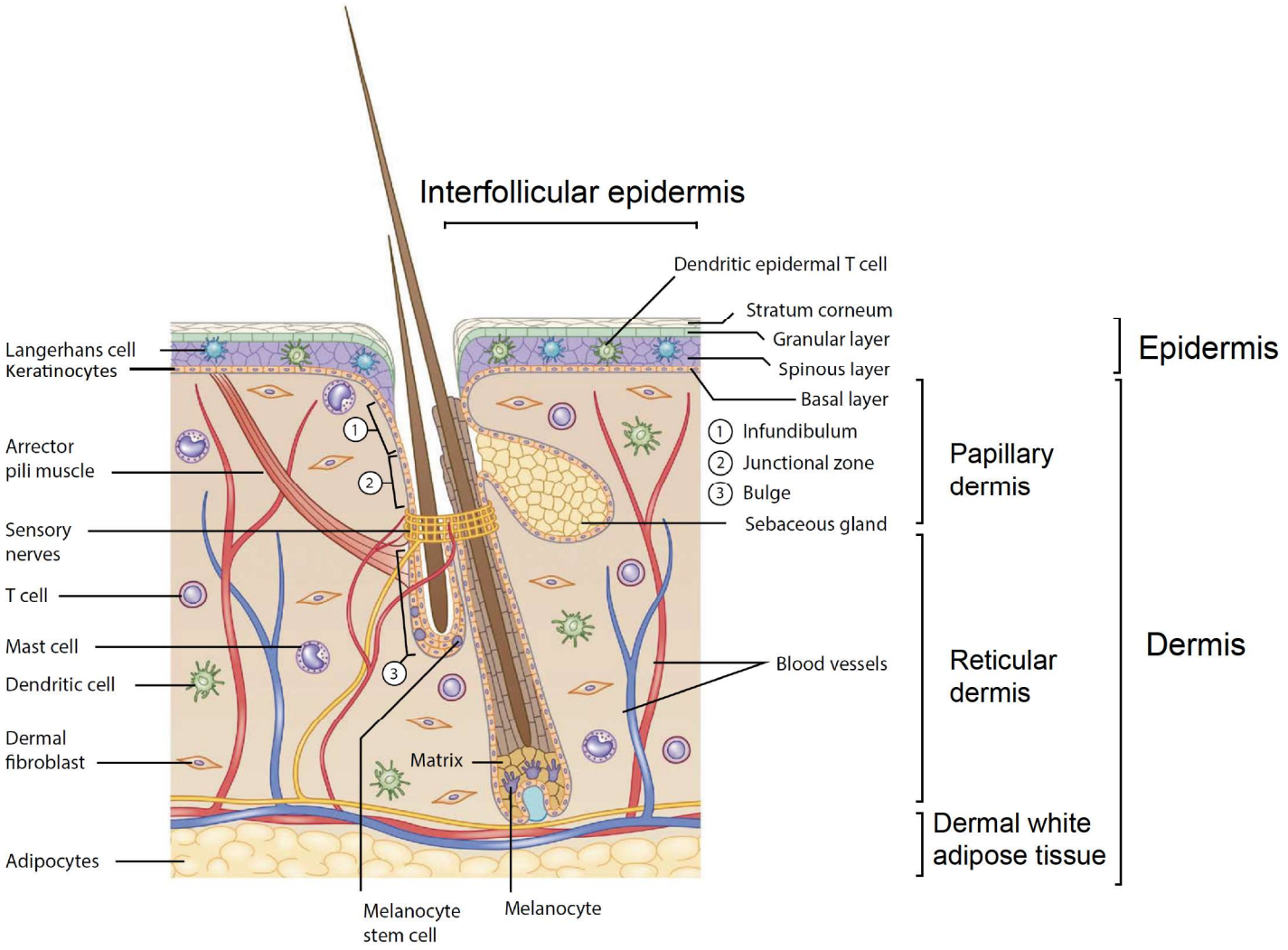

Figure 1. The structure of the skin. The skin is composed of the epidermis and the dermis. Epidermis is mainly composed of keratinocytes stacked in 4 layers : basal, spinous, granular and the stratum corneum. Immune cells such as Langerhans cells or DETCs are also present inside the epidermis. The dermis is composed of fibroblasts segregated in two layers, the upper papillary dermis and the lower reticular dermis, and a lower layer of adipocytes that form the DWAT. The HF crosses the epidermis and the dermis. It is composed of a bulge and a matrix zone, and is connected to its sebaceous glands through the junctional zone and to the IFE through the infundibulum. The arrector pili muscle ensures the hair movement. The dermis also contains blood vessels, sensory nerves and is populated by immune cells such as T cells, Mast cells or Dendritic cells. The IFE and the HF also contains Melanocytes. Adapted from *Hsu et al., Nature Medicine, 2014*.

2 INTRODUCTION

2.1 THE SKIN

2.1.1 Role and Structure

Skin is an essential barrier that covers the whole body, protects it from external infection, UV irradiation, dehydration and provide sensory perception[1]. In mammals, it is composed of 2 layers of tissue separated by a basement membrane (BM) or basal lamina : the epidermis and the underlying dermis (Figure 1). The dermis is composed of an upper (papillary) and a lower (reticular) layer[2]. The epidermis, the outermost layer of the skin, is a pluri-stratified epithelium made of keratinocytes which form an impermeable barrier[3]. The epidermis contains pilo-sebaceaous units that act as sensors and insulators, are composed of a hair follicle (HF) and their associated sebaceous glands (SG), and are connected to the interfollicular epidermis (IFE) by the infundibulum. The skin epidermis also contains sweat glands to regulate the body temperature by perspiration. Beside keratinocytes, other cell types also populate the epidermis. Melanocytes produce skin pigments for UV protection and immune cells such as Langerhans cells or Dendritic Epidermal γδ T cells (DETCs) act as sentinels to protect the epidermis[1]. The dermis is composed of fibroblasts that secrete collagen and extracellular matrix (ECM)[1,4]. It also contains specialized fibroblasts form the HF dermal papilla, which regulates hair follicle growth and the erector pili muscle, responsible for pilo-erection. The deeper layer of the dermis is made of adipocytes that form the dermal white adipose tissue (DWAT)[5]. The dermis is also populated by immune cells such as mast cells, dendritic cells and T cells that act as sentinels. Finally, the dermis contains blood vessels which ensure the proper gas exchange and provide nutrients to the tissues and sensory nerves that mediate sensory perception[1].

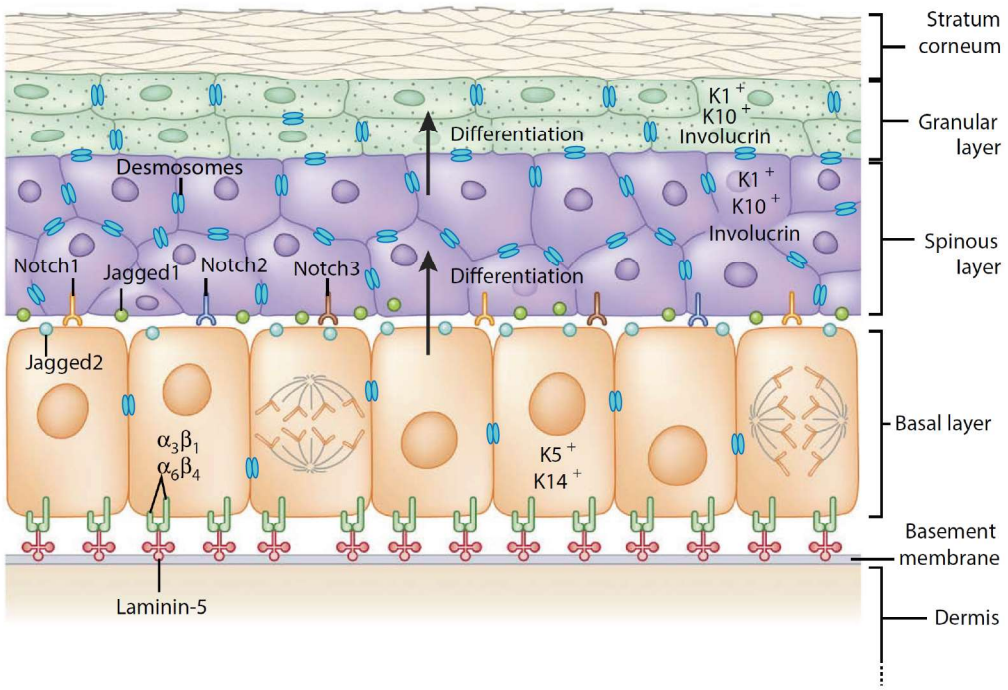

Figure 2. The structure of the interfollicular epidermis. The IFE is composed of 4 layers : basal, spinous and granular layers and the stratum corneum. Keratinocytes localized in the basal layer express K5 and K14 and are anchored to the basement membrane through integrins (α3β1, α6β4) which binds ECM component such as lam5. They also interact with suprabasal cells by secreting ligands implicated in signaling pathways, such as the Notch pathway. Basal keratinocytes sustain the IFE through cell divisions. When keratinocytes enter in differentiation, they loose their ability to divide, leave the basal layer and start to express differentiation markers such as K1, K10 and later Inv. They finally finish their differentiation process in the stratum corneum which is made of dead squames. Adapted from *Hsu et al., Nature Medicine, 2014*.

2.2 THE INTERFOLLICULAR EPIDERMIS

2.2.1 Structure

The IFE is a stratified epithelium and constitutes the first barrier protecting the animals from their environment (Figure 2). It is mainly composed of keratinocytes but other cell types such as the melanocytes, Langerhans cells, DETCs also reside in this epithelium[1]. As major building blocks of this tissue, the keratinocytes display high expression of intermediate filament cytokeratins, which confer mechanical resistance to the cells and are major components of the cytoskeletal structure. The innermost layer of keratinocytes, called the basal layer, composed of stem cells (SC) and undifferentiated progenitors, expresses keratins 5 and 14 (K5, K14) (Figure 2). It is the only proliferative layer and therefore supports the replenishment of the whole tissue. After cell division in the basal layer, daughter cells move upward in the suprabasal layers of IFE and enter into differentiation. In the spinous layer, they lose their ability to proliferate, change their transcriptional activity and start to express other keratins such as K1 and K10, as well as Involucrin (Inv). Constantly pushed upward by new cells generated underneath, they continue to differentiate in the granular layer where they start to express Filaggrin (Fil) and Loricrin (Lor) and acquire a cornified envelope, a feature essential for the establishment of the skin barrier. Terminaly differentiated keratinocytes finish their differentiation process in the outermost layer, the stratum corneum where they are enucleated and shed as squames[1,3].

The interfollicular epidermis is crucial to maintain body fluids in and pathogens out. To achieve this role of barrier, cells are anchored to the dermis through hemidesmosomes and Focal Adhesion (FA), and to each other through different cell junctions (Figure 3A). Hemidesmosomes are stable and robust junctions (Figure 3B, left). They are complex of proteins, including the transmembrane proteins α6β4 integrins which interact directly with extra-cellular matrix (ECM) component such as laminin 5 (Lam5), and indirectly with keratin cytoskeleton of the cells (Figure 3B, left). Mutations affecting intermediate filaments such as K14/K5 or hemidesmosomes are the cause of skin disorders termed Epidermolysis Bullosa (EB), characterized by blistering and skin fragility,

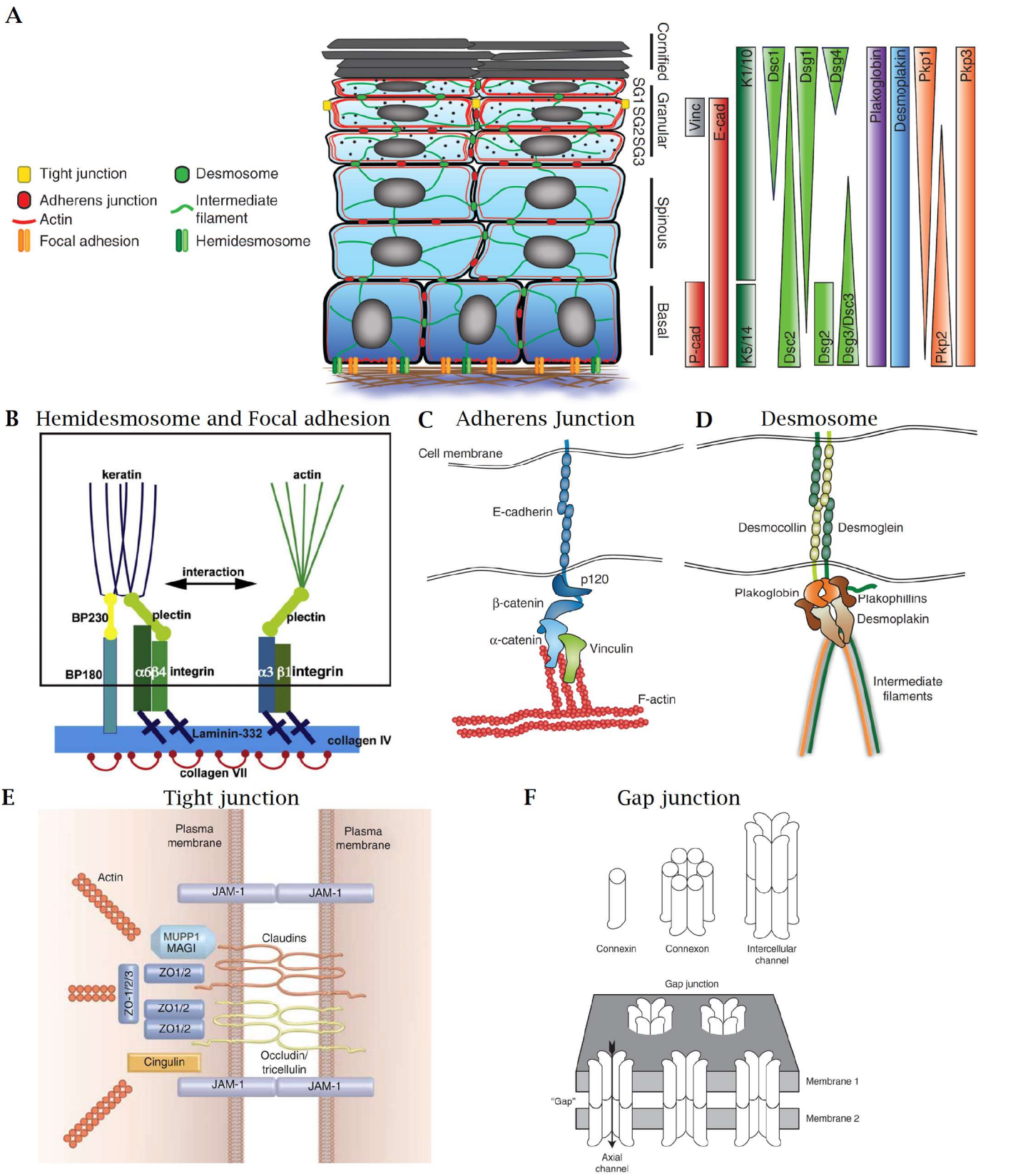

Figure 3. Cell junctions in the epidermis. (A) Spatial distribution of cell junctions and cytoskeleton in epidermis. Basal keratinocytes are connected to the basement membrane through Focal adhesion and hemidesmosomes. Basal and spinous keratinocytes are connected to each other through Adherens Junctions and Desmosomes. The spatial distribution of the proteins that constitute these two cell-cell junctions is also showed (right). Granular keratinocytes present Tight Junctions. Adapted from *Rübsam et al., Cold Spring Harbor Perspectives in Biology, 2018.* (B) Molecular composition of hemidesmosomes (left) and focal adhesion (right) in basal keratinocytes. *Tsuruta et al., Journal of Dermatological Science, 2011.*(C-D) Molecular composition of Adherens Junctions (C) and Desmosomes (D) in keratinocytes. *Rübsam et al., Cold Spring Harbor Perspectives in Biology, 2018.* (E) Molecular composition of Tight junctions, from *Niessen, Journal of Investigative Dermatology, 2007.* (F) Structural composition of Gap junctions, from *Goodenough & Paul, Cold Spring Harbor Perspectives in Biology, 2009.*

highlighting the importance of these proteins for skin integrity[6,7]. FA are large multi-protein assembly made of other integrins heterodimers such as α2β1, α3β1, α5β1 and connect the actin cytoskeleton of the cells with various matrix ligands outside the cells such as fibronectin, laminin and collagen (Figure 3B, right). FA are highly dynamics and important for cell motility and migration. More than providing the anchorage of the cells, focal adhesion are also involved in inside-out and outside-in signaling[7].

Basal and spinous keratinocytes are also connected to each other through cell-cell junctions: Adherens Junctions (AJ) and desmosomes. AJ are made by protein complexes such as transmembrane cadherin proteins (mainly E-cadherin) connected inside the cells to cytoskeletal actin filaments through β-catenin and α-catenin (Figure 3C). AJ mediates cell-cell adhesion, regulates the organization of the actin cytoskeleton and constitutes a hub for cell signaling[8]. Desmosomes are made of the transmembrane cadherin proteins, Desmocollin (Dsc) and Desmoglein (Dsg), which are connected to the cytokeratin intermediate filaments through plakophilin, plakoglobin and desmoplakin (Figure 3D). Desmosomes are essential to maintain the function and the structural integrity of the epidermis. A third type of cell-cell junctions, the Tight Junctions (TJ), is expressed in the apical part of suprabasal keratinocytes located in the granular layer (Figure 3E). TJ are composed of two families of transmembrane proteins, Occludin and Claudin, which bind actin cytoskeleton through Zonula Occludens (ZO) proteins[9]. The role of the TJ is to ensure a tight adhesion between cells[8]. Finally, Gap Junctions are also present at the surface of epidermal cells and support the intercellular communication[10] (Figure 3F). Gap junctions are made of intramembranous proteins, the connexins, organized in hexamers. Two hexamers from two neighbor cells form an intercellular channel through which ions and small molecules can transit, making these signaling molecules available for all cells within the tissue. The main connexins present in the skin epidermis are the connexin 43 (Cx43/Gja1), 26 (Cx26/Gjb2) and 30 (Cx30/Gjb6). Underlying their importance is cell communication for organ function, mutation of Cx26 or Cx30 are responsible for profound deafness and skin disorder in human[10].

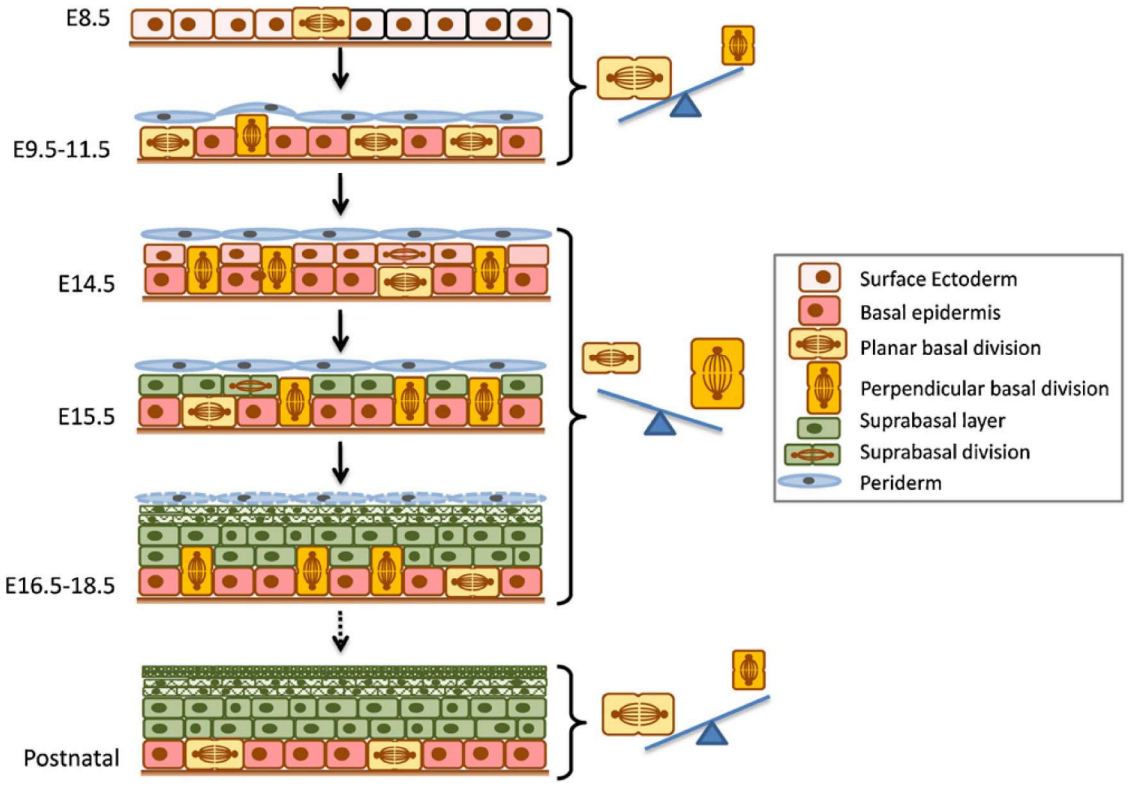

Figure 4. Stratification of the epidermis during embryonic development. At E8.5, the surface ectoderm surrounding the embryo is made of one single layer of cells expressing K8/18 and dividing parallel to the BM. Around E9.5, basal cells acquire an epidermal fate and express K5/K14. Until E11.5-E12.5, most of the cell division are still parallel to the BM producing only basal cells. At E14.5, basal keratinocytes start to divide perpendicularily to the BM, leading to the formation of an intermediate layer which express K1/K10 around E15.5. From E14.5 to E18.5, most of the cell division are perpendicular to the BM and lead to the rapid establishment of the epidermal suprabasal layers. After birth, most of the cell division are again parallel to the BM. Adapted from *Roshan and Jones, Seminars in Cell & Developmental Biology, 2012.*

2.2.2 Embryonic development and stratification

The establishment of the IFE layers is a complex and highly coordinated program that takes place during embryogenesis (Figure 4). In mice, this program occurs between embryonic day 9.5 (E9.5) and E18.5. Before E9.5, surface ectoderm cells are uncommitted and express K8 and K18. At E10.5, they acquire an epidermal fate and the prospective epidermis is composed of a single layer of keratinocytes that express basal markers such as K5 and K14 [11,12]. At E12.5, a large majority of cell divisions (92%) are oriented parallel to the basement membrane, resulting in the generation of two basal daughter cells. Around E14.5, by contrast, most of the cell divisions (70%) have their spindle poles oriented perpendicular to the basement membrane, generating suprabasal daughter cells that start to express K1 and K10[13,14]. Proper perpendicular division is dependent on cell-matrix and cell-cell interactions as disruption of FA (through β1 integrin knock-out) or AJ (through α-catenin knock-out) randomize division orientation[13]. This switch toward perpendicular cell division is a key step for epidermis stratification as it generates daughter cells that are not connected anymore to the basal lamina and acquire a suprabasal fate through asymmetrical partitioning of intracellular factors. This partitioning is controlled by two important complexes that are well conserved from worm to mammals : the Par complex (comprising Par3, Par6 and aPKC) which is a master polarity determinant and a complex that controls spindle orientation (LGN/Numa/Dctn1)[15]. In mice embryonic skin, downregulation of LGN, Numa or Dctn1 decreases the proportion of perpendicular division at E16.5 and prevent the proper stratification of the epidermis, leading to a thin and permeable epidermis at birth [16]. Interestingly, perpendicular divisions are specific to embryonic development and are very rare in adult epidermis[13]. Recent live-imaging studies performed on E15.5 mouse embryos suggest that the contraction of basal cells due to overcrowding may also have a role in stratification and epidermal cell differentiation[17].

In postnatal and adult epidermis, by contrast, orientation of cell division are uncoupled from cell fate as most of the division are parallel or oblique to the basal lamina. In this case, daughter cells start their differentiation program in the basal layer and move later on into the suprabasal layers through delamination[12,18]. This

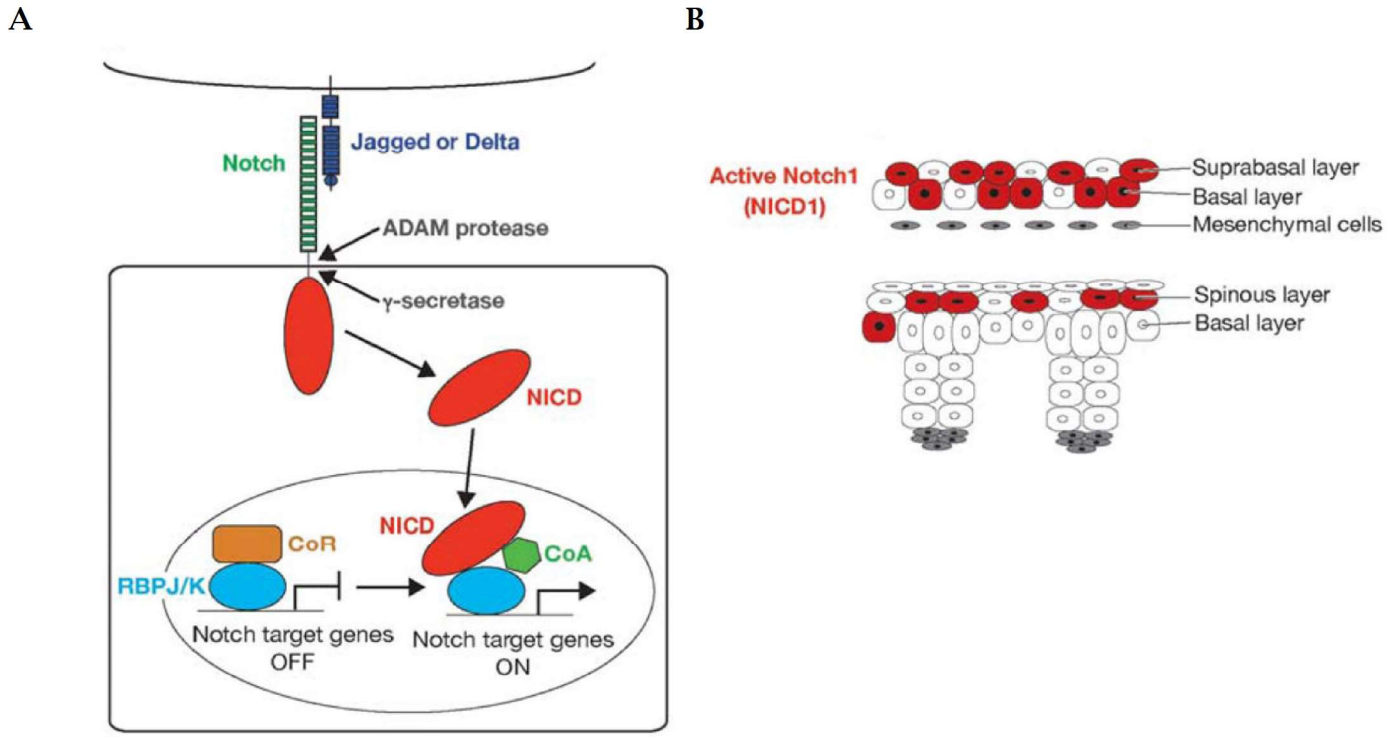

Figure 5. The Notch signaling pathway. (A) Molecular components of the canonical Notch signaling pathway. Ligands from Jagged or Delta family bind the Notch receptor and activate the pathway. After ligand binding, the NICD is cleaved by the ADAM protease and a γ-secretase and translocates into the nucleus where it associates with the DNA-binding protein RBPJ/K and activates target genes transcription. (B) Notch1 signaling is active during epidermis development in basal and suprabasal cells while it is only active in the suprabasal cells after birth. Notch1 signaling restricts basal fate and promotes differentiation in epidermis. Adapted from *Blanpain and Fuchs, Annual Review of Cell and Developmental Biology, 2006.*

upward movement is thought to be due to a combined loss of cell-matrix contact and dynamic cell-cell junctions re-arrangement which would reduce the cortical tension of the daughter cell compared to neighbor basal cells and initiate an upward movement and differentiation[19]. Interestingly, while recent reports showed that overcrowding triggers cell differentiation and stratification during embryogenesis[17], other studies suggest that, to the contrary, basal cell differentiation is the trigger to induce neighbor cell division in adult tissue[20]. It is possible that the mechanism differ depending on the proliferative status of the tissue or that both mechanisms may co-exist within the same tissue.

2.2.2.1 The role of Notch signaling in epidermis development

The control of asymmetrical division, cell fate and differentiation are key steps in epidermis development and several studies show the importance of the Notch signaling pathway in this process[3]. Notch signaling pathway is highly conserved and implicated in cell fate decision in the entire animal kingdom[21-23]. In mammals, the transmembrane receptor Notch exist in 4 isoforms (Notch 1-4). Upon binding with their transmembrane ligands Jagged (Jag1, Jag2) or Deltas (Dll1, Dll3 and Dll4), Notch receptors are sequentially cleaved by a metalloproteinase and a γ-secretase to release the active Notch IntraCellular Domain (NICD) which can translocates to the nucleus, associate with the DNA-binding protein CBF1/RBP-J and activates Notch target genes transcription[22] (Figure 5A). Several components of Notch signaling pathway are expressed in skin epidermis. During mouse epidermal development, Notch1-3 and Jag1 are expressed in suprabasal cells whereas Dll1 and Jag2 are expressed at the apical side of basal cells[16,24-26]. Notch target genes such as Hes1, and to a lesser extend Hey1, are also expressed in majority in suprabasal cells and in rare basal cells[27]. Several *in vivo* gain (GOF) and loss of function (LOF) experiments suggest multiple important roles of Notch signaling during embryonic development and post-natal life. Mice having a conditional deletion of Notch1 initiated at birth present a higher proliferation rate and aberrant expression of basal markers in the second layer, pointing a role for Notch1 in the control of proliferation and differentiation in post-natal life[26]. Similar epidermis hyperproliferation was also observed postnatally *in vivo* after complete blocking of Notch signaling through RBP-J ablation in a mosaic manner[28] or upon inactivation of γ-secretase complex[29]. The

role of Notch1 in controlling cell proliferation was further supported by *in vitro* experiments showing increased expression of the cell cycle arrest Cyclin-dependent kinase inhibitor 1A (cdkn1a or p21), after Notch1 overexpression, a mechanism that would occur through both a direct and indirect RBP-J dependent mechanism[26,30]. However, other *in vivo* experiments suggest a slightly different role for the Notch signaling during embryonic development. *In vivo K14-Cre* mediated conditional knock out of RBP-J or Notch1/Notch2 together showed that blocking Notch signaling from E14.5 in skin epidermis lead to a thinner epidermis, defect in the proper maintenance of spinous and granular layers and lower proliferation[27,31]. These mice die shortly after birth but grafting experiments confirm that an hyperproliferation can be observed later on, suggesting an indirect or delayed role of Notch signaling on proliferation *in vivo* or different role of Notch signaling in embryonic vs post-natal development[27,31]. The absence of spinous and granular layers observed after complete blocking of Notch signaling suggest an important role in promoting differentiation during embryonic development. Interestingly, Hes1 KO mice partially recapitulate RBP-J cKO phenotype (thinner epidermis, lack of spinous layer, low proliferation), except that the granular layer is present and even premature[31]. On the other hand, forced expression of Notch signaling through overexpression of NICD in all K14+ cells at E14.5 lead to thicker epidermis, increased spinous compartment (K1), decreased granular compartment (Lor, Fil), but also change in basal fate and decreased adhesion due to decreased expression of integrins (Itgα6, β1, β4)[27,31]. While overexpression of Hes1 in basal cells also lead to a thicker epidermis but does not show any difference in spinous or basal fate. These data suggest that basal fate restriction and promotion of spinous differentiation is controlled by Notch signaling but is not Hes1 dependent, contrasting with some *in vitro* experiments[27,31]. Finally, overexpression of NICD or Hes1 in suprabasal layer support a role of Notch signaling in both maintaining spinous fate (Hes1 dependent) and promoting granular differentiation (Hes1 independent)[31]. Altogether, these data support the model where Notch signaling is an important switch for the commitment of basal cells to differentiate (Figure 5B). First, Notch signaling restrict basal cell fate by repressing proliferation and adhesion and promote spinous differentiation through target genes different than Hes1. Second, through Hes1, Notch signaling maintains spinous fate and block granular differentiation. Finally, when Hes1 is downregulated, Notch

signaling also promote granular differentiation. In line with these results, it was suggested that embryonic asymmetrical division promote stratification by enhancing Notch signaling in the suprabasal cells[16].

2.2.2.2 The role of Wnt signaling in proliferation and HF SC maintenance

The Wnt/β-catenin signaling pathway is conserved throughout eukaryotes and plays important role in multiple tissues from embryonic to post-natal development[3,32]. Wnt ligands, a family of cysteine-rich secreted glycoproteins, interact with cell surface receptors of the Frizzeled (FZD) family and LDL-related protein (LRP) receptors, and lead to the intracellular stabilization of β-catenin (β-cat) (Figure 6). In absence of Wnt ligand, Frizzeled and LRP receptors are inactive and β-cat is recruited to a destruction complex composed of several proteins including Adenomatous polyposis coli (APC), Disheveld (Dsv) and Axin. B-cat is then phosphorylated by two kinases of this complex, caseine kinase-1 (CK1) and glycogen synthase kinase-3 (GSK-3), recognized by the E3 ubiquitin ligase (β-TrCP) and transported to the proteasome for degradation (Figure 6A). Activation of the pathway occurs when a Wnt ligand binds both FZD and LRP, which trigger the phosphorylation of the latter and enables, through Dsv, the recruitment of the destruction complex to the cell membrane. While the complex can still phosphorylate β-cat, it is no longer accessible for β-TrCP and free β-cat starts to accumulate in the cytoplasm and translocates in the nucleus. There, β-cat replaces a transcriptional repressor, Groucho, and interacts with transcription factors (TF) such as T-Cell Factor (TCFs) and Lymphoid Enhancer Factor (LEFs) to recruit transcriptional co-activators and histone modifiers and initiate gene transcription (reviewed in ref[32]). Wnt/β-cat signaling can be modulated through a variety of antagonists secreted or membrane-associated proteins. Secreted Frizzeled-Related Proteins (SFRPs) or Wnt Inhibitor (WIF) directly bind Wnt ligands whereas members of the Dikkopf (DKKs) family, Sclerostin (Sost) or Sclerostin Domain Containing-1 (Sostdc1) block Wnt signaling through their interaction with LRP receptor. Wnt/β-cat signaling can be enhanced thanks to the association of R-spondin secreted proteins with their receptor, the leucine rich repeat containing G protein-coupled receptors (LGRs) family, which prevent FZD and LRPs degradation and therefore prolong β-cat stabilization[33,34].

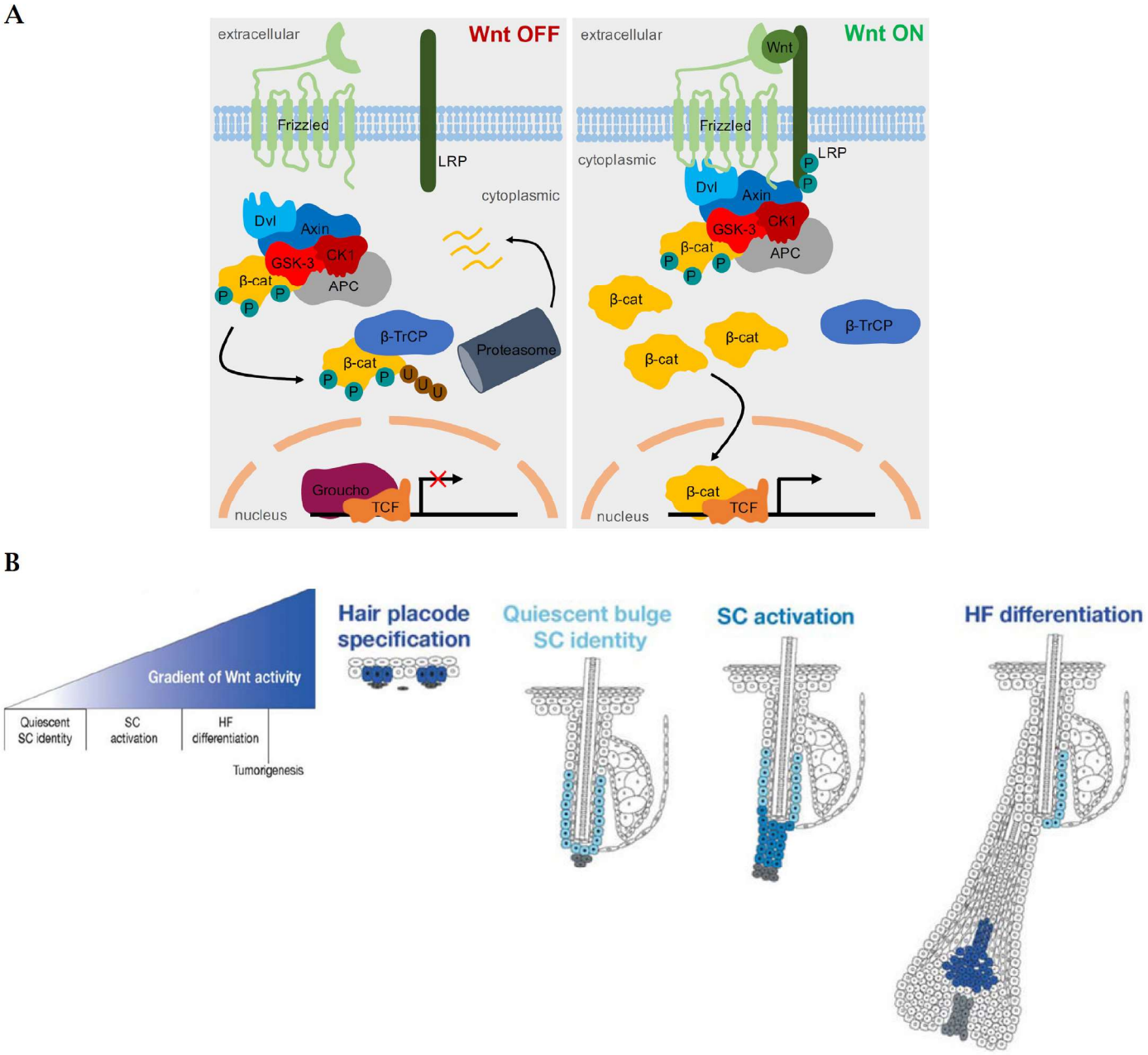

Figure 6. The Wnt signaling. (A) Molecular components of the canonical Wnt signaling pathway. In the abscence of Wnt ligand, the excess of cytoplasmic β-cat is bound by a protein complex and degraded by the proteasome (left). In the presence of Wnt ligand, the Frizzeled and LRP receptors are activated and recrut the destruction complex at the membrane. Free β-cat can transclocate to the nucleus, replace the transcriptionnal repressor Groucho and activate Wnt target genes transcription. From *Kretzschmar and Clevers, Developmental Biology, 2017.* (B) In the epidermis, the role of Wnt may depend on the level of activation of the pathway. Low Wnt activity would be essential to maintain quiescence of the bulge SC, light Wnt activity would be necessary to activate the SC and high Wnt activity would be essential for HF placode formation during embryonic development and HF differentiation in post-natal and adult life. Adapted fom *Blanpain and Fuchs, Annual Review of Cell and Developmental Biology, 2006.*

In the mammalian epidermis, Wnt/β-cat signaling pathway plays multiple roles in HF morphogenesis, HF stem cells specification and hair shaft differentiation. Conditional deletion of β-cat in epidermal cells at E15.5 blocks the formation of HF placode and in postnatal development prevent the initiation of the HF morphogenesis leading ultimately to hairless mice[35]. Similar hairless phenotype were observed in mice deficient for Lef1 or over expressing a Wnt inhibitor Dkk1[36-38]. More precisely, conditional deletion of β-cat post-natally lead to a decrease in proliferation of HF matrix and loss of HF SCs markers[38,39]. By contrast, forced activation of Wnt/β-cat signaling in transgenic mice through overexpression of Lef1 or constitutive activation of β-catenin in basal epidermal cells lead to precocious anagen re-entry, aberrant and supernumerary formation of HF within the IFE and later to the spontaneous development of hair tumors such as pilomatricomas[39-41]. All these data support the important role of Wnt/β-cat signaling in the control of matrix cells proliferation, HF morphogenesis and maintenance. Wnt/β-cat signaling directly controls keratinocyte differentiation within the HF as hair keratin genes possess LEF/TCF binding sites in their upstream promoter and the highest expression of Wnt signaling is observed in terminally differentiated cells of the cortex in the hair shaft[41,42]. By contrast, quiescent bulge SCs express a high level of Wnt inhibitors such as *Sfrp1* or *Dkk3,* downregulate *Wnt3* and *Wnt3a* but at the same time express Wnt receptors (*Fzd2/3/7*) suggesting that they keep the Wnt pathway inactive or at low level but nevertheless can potentially react to an increased Wnt stimulation[43]. Interestingly, a subset of bulge cells express the Lgr5 receptor during the resting phase of the HF cycle, suggesting that Wnt active and inactive cells coexistence may be important for HF maintenance[44]. Altogether, these data suggest a model where Wnt/β -cat signaling impact HF SC behavior differently depending on the intensity of its activity[3] (Figure 6B).

In hairy epidermis, such as backskin and tail, lineage tracing studies using *Axin2-CreER* mice showed that Wnt signaling is active in basal IFE progenitors[38]. Specific mosaic deletion of β-cat in *Axin2*+ IFE cells induces a decrease in their proliferation rate[38]. Similarily, in non hairy epidermis such as the footpad and the tongue, broad deletion of β-cat or ectopic expression of the Wnt inhibitor *Dkk1* lead to a decrease in epidermis thickness and basal proliferation but in this case induce

a premature differentiation[38,45]. These results suggest that, similarily to HF, Wnt signaling is important to sustain basal IFE proliferation during homeostasis and may play a different role in differentiation.

2.2.2.3 Transcription factors important for epidermis maintenance and stratification

TFs are important actors in cell fate determination. They integrate upstream signaling and ensures the downstream regulation of gene expression[46]. A key TF in epidermis development is *p63* (also *Tp63*)[47,48]. *P63* is a homolog of the *p53* tumor suppressor gene. *P63* can present six distinct isoforms due to alternative transcription start sites and splicing at the C-terminus leading to three trans-activating long isoforms (TA-p63 α, β and γ) and three short isoforms (ΔN-p63 α, β and γ)[49]. In human, germline mutations of *TP63* have been associated with several human syndromes presenting ectodermal dysplasia, limb malformations and orofacial clefting[50]. In mice, deletion of all *p63* isoforms lead to craniofacial malformations, limb truncation and severe defect in the formation of squamous epithelia such as skin, tongue, oesophagus, proximal stomach and the absence of ectodermal derivatives such as teeth, HFs, mammary, lacrymal and salivary glands[47,48]. In the skin epidermis, expression of the basal markers (K5/K14) as well as differentiation markers (K1/K10, Inv, Fil and Lor) are low or absent in *p63* deficient mice[47,48,51]. *P63* null mice die within hours after birth and present severe defect in skin barrier formation[47,48]. These data show that *p63* is important for epidermal cell fate and stratified epithelia development. While ectopic expression of both TA-p63 and ΔN-p63 isoforms trigger the expression of K14/K5 *in vitro* and induce a squamous phenotype in the lung epithelium *in vivo*[52-54] further studies showed that only the ΔN-p63 isoforms is important in skin epidermis[52,54-58]. First, despite initial confusion in the field, it appears that only the ΔN-p63 isoforms are presents at the protein level both in mouse and human keratinocytes[52,54,55]. Second, specific depletion of ΔN-p63 (but not the TA-p63) phenocopies the *p63* full deletion phenotype observed in human keratinocytes organotypic culture *in vitro* and during mouse development *in vivo*[55-57]. Third, genetic induction of ΔN-p63 or both α isoforms together (but not the TA-p63α alone) can partially rescue *p63* null phenotype[54,58]. All these data demonstrate that most of the phenotype observed in *p63* null mice in skin epidermis is attributable to ΔN-p63. Consistent with its role in

the control of epidermal fate, ΔN-p63 protein is observed at E10.5 during skin embryonic development, before the strong expression of K5/K14, when the ectoderm is still a single layer of cells expressing K8/K18[54,59]. Several experiments, including genetic deletion of ΔN-p63 in mice or siRNA in human keratinocytes, show that *p63* controls the expression of important epithelial markers implicated in cell adhesion (Itgβ4, Itgβ6), basement membrane formation (Lam5, Collagen IV) and would repress directly differentiation markers[55,56,58,60]. Importantly, p63 has also an important role in epigenetic regulation as *p63* motifs are present in enhancer elements upstream of the *K14* and *K5* genes[53,54]. Recent reports also suggest that p63 may act as a pioneer factor and cooperate with chromatin remodeler proteins to shape enhancers and open the chromatin in epithelial cells[61,62].

Interestingly, a direct feedback control exists between Notch and p63. Notch signaling inhibits p63 expression and sustained activity of p63 suppresses the cell cycle arrest and part of the differentiation program mediated by Notch, possibly through the downregulation of Hes1[63]. Pharmacological and genetic inhibition of Notch signaling promote p63 expression in human embryonic stem cells (hESCs) and mouse embryonic skin respectively[59]. These data suggest that the balance between p63 and Notch signaling may be critical for epidermal cell fate decision, a higher level of p63 being in favor of a basal proliferative state whereas a higher level of Notch would favor a differentiated state. Moreover, while Hes1 is mostly expressed in suprabasal cells, Hes1 KO mice display a lower proliferation and down regulation of p63 in basal cells, suggesting that a non-cell autonomous signal coming from suprabasal cells is also important to maintain proper basal proliferation[31].

C/EBPα and β are other TFs known to regulate proliferation and differentiation in many mammalian tissues[64]. They are expressed in suprabasal cells of the epidermis[65,66]. Mice lacking *Cebpa* or *Cebpb* show no or only mid perturbation in epidermis, respectively[67,68]. However, double conditional ablation of both genes in K14+ cells lead to perinatal death due to defect in barrier formation, as shown with dye penetration and downregulation of genes implicated in the formation of the cornified envelope (*Lor, Flg, Tgm3*)[69]. *K14-Cre/Cepba*$^{f/f}$*/Cebpb*$^{f/f}$ mice also display an hyperproliferative epidermis, ectopic expression of K14 in the suprabasal cells, decreased expression of K1, K10 and absent expression of Inv and Lor[69]. These data

suggest an important role of C/EBPα and β to repress proliferation and mediate the loss of basal marker and the acquisition of late differentiation markers.

Other TFs are important to initiate and ensures the progression of terminal differentiation. Among them, the Oct class of POU domain TFs : Pou2f1 (also called Oct-1), Pou3f1 (also called Tst-1, Oct-6 or SCIP) and Pou2f3 (also called Skn-1a/i, Oct-11 or Epoc)[46]. While Pou2f1 is expressed at similar level in basal and suprabasal cells, Pou2f3 and Pou3f1 expressions are higher in epidermal suprabasal cells and overlap with K10 expression[70]. *In vitro*, Pou3f1 and Pou2f3 can repress the expression of reporter genes placed under the control of the *K14* promoter, suggesting that they repress K14 expression, and overexpression of Pou2f3 in keratinocytes increases their ability to differentiate and express K10[70-72]. *In vivo*, double homozygous ablation of Pou2f3 and Pou3f1 genes lead to ectopic expression of K14 in suprabasal cells, in grafted murine epidermis[70]. These data highlight the role of these TFs to repress K14 and promote keratinocytes differentiation.

TFs from the Activator Protein 1 (AP-1) family also play important roles in epidermis differentiation[73]. AP-1 are transcriptional regulators composed of members of the DNA binding proteins Fos (Fos, FosB, Fosl1/Fra-1 and Fosl2/Fra-2) and Jun (Jun/c-Jun, JunB and JunD) families[73]. AP-1 act downstream of evolutionarily conserved signaling pathways such as Mitogen-Activated Protein Kinase (MAPK), Transforming Growth Factor beta (TGF-β) and Wnt[73]. Conditionnal deletion of Jun in basal epidermal cells show that it is an important mediator of Epidermal Growth Factor (EGF) signaling and primary keratinocytes lacking Jun display lower proliferation rate and increased K10 expression, a marker of early differentiation[74,75]. Interestingly, Jun and JunB have been shown to be downregulated in human inflammatory skin disease such as psoriasis, characterized by inflamed, scaly skin lesions[76]. Consistently, specific conditional ablation of Jun and JunB in K5+ cells in adult mice lead to the formation of an abnormally thickened epidermis, hyperkeratosis and recapitulate psoriasis like phenotype such as inflammatory infiltrates and enlarged blood vessels[76]. Deletion of Jun and JunB lead to the increased expression of the chemokines S100a8 and S100a9, which are known to recruit neutrophils[76]. These data suggest an important role for Jun and JunB to

maintain proper balance between proliferation and differentiation and to maintain proper epidermis integrity.

The AP-2 family of TFs is composed of 5 members : AP-2α, AP-2β, AP-2γ, AP-2δ and AP-2ε[77]. AP-2 sequence motif is found upstream of many regulatory regions of important epidermal genes, including keratins[77-80]. AP-2α and AP-2γ are both expressed in basal and suprabasal epidermal cells, although AP-2α has a higher expression in basal cells[80,81]. Conditional deletion of AP-2α *in vivo* show that it represses EGF receptor expression in suprabasal cells and basal cells commited for differentiation suggesting an important role in the control of keratinocytes proliferation[81]. AP-2α and AP-2γ also act synergistically with Notch on C/EBP TF expression to regulate basal to spinous transition[82]. Indeed, double conditional KO of AP-2α and γ lead to a decreased expression of early terminal differentiation genes in the epidermis such as K1, K10, Fil and also a decreased expression of C/EBP TF both, *in vivo* and *in vitro*[82]. These data suggest that AP-2α plays an important in the switch from proliferative to differentiated cells in skin epidermis.

Members of Krupper-Like Family (Klf) are charachterized by a Zinc finger DNA-binding domain. They are 17 mammalians proteins and several Klfs are expressed in skin epidermis[77]. Among them, Klf4 has been shown to play an essential role in epidermis development and barrier function[77]. Klf4 protein appears in spinous layers around E14.5 during embryonic epidermis development and mice lacking Klf4 die early after birth due to barrier function defect, highlighting an important role for Klf4 in IFE differentiation and barrier function acquisition[83]. Klf5, on the other hand, is expressed in both basal and suprabasal cells in the epidermis in mouse and human and may be important for basal to suprabasal cell transition[84,85]. Klf5 is a direct repressor of ΔNp63 and its overexpression during embryogenesis leads to skin barrier defect, abnormal K8 expression within the basal layer and defect in proliferation[86]. Klf5 may also have an important role in promoting HF stem cells differentiation, as suggested by the decrease in CD34+ fraction in adult skin upon Klf5 overexpression[86].

Among TF from the GATA family, composed of six members (Gata1 to 6), Gata3 plays key roles in skin epidermal development and lineage determination[77].

Gata3 is expressed at E15 and localized in basal and suprabasal layers of the epidermis[87,88]. *Gata3-/-* mice die at birth and show a delay in barrier function acquisition around E16.5, suggesting a positive role for Gata3 in epidermis differentiation[87,88]. Genes associated with lipid biosynthesis as well as epidermal differentiation such as Lor, K10 and Inv are downregulated in *Gata3* deficient mice at E15.5 and E16.5, confirming the critical role of Gata3 in keratinocyte differentiation[88]. By contrast, grafting experiments using *Gata3-/-* keratinocytes or specific deletion of *Gata3* in K14+ cells show an increase in epidermis thickness[87-89]. Interestingly, genes associated with epithelial defense and recruitment of inflammatory cells, such as S100a8 and S100a9, are upregulated in *Gata3-/-* epidermis[88]. The hyperproliferative epidermis observed in transplantation assays using *Gata3-/-* epidermis or in *K14-Cre/Gata3$^{f/f}$* mice may therefore be a compensatory mechanism related to the increase in inflammatory signals[88,89]. Altogether, these data show that Gata3 is dispensable for skin development but plays an important role in differentiation, barrier function and to control inflammatory signals.

Similarily to Gata3, Grainyhead Like transcription factor 3 (Grhl3) has been shown to be important for skin barrier acquisition[77]. Grhl3 is expressed early in the neurectoderm during embryonic development and is confined to epidermal suprabasal cells after birth[90,91]. Mice deficient for Grhl3 display a defect in barrier function and decreased expression of Inv, Lor and Fil, supporting a role in epidermal maturation[92,93].

2.3 MODELLING STEM CELL FATE DECISION IN EPIDERMIS

SC are able to self-renew indefinitely and give rise to all the cell lineages that constitute their tissue of origin[3]. Maintenance and tissue repair are achieved by SCs and has to be properly controlled to enable harmonious growth and healing. How SC balance between proliferation and differentiation in IFE during homeostasis has been a matter of debate and different models of epidermis self-renewal were proposed in the past (Figure 7). One model proposed in 1970's by Mackenzie and further supported by Potten in the 1980's proposed that epidermis was maintained by discrete and regular columns of cells called Epidermal Proliferative Units (EPU)

(Figure 7A-C)[94-96]. Each unit was thought to be sustained by a central basal self-renewing SC. Upon infrequent asymmetrical division, this SC gives rise to basal transit-amplifying (TA) daughter cells (around 9 in the backskin, 10 in the ear, 13-16 in the footpad and 24 in the tail)[94,97]. According to this model, these basal TA cells undergo a limited number of division and ultimately enter into terminal differentiation leaving the place for a new TA cell[94]. For both SC and TA cells, the unique proposed mode of division was invariant asymmetrical cell divisions, meaning that two different cells are produced after division : a cell identical to the mother and a more differentiated cell. This pattern of self-renewal is called invariant asymmetry and implies that each EPU converge toward a fixed size after some time (Figure 7A-C). While the EPU model has been largely accepted for decades, the progress made in lineage tracing techniques and whole-mount tissue preparation for 3D observations highlighted several results that were not consistent with this theory (Figure 7D-J). Indeed, in early 2000's lineage tracing experiments made with lac-z-carrying retrovirus showed epidermal clones having a size bigger than an expected EPU[98]. However, the experimental set-up implicated abrasion of the skin to increase basal proliferation and retrovirus insertion, leaving open the possibility that wound induced bigger EPU. A second lineage tracing study was performed with the use of a *STOP-EGFP* mouse where a premature STOP codon prevents the expression of the EGFP. Any mutation at any site of the STOP codon would restore EGFP expression[99]. Dorsal skin was treated with mutagen to induce randomly EGFP expression in epidermal cells and skin was collected 6 weeks after to enable EGFP+ suprabasal cells to be shed off. As the turnover of the epidermis is estimated at 2 weeks, the vast majority of labelled cells still present were coming from cells having self-renewal capacities and the low mutation frequency exclude the possibility that two basal cells next to each other would undergo the mutation. The data showed the presence of clones bigger than the size of an expected EPU, which was not consistent with the theory[99]. Here again, the treatment with the mutagen precluded to draw definitive conclusions about epidermis homeostasis. Finally, the first lineage tracing experiment performed in homeostatic conditions was made by Clayton and colleagues on mouse tail epidermis[100]. Using a tamoxifen inducible promoter (*Ah-CreERT*) and *Rosa-EYFP* mice they labeled scattered and isolated single basal cells in the adult epidermis. Mice were sacrificed at different time points from 2 days up to

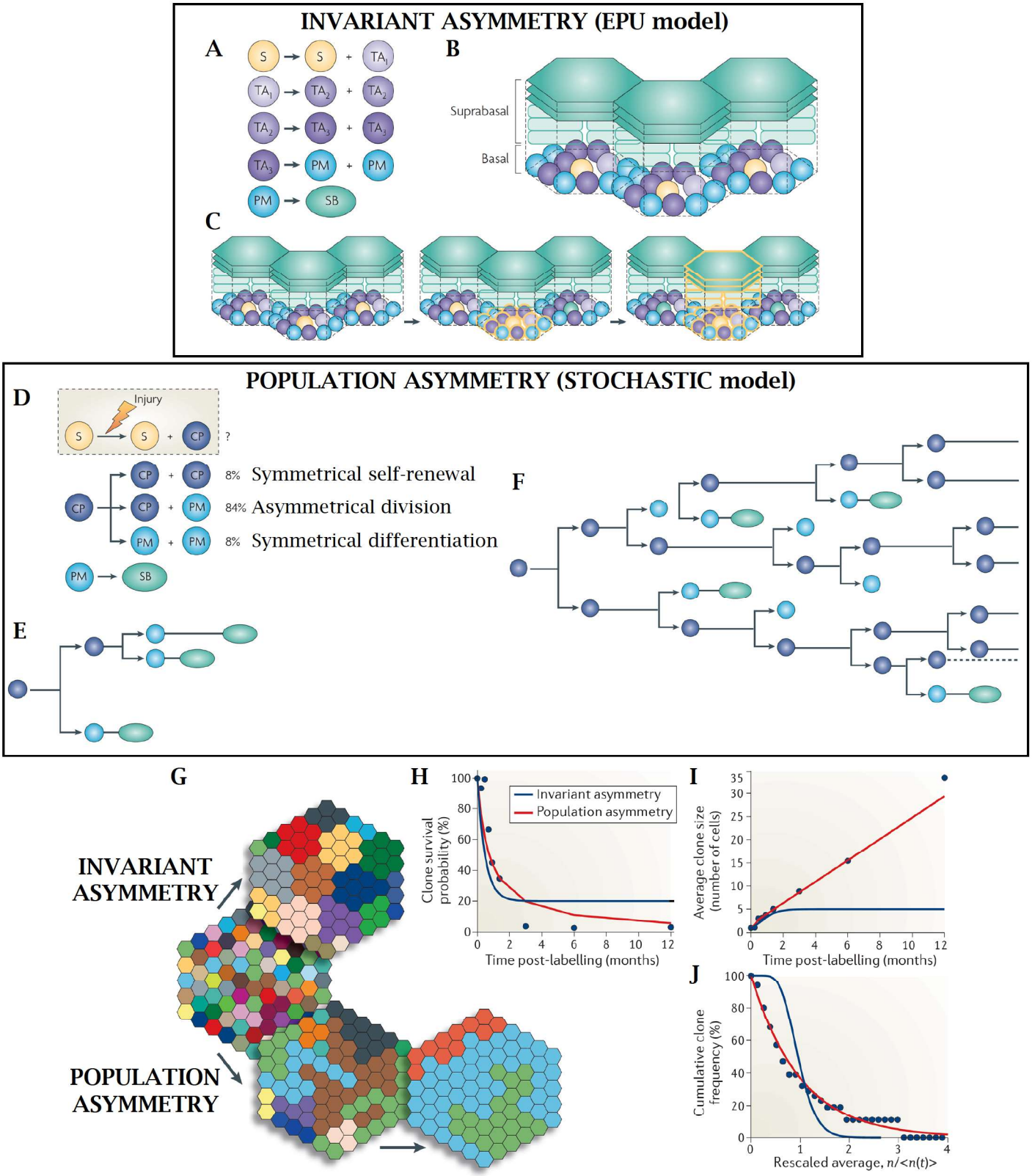

Figure 7. Models of IFE SC dynamics in epidermis. (A-C) The EPU hypothesis suggested that basal cells divide invariably asymmetrically. The stem cells (S) (yellow) generate the transit-amplifying (TA) population (purple) which after 3 rounds of division undergo terminal differentiation and become post-mitotic (PM) and suprabasal cells (SB) (A). Each unit is sustained by one S and has a fixed number of TA and PM basal cells (B). S would after some time renew the whole unit (C). (D-F) The stochastic model suggests that commited progenitors (CP) are all equipotent and adopt one of three possible cell fates at each division, with fixed probabilities (%) for each fate. CPs either remain proliferative (purple) either become post-mitotic (PM)(blue). This model does not exclude the existence of stem cells (S) which can be re-activated upon injury (D). Possible fate choices giving rise to a small clone (E) or a big (F) clone. Adapted from *Jones & Simons, Nature Reviews Molecular Cell Biology, 2008.* (G-J) Comparison of the invariant asymmetry and population asymmetry model and the expected outcomes upon clonal lineage tracing. Adapted from *Blanpain & Simons, Nature Reviews Molecular Cell Biology, 2013.*

1 year post-induction. Tail epidermis was collected as whole-mount and back skin as 60µm-thick sections, to observe the clonal dynamics over time, using 3D confocal microscopy. At 2 days post-induction, the vast majority of cells labeled in the basal layer of the tail IFE were single and the labeling frequency was 1/600, meaning that any clone observed in the later time point would be the progeny of a single cell. In the later time point, cohesive clones containing several labeled cells in the different layers of the epidermis were observed. The quantification of the number of basal and suprabasal cells per clone across the different time points showed that clones were progressively expanding in size over time. One year after the induction, the number of clones per surface area had decreased by more than 90% whereas almost 80% of the remaining clones were highly heterogeneous in size, ranging from 1 to 128 basal cells[100]. This dramatic loss of clones and the ever expanding ability of the remaining clones were in contradiction with the EPU model and the invariant asymmetry model (Figure 7G-J). Instead, these data were consistent with a neutral drift model in which IFE is maintained by only one compartment of equipotent proliferating cells which may undergo an unlimited number of division and compete neutrally for space : the stochastic model or population asymmetry (Figure 7D-F)[100,101]. According to this model, each division of an epidermal basal progenitor can lead to 3 different fate outcomes. In the vast majority of the cases (84%) the progenitor gives two different daughter cells (asymmetrical fate outcome) : one progenitor which remains in the basal layer and one postmitotic differentiated cell. However, if this was the only mode of division, the frequency of the labeled clone observed in the tissue should not decrease overtime and the size of the remaining clones would not be heterogeneous. Instead, the clonal data fit with the possibility that some progenitors can be lost by differentiation (symmetrical differentiation) and some other can self-renew (symmetrical self-renewal) and increase the number of basal cells within a clone. The data suggest that these 2 events occur in 16% of the cell division and are perfectly balanced (8% each) which guarantee the homeostasis of the tissue. In this case, the asymmetry is made at the level of the population (population asymmetry) and not at the level of the single cell (invariant asymmetry). The probabilities of cell fate outcomes are fixed but the model is called stochastic because the cell fate decision at each round of division cannot be predicted[100,101].

While this model suggested that the vast majority of basal cells are equipotent progenitors, it did not totally exclude the existence of small population of quiescent SC[100]. Indeed, using skin specific promoter such as *K14-CreER* and *Inv-CreER* crossed with *Rosa-YFP* mice, our lab demonstrated that different populations of basal progenitors could be labeled in the basal layer of the tail IFE during homeostasis[102,103]. After tamoxifen (TAM) induction, *Inv-CreER/Rosa-YFP* mice display clones having the same clonal distribution and dynamics as described by Clayton : 80% of asymmetrical division, 10% of self-renewal and 10% of symmetrical differentiation. Similarily to Clayton's data, 80% of the clones were lost after 3 months of tracing, whereas the remaining clones were expanding and highly heterogeneous in size[102]. By contrast, *K14-CreER/Rosa-YFP* targeted clones displayed a different dynamics. After 3 months, only 30% of the clones were lost and after one year at least 25% of the clones were still remaining contrasting with less than 10% of remaining clones in the *Inv-CreER* tracing. Further analysis of the clonal distributions showed that *K14-CreER* targeted cells were a mix of SC and committed progenitors (CP) and that *Inv-CreER* targeted cells were exclusively CPs[102]. These data suggest that IFE basal layer is heterogeneous and is not exclusively made of equipotent progenitors.

More recently, the entire clonal tracing was made a second time on independent cohorts of mice and taking into account the two compartments that follow distinct differentiation programs in the tail epidermis : the interscale (which surrounds HF triplets and is made of suprabasal cells expressing K10), and the scale (characterized by suprabasal cells expressing K31)[104-106]. This study revealed two different modes of tissue maintenance within the IFE tail epidermis during homeostasis[103] (Figure 8). In interscale regions, the previously described hierarchy of SC-CP was confirmed : SCs divide less frequently (once every 15 days) and, following a stochastic model of cell fate outcome, give rise to a SC and a CP in 94% of the case. In the remaining 6% of the cases SC either self-renew either is lost through differentiation, with equal probabilities. The CPs divide more frequently (once every 4 days) and undergo asymmetrical cell fate outcome in around 62% of the cases, or symmetrical cell fate outcomes in 38% of the cases that could lead either to CP loss or CP self-renewal. However, these two outcomes are not perfectly balanced and CPs are slightly biased toward symmetrical differentiation (21% over 17%), letting the space for new CP

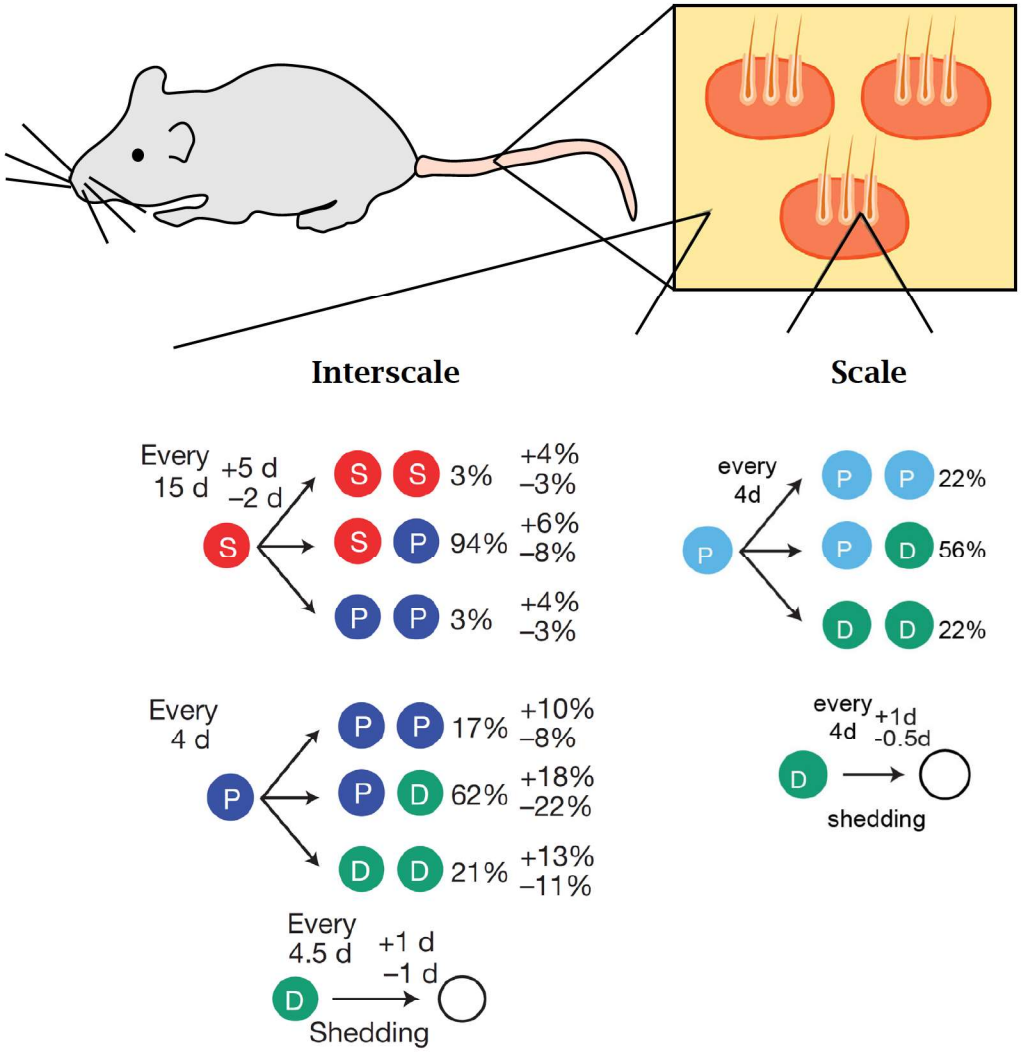

Figure 8. Current model of SC and CP dynamics in mouse tail epidermis during homeostasis. In interscale a hierarchy of SC and CP following a population asymmetry is observed. SCs (red) divide infrequently (once every 15days) and give rise to CP (blue) in 94% of the cases. SC also balance self-renewal (S+S, 3%) and symmetrical differentiation (P+P, 3%). CPs divide frequently (once every 4 days) and do asymmetrical division giving rise to differentiated cell (D, green) in 62% of the cases. CPs have a slight imbalance for symmetrical differentiation (D+D, 21%) over self-renewal divisions (P+P, 17%). In scale, an equipotent population of CPs divide frequently and undergo asymmetrical division in 56% of the cases while they perfectly balance their self-renewal division (P+P, 22%) and differentiation (D+D, 22%). In both interscale and scale, the equilibrium is maintained at the level of the population. Adapted from *Sanchez et al., Nature, 2016*. Scheme of scale-interscale pattern adapted from *Gonzales & Fuchs, Developmental Cell, 2017*.

coming from the SC pool (Figure 8). By contrast, scale regions are sustained by equipotent progenitors which undergo asymmetrical cell fate outcome in 56% of the cases and symmetrical cell fate outcome in 44% of the cases, CP loss and CP self-renewal being perfectly balanced[103]. The stochastic or population asymmetry model has been shown in several other epidermal areas such as paw[45,107] and ear epidermis[107,108] as well as in other squamous epithelia such as the oesophagus[109].

The stochastic model changed the perception that basal cells are intrinsically pre-programmed to undergo a limited number of division. To the contrary, this model implies that SCs and CPs can adapt their behavior to changing situations and opens the question of what are the molecular mechanisms that control cell fate decision and whether it is dictated by intrinsic or extrinsic factors. In homeostatic conditions, the majority of the divisions are asymmetrical and self-renewal and differentiation are balanced so the tissue does not grow but instead replaces the suprabasal cells that are shed off at the surface. By contrast, under expanding conditions such as postnatal growth or wound repair, the IFE surface must expand rapidly. How SCs and CPs adapt their proliferation and cell fate decision to achieve such expansion? Do the SC/CP increase their self-renewal decisions in order to rapidly increase the pool of SC/CP ? The mouse oesophagus is a squamous epithelia maintained through population asymmetry[109]. After a wound performed with microendoscopic biopsy, lineage tracing experiments showed clones expanding toward the damaged area after, suggesting that progenitors switch toward a regenerative behavior during tissue repair[109]. Moreover, recent *in vitro* experiments performed with human keratinocytes suggest that epidermal progenitors have the intrinsic capacity to switch between a “balanced” or “homeostatic” mode of division to an “expanding” mode of division[110]. Tracking keratinocytes division by live imaging, Roshan and colleagues showed that human epidermal cells displayed tree possible outcomes after cell division : symmetrical self-renewal (one dividing cell gives rise to two dividing cells), symmetrical differentiation (one dividing cell gives rise to two non-dividing cells) and asymmetrical division (one dividing cell gives rise to one dividing and one non dividing cell). In the center of the colony, a “balanced” or “homeostatic” mode of division is observed, characterized by an equal proportion of symmetrical self-renewal and differentiation. However, in the border of the colony

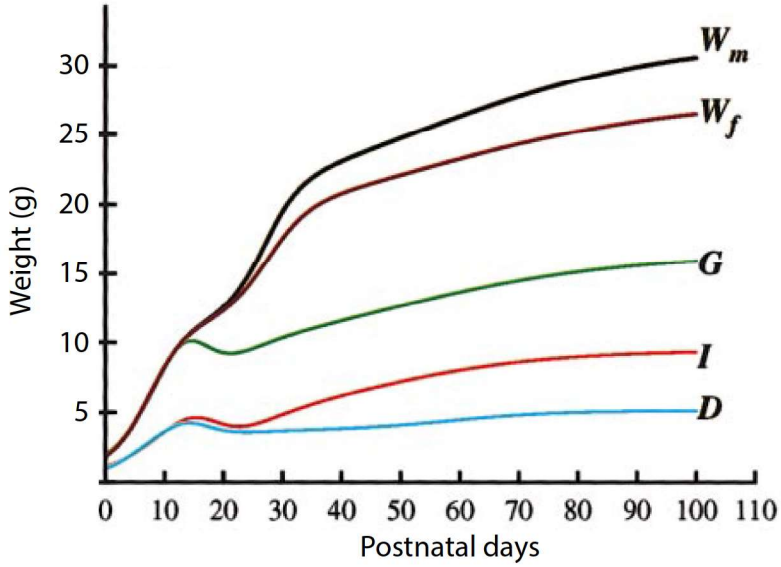

Figure 9. The mouse growth curve during post-natal development and the impact of Growth Hormone and Insulin-like Growth Factor 1 deficiency. Average growth curve of males (W_m) and females (W_f) wild type C57BL/6J animals and of mutants lacking GHR (*G*), IGF1 (*I*) or both (*D*). Adapted from *Lupu et al., Developmental Biology, 2001*.

or after a scratch wound assay, keratinocytes switch to an “expanding” mode of division, where the probability of self-renewal division is increased compared to the probability of symmetrical differentiation, creating an imbalance[110]. Whether this switch from “homeostatic” to “expanding” mode of division also happens *in vivo* is currently unknown.

2.4 THE POST-NATAL DEVELOPMENT

The process of growth in a living organism implies the size increase of the tissues through an excess of proliferation over apoptosis, or a change in cell size. In mammals, the growth starts during embryonic development and continues during post-natal life until a steady state is reached at the adulthood. It is also accompanied with a increase in the body mass. In mice postnatal growth follows an almost linear growth from birth (+/- 1g) to around 5 weeks of age (+/- 30 g) (Figure 9). Body growth is controlled by tissue specific growth factors and circulating hormones. Among them, the Growth Hormone (GH)-Insulin-like Growth factors (IGFs) axis is the most important as demonstrated by numerous mutations affecting this signaling pathway and leading to different form of dwarfism in mice and human[111]. GH is a ligand secreted by the pituitary gland in a pulsatile manner and act through the GH receptor (GHR). This interaction is further modulated by other GH-binding proteins (GHBPs). As other hormones, the production of GH decline gradually after puberty. GH stimulates the production of IGF ligands (IGF1 and IGF2), mainly produced by the liver. IGFs bind to their receptor (IGFR, type I and II) and can also be modulated by IGF binding proteins (IGFBPs) and IGFBP proteases[112]. In peripheral tissues, GH and IGFs binding to their receptors trigger the activation of several intracellular pathway implicated in proliferation or apoptosis. GH and IGFs are both important for post-natal growth as demonstrated with mouse lines harboring *Ghr* or *Igf1* or both null mutations and displaying a reduced weight and size (Figure 9)[113,114]. GH-IGF axis also plays a major role in skin development and keratinocytes proliferation[112]. Mice overexpressing Igf1 in K5+ basal cells exhibit increased proliferation, epidermal hyperplasia and develop spontaneous papillomas[115]. Human suffering from an excess of GH harbor a thicker dermis and elevated amount of IGFs have been associated with Psoriasis while GH-deficient patients harbor a thinner epidermis[112]. Fibroblasts are the major source of IGFs and keratinocytes express GHR and IGFR[112].

2.5 THE WOUND REPAIR

For this section, I would refer the readers to a recent Perspective I wrote with Cédric Blanpain, published in Nature Cell Biology (see here after).

PERSPECTIVE | FOCUS
https://doi.org/10.1038/s41556-018-0237-6
nature cell biology

Stem cell dynamics, migration and plasticity during wound healing

Sophie Dekoninck[1] and Cédric Blanpain[1,2]*

Tissue repair is critical for animal survival. The skin epidermis is particularly exposed to injuries, which necessitates rapid repair. The coordinated action of distinct epidermal stem cells recruited from various skin regions together with other cell types, including fibroblasts and immune cells, is required to ensure efficient and harmonious wound healing. A complex cross-talk ensures the activation, migration and plasticity of these cells during tissue repair.

The skin is the first barrier protecting animals against UV radiation and pathogens from the external environment. It is composed of an epithelial layer, the epidermis, and the underlying dermis, which are separated by a basement membrane[1]. The epidermis contains pilosebaceous units that include a hair follicle and sebaceous glands, and are connected with the interfollicular epidermis (IFE) through the infundibulum[1]. The skin epidermis also contains other appendages, such as sweat glands, which regulate body temperature through perspiration[1]. The dermis is composed of an upper (papillary) and a lower (reticular) layer of fibroblasts, blood vessels, immune cells and extracellular matrix (ECM)[2,3]. Specialized fibroblasts form the dermal papilla, which regulates hair follicle growth and the erector pili muscle, responsible for pilo-erection. Partially integrated into the reticular dermis is a layer of dermal adipocytes that form the dermal white adipose tissue[4]. Underneath the dermis, the hypodermis (or subcutaneous adipose tissue) is composed of adipocytes, blood vessels and inflammatory cells[4]. This layer is important for thermoregulation and mechanical protection[2,4] (Fig. 1a).

Upon tissue damage, the skin has to be repaired as quickly as possible to prevent excessive blood loss and infection. Wound healing occurs through distinct overlapping phases: haemostasis, inflammation, proliferation and remodelling[5]. Haemostasis occurs immediately after tissue damage and results in the formation of a blood clot, which stops the haemorrhage and triggers the recruitment of different immune cells, including neutrophils, macrophages and lymphocytes, to prevent infection and further activate the inflammatory response[5,6] (Fig. 1b). The proliferation phase coordinates epidermal re-epithelialization and dermal repair[5] (Fig. 1c). The remodelling phase removes cells that are no longer necessary and induces ECM remodelling[6]. In small excisional wounds (<1 cm in diameter in mice), hair follicles are not reformed and dermal scar tissue compensates for skin loss[7] (Fig. 1d). However, in large wounds (>1 cm in diameter), regeneration of hair follicles (wound-induced hair follicle neogenesis (WIHN)) can be observed after re-epithelialization during the remodelling phase, resembling hair follicle embryonic development and a regeneration phase, typically 13–14 days after injury in mice[7,8] (Fig. 1d).

Although the key steps of wound healing are well described at the tissue level, a more in-depth characterization of the behaviour of individual cells at the clonal level and their fate transitions has only yet begun. The emergence of lineage tracing and intravital microscopy, coupled with transcriptional and epigenetic profiling, provide important insights about cellular and molecular mechanisms responsible for wound healing[9–12]. In this Perspective, we describe recent advances with an emphasis on skin epithelial stem cell populations, their heterogeneity, clonal dynamics and remarkable plasticity during wound healing. Finally, we discuss the role of fibroblast populations and immune cells during repair and regeneration.

Skin epithelial stem cells during homeostasis

The skin epithelium renews throughout life in a continuous turnover ensured by stem and progenitor cells that balance proliferation and differentiation to replace dead and terminally differentiated cells[1,13,14]. Epithelial stem cells reside in a specific microenvironment called the niche that is composed of various cell types. Niche cells influence stem cell behaviour directly by cell contact or indirectly via ECM components and growth factors[15]. Although skin stem cells are able to regenerate the entire repertoire of skin epithelial lineages upon transplantation, lineage tracing has demonstrated that, during physiological conditions, epidermal compartments are sustained by their own pool of resident stem cells[14–16] (Fig. 2a).

During adult homeostasis, hair follicles undergo cycles of growth (anagen) and degeneration (catagen), followed by a resting stage (telogen)[1]. The hair follicle stem cells (HFSCs) responsible for cyclic regeneration are located in the permanent non-cyclic follicle portion called the bulge[17–20]. HFSCs were first identified based on their slow-cycling properties[19,21,22]. They have higher clonogenicity in vitro and give rise to IFE, hair follicle and sebaceous gland lineages upon transplantation[17,18,20,23,24]. Slow-cycling HFSCs were first isolated and characterized using *K5-tTA/TRE-H2BGFP* and *Krt15-EGFP* transgenic mice[25,26], and several studies revealed the expression of bulge specific markers, such as *Cd34* (refs [18,23]), *Krt15* (refs [27,28]), *Krt19* (ref. [29]), *Lgr5* (ref. [30]), *Sox9* (refs [31,32]) and *Tcf3* (ref. [33]). In sharp contrast to transplantation experiments, lineage tracing using *Krt15-CrePR*[34], *Shh-Cre*[35], *Lgr5-CreER*[30], *K19-CreER*[29], *Sox9-Cre*[32] and *Tcf3-CreER*[33] mouse strains established that HFSCs only contribute to hair follicle regeneration during physiological conditions and do not maintain the sebaceous gland, infundibulum or IFE (Fig. 2a).

The IFE is composed of a single layer of proliferative basal cells and several layers of differentiated non-proliferative cells[1]. Basal cells replenish the suprabasal cells that are lost as terminally differentiated squames. In mice, it takes about 1 week for a basal cell to transit to the surface of the skin and about 1 month to replenish the whole IFE[36]. Early proliferation kinetic experiments reported maintenance of the IFE by small proliferative units that contain stem cells and progenitors[37]. However, lineage tracing at clonal density later demonstrated that these units do not have a fixed size or predictable proliferation kinetics[38,39]. Instead, several studies, showed that IFE homeostasis was sustained by a single population of committed progenitors that balance renewal and differentiation in a stochastic manner[38,40–43]. However, further studies provided evidence that

[1]Laboratory of Stem Cells and Cancer, Université Libre de Bruxelles, Brussels, Belgium. [2]WELBIO, Université Libre de Bruxelles, Brussels, Belgium.
*e-mail: Cedric.blanpain@ulb.ac.be

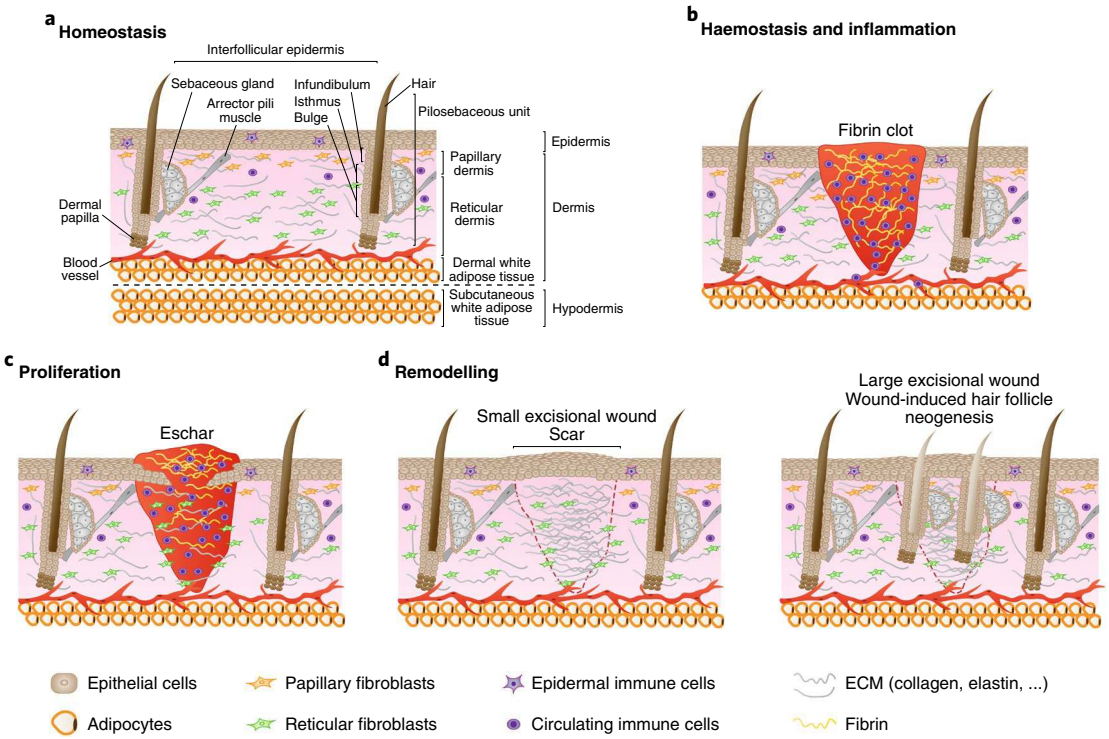

Fig. 1 | Overview of skin homeostasis and wound-healing phases. a, The skin is composed of the dermis and the epidermis. In the epidermis, epithelial cells are organized into a pilosebaceous unit (the hair follicle and its associated sebaceous glands) and the surrounding tissue (the IFE). The dermis consists of a papillary and a reticular layer located in the upper and lower part, respectively. Dermal papilla controls the hair follicle cycle and the arrector pili muscle ensures its movement. The dermis includes fibroblasts, blood vessels, immune cells, sensory nerves and, in its lower portion, the dermal white adipose tissue, which contains adipocytes. Below the skin lies the hypodermis or subcutaneous white adipose tissue. **b**, Haemostasis and inflammation start immediately after wounding. The fibrin clot prevents further blood loss and provides a scaffold for the migration of immune, dermal and epidermal cells. **c**, During the proliferation phase, keratinocytes, fibroblasts and endothelial cells proliferate and migrate to the wound site and reform the ECM. **d**, During the remodelling phase, the collagen in the dermis is remodelled and cells from earlier stages are removed. In small excisional wounds in mice, hair follicles are not regenerated and dermal scar tissue compensates for skin loss (left panel). In large excisional injuries, WIHN can be observed after complete re-epithelialization (right panel).

basal epidermal cells are heterogeneous and some cells, depending on the skin regions, exhibit stem cell characteristics[44,45]. These IFE stem cells (IFESCs) were more quiescent, persisted longer and could give rise to more rapidly cycling committed progenitors with a shorter lifespan[44,45] (Fig. 2a). Profiling of murine stem and progenitor cells showed that the two populations are molecularly different and that stem cells express a higher level of basal integrins, as do human epidermal stem cells, whereas committed progenitors are primed towards differentiation[44,46].

The isthmus, a region located between the bulge and sebaceous gland, contains its own pool of resident stem cells that express *Blimp1* (ref. [47]), *Lgr6* (ref. [48]), *Lrig1* (ref. [49]), *Gata6* (ref. [50]) or *Plet1* (ref. [51]). These multipotent cells give rise to all epidermal lineages upon transplantation[48–50,52]. Lineage tracing using *Blimp1-Cre*[47], *Lgr6-CreER*[48,53] and *Lrig1-CreER*[54] has confirmed that these cells maintain the isthmus and sebaceous gland during homeostasis (Fig. 2a). In addition, *Lrig1*-expressing cells also give rise to cells of the infundibulum[54] (Fig. 2a), whereas *Gata6*-expressing stem cells only contribute to the maintenance of the sebaceous gland ducts but not the gland itself during homeostasis[50] (Fig. 2a). Altogether, these data show that, during physiological conditions, skin stem cells are confined to restricted compartments. Presently, the molecular mechanisms that restrain the movement of these cells across different territories remain unclear. As in the intestine[55], cell-specific expression of different guidance molecules might confine cell types in specific territories.

Skin epithelial stem cells during wound healing

During wound healing, stem cells are activated and recruited from different skin regions. Interestingly, lineage restriction and spatial confinement of resident skin stem cells are transiently lost during repair, allowing contribution of multiple epidermal stem cells[15,34,54,56,57] (Fig. 2b).

The involvement of HFSCs in wound healing was already proposed 40 years ago after dermabrasion experiments in mice[58] and further confirmed by more-recent analyses of proliferation kinetics[22]. Lineage tracing targeting labelled retaining cells[26] or using *Krt15-CrePR*[34], *Shh-Cre*[57], *K19-CreER*[54] and *Lgr5-CreER*[54] reporter strains showed that HFSCs rapidly migrate from the bulge to the wound and contribute to epidermal repair (Fig. 2b). These data demonstrate that HFSCs are highly plastic during wound healing, similarly to their expanded fate potential upon transplantation[17,20,30,49,52].

Clonal analysis of IFESCs and committed progenitor cells following injury of mouse tail skin showed that IFESCs are recruited to the wound, contribute to epidermal repair and persist up to 35 days[44] (Fig. 2b). By contrast, committed progenitors are initially recruited, but their progeny do not remain in the wound long term[44]. Additional lineage tracing with *Dlx1-CreER* and *Slc1a3-CreER* reporters, which mark slow-cycling and rapidly cycling stem cells from different microdomains of tail and back skin IFE, demonstrated that, upon wounding, both stem cell populations repopulate the two IFE regions[59]. However, in the long term, both cell populations only persist in their region of origin and not in the region that

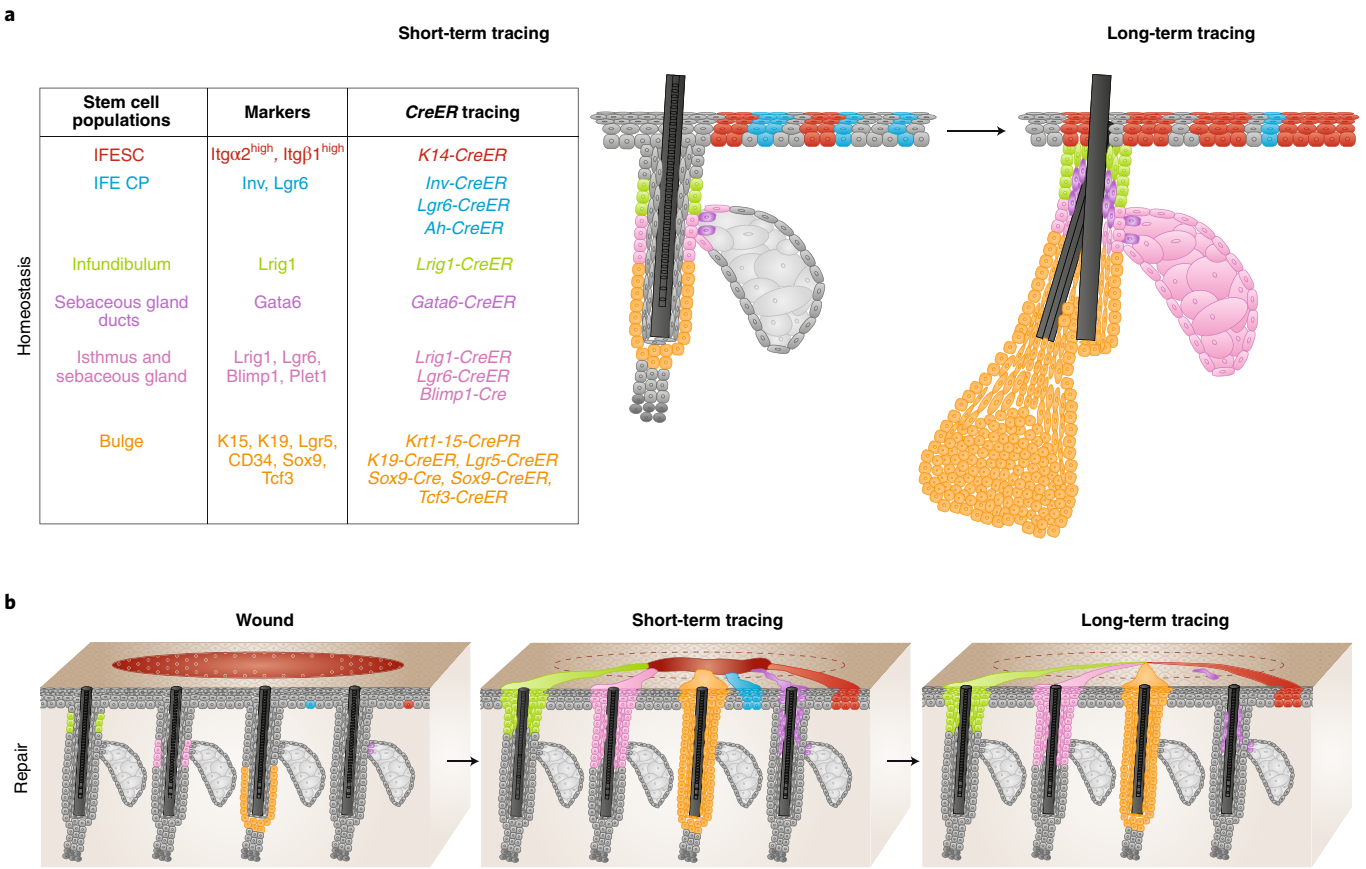

Fig. 2 | Skin epithelial stem cell populations during homeostasis and repair. a, Skin epithelial stem cells express specific markers and can be lineage traced with *CreER* mouse strains (left table). IFESCs and committed progenitors are located in the basal layer of the IFE and give rise to suprabasal, differentiated cells. Stem cells and committed progenitors can be traced using *K14-CreER* or *Inv-CreER* mouse strains induced at low dose, respectively. IFE committed progenitors (CPs) also express *Lgr6*. Infundibulum stem cells are located in the upper part of the isthmus and express *Lrig1*. A population of sebaceous gland duct stem cells expressing *Gata6* are located at the entrance of the gland but only maintains the junctional zone. Isthmus and sebaceous gland stem cells are basal cells located at the junction between the hair follicle and the gland, express *Lrig1*, *Lgr6* and *Blimp1* and give rise to the entire sebaceous gland and the isthmus. Bulge stem cells are located in the permanent lowest portion of the hair follicle, express *K15*, *K19*, *Lgr5*, *Cd34*, *Sox9* and *Tcf3* and give rise to the entire hair follicle. **b**, Upon wounding, both IFESCs and committed progenitors are recruited and contribute to tissue repair. Only IFESCs will reside in the newly formed IFE long term. Isthmus, sebaceous gland and infundibulum stem cells are recruited, contribute to IFE repair and remain long term. Bulge stem cells are recruited to the IFE and a small proportion can remain long term as IFESCs. *Gata6*-expressing sebaceous gland duct stem cells are recruited to the IFE, migrate suprabasally, dedifferentiate and are re-established as IFESCs in the long term.

they migrate to during wound healing[59]. These observations suggest that, during repair, all basal cells present some degree of plasticity, a change in behaviour and functional contribution, but the wound does not reset the clock completely and cells keep a memory of their original location and hierarchy.

Similarly to HFSCs, *Lrig1*-expressing and *Lgr6*-expressing stem cells from the upper isthmus are mobilized following wounding and are possibly activated even more rapidly than HFSCs[54]. HFSCs have been assumed to be quickly lost during regeneration and to only serve as a transient bandage that allows other stem cells from the IFE and upper isthmus/infundibulum to sustain long-term repair[34]. However, a more recent study showed that the proportion of hair follicle and Lrig1-derived cells located in the epidermis drops dramatically 3 weeks after an injury, whereas remaining cells can persist up to 1 year thereafter[54] (Fig. 2b). The persistence of these cells in the re-epithelialized IFE is proportional to the amount of stem cells labelled in the beginning and suggests a stochastic competition between equipotent stem cells rather than a hard-wired process[54]. Importantly, glabrous skin, such as the ventral (or palmar) part of the paw, heals correctly with slower kinetics than human skin, showing that HFSCs are dispensable for wound healing[60]. Moreover, similar to the contributions of hair follicles and the infundibulum in skin with hair, sweat gland duct progenitors help to regenerate the injured epidermis in mouse paws[61]. Altogether, these studies suggest that the vacant niche created by an injury activates a broad range of stem cells to assume characteristics that differ from their homeostatic roles. Additional studies will be required to better understand the signals that activate distant stem cells, respective timelines and the mechanisms that disrupt and re-establish the boundaries between skin compartments. It further remains unclear how differentiation programmes get rewired during wound healing and how the balance between proliferation, migration and differentiation is achieved.

Migration, proliferation and compartmentalization. Epidermal injury is typically followed by increased keratinocyte proliferation[5]. Interestingly, proliferation is not observed at the wound edge but rather at a distance of 0.5–1.5 mm away from the edge[9,10,62], in a proliferative zone that surrounds the wound. At the leading edge, keratinocytes do not proliferate but migrate as a cellular sheet[9,10] (Fig. 3).

Intravital microscopy during wound healing demonstrated that both basal and suprabasal layers migrate during wound healing[10].

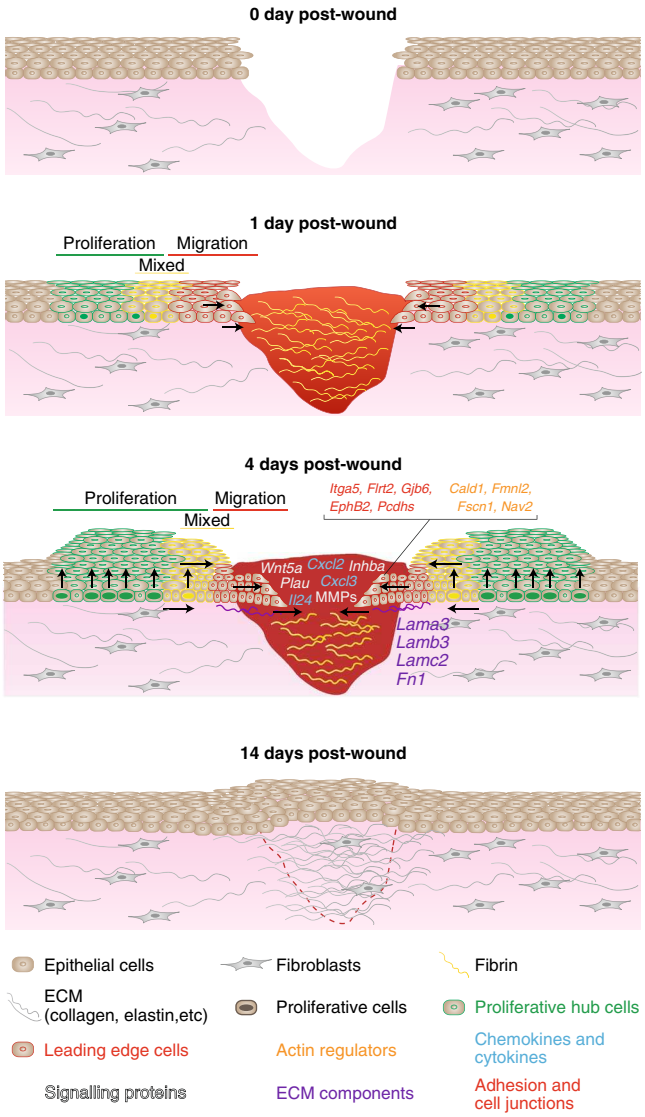

Fig. 3 | Epidermal migration, proliferation and compartmentalization during wound healing. Epithelial cells start to migrate into the wound bed within 12 hours after injury. The day after wounding, IFE cells located close to the wound show an elongated shape towards the direction of the wound (horizontal arrows) and are quiescent, whereas cells located at a distance start to proliferate, which leads to the establishment of a proliferative and a migrating leading edge compartment. Between these two zones, a mixed region is observed containing both migrating and proliferative cells. Four days after wounding, leading edge cells are compressed and upregulate the expression of specific genes that promote inflammation and regeneration. This gene signature is transient and disappears when the IFE is healed. Vertical arrows represent the movement of basal cells toward the differentiated layers. MMPs, matrix metalloproteinases.

The speed of migration is greatest closer to the leading edge and decreases thereafter[10]. At a distance of 0.5 mm from the edge, both migration and proliferation co-occur[10]. In this mixed region, basal cells are elongated towards the wound and orient their division in this direction[10]. In the tail epidermis, cells present at the leading edge are initially elongated parallel to the direction of the wound, suggesting active migration, but assume a perpendicular orientation 2–4 days after wounding, possibly because they are pushed and compressed by cells behind[9]. Whether proliferation is necessary for cell migration remains unclear. Pharmacological inhibition of cell proliferation prevents wound closure and cell compression at the leading edge in tail skin[9]. By contrast, proliferation is dispensable for wound closure in the mouse ear epidermis[10]. However, cells also display a more elongated shape in wounds with inhibited proliferation, suggesting a compensatory effect[10]. Differences in wound size and region-specific dermal populations could explain the discrepancies observed between the ear and tail IFE. However, in Rac1-knockout mice with perturbed cell migration and elongation, a defect in the orientation of cell division is evident, suggesting its control by migration of the leading edge[10]. Altogether, these observations imply that cell migration at the leading edge comes first after wounding and that the displacement of cells in this region triggers orientated cell division of the cells following behind. Increased proliferation can itself generate a surplus of migrating cells that later push the leading edge towards the wound centre.

Transcriptional profiling of cells from migration and proliferation zones indicated two molecularly distinct and transient regions[9]. Cells at the leading edge expressed transiently higher levels of matrix metalloproteinases, pro-inflammatory molecules, genes controlling the cytoskeleton, microtubule and actin remodelling, ECM ligands and cell-adhesion molecules, such as integrin α_5 (ref. [9]) (Fig. 3). The constant size of the leading edge and its independence of wound size or skin area suggest that the signals controlling marker expression are local and potentially propagated from cell to cell within the epidermis. The leading edge might act as a transient scaffold enabling harmonious wound healing. By secreting a higher level of proteins that control ECM remodelling and blood clot dissolution, the leading edge might promote the progression of tissue regeneration towards the wound centre and protect stem cells and their progeny from tissue remodelling.

In addition, the acquired migratory phenotype of keratinocytes displays some features of epithelial-to-mesenchymal transition, including downregulation of cell-adhesion molecules, increased motility and upregulation of epithelial-to-mesenchymal transition markers, such as Slug[63,64]. Whether epithelial-to-mesenchymal transition is required for efficient wound healing or leading edge migration will require further analysis.

Stem cell population dynamics. During homeostasis, IFESCs and committed progenitors divide asymmetrically at the population level to maintain a constant number of epidermal cells[65]. However, during wound healing, cell numbers need to increase to compensate for lost cells until re-epithelialization is completed. Excess of renewal over differentiation can be achieved by increasing symmetric renewal or decreasing the proportion of cells that undergo differentiation, as during oesophageal wound repair[66] or in vitro culture of keratinocytes[67]. Upon tail injury, clonal analysis of *K14-CreER* (IFESCs and progenitors) and *Lrig1-CreER* (infundibulum stem cells) mouse strains demonstrated streaks of labelled cells arising from single IFE or infundibulum cells, both basal and suprabasal, that project towards the wound centre[9]. IFE-derived clones decreased by more than 90% during the first week, due to rapid terminal differentiation of committed progenitors, but overall cell ratios demonstrated that committed progenitors continued to divide mostly asymmetrically at the population level[9]. The proportion of basal and suprabasal cells from *Lrig1-CreER*-derived clones was similar to IFE-derived clones, although the size of the infundibulum-derived clones was slightly bigger[9]. Clonal persistence, clone size and the basal/suprabasal cell ratio were consistent with a hierarchical model in which rare stem cells reside at the top of the hierarchy, dividing asymmetrically at a much more rapid pace than homeostasis and give rise to progenitors, so that the equilibrium between proliferation and differentiation remains balanced. Irrespective of their initial locations, wounding seems to induce the activation of a minor stem cell population, whereas lineage hierarchy and balance between self-renewal and differentiation of committed progenitors remain unchanged from homeostasis[9].

Recently, clonal analysis of the human skin epidermis was performed after grafting in vitro reconstructed, genetically engineered skin into a patient with a severe form of the genetic skin disorder epidermolysis bullosa[68]. Sequencing of the integration site of the retrovirus used to replace the mutated gene revealed that viral integration in keratinocyte colonies originating from progenitors rapidly decreased over time[68]. By contrast, the integration sites of the most clonogenic colonies derived from stem cells increased, supporting the notion that only human skin stem cell-derived colonies are able to renew and expand long term in vivo, whereas progenitor cells possess limited potential to self-renew and revert back into a stem cell-like state[68].

Stem cell plasticity. When stem cells from the hair follicle and infundibulum are recruited to the IFE upon injury, they progressively lose their initial identity and are reprogrammed to an IFE fate[34]. The molecular mechanisms responsible for this plasticity are still incompletely understood. In a comparison of chromatin landscapes of injured IFE and homeostatic HFSCs and IFESCs, the wounded IFE exhibited a hybrid signature between HFSCs and IFESCs, in which the open chromatin regions were enriched for both IFESC (Klf5) and HFSC (Sox9) transcription factors[12]. This hybrid stage called 'lineage infidelity' seems to ensure proper re-establishment of the epidermal barrier[12]. Although this hybrid state is transient during repair, it persists in skin cancer[12,69].

Differentiated suprabasal epidermal cells are able to revert back to a stem cell state upon wounding[70,71], a phenomenon also observed in airway epithelium after lineage ablation of basal stem cells[72]. However, lineage tracing and photolabelling of suprabasal IFE cells demonstrated that these cells cannot adopt a basal state again under wound-healing conditions[9,10]. Contrastingly, a population of *Gata6*-expressing cells residing in the isthmus, which during homeostatic conditions give rise to the sebaceous duct, can be mobilized during wound healing to migrate towards the injured IFE and revert from a differentiated to a basal stem cell fate[50]. This reversion does not occur immediately after injury, as the suprabasal cells require a few days to access the basal layer and undergo stem cell reprogramming[50]. This intriguing observation raises the question of whether other differentiated epidermal cells are also able to revert back to a stem cell state or whether this is a unique property of the *Gata6*-expressing population. It is possible that the timing of reversion is important and that experiments performed on the tail and ear epidermis induced the labelling of the suprabasal cells too early to observe the reversion[9,10]. Further experiments will be necessary to identify the mechanisms underlying this cellular plasticity and reprogramming of differentiated cells during wound healing. Other cases of dedifferentiation have been previously described in the hair follicle[73,74]. After depilation or laser ablation to induce the loss of bulge HFSCs, hair germ cells[73] and infundibulum or sebaceous gland cells[74] are able to repopulate the stem cell niche and establish functional HFSCs. Similarly to skin, cells in the gut epithelium that are committed to terminal differentiation can revert back to a progenitor-like state and contribute to tissue repair following injury[75–77]. However, intestinal stem cells are required to ensure tissue repair following ionizing radiation[78], demonstrating that, despite the ability of committed cells to re-assume stemness, regular tissue-resident stem cells are essential for repair.

The degree of damage can also influence cellular plasticity. In relatively small wounds, re-epithelialization occurs without reforming hair follicles, whereas de novo hair follicle formation is apparent in large wounds[8]. Lineage tracing confirmed that these de novo hair follicles do not originate from HFSCs but from IFE cells[8]. Analogous to hair follicle morphogenesis during embryonic development[79–81], WIHN depends on Wnt signalling, as overexpression of Dickkopf Wnt signalling pathway inhibitor 1 or β-catenin deletion in IFE basal cells prevents de novo hair follicle regeneration[8]. Epidermal deletion of *Wntless*, a gene required for the secretion of Wnt ligands, suppresses WIHN, suggesting that keratinocyte-derived Wnt is essential[82]. Different mouse strains have different susceptibilities to WIHN[83,84]. Toll-like receptor 3 (Tlr3) levels are increased in mouse strains with enhanced WIHN, and double-stranded RNA is a key signal that triggers skin regeneration through Tlr3 (ref. [84]). Msh homeobox 2 is also crucial for WIHN[85]. Fibroblast growth factor 9, secreted by γδ T cells, triggers Wnt expression by wound-induced fibroblasts, further amplifying the Wnt signal required for WIHN. These data illustrate the importance of a crosstalk between immune cells, fibroblasts and keratinocytes to enable successful WIHN[86].

Plasticity upon wound healing is also observed in other skin lineages. In the dermis, myofibroblasts, located close to de novo-formed hair follicles, are converted into adipocytes in large wounds[87]. This cell-fate conversion depends on bone morphogenetic protein signalling originating from newly formed hair follicles that activate the expression of Zfp423, a transcription factor that regulates adipocyte development[87]. Cell plasticity has also been described in other epithelia, such as the mammary gland, lung and intestinal epithelium[88]. It will be important to define whether generic mechanisms conserved across different tissues and species control cellular plasticity after lineage ablation and during tissue repair, inflammation or tumorigenesis.

Crosstalk between stem cells and the niche. During wound repair, fibroblasts are responsible for ECM synthesis in the dermis and for the fibrotic response leading to scar formation[5]. However, during embryonic development and in certain body locations, such as the oral cavity, wounds heal without forming scars[89]. The dermis of the mouse back skin is composed of fibroblasts of different developmental origin[90,91]. At least two fibroblastic lineages give rise to the upper (papillary fibroblasts, dermal papillae and erector pili muscle) and lower (reticular fibroblasts, preadipocytes and hypodermal adipocytes) dermis, respectively[90]. Upon wounding, fibroblasts of the lower dermis are recruited first, followed by fibroblasts of the upper dermis[90] (Fig. 1). Reticular fibroblasts secrete the collagens responsible for scar tissue formation and are unable to regenerate the hair follicle after transplantation[90]. This observation may potentially explain why de novo hair follicle formation rarely occurs during wound healing. The upper papillary dermis is the only fibroblast lineage competent to regenerate hair follicles after transplantation, but it is recruited late during repair[90]. Interestingly, activation of Wnt–β-catenin signalling in epidermal cells increases the recruitment of papillary fibroblasts and also the number of hair follicles regenerated in the wound bed[90]. By sharp contrast, inhibition of β-catenin in fibroblasts promotes hair follicle regeneration during wound healing and correlates with a decrease in the number of reticular fibroblasts and an increase in the number of papillary fibroblasts[92]. In addition to different locations, two distinct fibroblastic lineages can also be identified on the basis of the embryonic expression of Engrailed-1 (*En-1*)[91]. The En-1-positive lineage of fibroblasts produces ECM composed of collagen type I and type III, becomes more abundant postnatally and is responsible for fibrotic scarring after injury[91]. By contrast, the En-1-negative lineage becomes less abundant after birth but has a higher regenerative capacity and their dominance during embryonic development might explain why embryos are able to regenerate scarless skin[91,93]. Of note, the preferential location of En-1-positive lineage fibroblasts in the reticular dermis after birth suggests that they encompass the reticular populations previously described[90,91]. Altogether, these data support the importance of surrounding dermal fibroblasts in skin regeneration.

A crosstalk between epidermal and immune cells also plays a major role during wound healing. Interestingly, after epidermal stem cells have been challenged with an inflammatory stimulus, the skin retains a memory of past inflammation and heals faster upon wounding. This memory is associated with chromatin remodelling

that primes stem cells to respond more rapidly upon injury, in particular, by promoting cell migration, which is partly mediated by the AIM2 inflammasome[11]. This remarkable observation is reminiscent of an 'alert state', as described in muscle stem cells, in which stem cells contralateral to the injured muscle undergo accelerated cell cycle entry upon tissue damage[94]. By contrast, ageing is associated with a defect in wound healing, linked to a decrease in epidermal migration and impaired signalling between epidermal and dendritic epidermal T cells[95]. Aged epidermal cells demonstrate a defect in signal transducer and activator of transcription 3 (Stat3) activation following wounding, which in turn prevents the activation of *SKINTS* genes that encode immunoglobulins and activate dendritic epidermal T cells in the wound bed[95].

Upon wounding, skin stem cell populations are also activated by activin A, which is overexpressed in the dermis and the epidermis[9,96]. Overexpression of activin A enhances wound healing[96,97], promotes keratinocyte migration and the formation of granulation tissue by dermal cells[98,99]. Moreover, activin A recruits Foxp3-expressing regulatory T cells, which further supports accelerated healing[97]. These data illustrate the importance of the crosstalk between immune cells, dermal cells and keratinocytes during wound healing[97].

Conclusions and outlook

Taken together, this body of work provides previously unappreciated insights into the cellular and molecular mechanisms regulating wound healing and the importance of a crosstalk between different skin cell populations. However, many open questions remain regarding the signals that stimulate stem cells to migrate to the wound centre. We also know little about the control of skin compartmentalization during homeostasis and repair. How rapidly after wounding are these boundaries re-established? Mechanistically, it will be interesting to further elucidate how cells move between and within basal and suprabasal layers and learn more about the role of the leading edge. Factors controlling chromatin remodelling and lineage infidelity in chronic wounds and cancer also remain to be discovered.

Lineage ablation experiments at the leading edge should aid in defining the role and function of involved compartments during wound repair. Moreover, single-cell RNA sequencing and ATAC (assay for transposase accessible chromatin with high-throughput) sequencing of stem cell populations isolated during different regeneration stages should provide insights into the chromatin and transcriptional landscape associated with cellular heterogeneity. These studies might also elucidate further mechanisms that mediate the reprogramming of cells from the hair follicle and infundibulum as they are recruited to the IFE. Finally, understanding the role of the niche in the reprogramming of differentiated cells towards a stem cell fate will be an important challenge for the future.

Received: 24 July 2018; Accepted: 24 October 2018;
Published online: 2 January 2019

References

1. Blanpain, C. & Fuchs, E. Epidermal stem cells of the skin. *Annu. Rev. Cell Dev. Biol.* **22**, 339–373 (2006).
2. Hsu, Y. C., Li, L. & Fuchs, E. Emerging interactions between skin stem cells and their niches. *Nat. Med.* **20**, 847–856 (2014).
3. Lynch, M. D. & Watt, F. M. Fibroblast heterogeneity: implications for human disease. *J. Clin. Invest.* **128**, 26–35 (2018).
4. Driskell, R. R., Jahoda, C. A., Chuong, C. M., Watt, F. M. & Horsley, V. Defining dermal adipose tissue. *Exp. Dermatol.* **23**, 629–631 (2014).
5. Sun, B. K., Siprashvili, Z. & Khavari, P. A. Advances in skin grafting and treatment of cutaneous wounds. *Science* **346**, 941–945 (2014).
6. Gurtner, G. C., Werner, S., Barrandon, Y. & Longaker, M. T. Wound repair and regeneration. *Nature* **453**, 314–321 (2008).
7. Wang, X. et al. Principles and mechanisms of regeneration in the mouse model for wound-induced hair follicle neogenesis. *Regeneration (Oxf.)* **2**, 169–181 (2015).
8. Ito, M. et al. Wnt-dependent de novo hair follicle regeneration in adult mouse skin after wounding. *Nature* **447**, 316–320 (2007).
9. Aragona, M. et al. Defining stem cell dynamics and migration during wound healing in mouse skin epidermis. *Nat. Commun.* **8**, 14684 (2017).
10. Park, S. et al. Tissue-scale coordination of cellular behaviour promotes epidermal wound repair in live mice. *Nat. Cell Biol.* **19**, 155–163 (2017).
11. Naik, S. et al. Inflammatory memory sensitizes skin epithelial stem cells to tissue damage. *Nature* **550**, 475–480 (2017).
12. Ge, Y. et al. Stem cell lineage infidelity drives wound repair and cancer. *Cell* **169**, 636–650.e14 (2017).
13. Blanpain, C. & Fuchs, E. Epidermal homeostasis: a balancing act of stem cells in the skin. *Nat. Rev. Mol. Cell Biol.* **10**, 207–217 (2009).
14. Belokhvostova, D. et al. Homeostasis, regeneration and tumour formation in the mammalian epidermis. *Int. J. Dev. Biol.* **62**, 571–582 (2018).
15. Gonzales, K. A. U. & Fuchs, E. Skin and its regenerative powers: an alliance between stem cells and their niche. *Dev. Cell* **43**, 387–401 (2017).
16. Kretzschmar, K. & Watt, F. M. Markers of epidermal stem cell subpopulations in adult mammalian skin. *Cold Spring Harb. Perspect. Med.* **4**, a013631 (2014).
17. Rochat, A., Kobayashi, K. & Barrandon, Y. Location of stem cells of human hair follicles by clonal analysis. *Cell* **76**, 1063–1073 (1994).
18. Blanpain, C., Lowry, W. E., Geoghegan, A., Polak, L. & Fuchs, E. Self-renewal, multipotency, and the existence of two cell populations within an epithelial stem cell niche. *Cell* **118**, 635–648 (2004).
19. Cotsarelis, G., Sun, T. T. & Lavker, R. M. Label-retaining cells reside in the bulge area of pilosebaceous unit: implications for follicular stem cells, hair cycle, and skin carcinogenesis. *Cell* **61**, 1329–1337 (1990).
20. Oshima, H., Rochat, A., Kedzia, C., Kobayashi, K. & Barrandon, Y. Morphogenesis and renewal of hair follicles from adult multipotent stem cells. *Cell* **104**, 233–245 (2001).
21. Braun, K. M. et al. Manipulation of stem cell proliferation and lineage commitment: visualisation of label-retaining cells in wholemounts of mouse epidermis. *Development* **130**, 5241–5255 (2003).
22. Taylor, G., Lehrer, M. S., Jensen, P. J., Sun, T. T. & Lavker, R. M. Involvement of follicular stem cells in forming not only the follicle but also the epidermis. *Cell* **102**, 451–461 (2000).
23. Trempus, C. S. et al. Enrichment for living murine keratinocytes from the hair follicle bulge with the cell surface marker CD34. *J. Invest. Dermatol.* **120**, 501–511 (2003).
24. Claudinot, S., Nicolas, M., Oshima, H., Rochat, A. & Barrandon, Y. Long-term renewal of hair follicles from clonogenic multipotent stem cells. *Proc. Natl Acad. Sci. USA* **102**, 14677–14682 (2005).
25. Morris, R. J. et al. Capturing and profiling adult hair follicle stem cells. *Nat. Biotechnol.* **22**, 411–417 (2004).
26. Tumbar, T. et al. Defining the epithelial stem cell niche in skin. *Science* **303**, 359–363 (2004).
27. Lyle, S. et al. The C8/144B monoclonal antibody recognizes cytokeratin 15 and defines the location of human hair follicle stem cells. *J. Cell Sci.* **111**, 3179–3188 (1998).
28. Liu, Y., Lyle, S., Yang, Z. & Cotsarelis, G. Keratin 15 promoter targets putative epithelial stem cells in the hair follicle bulge. *J. Invest. Dermatol.* **121**, 963–968 (2003).
29. Youssef, K. K. et al. Identification of the cell lineage at the origin of basal cell carcinoma. *Nat. Cell Biol.* **12**, 299–305 (2010).
30. Jaks, V. et al. Lgr5 marks cycling, yet long-lived, hair follicle stem cells. *Nat. Genet.* **40**, 1291–1299 (2008).
31. Vidal, V. P. et al. Sox9 is essential for outer root sheath differentiation and the formation of the hair stem cell compartment. *Curr. Biol.* **15**, 1340–1351 (2005).
32. Nowak, J. A., Polak, L., Pasolli, H. A. & Fuchs, E. Hair follicle stem cells are specified and function in early skin morphogenesis. *Cell Stem Cell* **3**, 33–43 (2008).
33. Howard, J. M., Nuguid, J. M., Ngole, D. & Nguyen, H. Tcf3 expression marks both stem and progenitor cells in multiple epithelia. *Development* **141**, 3143–3152 (2014).
34. Ito, M. et al. Stem cells in the hair follicle bulge contribute to wound repair but not to homeostasis of the epidermis. *Nat. Med.* **11**, 1351–1354 (2005).
35. Levy, V., Lindon, C., Harfe, B. D. & Morgan, B. A. Distinct stem cell populations regenerate the follicle and interfollicular epidermis. *Dev. Cell* **9**, 855–861 (2005).
36. Potten, C. S. Epidermal cell production rates. *J. Invest. Dermatol.* **65**, 488–500 (1975).
37. Potten, C. S. The epidermal proliferative unit: the possible role of the central basal cell. *Cell Tissue Kinet.* **7**, 77–88 (1974).
38. Clayton, E. et al. A single type of progenitor cell maintains normal epidermis. *Nature* **446**, 185–189 (2007).
39. Ro, S. & Rannala, B. A stop-EGFP transgenic mouse to detect clonal cell lineages generated by mutation. *EMBO Rep.* **5**, 914–920 (2004).
40. Roy, E. et al. Bimodal behaviour of interfollicular epidermal progenitors regulated by hair follicle position and cycling. *EMBO J.* **35**, 2658–2670 (2016).

41. Lim, X. et al. Interfollicular epidermal stem cells self-renew via autocrine Wnt signaling. *Science* **342**, 1226–1230 (2013).
42. Doupe, D. P., Klein, A. M., Simons, B. D. & Jones, P. H. The ordered architecture of murine ear epidermis is maintained by progenitor cells with random fate. *Dev. Cell* **18**, 317–323 (2010).
43. Rompolas, P. et al. Spatiotemporal coordination of stem cell commitment during epidermal homeostasis. *Science* **352**, 1471–1474 (2016).
44. Mascre, G. et al. Distinct contribution of stem and progenitor cells to epidermal maintenance. *Nature* **489**, 257–262 (2012).
45. Sanchez-Danes, A. et al. Defining the clonal dynamics leading to mouse skin tumour initiation. *Nature* **536**, 298–303 (2016).
46. Jones, P. H. & Watt, F. M. Separation of human epidermal stem cells from transit amplifying cells on the basis of differences in integrin function and expression. *Cell* **73**, 713–724 (1993).
47. Horsley, V. et al. Blimp1 defines a progenitor population that governs cellular input to the sebaceous gland. *Cell* **126**, 597–609 (2006).
48. Snippert, H. J. et al. Lgr6 marks stem cells in the hair follicle that generate all cell lineages of the skin. *Science* **327**, 1385–1389 (2010).
49. Jensen, K. B. et al. Lrig1 expression defines a distinct multipotent stem cell population in mammalian epidermis. *Cell Stem Cell* **4**, 427–439 (2009).
50. Donati, G., Rognoni, E., Hiratsuka, T., Liakath-Ali, K. & Hoste, E. Wounding induces dedifferentiation of epidermal Gata6$^+$ cells and acquisition of stem cell properties. *Nat. Cell Biol.* **19**, 603–613 (2017).
51. Nijhof, J. G. et al. The cell-surface marker MTS24 identifies a novel population of follicular keratinocytes with characteristics of progenitor cells. *Development* **133**, 3027–3037 (2006).
52. Jensen, U. B. et al. A distinct population of clonogenic and multipotent murine follicular keratinocytes residing in the upper isthmus. *J. Cell Sci.* **121**, 609–617 (2008).
53. Fullgrabe, A. et al. Dynamics of Lgr6$^+$ progenitor cells in the hair follicle, sebaceous gland, and interfollicular epidermis. *Stem Cell Rep.* **5**, 843–855 (2015).
54. Page, M. E., Lombard, P., Ng, F., Gottgens, B. & Jensen, K. B. The epidermis comprises autonomous compartments maintained by distinct stem cell populations. *Cell Stem Cell* **13**, 471–482 (2013).
55. Batlle, E. et al. β-Catenin and TCF mediate cell positioning in the intestinal epithelium by controlling the expression of EphB/ephrinB. *Cell* **111**, 251–263 (2002).
56. Jaks, V., Kasper, M. & Toftgard, R. The hair follicle—a stem cell zoo. *Exp. Cell Res.* **316**, 1422–1428 (2010).
57. Levy, V., Lindon, C., Zheng, Y., Harfe, B. D. & Morgan, B. A. Epidermal stem cells arise from the hair follicle after wounding. *FASEB J.* **21**, 1358–1366 (2007).
58. Argyris, T. Kinetics of epidermal production during epidermal regeneration following abrasion in mice. *Am. J. Pathol.* **83**, 329–340 (1976).
59. Sada, A., Jacob, F., Leung, E., Wang, S. & White, B. S. Defining the cellular lineage hierarchy in the interfollicular epidermis of adult skin. *Nat. Cell Biol.* **18**, 619–631 (2016).
60. Ito, M. & Cotsarelis, G. Is the hair follicle necessary for normal wound healing? *J. Invest. Dermatol.* **128**, 1059–1061 (2008).
61. Lu, C. P. et al. Identification of stem cell populations in sweat glands and ducts reveals roles in homeostasis and wound repair. *Cell* **150**, 136–150 (2012).
62. Coulombe, P. A. Wound epithelialization: accelerating the pace of discovery. *J. Invest. Dermatol.* **121**, 219–230 (2003).
63. Savagner, P. et al. Developmental transcription factor slug is required for effective re-epithelialization by adult keratinocytes. *J. Cell. Physiol.* **202**, 858–866 (2005).
64. Haensel, D. & Dai, X. Epithelial-to-mesenchymal transition in cutaneous wound healing: where we are and where we are heading. *Dev. Dyn.* **247**, 473–480 (2018).
65. Blanpain, C. & Simons, B. D. Unravelling stem cell dynamics by lineage tracing. *Nat. Rev. Mol. Cell Biol.* **14**, 489–502 (2013).
66. Doupe, D. P. et al. A single progenitor population switches behavior to maintain and repair esophageal epithelium. *Science* **337**, 1091–1093 (2012).
67. Roshan, A. et al. Human keratinocytes have two interconvertible modes of proliferation. *Nat. Cell Biol.* **18**, 145–156 (2016).
68. Hirsch, T. et al. Regeneration of the entire human epidermis using transgenic stem cells. *Nature* **551**, 327–332 (2017).
69. Latil, M. et al. Cell-type-specific chromatin states differentially prime squamous cell carcinoma tumor-initiating cells for epithelial to mesenchymal transition. *Cell Stem Cell* **20**, 191–204.e5 (2017).
70. Fu, X., Sun, X., Li, X. & Sheng, Z. Dedifferentiation of epidermal cells to stem cells in vivo. *Lancet* **358**, 1067–1068 (2001).
71. Mannik, J., Alzayady, K. & Ghazizadeh, S. Regeneration of multilineage skin epithelia by differentiated keratinocytes. *J. Invest. Dermatol.* **130**, 388–397 (2010).
72. Tata, P. R. et al. Dedifferentiation of committed epithelial cells into stem cells in vivo. *Nature* **503**, 218–223 (2013).
73. Ito, M., Kizawa, K., Hamada, K. & Cotsarelis, G. Hair follicle stem cells in the lower bulge form the secondary germ, a biochemically distinct but functionally equivalent progenitor cell population, at the termination of catagen. *Differentiation* **72**, 548–557 (2004).
74. Rompolas, P., Mesa, K. R. & Greco, V. Spatial organization within a niche as a determinant of stem-cell fate. *Nature* **502**, 513–518 (2013).
75. van Es, J. H. et al. Dll1$^+$ secretory progenitor cells revert to stem cells upon crypt damage. *Nat. Cell Biol.* **14**, 1099–1104 (2012).
76. Buczacki, S. J. et al. Intestinal label-retaining cells are secretory precursors expressing Lgr5. *Nature* **495**, 65–69 (2013).
77. Tian, H. et al. A reserve stem cell population in small intestine renders Lgr5-positive cells dispensable. *Nature* **478**, 255–259 (2011).
78. Metcalfe, C., Kljavin, N. M., Ybarra, R. & de Sauvage, F. J. Lgr5$^+$ stem cells are indispensable for radiation-induced intestinal regeneration. *Cell Stem Cell* **14**, 149–159 (2014).
79. Zhang, Y. et al. Reciprocal requirements for EDA/EDAR/NF-κB and Wnt/β -catenin signaling pathways in hair follicle induction. *Dev. Cell* **17**, 49–61 (2009).
80. Huelsken, J., Vogel, R., Erdmann, B., Cotsarelis, G. & Birchmeier, W. β -Catenin controls hair follicle morphogenesis and stem cell differentiation in the skin. *Cell* **105**, 533–545 (2001).
81. Andl, T., Reddy, S. T., Gaddapara, T. & Millar, S. E. WNT signals are required for the initiation of hair follicle development. *Dev. Cell* **2**, 643–653 (2002).
82. Myung, P. S., Takeo, M., Ito, M. & Atit, R. P. Epithelial Wnt ligand secretion is required for adult hair follicle growth and regeneration. *J. Invest. Dermatol.* **133**, 31–41 (2013).
83. Nelson, A. M. et al. Prostaglandin D_2 inhibits wound-induced hair follicle neogenesis through the receptor, Gpr44. *J. Invest. Dermatol.* **133**, 881–889 (2013).
84. Nelson, A. M. et al. dsRNA released by tissue damage activates TLR3 to drive skin regeneration. *Cell Stem Cell* **17**, 139–151 (2015).
85. Hughes, M. W. et al. Msx2 supports epidermal competency during wound-induced hair follicle neogenesis. *J. Invest. Dermatol.* **138**, 2041–2050 (2018).
86. Gay, D. et al. Fgf9 from dermal γδ T cells induces hair follicle neogenesis after wounding. *Nat. Med.* **19**, 916–923 (2013).
87. Plikus, M. V. & Guerrero-Juarez, C. F. Regeneration of fat cells from myofibroblasts during wound healing. *Science* **355**, 748–752 (2017).
88. Blanpain, C. & Fuchs, E. Stem cell plasticity. Plasticity of epithelial stem cells in tissue regeneration. *Science* **344**, 1242281 (2014).
89. Szpaderska, A. M., Zuckerman, J. D. & DiPietro, L. A. Differential injury responses in oral mucosal and cutaneous wounds. *J. Dent. Res.* **82**, 621–626 (2003).
90. Driskell, R. R. et al. Distinct fibroblast lineages determine dermal architecture in skin development and repair. *Nature* **504**, 277–281 (2013).
91. Rinkevich, Y. et al. Skin fibrosis. Identification and isolation of a dermal lineage with intrinsic fibrogenic potential. *Science* **348**, aaa2151 (2015).
92. Rognoni, E. et al. Inhibition of β-catenin signalling in dermal fibroblasts enhances hair follicle regeneration during wound healing. *Development* **143**, 2522–2535 (2016).
93. Jiang, D. et al. Two succeeding fibroblastic lineages drive dermal development and the transition from regeneration to scarring. *Nat. Cell Biol.* **20**, 422–431 (2018).
94. Rodgers, J. T. et al. mTORC1 controls the adaptive transition of quiescent stem cells from G_0 to G_{Alert}. *Nature* **510**, 393–396 (2014).
95. Keyes, B. E. et al. Impaired epidermal to dendritic T cell signaling slows wound repair in aged skin. *Nat. Cell Biol.* **167**, 1323–1338.e14 (2016).
96. Munz, B. et al. Overexpression of activin A in the skin of transgenic mice reveals new activities of activin in epidermal morphogenesis, dermal fibrosis and wound repair. *Eur. J. Immunol.* **18**, 5205–5215 (1999).
97. Haertel, E., Joshi, N., Hiebert, P., Kopf, M. & Werner, S. Regulatory T cells are required for normal and activin-promoted wound repair in mice. *Eur. J. Immunol.* **48**, 1001–1013 (2018).
98. Wankell, M. et al. Impaired wound healing in transgenic mice overexpressing the activin antagonist follistatin in the epidermis. *EMBO J.* **20**, 5361–5372 (2001).
99. Bamberger, C. et al. Activin controls skin morphogenesis and wound repair predominantly via stromal cells and in a concentration-dependent manner via keratinocytes. *Am. J. Pathol.* **167**, 733–747 (2005).

Acknowledgements

We apologize to all authors whose work could not be cited owing to space constraints. C.B. is an investigator of WELBIO. S.D. is supported by a fellowship of the FNRS/TELEVIE. This work was supported by a consolidator grant of the European Research Council.

Competing interests

The authors declare no competing interests.

Additional information

Reprints and permissions information is available at www.nature.com/reprints.

Correspondence should be addressed to C.B.

Publisher's note: Springer Nature remains neutral with regard to jurisdictional claims in published maps and institutional affiliations.

3 OPEN QUESTIONS

The SC and CP dynamics unraveled in the mouse tail epidermis during homeostasis raises a lot of questions. How SCs and CPs adapt their proliferation and cell fate decisions when the tissue needs to expand, such as in wound healing or during post-natal development ? Are the SC/CP able to change their cell fate decision ? Do they increase their self-renewal decisions in order to rapidly increase the pool of SC/CP ? What are the molecular signals controlling these fate decisions ?

Modeling the cell fate probabilities in expansion conditions could be critical and would help to better understand what is deregulated in term of cell fate decision during pathological conditions such as tumor initiation or chronic wound. Skin Chronic wound affect more than 6 million people and cost more than $25 billons per year in USA[116]. Improving our knowledge in wound healing and skin growth mechanisms is therefore an important challenge for our future economy and society.

.

4 RESULTS

4.1 DEFINING STEM CELL DYNAMICS AND MIGRATION DURING WOUND HEALING IN MOUSE SKIN EPIDERMIS

4.1.1 Focus

The skin epidermis is constantly renewed throughout life[117]. Using lineage tracing experiments, we and others previously demonstrated that the mouse tail IFE is maintained by a hierarchy of SCs and CPs that present tree possible cell fate decisions : asymmetrical cell fate decisions, symmetrical renewal and symmetrical differentiation, the two last outcomes harboring similar probabilities during homeostasis[100,102,103]. When the skin barrier is disrupted, a cascade of cellular and molecular events is activated to repair the damage and restore skin integrity[118]. Different epidermal SCs coming from the HF, isthmus, infundibulum and IFE have been shown to contribute to IFE repair after wound[43,44,102,119-123]. However, it remains unclear whether these cells only increase their proliferation rate, maintaining an equal proportion of symmetrical renewal and differentiation, or whether they switch to an “expanding” mode of division leading to more symmetrical self-renewal. It also remains unclear whether basal cells can uncouple proliferation, differentiation and migration during the healing process, and whether two different SCs populations achieve the same proliferative dynamics.

In this study, we used BrdU incorporation on 3D whole-mount tissues from mouse tail epidermis and microarray analysis to shed more lights on the reepithelization phase and the molecular identity of the different compartments taking place during wound healing. Moreover, using inducible CreER recombinase under the control of two promoters to target IFE SCs (*K14-CreER*)[124] and upper isthmus (or infundibulum) SCs (*Lrig1-CreER*)[125] combined with the *Rosa-Confetti* (Brainbow 2.1) reporter[126], we deciphered the proliferation dynamics and cell fate decisions occurring in these two distinct SCs populations during IFE repair.

4.1.2 Methods and results

We used 3 mm punch biopsy to generate circular wounds on the tail of transgenic mice and collected the epidermis at 0, 2, 4, 7, 10 and 14 days post-wound. Our data show that proliferation increases from 2 days to 7 days post wound and that rapidly dividing cells are localized in a specific zone defined within a circle around the wound, on average 1 mm large, delimitating a proliferative hub. Within 500µm from the edge of the wound, a region called the leading edge (LE) is by contrast devoid of proliferative cells (Figure 1, page 36). Two and for days after wound, LE cells were oriented perpendicularly to the wound direction, suggesting that some forces were compressing them. Treating mice with 5-Fluorouracile (5-FU), a pyrimidine analog that blocks DNA synthesis, delayed wound closure and partially relieved LE cells from the compression, suggesting that proliferation was important for the compression of the LE cells (Figure 2, page 37).

To define the molecular identity of the wounded epidermis we performed microarray analysis on basal cells from the LE and proliferative hub, isolated with 4mm and 6mm diameter punch biopsies, respectively, 4 and 7 days after wound and compared with unwounded epidermis (Figure 3, page 38). We identified upregulated genes implicated in cell adhesion/cytoskeleton, cell signaling, inflammation and cell cycle regulators (Supplementary figure 2, page 49). We validated the specific and rapid upregulation of Itgα5 in the LE and used it as a marker to isolate LE cells 4 days after wound by FACS (Figure 3, page 38). We found a similar LE signature as identified in the first analysis, validating our first approach. Gene ontology enrichment (GO) analysis revealed that the LE signature was enriched in genes associated with cell migration, inflammation, cell adhesion, ECM ligands, cytoskeleton and actin regulators, cell signaling, and coding for specific TFs. This analysis allowed us to propose a spatial molecular signature of the LE and proliferative cells upon wound healing (Figure 3, page 38). We confirmed the local and transient upregulation of genes not previously described in wound epidermis, such as *Flrt2/3*, *Gprc5a* and *Myo1b* at the protein level by immunostaining (Figure 4, page 40). These observations support the notion of a spatially restricted and transient LE compartment formed during wound healing. 5-FU treatment decreased

the proliferation within the epidermis, but did not change the expression of the leading edge marker, suggesting that these markers were induced independently of cell division (Figure 5, page 41). Wounded mice treated with dexamethasone, an anti-inflammatory drug of the glucocorticoid (GC) family, partially re-established proliferation in the LE cells but did not impair the expression of the LE markers, suggesting that the quiescent status of the LE cells can be functionally and molecularly uncoupled from the expression of the LE specific markers (Figure 5, page 41).

To address the cell fate decisions of the IFE SCs and infundibulum cells upon wound healing, we performed lineage tracing at clonal density using Cre-recombinase under the control of IFE SCs promoter (*K14-CreER*)[102,124] or upper isthmus/infundibulum SCs promoter (*Lrig1-CreER*)[125] combined with the *Rosa-Confetti* (brainbow 2.1)[126,127] reporter. Clones appeared as long unicolor fragmented streaks pointing toward the center of the wound (Figure 6, page 42). 80% of the *K14-CreER/Rosa-Confetti* clones were lost between 0 and 4 days post-wound while the thickness of the epidermis increased 4 to 5 fold, consistent with the increased proliferation observed at 2 and 4 days post-wound. *Lrig1-CreER/Rosa-Confetti* clones were all confined in the infundibulum at 0 day post-wound but later appeared as long unicolor fragmented streaks of cells projecting outside the HF toward the wound center (Figure 7, page 43). We quantified the number of basal and suprabasal cells per unicolor streak 0, 4, 7 and 14 days after wound (Figure 8, page 44). Mathematical modeling showed that, despite a more rapid increase in size in *Lrig1-CreER* clones, both Infundibulum and IFE derived clones harbor a similar proliferation dynamics in which the majority of cell fate decisions are asymmetrical, while self-renewal and differentiation are balanced. Finally, spinous cells were traced using the *Inv-CreER*[128] promoter and *Rosa-YFP* reporter[129]. No YFP+ cells were observed in the new IFE after wound, ruling out the possibility that suprabasal cells revert back to basal upon wound healing (Supplementary figure 5, page 52).

4.1.3 Conclusion

Using BrdU incorporation, immunostaining and spatially distinct transcriptional analysis we refined the molecular mechanism and the cellular dynamics occurring during wound healing in mouse tail epidermis. We confirmed

that two compartments are formed during the re-epithelialization stage, a quiescent/ migrating LE and a proliferative hub, and that they are spatially and molecularly distinct. We show that LE cells have a specific transcriptional signature that can be uncoupled from their quiescent state and define new markers not previously described in wounded epidermis (Figure 9, page 45). Moreover, using lineage tracing and mathematical modeling we uncovered the proliferation dynamics and cell fate decision of two skin SCs populations upon wound healing. We show that, while Infundibulum and IFE SCs reside in different regions in the skin, they acquire the same dynamics upon wound healing, activating their SCs but maintaining a majority of asymmetrical cell fate decisions leading to linear growth of the clones.

nature COMMUNICATIONS

ARTICLE

Received 11 Jan 2017 | Accepted 23 Jan 2017 | Published 1 Mar 2017

DOI: 10.1038/ncomms14684 OPEN

Defining stem cell dynamics and migration during wound healing in mouse skin epidermis

Mariaceleste Aragona[1,*], Sophie Dekoninck[1,*], Steffen Rulands[2], Sandrine Lenglez[1], Guilhem Mascré[1], Benjamin D. Simons[2,3,4] & Cédric Blanpain[1,5]

Wound healing is essential to repair the skin after injury. In the epidermis, distinct stem cells (SCs) populations contribute to wound healing. However, how SCs balance proliferation, differentiation and migration to repair a wound remains poorly understood. Here, we show the cellular and molecular mechanisms that regulate wound healing in mouse tail epidermis. Using a combination of proliferation kinetics experiments and molecular profiling, we identify the gene signatures associated with proliferation, differentiation and migration in different regions surrounding the wound. Functional experiments show that SC proliferation, migration and differentiation can be uncoupled during wound healing. Lineage tracing and quantitative clonal analysis reveal that, following wounding, progenitors divide more rapidly, but conserve their homoeostatic mode of division, leading to their rapid depletion, whereas SCs become active, giving rise to new progenitors that expand and repair the wound. These results have important implications for tissue regeneration, acute and chronic wound disorders.

[1] Université Libre de Bruxelles, IRIBHM, Brussels B-1070, Belgium. [2] Cavendish Laboratory, Department of Physics, University of Cambridge, J.J. Thomson Avenue, Cambridge CB3 0HE, UK. [3] The Wellcome Trust/Cancer Research UK Gurdon Institute, University of Cambridge, Tennis Court Road, Cambridge CB2 1QN, UK. [4] Wellcome Trust-Medical Research Council Stem Cell Institute, University of Cambridge, Cambridge CB2 1QR, UK. [5] WELBIO, Université Libre de Bruxelles, Brussels B-1070, Belgium. * These authors contributed equally to this work. Correspondence and requests for materials should be addressed to C.B. (email: Cedric.Blanpain@ulb.ac.be).

The skin epidermis is a stratified epithelium that acts as a barrier protecting the animals against infections, trauma and water loss[1]. When the skin barrier is disrupted, a cascade of cellular and molecular events is activated to repair the damage and restore skin integrity. Defects in these events can lead to improper repair causing acute and chronic wound disorders[2].

Wound healing (WH) is organized in three stages[1–4]: the inflammation stage starts immediately, and is associated with the formation of the blood clot and the recruitment of inflammatory cells. The second stage is the regenerative phase associated with re-epithelialization of the wound, the creation of new epidermal cells and the formation of the granulation tissue. Finally, the last stage, which can last for months, involves the remodelling of the epidermis, dermis and extracellular matrix (ECM). Different epidermal SCs coming from the hair follicle (HF), isthmus, infundibulum and interfollicular epidermis (IFE) contribute to WH[5–12]. However, it remains unclear how different SCs populations can balance proliferation, differentiation and migration during the healing process, and whether they conform to the same proliferative dynamics. It also remains unclear whether these cells simply increase their proliferation rate, maintaining a homoeostatic mode of division, or whether they switch to a proliferative mode of division leading to more symmetrical cell duplication to facilitate the expansion of newly formed skin.

Here, using whole-mount tail epidermis, we identify and characterize molecularly and functionally two spatially distinct epithelial compartments surrounding the wound: a proliferative hub and a migrating leading edge (LE). We define the spatiotemporal dynamics of these two compartments over the re-epithelialization stage. We uncover the molecular signatures associated with these two distinct epidermal compartments and demonstrate that proliferation, migration and differentiation can be uncoupled during the early stage of wound repair. To understand the mode of division and the cellular hierarchy of different populations of epidermal cells, we perform a detailed quantitative clonal analysis and mathematical modelling of the individual behaviour IFE and infundibulum cells during WH. We show that at the beginning of WH, because of the incapacity of progenitors to switch from homoeostatic (asymmetric cell fate outcome at the population level) to a proliferative (symmetric renewal) mode of division, the important increase in cell proliferation leads to minimal tissue regeneration with a massive loss of progenitors through differentiation. As SCs become activated, they undergo rapid asymmetric cell fate outcome generating new SCs and progenitors that promote tissue expansion, visible as streaks of cells spanning from the proliferative hub to the centre of the wound. This clonal dynamic is very similar for different populations of epidermal SCs coming from different skin regions, suggesting that this cellular behaviour helps to maximize the regenerative process.

Results

Spatiotemporal proliferation and migration during WH. To define the role of cell proliferation during the regenerative stage of WH, we performed a 3 mm punch biopsy in the tail skin of adult mice and analysed the result of short-term BrdU incorporation by confocal microscopy on whole-mount epidermis at different time points during WH (Fig. 1a). Immediately after wounding, there was no increase in BrdU incorporation. However, at day 2 (D2) and even more at D4 following wounding, we found that BrdU incorporation was increased by 5-fold in a zone spanning from 500 µm to 1.5 mm from the LE, with 40% of basal cells entering into cycle during a period of 4 h (Fig. 1b). The width of the annulus of cells that proliferated around the wound progressively decreased with time (Fig. 1a,c,d). We found that epidermal cells at the LE, spanning a distance of 500 µm from the wound front, did not incorporate BrdU at any time point from D2 to D7 following wounding (Fig. 1a–c). This showed that cells at the LE of the epidermal sheath, which ensures skin regeneration, do not proliferate actively, but migrate to the centre of the wound. These results confirm the existence of a migrating LE that has been hypothesized for several decades based on the histological examination of wounded tissues and *ex-vivo* skin explants[3]. Reaching a maximal size at D4 following wounding, the size of the non-proliferating LE zone progressively decreased over time, suggesting that the specification and differentiation of LE cells occurs only during the early stage of WH (Fig. 1a,d). After D14, the wound edges fused at midline and proliferation resumed at the centre of the wound region (Fig. 1a,e).

As wound contraction contributes to wound closure[13], we assessed the relative importance of epidermal regeneration and wound contraction to the overall wound repair. As *de novo* HF formation only occurs with more extensive wounding and at a later stage[14], wound contraction was measured by the distance between the HF and the wound centre at D0 minus the same measurement at a given time point, while the newly formed epidermis was measured by the difference between the radius at D0 (1.5 mm) and the radius at any time point minus the contraction. Surprisingly, we found that the distance between HF triplets and the centre of the wound after the punch biopsy did not decrease significantly from D0 to D7, where proliferation was maximum, suggesting that proliferation is not very productive during the initial stage of wound repair (Fig. 1e,f). From D10 to D14, this distance decreased linearly in time until re-epithelialization was completed (Fig. 1e,f). At this stage the average distance between the HF triplets and the wound centre is 0.9 mm, suggesting that an epithelial regeneration contributes approximately to two-thirds of the healing process, and wound contraction (0.6 mm) is responsible for the remainder.

Cell shape and polarity during WH. The shape and size of the epidermal cells, which is the reflection of the forces that epidermal cells experience during the regeneration process, was very different depending on the wound region and the time point following wounding (Fig. 2a–c). At D0, the basal cells of the LE appeared less compacted (Fig. 2a), consistent with a relaxation in the force exerted on the wound edge. At D1, the LE cells were elongated toward the wound centre (Fig. 2a), as previously shown[15], consistent with the active migration of the LE cells toward this point. At D4, basal cells far from the wound presented a regular cuboidal/hexagonal shape (Fig. 2b). The density of basal cells in the proliferative zone was increased, leading to a more compressed cell shape (Fig 2b,d). In contrast, in the non-proliferative zone, the basal cells were bigger, polarized in the same direction, and elongated along an axis perpendicular to the direction of the wound closure (Fig. 2b). This suggests that, at D4 and thereafter, the movement of the LE is a passive process possibly mediated by the proliferating cells (Fig. 2b). Consistent with this notion, blocking epidermal cell proliferation by 5-fluorouracil (5-FU), which inhibited the re-epithelialization process and WH (Fig. 2e), prevented the perpendicular polarization of the LE at D4 (Fig. 2f). These data demonstrate that the two distinct epidermal compartments, the proliferative hub and the LE, present different cell shape and polarity that change with time, likely reflecting the difference in the physical forces that these different zones experience at the different stages of WH.

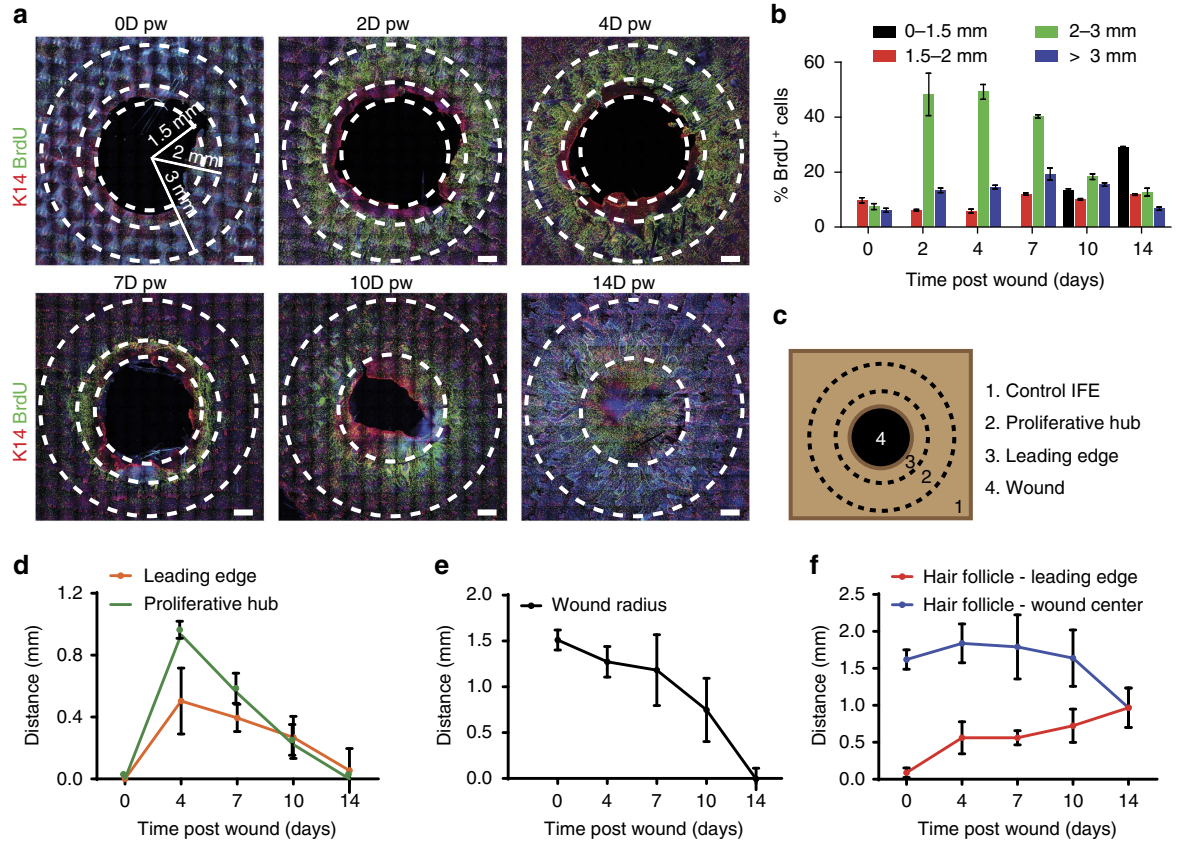

Figure 1 | Respective contribution of cell proliferation and migration during WH. (**a**) Representative immunostaining of K14 (red) and BrdU (green) in whole-mount skin epidermis of the wounded region at the different time points. Dashed lines limit the wounded area, the LE and the proliferative hub. Scale bar, 500 µm. (**b**) Quantification of the percentage of BrdU positive cells according to the distance from the wound centre ($n=5{,}000$ cells/region counted from three different mice). (**c**) Descriptive scheme showing the situation in the early days after wound and the localization of the two different areas around the wound between 2 and 7 days after wound. (**d**) Measure of the width of the LE (orange line) and the proliferative hub (green line) overtime. Five measures were taken per wound ($n=3$ mice). (**e**) Measure of the average wound radius overtime. Five different measures were taken per wound ($n=3$ mice). (**f**) Measure of the distance between the nearest HF and the LE (red line) and the distance between the HF and the wound centre (blue line). Five different measures were taken per wound ($n=3$ mice).

Molecular signature of LE and proliferation hub during WH. To define the molecular features associated with the formation of the proliferative hub and the LE, we performed transcriptional profiling of different concentric rings of the wound using different sizes of punch biopsy and fluorescence-activated cell sorting (FACS) sorting. A first punch biopsy of 4 mm in diameter around the wound was used to enrich for LE cells (spanning two times 500 µm, the average width of the LE), and a second punch biopsy (6 mm) was enriched for the proliferative hub of the wound (Fig. 3a; Supplementary Fig. 1). We performed a third biopsy far from the wound corresponding to control normal unwounded epidermis. We performed duplicate microarrays of these three skin regions at D4 and D7 post-wounding. We found genes upregulated in both wound regions at the two different time points, which correspond to a generic wound-healing signature. This gene signature included genes regulating cell adhesion (for example, *Dsc2*), cytoskeleton (for example, *Krt6*, *Krt17*), inflammation (for example, *Il24*, *Il33 S100a8/a9*), cell signalling (for example, *Areg*, *Ereg*, *Emb*, *Epgn*), (Supplementary Fig. 2a) and cell cycle-related genes (for example, *Ccna2*, *Ccnb1*) (Supplementary Fig. 2b). For some genes, such as *Krt6* (refs 3,16–19), in which expression was confirmed by immunofluorescence (Supplementary Fig. 2c), *Il24*, *S100a8/a9* or the EGFR ligands, their role in the regulation of WH has previously been described[20–23]. In other cases, including *Fscn1*, *Emb*, *Sprr1b and Sprr2h*, genes were not known to be involved in skin WH.

We next defined which genes were preferentially upregulated and downregulated in the LE as compared with the proliferative hub (the LE signature) (Supplementary Fig. 2d–f). We found that *α5-integrin* was highly enriched in the LE signature (Supplementary Fig. 2e); consistent with a previous study that showed that *α5-integrin* was expressed at the LE of human skin explants *ex vivo*[24–27] and at the LE during eyelid closure, a developmental process that involves epidermal cell migration[28], reminiscent of the LE during WH. Whole-mount immunostaining confirmed the rapid upregulation of α5-integrin in the non-proliferative cells of the LE *in vivo* (Fig. 3b). To refine the molecular signature of the LE without contamination of proliferative cells, we isolated α5-integrin positive cells from a 4 mm punch biopsy by FACS at D4 following wounding (Supplementary Fig. 3) and performed microarray analysis in triplicates. These molecular analyses confirmed the preferential expression of many of the previously described genes expressed during WH, validating the approach used here and allowing for the first time to distinguish the spatial localization of these genes at the LE and/or in the proliferative hub. In addition, the gene signatures of the proliferative and LE cells during wounding uncover many novel genes not previously described during WH and tissue regeneration (Fig. 3c–j). Gene Ontology Enrichment (GO) analysis revealed that the genes upregulated in the LE comprised genes regulating cell adhesion, cytoskeleton organization, epidermal differentiation, cell migration and other

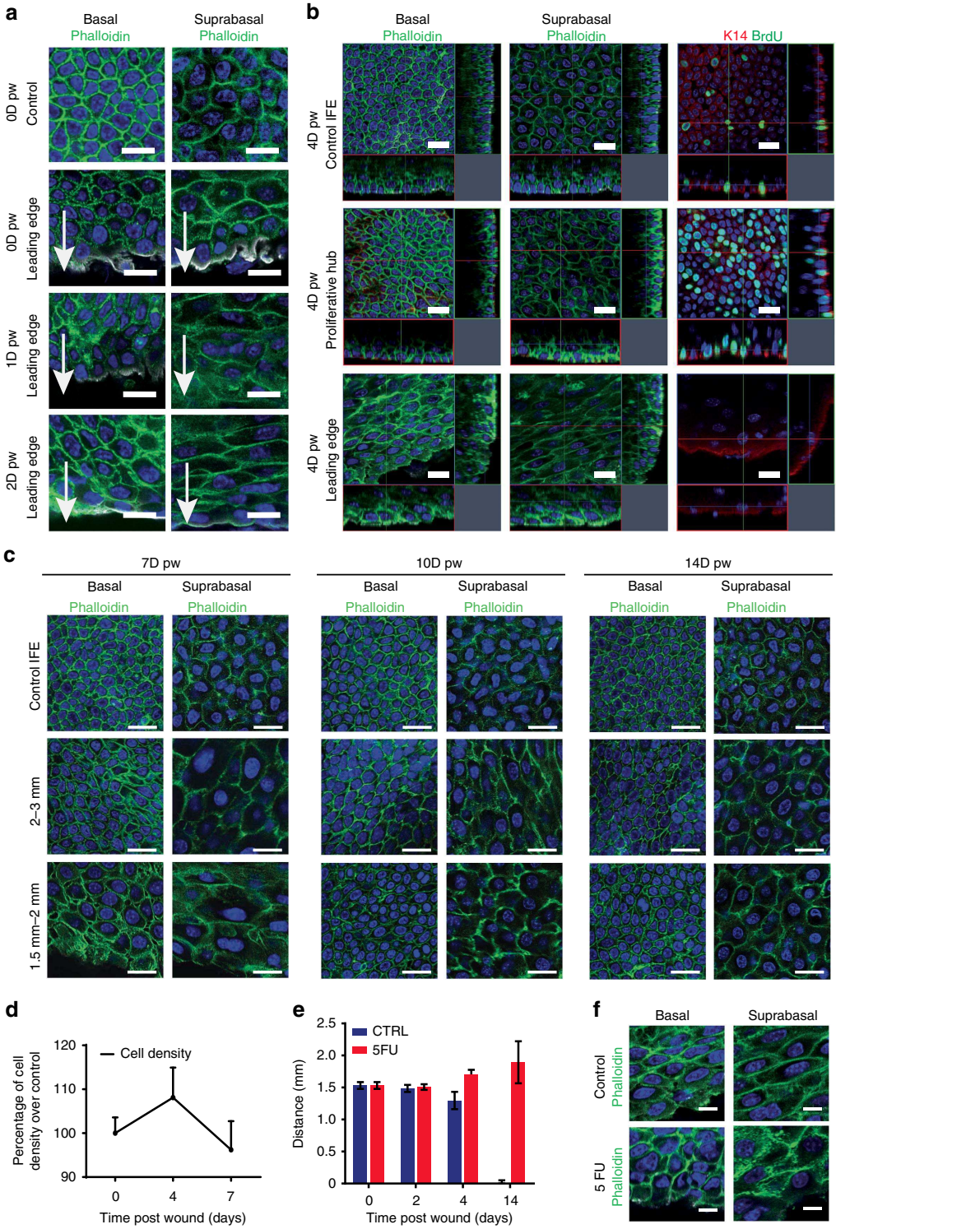

Figure 2 | Modifications of cell polarity and cell shape during WH. (**a**) Representative confocal analysis of whole-mount epidermis stained for F-actin with phalloidin (green) and β4-integrin (white) showing the different shape of basal (left) and suprabasal (right) cells at the LE 0, 1 and 2 days after wound compare to a control area. Arrows indicate the direction of the wound. Scale bar, 20 μm. (**b**) Left and middle panels: representative confocal analysis of whole-mounted epidermis stained for F-actin with phalloidin (green) and β4-integrin (white) showing the shape of the basal (left) and suprabasal (middle) cells in the different regions, 4 days after wound. Right panel: immunostaining for BrdU (green) and K14 (red) in the different regions 4 days after wound. (**c**) Representative confocal pictures of whole-mounted epidermis immunostained for F-actin with phalloidin (green) showing the shape of the basal and suprabasal keratinocytes in the control area, proliferative hub (2–3 mm) and LE (0–2 mm) 7, 10 and 14 days after wound. Nuclei are stained with Hoechst (blue). Scale bar, 20 μm. (**d**) Percentage of cell density at 0, 4 and 7 days post wound in the proliferative hub normalized by a control area. Five different measures were taken per wound ($n=4$ mice). (**e**) Measure of the wound radius after 5-FU topical treatment compared to control-untreated mice ($n=3$ mice). (**f**) Representative confocal pictures of whole-mounted epidermis stained for F-actin with phalloidin (green) showing the elongated cells at the LE in the untreated mice and the random orientation of the cells in the same area after 5-FU treatment. Nuclei are stained with Hoechst (blue). Scale bar, 20 μm. Wound centre is at the bottom edge of the pictures.

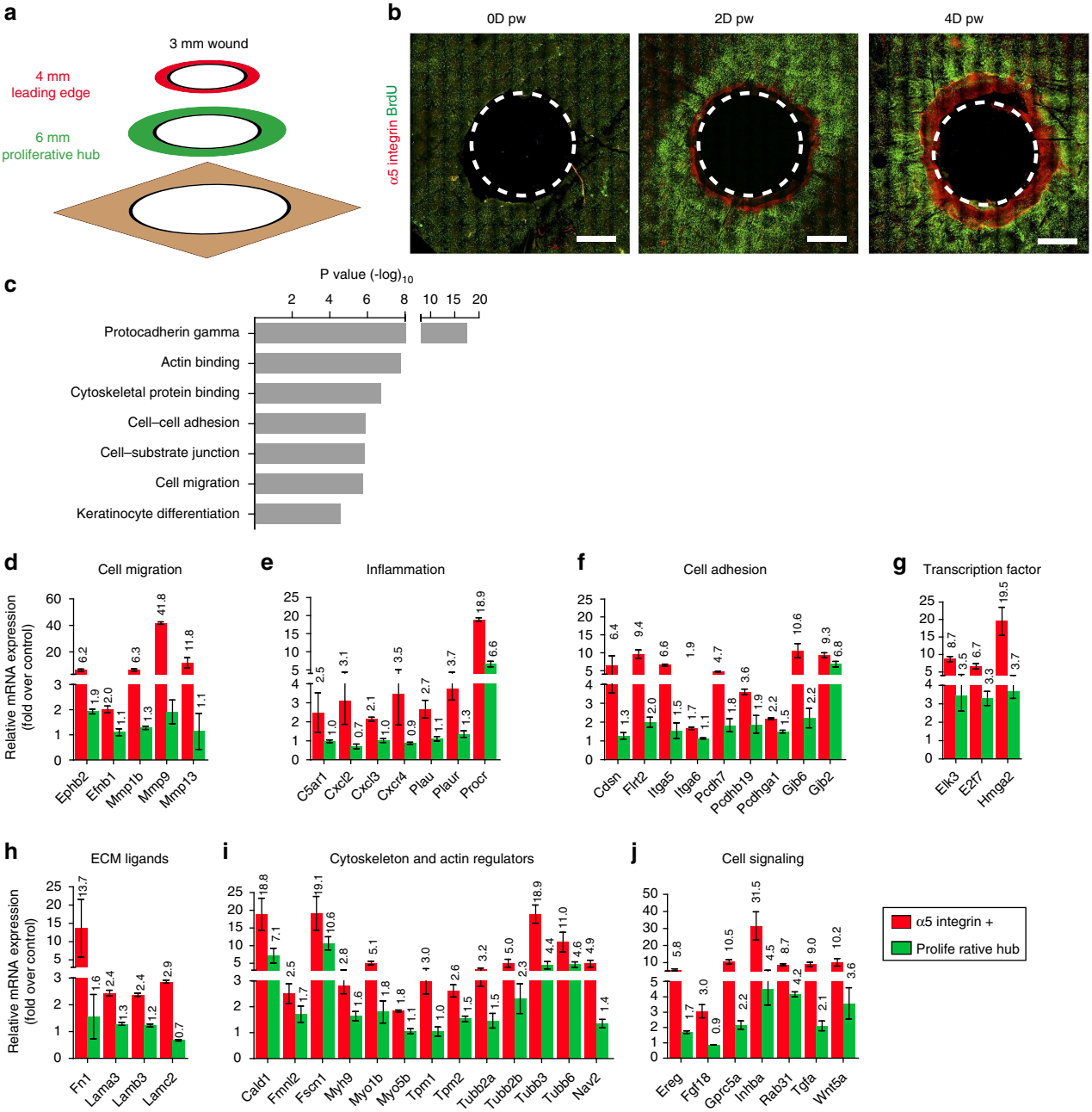

Figure 3 | Molecular signature of the proliferative hub and the LE during WH. (**a**) Scheme showing the strategy used to isolate the LE with a 4 mm punch biopsy and the proliferative hub with a 6-mm-punch biopsy. (**b**) Representative maximum intensity projection of confocal pictures showing the immunostaining of whole-mount epidermis with α5-integrin (red) and anti-BrdU (green) 0, 2 and 4 days after wound. Note the expression of the α5-integrin by the non-proliferative LE cells only. (**c**) Gene ontology enrichment in the LE 4 days after wound ($n=3$). (**d**–**j**) LE signature. List of genes upregulated in the α5-integrin positive cells of the LE compared with the proliferative hub ($n=3$). These genes are implicated in cell migration (**d**), inflammation (**e**), cell adhesion (**f**), transcription (**g**), ECM composition (**h**), cytoskeleton and actin regulators (**i**) and cell signalling (**j**).

processes involved in WH (Fig. 3c). The most upregulated genes of the LE signature were genes coding for proteins regulating cell migration including several metalloproteinases (MMPs) (*Mmp9*, *Mmp13*, *Mmp1b*) (Fig. 3d), whereas *Timp3*, an inhibitor of metalloproteinase, was the most downregulated gene (Supplementary Fig. 2f), suggesting that the high level of MMPs expressed by the cells of the LE promote the remodelling of the ECM at the wound front allowing the front cells to progress toward the centre. MMPs also help the breakdown of the hemi desmosomes that anchor the cells at the basal membrane and are therefore essential for the movement of basal cells. MMPs deletion in flies and mice results in wound-healing defects due to defective cell elongation, cytoskeleton and basal membrane remodelling as well as cell migration[29–33]. The migrating zone also expressed high level of *urokinase* (*Plau*) and *plasminogen activator* (*Plaur*) (Fig. 3e), two key fibrinolytic proteins contributing to the remodelling of the blood clot during WH[34]. The LE also expressed high level of *Ephb2* and *Efnb1* (Fig. 3d), a receptor and its ligand, which have recently been shown to control WH[35] as well as other genes such as *Cxcr4*, *C5ar1*, *Myh9*, *Procr*, *Wnt5a*, *Elk3* (Fig. 3e,g,i,j), which regulate cell migration in other cellular contexts. We found that *Inhibin-βa*, a subunit of

Activin A was overexpressed preferentially at the LE (Fig. 3j), in good accordance with in-situ hybridization of *Inhibin-βa* during WH[36] and the previously reported role of Activin A during WH in mice[37–42].

Our LE signature encompassed many genes controlling cell adhesion, including several protocadherins (*Pcdh7*, *Pcdhb19*, *Pcdhga1*) (Fig. 3f), integrins (*Itga5*, *Itga6*) (Fig. 3f) and some of their ECM ligands (*Fn1*, *Lama3*, *Lamb3*, *Lamc2*) (Fig. 3h), desmosomes (*Cdsn*)[43] and gap junction proteins (*Gjb6/Cx30* and *Gjb2/Cx26*) (Fig. 3f). Corneodesmosin (*Cdsn*), a desmosome protein of the wound edge signature (Fig. 3f) was reported to be expressed using transgenic reporter mice in the wound edge and in the inner root sheath (IRS) of the hair[44].

Many genes controlling cell cytoskeleton and actin remodelling including actin regulators (*Fscn1*, *Cald1*, *Nav2*, *Fmnl2*), myosin (*Myo1b*, *Myo5b*, *Myh9*, *Tpm1*, *Tpm2*) and tubulin (*Tubb2a*, *Tubb3*, *Tubb6*), were preferentially overexpressed at the LE (Fig. 3i), and *Tubb6* was previously shown to be upregulated during wounding[19]. These genes may control the morphology, polarity, rigidity of the cell cortex and migration during WH.

Several genes that might regulate the quiescence of the LE surfaced from the microarray analysis. *Gprc5a*, an orphan G protein coupled receptor, acting as tumour suppressor genes in the lung by negatively regulating EGFR and Stat3 signalling[45–47], was strongly upregulated at the LE (Fig. 3j.). The upregulation of *E2f7* (ref. 48) or *Fgf18* (ref. 49), genes that promote cell quiescence in other contexts may also contribute to shut down of proliferation in the wound LE (Fig. 3g,j).

Spatiotemporal expression of the LE signature during WH. Immunostaining performed against several of these newly identified markers of the LE signature including cell adhesion, receptor and cytoskeleton proteins (*Flrt2*, *Gprc5a*, *Tubb2*, *Myo1b*, *Itga5*) confirmed their preferential enrichment at the LE of the wound as predicted by our microarray analysis (Fig. 4a–e). Itga5 was expressed preferentially in the basal cells of the LE (Fig. 4a). Flrt2, a repulsive guidance protein that regulates the migration of neuronal progenitors during embryonic development[50] was more expressed in the cells of the wound edge than in the proliferation zone, but was not present in the normal skin epidermis (Fig. 4b). Gprc5a was expressed at the LE of the wound at D4 (Fig. 4c), and similarly to Cdsn[44], Flrt2 or Tubb2, to the IRS or precortex cells of the HFs (Fig. 4b–d; Supplementary Fig. 4a–c). Myosin 1b, a tension-sensitive myosin was also expressed in all cell types of the LE (Fig. 4e), which by regulating actin foci stability, controls cell migration or repulsion. Myosin 1b was also expressed in the bulge and outer root sheath (ORS) of the HFs (Supplementary Fig. 4d). The expression of all these newly identified molecular markers of the wound LE signature decreased overtime and at D14 post-wound, when the opposite margin of epidermal cells fused together, these markers were not expressed anymore (Fig. 4a–e). These data demonstrate the transient nature of this wound LE structure.

Uncoupling proliferation and differentiation during WH. To gain further insights into the mechanisms that specify these two distinct regions, we determined whether the fate and the differentiation programme of the LE are linked to cell division, by assessing the impact of blocking cell proliferation on the fate of LE cells. Topical application of 5-FU, which strongly decreased epidermal cell proliferation, did not prevent or impair the expression of LE markers (Fig. 5a–c), demonstrating that the particular differentiation programme of the LE is specified independently of cell division.

As inflammation plays an important role in orchestrating the early step of WH[1,2,51], we assessed the impact of blocking inflammation on these two distinct epidermal compartments during re-epithelialization. Interestingly, treating the wounded mice with dexamethasone, a potent anti-inflammatory drug, reactivate proliferation in the LE without impairing its particular gene expression signature (Fig. 5d–g) demonstrating that, the LE-specific gene signature is not associated with terminal differentiation (Fig. 5f,g). These data show that glucocorticoid treatment suppresses a negative regulator of cell cycle acting on the LE. As glucocorticoid can also directly act on keratinocytes[52], this negative regulator may originate either from the keratinocytes or from the inflammatory cells and the granulation tissue. Although, these data do not allow to discriminate whether the inhibition of proliferation at the LE is regulated by an intrinsic or an extrinsic mechanism, these results provide compelling evidence that the LE-specific cellular quiescence and gene expression signature can be functionally and molecularly uncoupled.

Clonal analysis of IFE SC during WH. To follow the progeny of the basal epidermal cells, and study their cellular dynamics at the single cell level, we performed clonal analysis on *K14CREER/Rosa Confetti* mice targeting preferentially IFE SCs[12] (Fig. 6a). We administrated Tamoxifen (TAM) 14 days before wounding and analysed the respective clonal contribution during the healing process (Fig. 6b). At the end of the re-epithelialization, K14-labelled cells gave rise to long streaks of labelled cells directed toward the LE of the wound (Fig. 6c–e). With a clone merger probability estimated at roughly 5% (Fig. 6f; Supplementary Note 1), we deduced that streaks labelled with the same fluorescent protein were clonal in origin, derived from single SCs. The clonal lines were often interrupted by unlabelled cells (Fig. 6d,e), suggesting that a cycle of active SC proliferation followed by cell intercalation from neighbouring clones (or clonal fragmentation) occurs repetitively during WH. Interestingly, all of these fragmented clonal streaks originate from the proliferative hub previously described (Fig. 6g). Quantification of the clonal persistence revealed that more than 90% of IFE-labelled clones were lost during the first week following wounding (Fig. 6h), consistent with the majority of progenitors maintaining homoeostatic behaviour, leading to a progressive decrease in the labelled cell fraction[12,53,54]. Importantly, this clonal dynamic contrasts with that reported for oesophagus, where repair seems to involve a switch of progenitors to a proliferative mode of division[55], or following *in vitro* culture of human keratinocytes[56]. Consistent with a major increase in the rate of terminal differentiation, as measured by clonal persistence, the epidermal thickness increased during the same period (Fig. 6i).

Three-dimensional analysis of labelled clones revealed that, in contrast to clones in the control regions that are composed of stacks of cells that lie on the top of each other (Fig. 6j), at D4 K14CREER IFE SCs gave rise to basal and suprabasal cells that migrate toward the wound edge (Fig. 6k). The restriction of the basal footprint of the clone at the trailing edge suggest that marked SCs undergo predominantly asymmetric cell division, giving rise to a steady production of progenitors. Interestingly, despite the high rate of proliferation observed in the first days following wounding, at this time point, K14CREER clones are not on average bigger as compared to D0, suggesting that the effect of SC renewal is not yet observed at the population level.

By D14, most of the persisting K14CREER clones became enlarged in their basal attachment and were composed of a majority of suprabasal cells (Fig. 6l), while others formed long streaks of basal cells and suprabasal cells (Fig. 6m), suggesting that these clones produced an increased number of basal

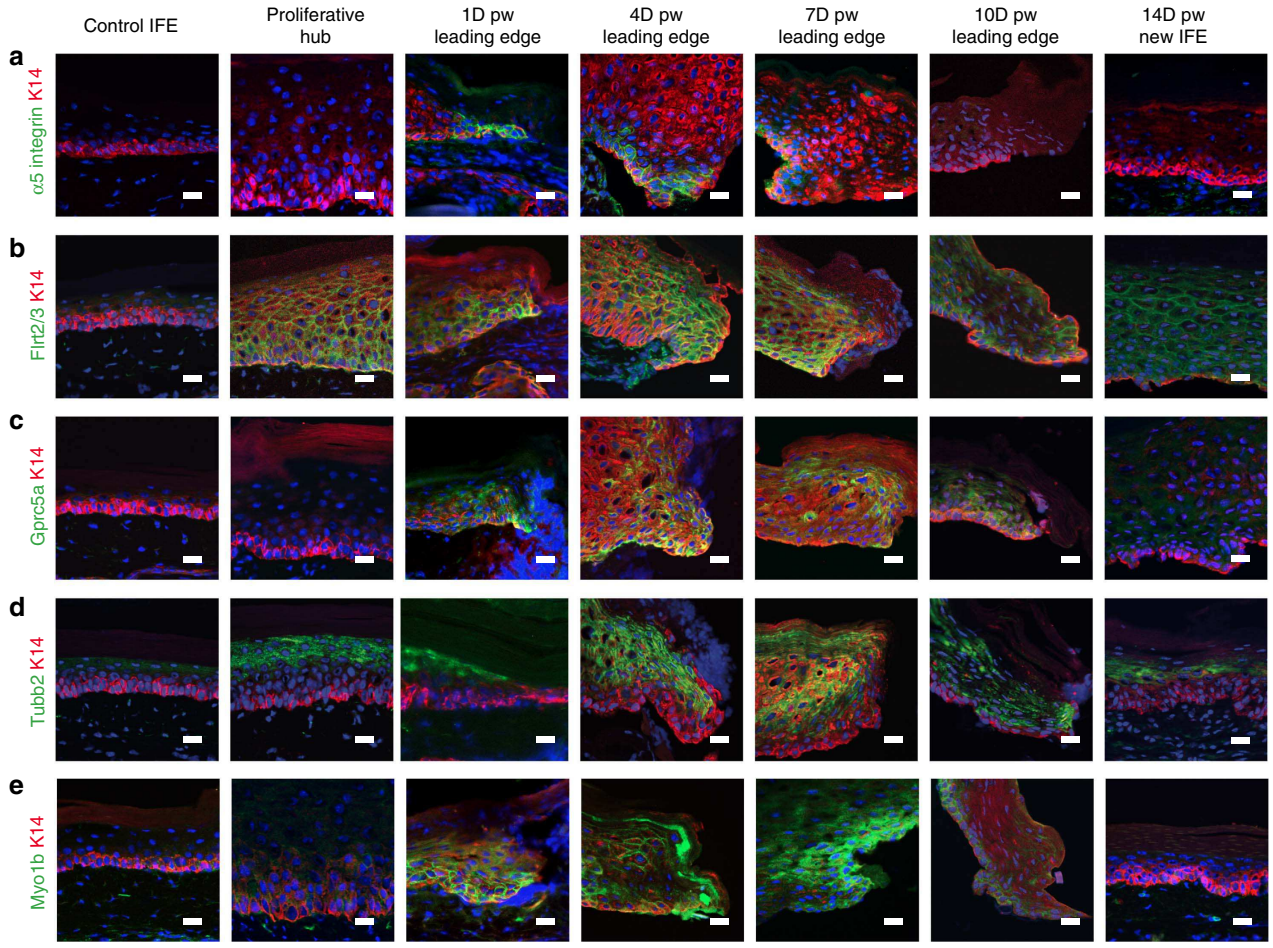

Figure 4 | Spatiotemporal expression of the LE signature during WH. (**a**) Representative immunofluorescence of α5-integrin (green) on skin section showing a strong and transient expression of Itgα5 in the basal cells of the LE at D1, D4 and D7 after wound. (**b**) Representative immunofluorescence of Flrt2/3(green) on skin section showing its expression in the proliferative hub and the LE in basal and suprabasal cells from 1 to 7 days after wound and progressively decreasing 10 and 14 days after wound. (**c**) Representative immunofluorescence of Gprc5a (green) on skin sections showing its overexpression in the basal and suprabasal cells at the LE at the different time points. (**d**) Representative immunofluorescence of Tubb2 (green) showing its higher expression in the suprabasal cells both in the proliferative hub and the LE after wound. (**e**) Representative immunofluorescence for Myo1b (green) showing positive signal in the cells of the LE from D1 to D7. In all the pictures from **a**–**e** K14 is in red and the nuclei are stained with Hoechst (blue). Scale bar, 20 μm.

progenitors leading to basal cell expansion. Interestingly, these streaks originate from a minority (>1%) of K14CREER-induced cells and seem to be responsible for only part of the wound regeneration (for details see Supplementary Note 1).

It has been proposed that, during wounding, differentiated suprabasal cells can revert back to a progenitor state and actively contribute to repair[57,58]. To test this possibility, we administrated TAM to *InvCREER/RosaYFP* that labelled suprabasal cells and rare basal cells (Supplementary Fig. 5a,b), performed a punch biopsy and analysed the contribution of labelled suprabasal cells during wounding. Ten days after wounding, most of the lineage labelled suprabasal cells had been shed from the skin surface or remained present as spinous or granular cells. Despite the high frequency of suprabasal cell labelling, we found only very rare basal cells initially targeted by the InvCREER, and these contribute minimally and transiently to the wound repair as previously described[3]. We found no evidence that suprabasal cells can revert back to a progenitor-like state, as the density of basal cells contributing to the wound repair is much lower compared to that of basal cells labelled at induction (Supplementary Fig. 5a,b). These data suggest that dedifferentiation of differentiated suprabasal cells does not contribute to WH in the tail epidermis.

Clonal analysis of infundibulum SC during WH. To assess whether different types of SCs arising from distinct epidermal regions present different clonal dynamics during WH, we performed clonal analysis on *Lrig1CREER/Rosa Confetti* mice targeting the upper HF SCs that include cells from the infundibulum, junctional zone and sebaceous gland, and that have been shown to contribute to WH[8] (Fig. 7a,b). At D14, most of the Lrig1-labelled cells give rise to long streaks of progeny from the infundibulum to the LE (Fig. 7c) with the clones presenting the same fragmentation reported for the K14 tracing (Figs 6d,e and 7c). The 3D reconstruction showed that the Lrig1 clones, starting from D7, had an analogous cellular composition as the K14 with long streak of basal and suprabasal cells emanating from the infundibulum and directed toward the wound centre (Fig. 7d–f).

Similar clonal dynamic of different epidermal SCs during WH. To gain further insight into the clonal dynamics of the IFE and the HF-derived SCs populations, we used a previously validated biostatistical framework[59–61] to infer with high confidence the number of cells and cellular composition of clones (basal versus suprabasal cells) arising from single *K14* and

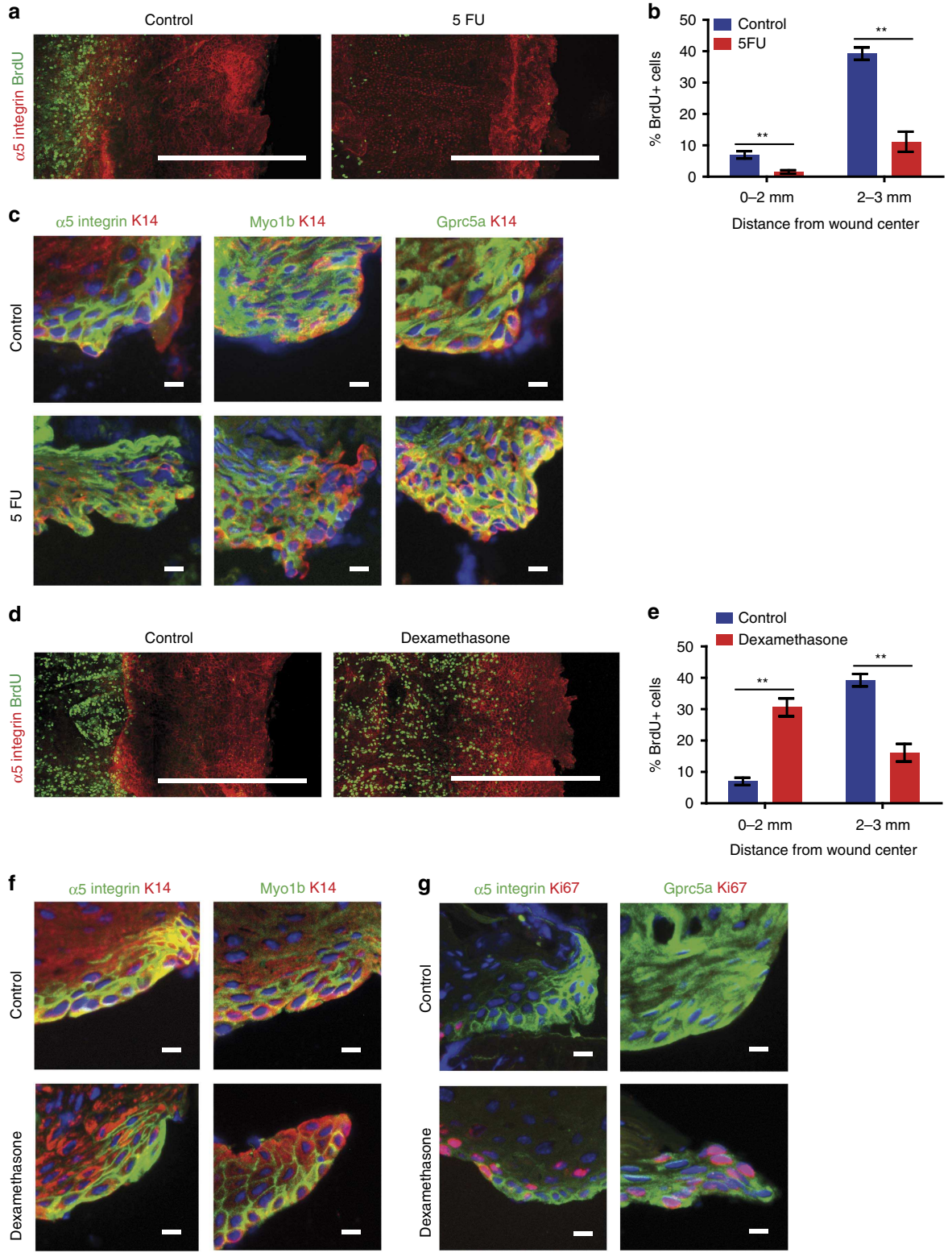

Figure 5 | Mechanisms regulating the formation of the LE during WH. (**a**) Maximum intensity projection of representative confocal pictures of untreated (control) and 5-FU-treated mice (right). Scale bar, 500 μm. (**b**) Quantification of the percentage of BrdU positive cells in the LE (0–2 mm) and the proliferative hub (2–3 mm) of untreated (control) and 5-FU-treated mice (**$P = 0.0079$ by Mann–Whitney test, $n = 5$ mice). (**c**) Representative immunostaining of skin sections showing the presence of the α5-integrin, Myo1b and Gprc5a (green), and K14 (red) at the LE in normal wound and after 5-FU treatment. Scale bar, 10 μm. (**d**) Maximum intensity projection of representative confocal pictures showing whole-mounted epidermis stained for α5-integrin (red) and BrdU (green) 4 days after wound under normal condition (left) and after anti-inflammatory treatment with dexamethasone (right). Scale bar, 500 μm. (**e**) Quantification of the percentage of BrdU positive cells in the LE (0–2 mm) and the proliferative hub (2–3 mm) of untreated and dexamethasone-treated mice (**$P = 0.0079$ by Mann–Whitney test, $n = 5$ mice). (**f**,**g**) Representative immunostaining on skin sections showing the expression of the α5-integrin, Myo1b (green) and K14 (red) (**f**), and the expression of α5-integrin, Gprc5a (green) and Ki67 (red) (**g**) at the LE in untreated and dexamethasone-treated mice. Scale bar, 10 μm.

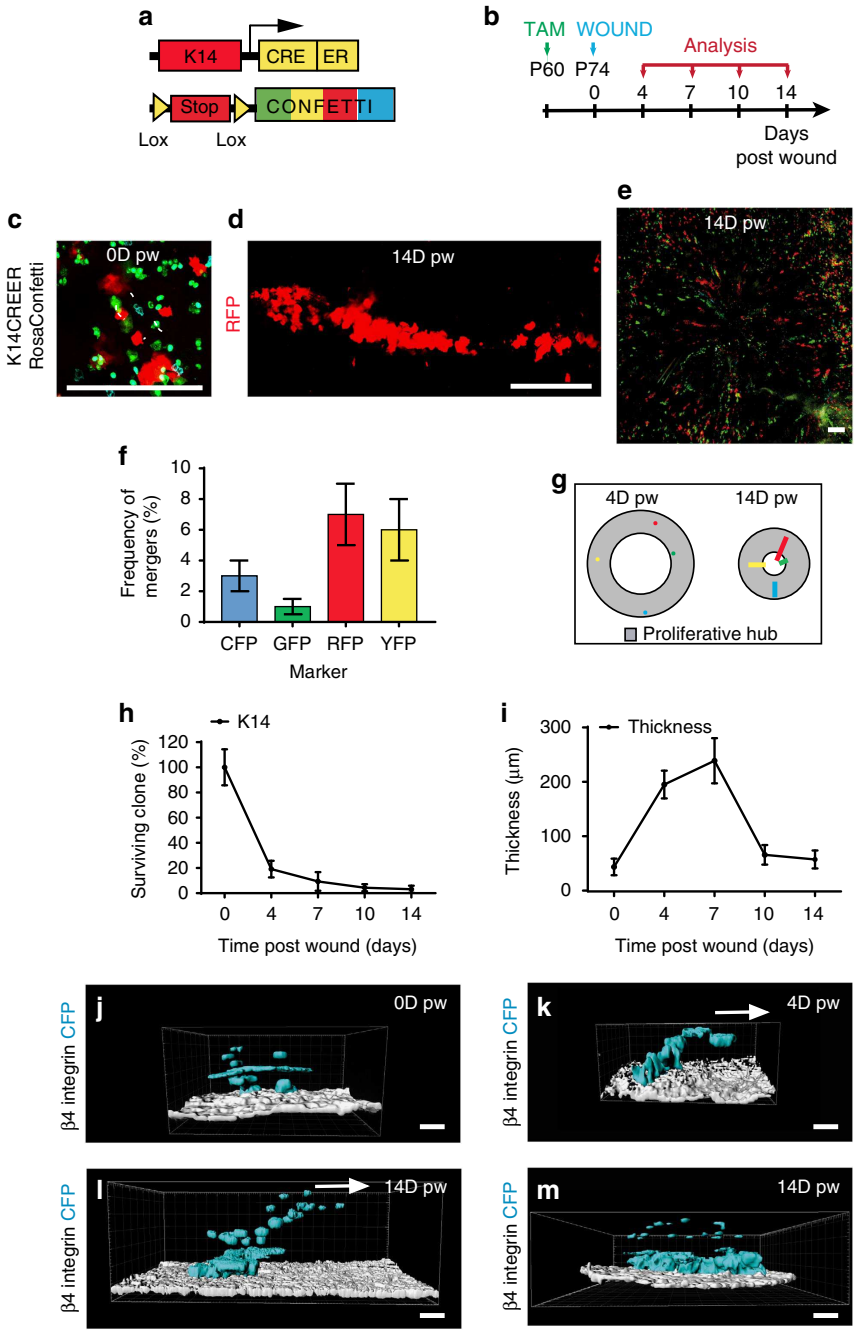

Figure 6 | Clonal analysis of IFE SC and progenitors during WH. (**a**) Genetic labelling strategy used to trace K14 IFE progenitors during WH. (**b**) Time line of the wound experiment. *K14CREER/RosaConfetti* mice were induced with Tamoxifen at 2 months of age and wounded 2 weeks after. The samples were collected 0, 4, 7, 10 and 14 days after wound. (**c**,**d**) Maximum intensity projection of representative confocal pictures showing K14CREER clones 0 days (**c**) and 14 days (**d**) after wound. (**e**) Maximum intensity projection of a representative confocal picture showing whole-mounted wounded epidermis from *K14CREER RosaConfetti* 14 days after wound. Scale bar, 500 µm. (**f**) Frequency of mergers calculated for each confetti colour. (**g**) Representative scheme showing the position of the clones (coloured dots) in the proliferative hub (grey area) 4 days after wound and the streaks they form 14 days after wound (coloured lines). (**h**) Quantification of the percentage of K14CREER surviving clones overtime after wound showing the massive loss of basally attached clones between day 0 and day 4 post wound. (**i**) Measure of the thickness of the epidermis in the proliferative hub 0, 4, 7, 10 and 14 days after wound. (**j**–**m**) 3D reconstruction using Imaris software of representative *K14CREER RosaConfetti* CFP clones imaged by confocal microscopy during WH. To identify the basal cells attached to the basal lamina, samples were stained for b4 integrin (white). In the control unwounded area (**j**), suprabasal cells are found on the top of basal cells. The picture shows a clone composed of 11 cells, 4 basal and 7 suprabasal cells. In contrast, during healing, the newly produced suprabasal cells are migrating on the top of basal cells toward the wound centre (on the right) (**k**–**m**). In **k**, the clone has the same size as the control (11 cells) but has more suprabasal cells (9 suprabasal and only 2 basal cells). The clone at D14 shown in **l** has expanded to reach 39 cells in total (4 of them are basal cells). In **m**, another clone by contrast expanded basally (83 total cell size, 33 basal cells) at D14 post wound. Arrows indicate cell movement. Scale bar, 20 µm.

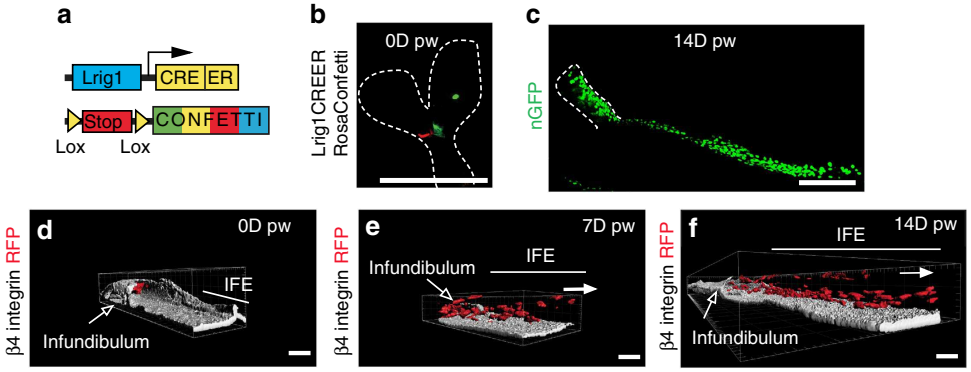

Figure 7 | Clonal analysis of infundibulum SC during WH. (**a**) Genetic labelling strategy used to trace Lrig1 upper HF cells during WH. (**b**,**c**) Maximum intensity projection of representative confocal pictures showing Lrig1CREER clones 0 days (**b**) and 14 days (**c**) after wound. (**d**–**f**) 3D reconstruction of RFP (red) positive Lrig1-targeted clones with Imaris software. The β4-integrin (white) is marking the basal side. Initially and in normal conditions, Lrig1-targeted clone is confined in the upper part of the HF/infundibulum (**d**). Upon wound, the progeny of the clone is moving outside of the HF/infundibulum and lines of cells can be seen in the IFE 7 days (**e**) and 14 days after wound (**f**). The white arrows show the direction of the wound. Scale bar, 50 μm.

Lrig1CREER/Rosa Confetti-targeted cells (Fig. 8a–e; Supplementary Note 1). To define how SCs balance proliferation and differentiation in the proliferative hub surrounding the wound edge, we analysed the clonal composition of *K14* and *Lrig1CREER/Rosa Confetti*-derived clones from D0 to D14 after wounding. From D4 to D14, the basal size of clones of both K14 and Lrig1CREER grew remarkably linearly (Fig. 8a,c). At first sight, this behaviour could indicate neutral competition, as has been reported for uninjured epidermis[12,62]. However, adapting the standard model of balanced stochastic progenitor cell fate, the observed rate of increase in the average basal size would translate to an unreasonably fast cell cycle time of >6 h. Rather, in this case, the linear increase indicates the labelling of an asymmetrically dividing subpopulation that drives the basal expansion through the steady production of progenitors (Supplementary Note 1). On the basis of the quantitative clonal analysis, we find that the data are consistent with a proliferative hierarchical model in which, during WH, a putative SC population at the apex divide perfectly asymmetrically giving rise to self-renewing progenitors in which the frequency of symmetrical duplication is balanced by symmetrical differentiation (Fig. 8f). Indeed, the existence of a persistent (SC) and a transient (progenitor) basal subpopulation might explain the fragmentation of clonal streaks. From the modelling of the clonal dynamics, we found that such model indeed predicts not only the increase in average basal clone size (Fig. 8c) but also recapitulates the detailed distributions of basal clones sizes in the K14CREER assay (Fig. 8d; Supplementary Note 1). Notably, such a hierarchical model coincides with that inferred from the study of homoeostatic turnover of interscale epidermis, but where the proliferation rate of SCs and progenitors have been massively increased[54]. Surprisingly, the conserved linearity of the average basal clone size and the shape of the size distribution suggested that Lrig1CREER targets SCs belonging to the same hierarchy as that targeted by K14CREER, but where a burst of proliferative activity at the earliest stages of regeneration expands the average number of SCs in each clone (Fig. 8c–f; Supplementary Note 1). Altogether, these data suggest that, irrespective of the epidermal origin, the regenerative stage of WH involves a sustained increase in proliferative activity of a minority of SCs, while keeping the fate behaviour and lineage relationship of SCs and progenitors largely unperturbed from their homoeostatic dependences.

Discussion

Our study uncovers the clonal dynamics and individual contribution of SCs coming from different epidermal compartments during skin WH in mice. In contrast to what has been proposed for oesophagus repair and the growth of human keratinocytes *in vitro*[55,56], our data show that WH does not increase the self-renewal capacities of progenitors, but rather leads to their massive depletion as proliferation increases. The repair of the skin epidermis does not induce a change in the cellular hierarchy of SCs and progenitors, or a change in the balance between renewal and differentiation but rather involves an increase in the proliferation rate of a small population of SCs that gives rise to progenitors upon asymmetric division leading to a linear increase in the individual clone size over time. Interestingly, IFE and infundibulum SCs present very similar clonal dynamics during wound repair, despite the fact that they are recruited from different regions of the epidermis.

Our study confirms the existence of two distinct epidermal zones during wound repair; a proliferative hub composed of the IFE and HF-derived SCs and their progeny and a LE composed of non-proliferative cells[3], and uncovers the timing, gene expression signature and mechanisms that specify these two distinct compartments during WH (Fig. 9). We propose that the non-proliferative LE of the wound acts as a scaffold allowing a harmonious healing process, by creating a platform secreting high level of enzymes that remodel the surrounding ECM and fibrin clot allowing tissue regeneration to progress toward the centre of the wound and protecting the SCs and their progeny from the immediate vicinity of the wound front and infection.

A similar wound margin structure with elongated migrating cells has been described during the early stages of WH following incisional wound in humans[63], supporting the notion that this mode of wound repair has been conserved during evolution. Further functional studies will be needed to refine the respective role of the genes identified here in the LE signature. The high level of expression of several of these genes in patients with chronic ulcers[64,65] suggests that defects in the formation and/or function of this structure may induce wound-healing problems leading to chronic ulcer formation.

Methods

Mice. *K14CREER* transgenic mice were provided by Fuchs[66]. *Lrig1-CreERT2* mice were a kind gift from Jensen[67]. *Involucrin-CreERT2* were previously described[12]. *Rosaconfetti* mice were provided by Clevers[68]. *Rosa YFP*[69] mice were obtained from Jackson Laboratory. All animals were mixed strains. No statistical methods were used to predetermine sample size. The experiments were not randomized. The investigators were not blinded to allocation during experiments and outcome assessment. Mice colonies were maintained in a certified animal facility in accordance with European guidelines. The experiments were approved by the local ethical committee (CEBEA).

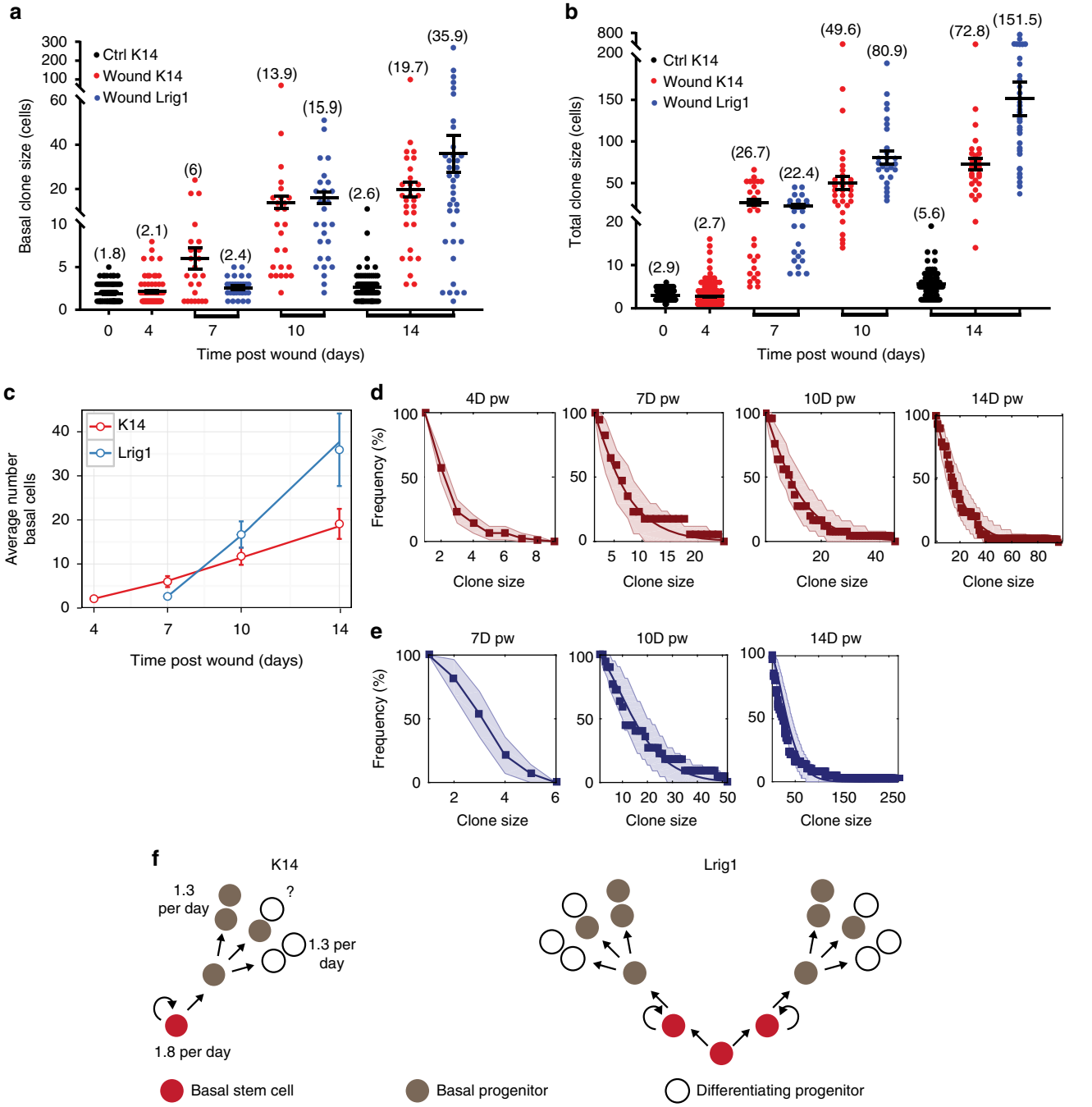

Figure 8 | Distinct epidermal stem cells present similar clonal dynamic during WH. (**a**,**b**) Clone size distribution showing the number of basal cells (**a**) and the total number of cells (**b**) per clone counted in *K14CREER* and *Lrig1CREER RosaConfetti* mice. (**c**) Average number of basal cells per clone in K14CREER (red) and Lrig1CREER (blue) clones. Solid lines are model predictions. The linear growth of both populations suggests that the stem cells fate outcomes are balanced but Lrig1 SCs achieved at the beginning one more symmetric division initially than K14 SCs. (**d**,**e**) Cumulative frequencies of K14CREER (**d**) and Lrig1CREER (**e**) basal clone size at different days after wound (dots). Solid lines give the model prediction and shaded areas denote the uncertainty of the model given the experimental data (95% confidence intervals). (**f**) Model of SC and progenitors cell fate outcome in IFE for K14 (left) and Lrig1 (right) populations during WH. K14-targeted SCs (red, left panel) divide asymmetrically 1.8 ($+0.6$; -0.3) times per day and give rise to progenitors (grey, left panel) that divide 1.3 ($+1.1$; -0.6) times per day which then give rise to differentiated cells following a balanced cell fate outcome. Lrig1-targeted SCs (red, right panel) achieve initially one symmetrical division and then asymmetrical divisions giving rise to progenitors (left grey) which follows the same cell fate outcome as described for K14 SCs.

Targeting Confetti or YFP expression in wound experiments. For lineage tracing experiment, *K14CreER/RosaConfetti*, *Lrig1-CreERT2/RosaConfetti* and *Involucrin-CRERT2/Rosa-YFP* male and female adult (between 2 and 6 months old) mice were induced at 2 months with 0.03 mg g^{-1}, 0.27 mg g^{-1} or 0.08 mg g^{-1} of TAM (Sigma-Aldrich), respectively, by intra-peritoneal (IP) injection. For K14-CreER and Lrig1-CreERT2 tracing, 2 weeks after TAM induction, mice were anesthetized (5% xylazine 10% ketamine in PBS) and circular pieces of epidermis were removed from the tail epidermis using a 3 mm diameter biopsy punch (Stiefel, Ireland). For *Involucrin-CRERT2/Rosa-YFP* mice the wound was performed 4 days after TAM injection to analyse the contribution of suprabasal cells. Each mouse was subjected to three different punches in the tail and at least five mice per time points were analysed.

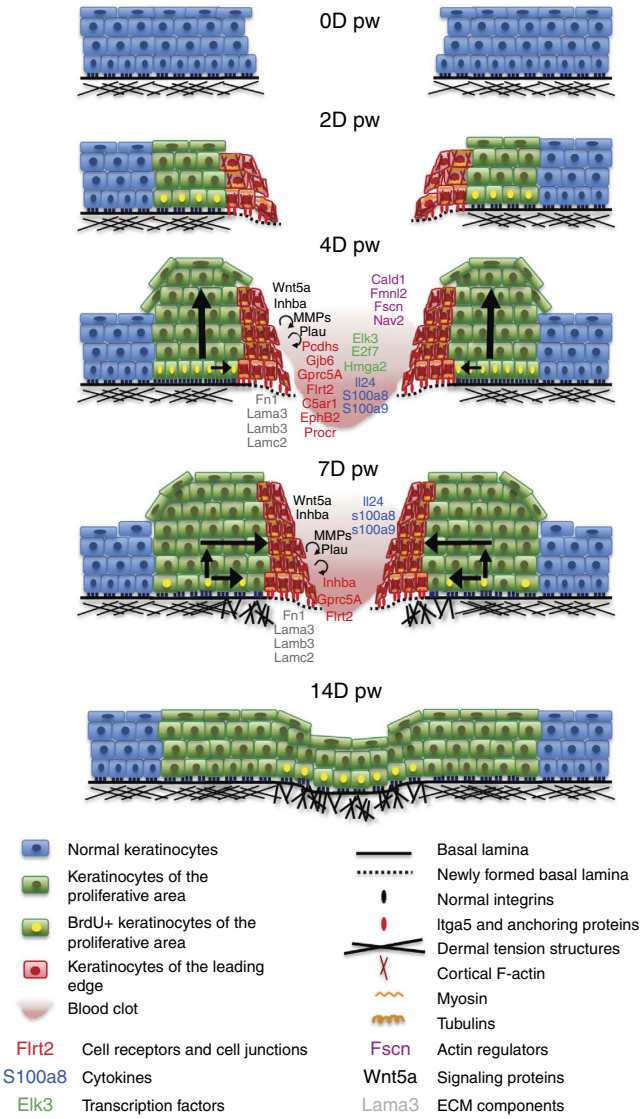

Figure 9 | Model of WH in mice. Cartoons representing the different steps occurring during re-epithelialization of WH. Important genes expressed preferentially during wounding are highlighted. The arrows represent the movement of cells from the basal to the suprabasal compartment including their suprabasal migration.

Proliferation experiments. For BrdU experiments, CD1 male and female adult (between 2 and 6 months old) mice were wounded, injected with one single injection IP of BrdU (50 mg kg^{-1} in PBS) at the different time points and killed 4 h after. For the quantification at least an area of 1.5 mm^2 per region per wound was analysed with Imaris software (Bitplane) to determine the percentage of BrdU positive cells.

Epidermal whole-mount and immunostaining. Pieces of skin tail surrounding the wound were incubated in PBS/EDTA (20 mM) on a rocking plate at 37 °C for 1 h. Epidermis was separated from the dermis using forceps as an intact sheet and washed two times with PBS. Pieces of epidermis were pre-fixed in 4% paraformaldehyde for 1 h at room temperature. Epidermis were rinsed two times with PBS for 5 min and conserved in PBS with 0.2% azide at 4 °C. For the immunofluorescence staining, the entire pieces of epidermis were incubated in blocking buffer (1% BSA, 5% horse serum, 0.8% Triton in PBS) for 3 h at room temperature on a rocking plate (100 r.p.m.). The samples were incubated in primary antibodies overnight at 4 °C. The primary antibodies used were the following: anti-Integrinβ4 (rat, 1:200, BD Biosciences), anti-K14 (chicken, 1:2,000, custom batch, Thermo Fischer), anti-GFP (rabbit, 1:200, Molecular Probes). Samples were then washed three times in PBS with 0.2% tween during 1 h and incubated in appropriate secondary antibodies diluted 1:400 in blocking buffer for 1 h at room temperature on the rocking plate. For BrdU staining, samples were incubated in HCl 1 M at 37 °C for 45 min, washed with PBS 0.2% tween, stained with anti-BrdU (rat, 1:200, Abcam) in blocking buffer and with appropriate secondary antibody. The following secondary antibodies were used: anti-rat, anti-chicken, anti-rabbit conjugated to AlexaFluor488 (Molecular Probes), to Rhodamine Red-X or to Cy5 (Jackson Immuno Research). Alexa488-conjugated phalloidin (Life Technologies) was used 1:200 in blocking buffer to visualize F-actin microfilaments. Nuclei were stained in Hoechst solution diluted 1:5,000 for 30 min and mounted in DAKO-mounting medium supplemented with 2.5% Dabco (Sigma). Immunostaining pictures of the whole mounts presented in the figures are representative images of at least five different experiments.

Microscope image acquisition and measurements. All pictures of section immunostaining were acquired using the Axio Imager M1 Microscope, the AxioCamMR3 or MrC5 camera and using the Axiovision software (Carl Zeiss). Acquisitions were performed at room temperature using ×20 numerical aperture (NA) 0.4 (Carl Zeiss). All confocal images were acquired at room temperature with a LSM780 confocal system fitted on an AxioExaminer Z1 upright microscope equipped with C-Apochromat ×40/1.1 or Plan Apochromat ×25/0.8 water immersion objectives (Zeiss, Iena, Germany). Optical sections 512 × 512 pixels were collected sequentially for each fluorochrome. The data sets generated were merged and displayed with the ZEN2012 software (Zeiss). 3D reconstitution images were processed using Imaris (Bitplane) software.

Histology and immunostaining on sections. Skin epidermis was removed from tailbone, embedded in OCT and kept at −80 °C. Sections of 6 µm were cut using a CM3050S Leica cryostat (Leica Mycrosystems). After fixation in 4% paraformaldehyde for 10 min at room temperature, tissues were washed three times in PBS for 5 min and incubated in blocking buffer (1% BSA, 5% Horse serum, 0, 2% Triton in PBS) for 1 h at room temperature. Primary antibodies were incubated overnight at 4 °C. Sections were rinsed three times in PBS and incubated with secondary antibodies and Hoechst in blocking buffer for 1 h at room temperature. Sections were again washed three times with PBS. The following primary antibodies were used: anti-K14 (chicken, 1:20,000, custom batch, Thermo Fischer); anti-K6 (rabbit, 1:6,000, Covance), anti-Flrt2/3 (rabbit, 1:100, Sigma); anti-Gprc5a (rabbit, 1:100, Sigma); anti-Myo1b (rabbit, 1:100, Sigma) and anti-α5-integrin (PE-conjugated rat, 1:200, BD or rabbit, 1:200, Abcam). For the anti-Tubb2 (rabbit, 1/1,000, Abcam) staining, fixation was performed in methanol at −20 °C for 2.5 min and the rest of the protocol was performed as described. The following secondary antibodies were used diluted to 1:400: anti-rabbit, anti-rat, anti-chicken conjugated to Alexa Fluor 488 (Molecular Probes), to rhodamine Red-X (Jackson Immunoresearch) or to Cy5 (Jackson Immunoresearch). Nuclei were stained in Hoechst solution (1:2,000) and slides were mounted in DAKO-mounting medium supplemented with 2.5% Dabco (Sigma). Immunostaining pictures of the skin sections presented in the figures are representative images of at least five different experiments.

Dissociation of epidermal cells and cell sorting. The dermis and epidermis were removed from the tail bone and micro dissection was performed using two different sizes of punch biopsy: one punch of 4 mm in diameter was done, around the wound of 3 mm in diameter, to remove the LE zone and one punch of 6 mm in diameter was used to remove the proliferative centre, at D4 and D7 after wound. Another piece of skin was taken, as control, from a region far from the wounded area. The two replicate samples at each time points were a pull of five CD1 mice. The samples were incubated in HBSS (Gibco) 0,25% trypsin (Gibco) at 37 °C until the epidermis was separated from the dermis (30 min). Epidermis was then incubated on a rocking plate (100 r.p.m.) at room temperature for 5 min. Basal cells were mechanically separated from the epidermis by flushing 10 times under the epidermis. Tissues were then cut in small pieces with a scalpel and incubated again for 5 min on a rocking plate (100 r.p.m.) at room temperature. Trypsin was then neutralized by adding DMEM medium (Gibco) supplemented with 2% Chelex Fetal Calf Serum (FCS) and the cells were mechanically separated by pipetting 90 times and filtrated on 70 µm filter (Falcon). Cells were incubated in 2% FCS/PBS with primary antibodies for 30 min on ice, protected from the light, with shaking every 10 min. Primary antibodies were washed with 2% FCS/PBS and cells incubated for 30 min in APC-conjugated streptavidin (BD Biosciences), on ice, with shaking every 10 min. Living epidermal cells were gated by forward scatter, side scatter and negative staining for Hoechst dye. For the first microarray analysis, basal IFE and infundibulum cells were stained using PE-conjugated anti-α6-integrin (clone GoH3; 1/200, ebioscience) and bulge cells were stained with biotinylated CD34 (clone RAM34; 1:50, BD Biosciences). Basal cells from the IFE were targeted using CD34 negative and α6-integrin positive gating. For the second microarray analysis, FITC-conjugated anti-α6-integrin (CD49f) (clone GoH3: 1:200, ebioscience) and PE-conjugated anti-α5-integrin (CD49e) (clone 5H10-27, 1:200, BD Bioscience) and biotinylated CD34 antibodies were used. The cells were sorted using CD34 negative α6-integrin positive α5-integrin positive gating. Before sorting, the cells were filtered again on 70 µm filter (Falcon). Fluorescence-activated cell sorting analysis was performed using FACSAria I at high pressure (70 psi) and FACSDiva software (BD Biosciences).

Microarray analysis. Sorted cells (300 cells per sample) were collected directly in 45 µl of lysis buffer (20 mM DTT, 10 mM Tris–HCl pH 7.4, 0.5% SDS, 0.5 µg µl^{-1}

proteinase K). Samples were then lysed at 65 °C for 15 min and frozen. RNA isolation, amplification and microarray were performed in the Functional Genomics Core, Barcelona. cDNA synthesis, library preparation and amplification were performed as described[70]. Microarrays were then performed on Mouse Genome 430 PM strip Affymetrix array at IRB Functional Genomics Core (Barcelona, Spain). The data were normalized using RMA algorithm. The entire procedure was repeated in three technical independent samples. Genetic signatures were obtained by considering genes presenting a fold change greater or smaller than 2 or −2, respectively, in each replicates. The accession number for the microarray data are GEO: GSE76795 and GSE93638.

5-FU and dexamethasone experiments. For the 5-FU experiments, mice were treated shortly after wound surgery with Efudix 5% cream (Meda Pharma) applied topically on the upper part of the tail three times per day until the sacrifice. For the dexamethasone experiments, dexamethasone powder (Sigma) was resuspended at 1 mg ml^{-1} in ethanol 100% and diluted 5 × in sterile PBS. The mice were injected intraperitoneally once per day at the dose of 1 mg kg^{-1}. The treatment started 2 days before the wound surgery and was sustained until the end of the experiment.

Data availability. Data supporting the findings of this study are available within the article (and its Supplementary Information files) and from the corresponding author on reasonable request. The accession number for the microarray data are GEO: GSE76795 and GSE93638.

References

1. Arwert, E. N., Hoste, E. & Watt, F. M. Epithelial stem cells, wound healing and cancer. *Nat. Rev. Cancer.* **12,** 170–180 (2012).
2. Gurtner, G. C., Werner, S., Barrandon, Y. & Longaker, M. T. Wound repair and regeneration. *Nature* **453,** 314–321 (2008).
3. Coulombe, P. A. Wound epithelialization: accelerating the pace of discovery. *J. Invest. Dermatol.* **121,** 219–230 (2003).
4. Plikus, M. V. *et al.* Epithelial stem cells and implications for wound repair. *Semin. Cell Dev. Biol.* **23,** 946–953 (2012).
5. Tumbar, T. *et al.* Defining the epithelial stem cell niche in skin. *Science* **303,** 359–363 (2004).
6. Ito, M. *et al.* Stem cells in the hair follicle bulge contribute to wound repair but not to homeostasis of the epidermis. *Nat. Med.* **11,** 1351–1354 (2005).
7. Jaks, V. *et al.* Lgr5 marks cycling, yet long-lived, hair follicle stem cells. *Nat. Genet.* **40,** 1291–1299 (2008).
8. Jensen, K. B. *et al.* Lrig1 expression defines a distinct multipotent stem cell population in mammalian epidermis. *Cell Stem Cell* **4,** 427–439 (2009).
9. Levy, V., Lindon, C., Harfe, B. D. & Morgan, B. A. Distinct stem cell populations regenerate the follicle and interfollicular epidermis. *Dev. Cell* **9,** 855–861 (2005).
10. Levy, V., Lindon, C., Zheng, Y., Harfe, B. D. & Morgan, B. A. Epidermal stem cells arise from the hair follicle after wounding. *Faseb J.* **21,** 1358–1366 (2007).
11. Snippert, H. J. *et al.* Lgr6 marks stem cells in the hair follicle that generate all cell lineages of the skin. *Science* **327,** 1385–1389 (2010).
12. Mascre, G. *et al.* Distinct contribution of stem and progenitor cells to epidermal maintenance. *Nature* **489,** 257–262 (2012).
13. Chen, L., Mirza, R., Kwon, Y., DiPietro, L. A. & Koh, T. J. The murine excisional wound model: contraction revisited. *Wound Repair Regen.* **23,** 874–877 (2015).
14. Ito, M. *et al.* Wnt-dependent de novo hair follicle regeneration in adult mouse skin after wounding. *Nature* **447,** 316–320 (2007).
15. Paladini, R. D., Takahashi, K., Bravo, N. S. & Coulombe, P. A. Onset of re-epithelialization after skin injury correlates with a reorganization of keratin filaments in wound edge keratinocytes: defining a potential role for keratin 16. *J. Cell Biol.* **132,** 381–397 (1996).
16. Weiss, R. A., Eichner, R. & Sun, T. T. Monoclonal antibody analysis of keratin expression in epidermal diseases: a 48- and 56-kdalton keratin as molecular markers for hyperproliferative keratinocytes. *J. Cell Biol.* **98,** 1397–1406 (1984).
17. Leigh, I. M. *et al.* Keratins (K16 and K17) as markers of keratinocyte hyperproliferation in psoriasis *in vivo* and *in vitro*. *Br. J. Dermatol.* **133,** 501–511 (1995).
18. Wojcik, S. M., Bundman, D. S. & Roop, D. R. Delayed wound healing in keratin 6a knockout mice. *Mol. Cell Biol.* **20,** 5248–5255 (2000).
19. Schafer, M. & Werner, S. Transcriptional control of wound repair. *Annu. Rev. Cell Dev. Biol.* **23,** 69–92 (2007).
20. Schelfhout, V. R. *et al.* The role of heregulin-alpha as a motility factor and amphiregulin as a growth factor in wound healing. *J. Pathol.* **198,** 523–533 (2002).
21. Poindexter, N. J. *et al.* IL-24 is expressed during wound repair and inhibits TGFalpha-induced migration and proliferation of keratinocytes. *Exp. Dermatol.* **19,** 714–722 (2010).
22. Kerkhoff, C. *et al.* Novel insights into the role of S100A8/A9 in skin biology. *Exp. Dermatol.* **21,** 822–826 (2012).
23. Barrandon, Y. & Green, H. Cell migration is essential for sustained growth of keratinocyte colonies: the roles of transforming growth factor-alpha and epidermal growth factor. *Cell* **50,** 1131–1137 (1987).
24. Marchisio, P. C., Bondanza, S., Cremona, O., Cancedda, R. & De Luca, M. Polarized expression of integrin receptors (alpha 6 beta 4, alpha 2 beta 1, alpha 3 beta 1, and alpha v beta 5) and their relationship with the cytoskeleton and basement membrane matrix in cultured human keratinocytes. *J. Cell Biol.* **112,** 761–773 (1991).
25. Larjava, H., Salo, T., Haapasalmi, K., Kramer, R. H. & Heino, J. Expression of integrins and basement membrane components by wound keratinocytes. *J. Clin. Invest.* **92,** 1425–1435 (1993).
26. Hertle, M. D., Kubler, M. D., Leigh, I. M. & Watt, F. M. Aberrant integrin expression during epidermal wound healing and in psoriatic epidermis. *J. Clin. Invest.* **89,** 1892–1901 (1992).
27. Guo, M. *et al.* Altered processing of integrin receptors during keratinocyte activation. *Exp. Cell Res.* **195,** 315–322 (1991).
28. Heller, E., Kumar, K. V., Grill, S. W. & Fuchs, E. Forces generated by cell intercalation tow epidermal sheets in mammalian tissue morphogenesis. *Dev. Cell* **28,** 617–632 (2014).
29. Stevens, L. J. & Page-McCaw, A. A secreted MMP is required for reepithelialization during wound healing. *Mol. Biol. Cell* **23,** 1068–1079 (2012).
30. Hattori, N. *et al.* MMP-13 plays a role in keratinocyte migration, angiogenesis, and contraction in mouse skin wound healing. *Am. J. Pathol.* **175,** 533–546 (2009).
31. Hartenstein, B. *et al.* Epidermal development and wound healing in matrix metalloproteinase 13-deficient mice. *J. Invest. Dermatol.* **126,** 486–496 (2006).
32. Madlener, M., Parks, W. C. & Werner, S. Matrix metalloproteinases (MMPs) and their physiological inhibitors (TIMPs) are differentially expressed during excisional skin wound repair. *Exp. Cell Res.* **242,** 201–210 (1998).
33. Okada, A. *et al.* Expression of matrix metalloproteinases during rat skin wound healing: evidence that membrane type-1 matrix metalloproteinase is a stromal activator of pro-gelatinase A. *J. Cell Biol.* **137,** 67–77 (1997).
34. Lund, I. K. *et al.* Concomitant lack of MMP9 and uPA disturbs physiological tissue remodeling. *Dev. Biol.* **358,** 56–67 (2011).
35. Nunan, R. *et al.* Ephrin-Bs drive junctional downregulation and actin stress fiber disassembly to enable wound re-epithelialization. *Cell Rep.* **13,** 1380–1395 (2015).
36. Hubner, G., Hu, Q., Smola, H. & Werner, S. Strong induction of activin expression after injury suggests an important role of activin in wound repair. *Dev. Biol.* **173,** 490–498 (1996).
37. Munz, B. *et al.* Overexpression of activin A in the skin of transgenic mice reveals new activities of activin in epidermal morphogenesis, dermal fibrosis and wound repair. *Embo J.* **18,** 5205–5215 (1999).
38. Beer, H. D. *et al.* Expression and function of keratinocyte growth factor and activin in skin morphogenesis and cutaneous wound repair. *J. Investig. Dermatol. Symp. Proc.* **5,** 34–39 (2000).
39. Wankell, M. *et al.* Impaired wound healing in transgenic mice overexpressing the activin antagonist follistatin in the epidermis. *Embo J.* **20,** 5361–5372 (2001).
40. Bamberger, C. *et al.* Activin controls skin morphogenesis and wound repair predominantly via stromal cells and in a concentration-dependent manner via keratinocytes. *Am. J. Pathol.* **167,** 733–747 (2005).
41. Antsiferova, M. *et al.* Keratinocyte-derived follistatin regulates epidermal homeostasis and wound repair. *Lab. Invest.* **89,** 131–141 (2009).
42. Lewis, C. J. *et al.* Bone morphogenetic protein signaling suppresses wound-induced skin repair by inhibiting keratinocyte proliferation and migration. *J. Invest. Dermatol.* **134,** 827–837 (2014).
43. Moll, I., Houdek, P., Schafer, S., Nuber, U. & Moll, R. Diversity of desmosomal proteins in regenerating epidermis: immunohistochemical study using a human skin organ culture model. *Arch. Dermatol. Res.* **291,** 437–446 (1999).
44. Gallinaro, H. *et al.* A 4.2kb upstream region of the human corneodesmosin gene directs site-specific expression in hair follicles and hyperkeratotic epidermis of transgenic mice. *J. Invest. Dermatol.* **122,** 730–738 (2004).
45. Tao, Q. *et al.* Identification of the retinoic acid-inducible Gprc5a as a new lung tumor suppressor gene. *J. Natl Cancer Inst.* **99,** 1668–1682 (2007).
46. Chen, Y. *et al.* Gprc5a deletion enhances the transformed phenotype in normal and malignant lung epithelial cells by eliciting persistent Stat3 signaling induced by autocrine leukemia inhibitory factor. *Cancer Res.* **70,** 8917–8926 (2010).
47. Zhong, S. *et al.* Lung tumor suppressor GPRC5A binds EGFR and restrains its effector signaling. *Cancer Res.* **75,** 1801–1814 (2015).
48. Endo-Munoz, L. *et al.* E2F7 can regulate proliferation, differentiation, and apoptotic responses in human keratinocytes: implications for cutaneous squamous cell carcinoma formation. *Cancer Res.* **69,** 1800–1808 (2009).
49. Blanpain, C., Lowry, W. E., Geoghegan, A., Polak, L. & Fuchs, E. Self-renewal, multipotency, and the existence of two cell populations within an epithelial stem cell niche. *Cell* **118,** 635–648 (2004).

50. Yamagishi, S. *et al.* FLRT2 and FLRT3 act as repulsive guidance cues for Unc5-positive neurons. *Embo J.* **30,** 2920–2933 (2011).
51. Sun, B. K., Siprashvili, Z. & Khavari, P. A. Advances in skin grafting and treatment of cutaneous wounds. *Science,* **346,** 941–945 (2014).
52. Sanchis, A. *et al.* Keratinocyte-targeted overexpression of the glucocorticoid receptor delays cutaneous wound healing. *PLoS ONE* **7,** 1–10 (2012).
53. Blanpain, C. & Simons, B. D. Unravelling stem cell dynamics by lineage tracing. *Nat. Rev. Mol. Cell Biol.* **14,** 489–502 (2013).
54. Sánchez-Danés, A. *et al.* Defining the clonal dynamics leading to mouse skin tumour initiation. *Nature* **536,** 298–303 (2016).
55. Doupe, D. P. *et al.* A single progenitor population switches behavior to maintain and repair esophageal epithelium. *Science* **337,** 1091–1093 (2012).
56. Roshan, A. *et al.* Human keratinocytes have two interconvertible modes of proliferation. *Nat. Cell Biol.* **18,** 145–156 (2016).
57. Fu, X., Sun, X., Li, X. & Sheng, Z. Dedifferentiation of epidermal cells to stem cells *in vivo*. *Lancet* **358,** 1067–1068 (2001).
58. Mannik, J., Alzayady, K. & Ghazizadeh, S. Regeneration of multilineage skin epithelia by differentiated keratinocytes. *J. Invest. Dermatol.* **130,** 388–397 (2010).
59. Lescroart, F. *et al.* Early lineage restriction in temporally distinct populations of Mesp1 progenitors during mammalian heart development. *Nat. Cell Biol.* **16,** 829–840 (2014).
60. Chabab, S. *et al.* Uncovering the number and clonal dynamics of Mesp1 progenitors during heart morphogenesis. *Cell Rep.* **14,** 1–10 (2016).
61. Wuidart, A. *et al.* Quantitative lineage tracing strategies to resolve multipotency in tissue-specific stem cells. *Genes Dev.* **30,** 1261–1277 (2016).
62. Clayton, E. *et al.* A single type of progenitor cell maintains normal epidermis. *Nature* **446,** 185–189 (2007).
63. Odland, G. & Ross, R. Human wound repair. I. Epidermal regeneration. *J. Cell Biol.* **39,** 35–151 (1968).
64. Rayment, E. A., Upton, Z. & Shooter, G. K. Increased matrix metalloproteinase-9 (MMP-9) activity observed in chronic wound fluid is related to the clinical severity of the ulcer. *Br. J. Dermatol.* **158,** 951–961 (2008).
65. Shih, B. *et al.* Identification of biomarkers in sequential biopsies of patients with chronic wounds receiving simultaneous acute wounds: a genetic, histological, and noninvasive imaging study. *Wound Repair Regen.* **20,** 757–769 (2012).
66. Vasioukhin, V., Degenstein, L., Wise, B. & Fuchs, E. The magical touch: genome targeting in epidermal stem cells induced by tamoxifen application to mouse skin. *Proc. Natl Acad. Sci. USA* **96,** 8551–8556 (1999).
67. Page, M. E., Lombard, P., Ng, F., Gottgens, B. & Jensen, K. B. The epidermis comprises autonomous compartments maintained by distinct stem cell populations. *Cell Stem Cell* **13,** 471–482 (2013).
68. Snippert, H. J. *et al.* Intestinal crypt homeostasis results from neutral competition between symmetrically dividing Lgr5 stem cells. *Cell* **143,** 134–144 (2010).
69. Srinivas, S. *et al.* Cre reporter strains produced by targeted insertion of EYFP and ECFP into the ROSA26 locus. *BMC Dev. Biol.* **1,** 4 (2001).
70. Gonzalez-Roca, E. *et al.* Accurate expression profiling of very small cell populations. *PLoS ONE* **5,** e14418 (2010).

Acknowledgements

We would like to thank J.-M. Vanderwinden and the LiMiF for the help with confocal microscopy. C.B. is an investigator of WELBIO. M.A. and S.D. are supported by a long-term fellowship of the HFSPO and a TELEVIE fellowship, respectively. This work was supported by the FNRS, TELEVIE, the PAI programme, a research grant from the Fondation contre le Cancer, the ULB fondation, the foundation Bettencourt Schueller, the foundation Baillet Latour and a consolidator grant the European Research Council (ERC-EXPAND).

Author contributions

M.A., S.D. and C.B. designed the experiments and performed data analysis; M.A., S.D. performed most of the experiments; S.L. provided technical support. G.M. made initial observations pertinent to the study. S.R. and B.D.S. performed the mathematical modelling and statistical analysis of the clonal data.

Additional information

Supplementary Information accompanies this paper at http://www.nature.com/naturecommunications

Competing financial interests: The authors declare no competing financial interests.

Reprints and permission information is available online at http://npg.nature.com/reprintsandpermissions/

How to cite this article: Aragona, M. *et al.* Defining stem cell dynamics and migration during wound healing in mouse skin epidermis. *Nat. Commun.* **8,** 14684 doi: 10.1038/ncomms14684 (2017).

Publisher's note: Springer Nature remains neutral with regard to jurisdictional claims in published maps and institutional affiliations.

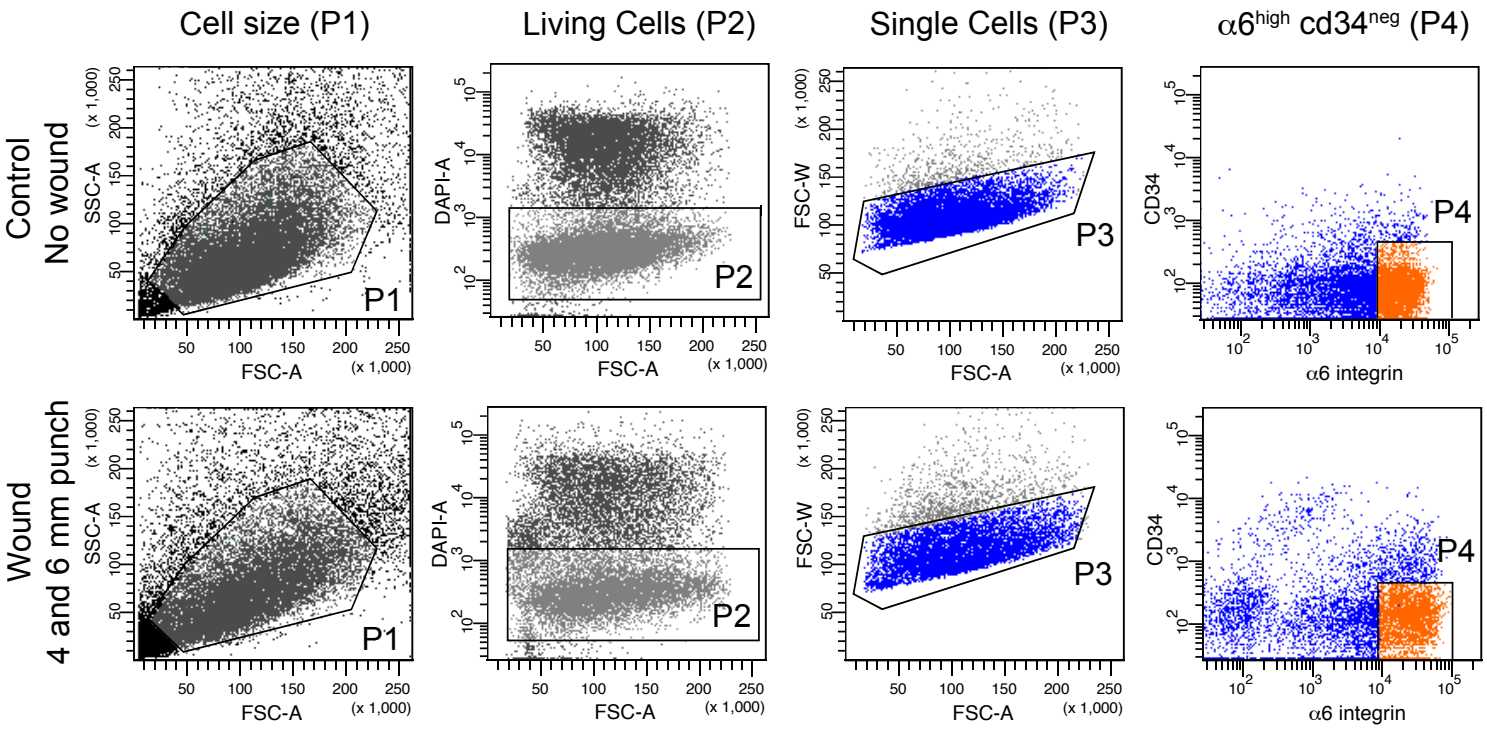

Supplementary Figure 1. FACS strategy used to isolate basal cells from the LE and the proliferative hub 4 and 7 days after wound.

Representative FACS plots showing the strategy used to isolate basal cells from the LE and the Proliferative hub. 4 and 7 days after wound, pieces of tail skin located far from the wound (control) and surrounding the wound obtained with the 6mm (proliferative hub) and the 4mm (leading edge) punches were dissociated by enzymatic and mechanical separation. Isolated epidermal cells were stained with α 6 integrin and CD34 antibodies. Single living cells were gated by debris exclusion (P1), DAPI exclusion (P2), doublet elimination (P3) and basal IFE $\alpha6^{high}$ $CD34^{neg}$ cells were sorted (P4).

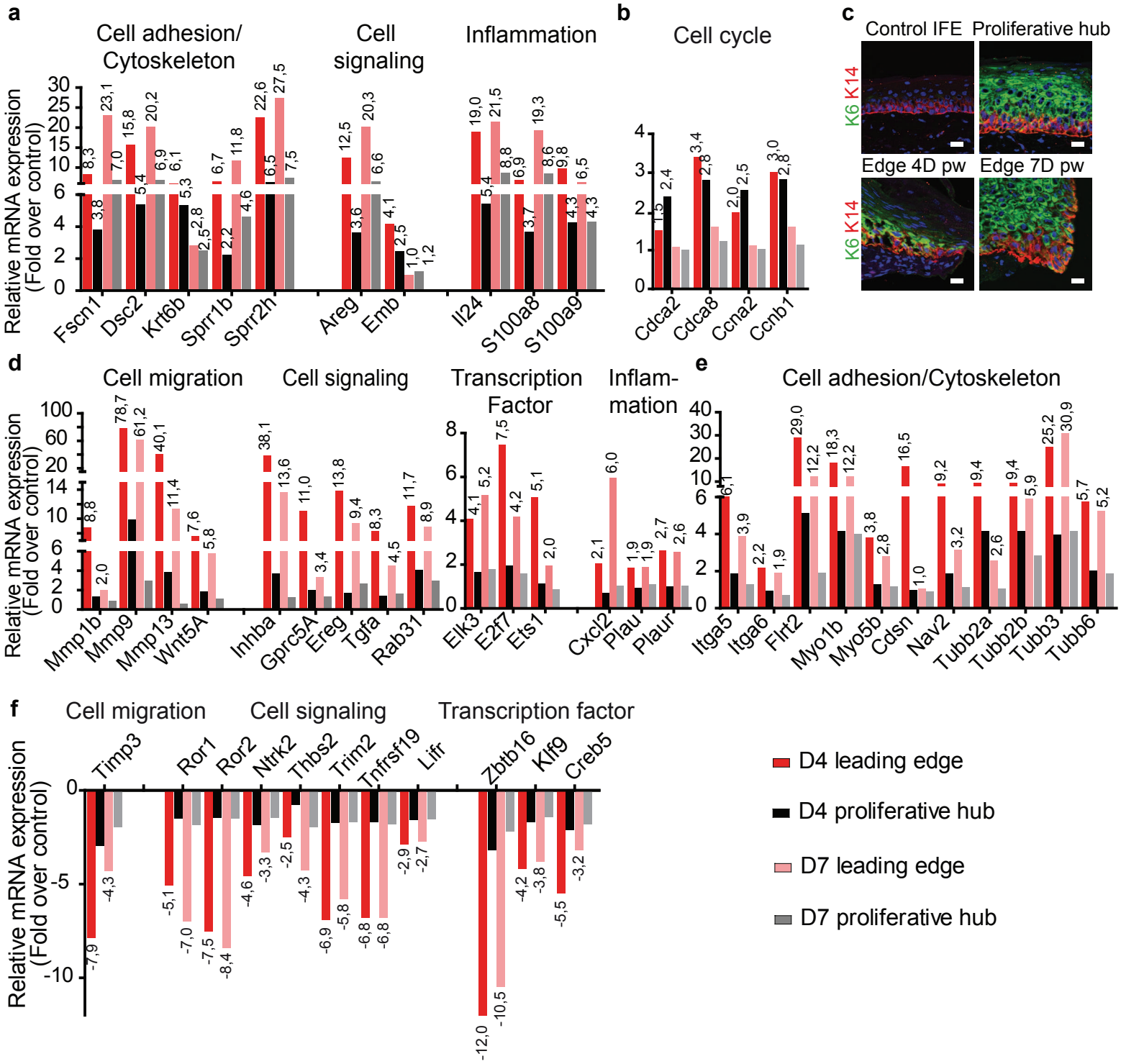

Supplementary Figure 2. Gene expression in the proliferative hub and leading edge as a wound signature.

a-**b**, Relative expression measured by microarray of genes upregulated in both proliferative hub and LE 4 and 7 days after wound. These genes are implicated in cell adhesion and cytoskeleton, cell signaling, inflammation (**a**) or cell cycle regulation (**b**). The fold changes are presented over the control (n=2). **c**, Immunofluorescence showing the expression of K6 (green) and K14 (red) on sections of epidermis in the proliferative hub and the leading edge 4 and 7 days after wound. Scale bar = 20µm. **d**-**e**, Relative expression measured by microarray of genes more specifically up regulated in the leading edge compared to the proliferative hub 4 and 7 days after wound. The genes are implicated in cell migration, cell signaling, transcription, inflammation (**d**) as well as cell adhesion and cytoskeleton (**e**). The fold changes are presented over the control (n=2). **f**, Relative expression of genes down regulated in the leading edge compared to the proliferative hub 4 and 7 days after wound. The fold changes are presented over the control (n=2).

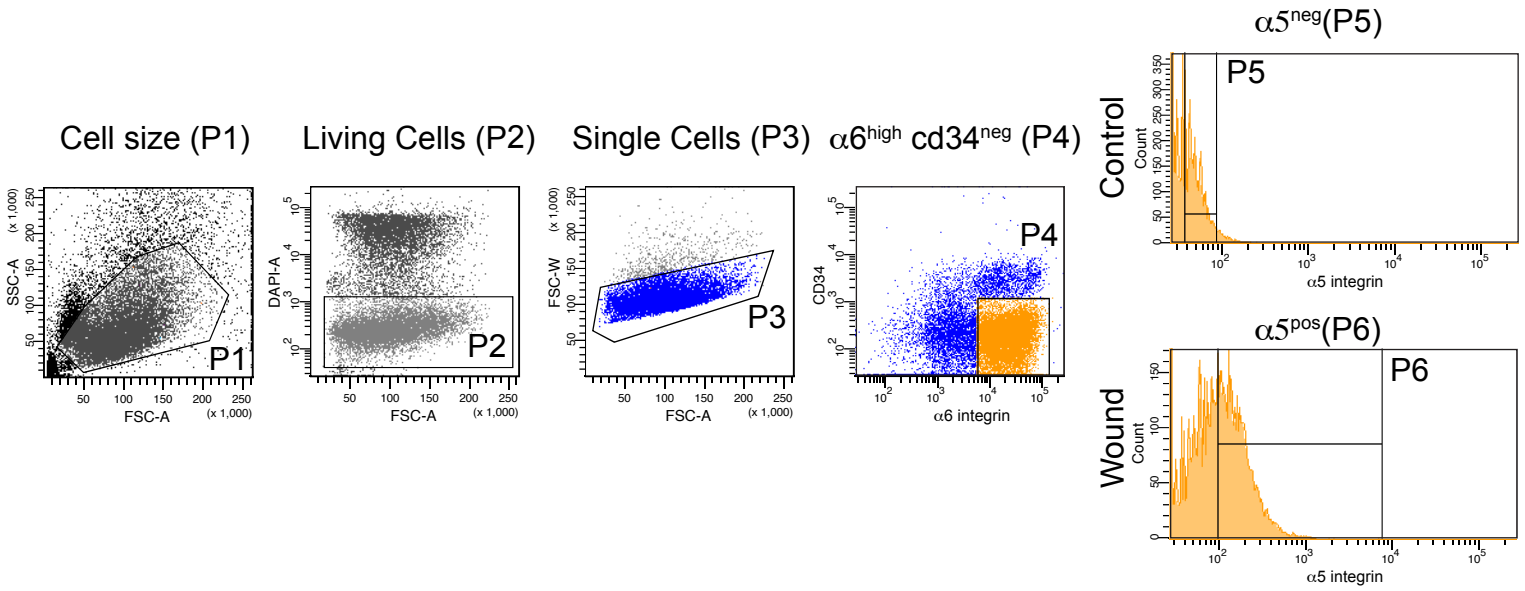

Supplementary Figure 3. FACS strategy used to isolate LE basal cells using their α5 integrin specific expression 4 days after wound.

Representative FACS plots showing the strategy used to isolate LE basals cells based on α5 integrin expression. 4 days after wound, pieces of tail skin located far from the wound (control) and surrounding the wound obtained with the 4mm punch were dissociated by enzymatic and mechanical separation. Isolated epidermal cells were stained with α5 integrin, α6 integrin and CD34 antibodies. Single living cells were gated by debris exclusion (P1), DAPI exclusion (P2), doublet elimination (P3). Within the $\alpha6^{high}$ $CD34^{neg}$ gate (P4), basal IFE cells were sorted according to their α5 integrin expression.

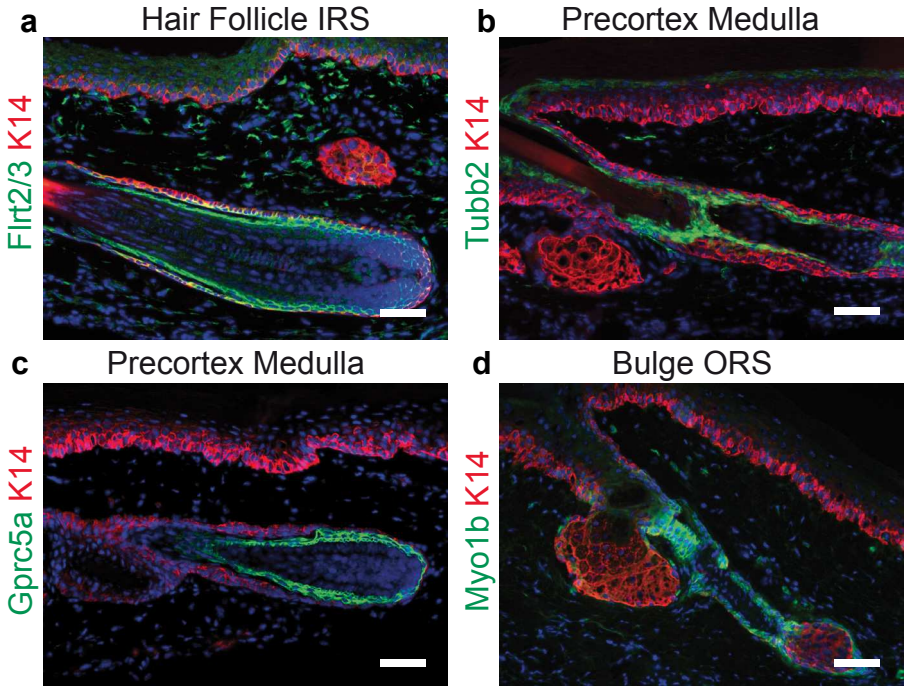

Supplementary Figure 4. Expression of the LE markers in the hair follicle.

a-**d**, Immunofluorescence of the wound markers (green) in normal unwounded skin. Flrt2/3 is expressed in the inner root sheath (IRS) of the normal hair follicle (**a**), Tubb2 and Gprc5a are expressed in the precortex medulla (**b**-**c**) and Myo1b is expressed in the bulge outer root sheet (ORS) (**d**). In all the pictures K14 is in red and the nuclei are stained with Hoechst (blue). Scale bar =50μm.

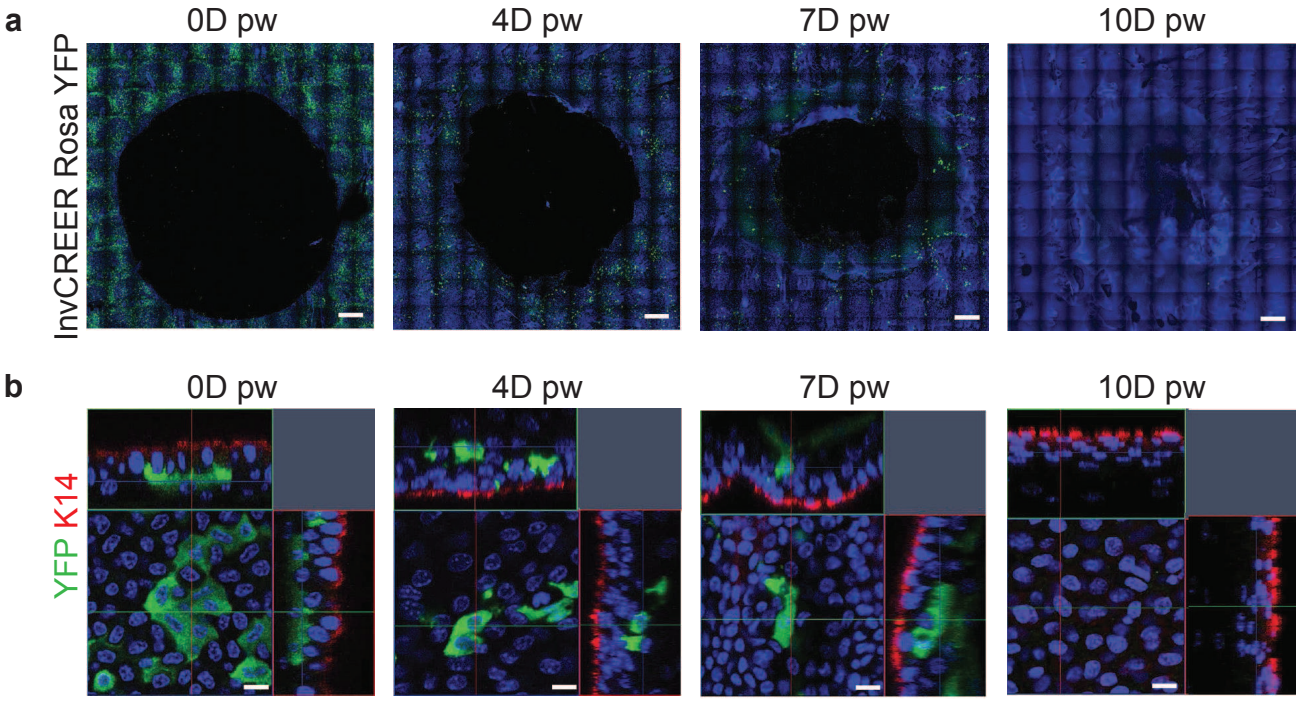

Supplementary Figure 5. Suprabasal cells do not revert back to basal cells during WH.

a, Maximum intensity projection of representative confocal pictures showing YFP immunostaining performed on whole-mount of wounded tail epidermis 4 days after TAM administration to *InvCREER/RosaYFP* mice and analysed at different times following wounding. Most of the Inv suprabasal cells are lost during the healing process. Scale bar = 500µm. **b**, Representative confocal pictures of YFP (green) and K14 (red) expression in *InvCREER/RosaYFP* mice in whole mount immunostaining at the different time points following wounding, showing the departure of the suprabasal Inv YFP labelled clones from the IFE. Scale bar = 20µm.

Supplementary Note 1

In this Supplementary Note we present further details of the biophysical and statistical approach used to infer the lineage hierarchy and proliferation kinetics of progenitors involved in skin wound healing. By taking into account the potential frequency of mergers we estimate the fraction of K14CREER cells contributing to wound healing. We then make use of stochastic modelling approach to infer the simplest model which is capable of describing the broad range of clonal dynamics observed in experiment.

Fraction of K14CREER progenitors contributing to wound healing

We begin our analysis by determining the fraction of K14CREER cells contributing to skin regeneration. To this end we first note that if labelling of K14CREER cells is statistically independent and representative this fraction is equal to the fraction of *labelled* K14CREER cells contributing to the wound. Denoting by n the number of labelled clones involved in wound healing and by N the total number of labelled clones that are capable of wound healing this fraction is given by $f = n/(mN)$. Here, m is the average number of basal cells in K14CREER clones. For the purpose of this analysis we define clones that contribute to wound healing as unicolour stripe-like structures that radially extend from the tissue surrounding the wound towards the centre of the wound. As the wound in most samples is closed at day 14 post wounding the number of stripes in a given wound is a proxy for n. The analysis of the experimental data is complicated by the relatively high induction frequency and the possibility that a given stripe is the merger of two different clones. To correct for possible merging events we therefore calculate the probability of merging for stripes of

a given colour c. If induction and stripe formation are each statistically independent and uniformly distributed around the wound the probability that neighbouring stripes are located at a distance d is $g(d) = \rho_c \exp(-\rho_c d)$, where ρ_c is the density of stripes of colour c . Then, if w is the typical width of stripes, the probability that nearest neighbours overlap is $G^c_{\text{unicolour}} = 1 - \exp(\rho_c w)$. If the density of stripes is low, $\rho_c \ll 1$, we can approximate the merging probability by expanding the exponential,

$$G^c_{\text{unicolour}} \approx \rho_c w \,. \tag{1}$$

As we do not know ρ_c we proceed by investigating merging events of stripes in different colours. The probability that clones of different colours merge is equal to the probability of mergers between any two colours times the probability that two stripes are of different colour,

$$G_{\text{bicolour}} \approx \rho_{\text{tot}} w \left(1 - \sum_c r_c^2\right) \tag{2}$$

Here, r_c is the relative frequency of colour c, which we can calculate from relative colour abundances in the control region and $\rho_{\text{tot}} = \sum_c \rho_c$. We can solve this equation for w and substitute into the expression for $G^c_{\text{unicolour}}$ to obtain

$$G^c_{\text{unicolour}} \approx \frac{G_{\text{bicolour}}}{1 - \sum_c r_c^2} \frac{\rho_c}{\rho_{\text{tot}}} \,. \tag{3}$$

The second fraction on the right hand side is the ratio of the density of stripes labelled in colour c and the total density of labelled stripes. This ratio is equal to the relative recombination frequency of colour $\rho_c/\rho_{\text{tot}} = r_c$, and it can therefore be calculated from the control region.

To infer the frequency of mergers of a given colour we still need to calculate the fraction of bicolour mergers, G_{bicolour}, from the experimental data. This fraction is simply the number of bicolour

mergers of any colour combination, n_{bicolour}, divided by to total number of stripes. For the latter we again need to correct for the possibility of mergers and obtain

$$G_{\text{bicolour}} \approx \frac{n_{\text{bicolour}}}{n_{\text{stripes}}\left(1+\sum_c r_c G^c_{\text{unicolour}}\right)}\,. \tag{4}$$

Substituting this into the expression for $G^c_{\text{unicolour}}$ we obtain

$$G^c_{\text{unicolour}} + G^c_{\text{unicolour}} \sum_c r_c G^c_{\text{unicolour}} \approx \frac{n_{\text{bicolour}} r_c}{n_{\text{stripes}}\left(1-\sum_c r_c^2\right)}\,. \tag{5}$$

To proceed we again note that ρ_c is small, such that we may restrict our analysis to the highest order contributions in ρ_c. As $G^c_{\text{unicolour}}$ is proportional to ρ_c the first term on the left hand side is of order ρ_c while the other terms on the left hand side are of order ρ_c^2 and can therefore be neglected. By not taking into account these terms we slightly overestimate the frequency of mergers. We finally obtain the following approximate expression for the frequency of mergers in colour c,

$$G^c_{\text{unicolour}} \approx \frac{n_{\text{bicolour}} r_c}{n_{\text{stripes}}\left(1-\sum_c r_c^2\right)}\,. \tag{6}$$

Calculating the frequency of mergers for the different colours in all wounds we found that mergers are relatively rare, constituting on average less than 10% of all unicolour stripes (Extended Data Fig. 2d). With this, the total number of stripes in a given colour is $n^c = n^c_{\text{stripes}}\left(1+\sum_{c'} r^{c'} G^{c'}_{\text{unicolour}}\right)$. Summation over all colours finally gives $n = n_{\text{stripes}}\left(1+\sum_c r^c G^c_{\text{unicolour}}\right)$.

We now calculate the number of labelled K14CREER cells in the recruitment area around the wound. To this end we multiply the density of clones at the time of initiation of stripes, ρ_0, with the recruitment area, A, from which K14CREER cells can be activated to form stripes: $N = \rho_0 A$. We quantified the clonal density in the recruitment area at day 4 post wounding, when stripe formation

is initiated. We found that, on average, roughly 306 ± 84 (95% confidence intervals) K14CREER clones populate an area of 1mm^2. We defined the recruitment area by the ring spanned by the 10th and the 90th percentiles of the distances between the starting positions of stripes to the center of the wound. As we took these positions at day 14 post wounding we corrected these distances for the contraction of the tissue surrounding the wound. We found that until day 14 tissue contraction led to a 30% decrease of the distance between the hair follicles and the centre of the wound (Figure 1f of the main text). We therefore increased these distances by 30% to take account for the fact that the recruitment area was larger at the time of initiation than at day 14. With this we found that the recruitment area is roughly 16 mm^2, corresponding to a ring of width 1 mm around the boundary of the wound. Therefore, on average 4853 ± 1336 clones were labelled at day 4 in the recruitment area. With an average number of basal cells in these clones of 0.67 ± 0.16 we find that, on average, 3242 ± 868 basal cells were labelled at the initiation of stripe formation.

Taken together we obtain that $0.2 \pm 0.2\%$ of K14CREER cells contribute to wound healing by forming stripes. To calculate confidence intervals we employed standard methods for the propagation of uncertainty. It is important to note that the confidence intervals we report here do not cover the full uncertainty, as they necessarily do not take into account sources of uncertainty that are difficult to quantified. For example the uncertainty associated with the definition of the time point of stripe initiation (here taken as day 4 post wounding) depends on the unknown clonal dynamics in this time interval.

Number of stripes contributing to wound healing

Having determined the fraction of K14CREER basal cells that contribute to wound healing we now investigate the total number of these cells. To begin, we first ask how many progenitors are hypothetically needed to fill the wound. At day 4 post wounding the radius of the wound is roughly 1 mm. At day 14 post wounding we measured, on average, 12089 ± 1120 basal cells per mm^2, which means that roughly 38000 basal cells are needed for wound healing. To the contribution of a single stripe to wound healing we then counted the number of basal and suprabasal cells in stripes. While the frequency of mergers is relatively low these events can have a large impact on the average number of cells in clones. To take into account the possibility of mergers we identified, based on their morphology and location, stripes which we were confident to be monoclonal. The average number of basal cells in the remaining monoclonal stripes at day 14 is 19 ± 7, suggesting that if wound healing was entirely achieved by stripe formation 2054 ± 754 stripes were needed.

We compare this number to the total number of stripes that contribute to wound healing. Based on the number of labelled stripes, n, the total number of stripes is n/p_{ind}, where p_{ind} is the probability that a K14CREER cell is induced at day 4. The latter can be obtained by dividing the density of labelled clones in the recruitment area at day 4 by the density of basal cells, which we obtained from an uninjured control region. With this, in stark contrast to the number of stripes needed to regenerate the tissue, we found that in total 343 ± 120 stripes contribute to wound healing. This discrepancy suggests that other subpopulations contribute to wound healing, for example Lrig1CREER cells located at the hair follicles. It is important to note, however, that the labelling

is likely not representative and we don't know the relative induction of basal stem and progenitor cells. If the proportion of labelled progenitors differs significantly from that found in previous studies [1] this number might be significantly higher.

Stochastic modelling of clonal dynamics

To define cell fate behaviour in skin wound healing we extend the biophysical modelling approach introduced in Refs. [2–4]. In this model, stem cells and their differentiating progenitor cell progeny function as equipotent cell populations in which their proliferation kinetics and fate behaviour follow defined statistical dependencies. These stochastic "rules" summarize the product of the complex gene regulatory processes that regulate cell fate behaviours. For simplicity, following Refs. [2,3], we consider a model based on intrinsic (cell-autonomous) regulation. However, in the two-dimensional geometry of the epidermis, models of fate behaviour based on external (cell extrinsic) regulation are difficult to discriminate from intrinsically regulated systems. The clonal analysis described here therefore leaves the question of the underlying regulatory dynamics unspecified.

Maximum likelihood estimation

In infer cell fate behaviour in skin wound healing we employ *Bayesian inference* [5]. In particular, we seek to define the model which describes the experimental data with the highest probability. A detailed description of this approach is given in Ref. [4]. Briefly, the probability $P(\Theta|E)$ of a model, Θ given the experimental evidence E is, following *Bayes' Theorem*, proportional to the product of

the probability of obtaining the experimental evidence given the validity of the model, $P(E|\Theta)$, and the *a priori* belief in a certain model, $P(\Theta)$:

$$P(\Theta|E) = \frac{P(E|\Theta)P(\Theta)}{\int_\Theta \mathrm{d}\,\Theta P(E|\Theta)P(\Theta)}\,. \tag{7}$$

If the prior distribution $P(\Theta)$ is uniform we can infer the best fitting model by maximising the likelihood function $\mathcal{L}_E(\Theta) \equiv P(E|\Theta)$.

With the frequency $f_{n,t}$ of observations of clones with given numbers of basal cells n at a given time point t after wounding and since measurements are statistically independent, the likelihood function takes the form of a multinomial distribution [4],

$$\mathcal{L}_E(\Theta) = \frac{\left(\sum_{n,t} f_{n,t}\right)!}{\prod_{n,t} f_{n,t}!} \prod_t \prod_n P(n,t|\Theta)^{f_{n,t}}. \tag{8}$$

To obtain approximations for $P(n,t|\Theta)$ we numerically solved *Master equations* of the form

$$\frac{\mathrm{d}}{\mathrm{d}t}P(n,t|\Theta) = \sum_{n'=0}^{\infty} \mathcal{W}_{n',n}P(n',t|\Theta) - \mathcal{W}_{n,n'}P(n,t|\Theta), \tag{9}$$

using *Gillespie's algorithm* [6]. These solutions of the Master equations give the probability to find any stochastic fate of a single clone. From this we obtain the distribution of persisting clones as

$$P^p_{n>0}(n,t|\Theta) = \frac{P(n,t|\Theta)}{1-P(0,t|\Theta)}\,. \tag{10}$$

With this, the logarithm of the likelihood function is given by

$$\log \mathcal{L}_E(\Theta) = \log \mathcal{N}^{-1} + \sum_t \sum_n N_{n,t} \log P^p_{n>0}(n,t|\Theta)\,. \tag{11}$$

To determine the maximum of the likelihood function we rasterised parameter space determine the best fit parameters and to calculate credible intervals, as defined below.

To estimate the uncertainty associated with the maximum likelihood parameters define credibility intervals comprising all parameter value whose likelihood is above a threshold, $\alpha = 0.05$, such that the resulting credible region (CR) is

$$\text{CR} = \left\{ \Theta \;\middle|\; \frac{\mathcal{L}_E(\Theta)}{\mathcal{L}_E(\Theta^*)} > \alpha \right\} . \tag{12}$$

This approach is most powerful in classifying sets of credible parameters [5]. For a specific model parameter, Θ_i, we report credible intervals in the form $\Theta_i^* \pm (\max_{\text{CR}}\{\Theta_i\} - \Theta_i^*, \Theta_i^* - \min_{\text{CR}}\{\Theta_i\})$.

Inference of the best fitting model

We are now in a position to perform maximum likelihood estimation in order to estimate the model, which describes the experimental data with the highest likelihood. The clonal analysis is complicated by the fact that skin wound healing comprises two temporal regimes: an early, highly proliferative phase with a strong bias towards the suprabasal layer is followed by a phase where overall proliferation reaches lower levels and where stripe formation is observed. While we here study the second regime, the clonal data might be compromised by labelled remainders from the early dynamics. Indicative of this is the large fraction of clones containing only suprabasal cells at day 4 and 7 post wounding as well as the large clonal loss rate. To avoid the presence of these clones distorting the results we focussed on clones containing basal cells and fitted the model to the basal compartment only.

To unveil the clonal dynamics constituting stripe formation we seek to define the simplest model which is capable of predicting the clonal data. To begin we study the time evolution of the average number of basal cells in K14CREER clones. We find that this increase is surprisingly linear. At first sight this could indicate neutral dynamics of a single progenitor population, where loss of clones due to symmetric differentiation is balanced by the growth of surviving clones [2,3]. A model comprising neutral dynamics has been proposed for the clonal dynamics in homeostatic epidermis [7]. However, in this modelling scheme the rate of increase of the average number of basal cells is given by the rate of symmetric proliferative divisions, which would correspond corresponding to an unreasonable cell cycle time of less than six hours. Further, neutral dynamics would give rise to an equally high rate of loss of stripes. In the clonal data there is no clear trend indicating a decreasing number of stripes over time (3.7 ± 1.6, 14.0 ± 7.6 , 6.7 ± 2.3 for days 7, 10, and 14pw, respectively).

To understand the rapid linear increase in the average number of basal cells we considered a situation where the neutral dynamics in the intact skin arises from an asymmetrically dividing subpopulation in the basal layer. Such a model can be summarised as

$$A \xrightarrow{\alpha} AB\,, \tag{13}$$

$$B \xrightarrow{\beta_1} BB\,, \tag{14}$$

$$B \xrightarrow{\beta_2} BC\,, \tag{15}$$

$$B \xrightarrow{\beta_3} CC\,, \tag{16}$$

where A is an asymmetrically dividing basal stem cell and B is a basal progenitor. C denotes

suprabasal cells. As the third process does not change the number of basal cells in a clone we cannot infer the rate β_2 from the basal data alone.

The time evolution of the probability to find a clone with n_B basal cells is described by Master equations of the form [8]

$$\frac{\mathrm{d}}{\mathrm{d}t}P(n_B,t) = \left[\alpha+\beta_1(n_B-1)\right]P(n_B-1,t)+\beta_3(n_B+1)P(n_B+1,t) \tag{17}$$

$$-\left[\alpha+(\beta_1+\beta_3)n_B\right]P(n_B,t)\,. \tag{18}$$

The solution has been shown to be a negative binomial distribution,

$$P(n_B,t)=\binom{\alpha+n_B-1}{n_B}(1-b_t)^{\alpha}b_t^{n_B}\,, \tag{19}$$

with the time dependent parameter

$$b_t=\frac{\exp[(\beta_1-\beta_3)t]-\beta_1}{\exp[(\beta_1-\beta_3)t]-\beta_3}\,. \tag{20}$$

The average number of basal cells follows

$$\langle n_B(t)\rangle=\frac{\alpha}{\beta_1-\beta_3}\left[e^{(\beta_1-\beta_3)t}-1\right]\,. \tag{21}$$

Therefore, if differentiation of basal progenitors is balanced with proliferation, $\beta_1=\beta_3\equiv\beta$, the average number of basal cells increases linearly with time,

$$\langle n_B(t)\rangle=\alpha t\,, \tag{22}$$

and the rate of increase is given by the division rate of basal stem cells.

A model comprising an asymmetrically dividing subpopulation which gives rise to balanced basal progenitors is therefore capable of predicting the time evolution of the average number of basal

cells in clones. The more challenging test is whether such a model is also able to predict the full distributions. We employed maximum likelihood estimation to infer the parameters that have the highest probability in describing the experimental data. We found that according to the so defined model basal progenitors divide asymmetrically with a rate $\alpha = 1.8 \pm (0.6, 0.4)\, d^{-1}$. Therefore, basal stem cells divide, on average, once every 13 hours. The most likely rates of symmetric proliferative and differentiating divisions of basal progenitors are $\beta = 1.3 \pm (1.1, 0.6)\, d^{-1}$, while the rate of asymmetric divisions of these cells cannot be inferred. Given that maximum likelihood estimation predicts a cell cycle time of at least 17 hours by symmetric divisions alone it is unlikely that, as in healthy epidermis, the majority of divisions is asymmetric. Notably, such a model resembles the clonal dynamics in the intact epidermis, where the basal compartment is comprised of basal stem cells, who divide mostly asymmetrically, and committed progenitors, who have a higher probability of symmetric divisions [1,9].

Having determined the clonal dynamics of K14CREER basal cells we then asked whether Lrig1CREER cells follow similar patterns of fate choice. The average number of basal cells in Lrig1CREER clones is significantly larger than in K14CREER clones. Remarkably, in common with the K14CREER clones this average increases linearly in time, suggesting that Lrig1CREER cells might show qualitatively similar behaviour. In principle, the higher rate of increase in the basal clone size might simply be the result of a reduced cell cycle time in Lrig1CREER cells. However, we found that in such a scenario the experimental data could again only be explained by assuming unreasonably fast division rates. Rather, we hypothesised that the increased size of Lrig1CREER clones might be the result of an initial round of symmetric divisions of basal stem cells. We approximate the

number of basal stem cells after the initial set of symmetric divisions by a Poisson distribution, such that the clone size distribution follows

$$\tilde{P}(n_B, t) = \sum_{k=1}^{\infty} \frac{\lambda^k}{k!} e^{-\lambda} P(n_B, t)^{*k}\,, \tag{23}$$

where the exponent denotes a k-fold convolution:

$$P(n_B, t)^{*k} = \sum_{n_B^1=1}^{n_B} P(n_B^1, t) \sum_{n_B^2=1}^{n_B^1} P(n_B^2, t) \ldots \sum_{n_B^k}^{n_B^{k-1}} P(n_B^k, t) P(n_B - n_B^k, t)\,. \tag{24}$$

We found that we could predict the clone size distributions of Lrig1CREER stripes by taking $\lambda = 3$ and using otherwise the same maximum likelihood parameters as for K14 cells. This suggests that the clonal dynamics of K14 expressing cells might be preceded burst of proliferation in Lrig1 expressing cells. However, we need to exercise some caution in the interpretation of these results: while we expect the merging rate of these clones to be only slightly higher than for K14CREER clones, abundant merging could potentially explain the differences between K14CREER and Lrig1CREER clones equally well.

In summary, clonal analysis suggests that K14 expressing cells that form stripes into the wound largely recapitulate the clonal dynamics of clonal dynamics in homeostasis. This dynamics is, up to a time independent convolution, maintained for Lrig1CREER stripes originating from hair follicles.

Supplementary References

1. Mascre, G. *et al.* Distinct contribution of stem and progenitor cells to epidermal maintenance. *Nature* **489**, 257–262 (2012).

2. Klein, A. M. & Simons, B. D. Universal patterns of stem cell fate in cycling adult tissues. *Development* **138**, 3103–11 (2011).

3. Klein, A., Doupé, D., Jones, P. & Simons, B. Kinetics of cell division in epidermal maintenance. *Phys. Rev. E* **76**, 021910 (2007).

4. Watson, J. K. *et al.* Clonal dynamics reveal two distinct populations of basal cells in slow-turnover airway epithelium. *Cell Reports* **12**, 90–101 (2015).

5. Box, G. E. P. & Tiao, G. C. *Bayesian inference in statistical analysis*, vol. 40 (John Wiley & Sons, 2011).

6. Gillespie, D. T. Exact stochastic simulation of coupled chemical reactions. *J. Phys. Chem.* **81**, 2340–2361 (1977).

7. Clayton, E. *et al.* A single type of progenitor cell maintains normal epidermis. *Nature* **446**, 185–189 (2007).

8. Bailey, N. T. J. *The Elements of Stochastic Processes with Applications to the Natural Sciences* (John Wiley & Sons, 1990).

9. Sánchez-Danés, A. *et al.* Defining the clonal dynamics leading to mouse skin tumour initiation. *Nature* DOI 10.1038/nature19069 (2016).

4.2 DEFINING THE DESIGN PRINCIPLES OF SKIN EPIDERMIS POSTNATAL GROWTH

4.2.1 Focus

In the past decades, several studies tried to decipher the cellular dynamics underlying epidermis maintenance during homeostasis [100,102,103,107]. In a homeostatic tissue, the number of cells that are lost must be compensated by new cells produced. Recent lineage tracing studies performed in our laboratory on the mouse tail epidermis suggest that a hierarchy of SC and CPs sustain skin epidermis through a majority of asymmetrical cell fate decisions but also balance self-renewal and cell differentiation so that the equilibrium is maintained at the population level [102,103]. However, little is known about the cellular dynamics taking place when the tissue needs to increase in size. Moreover, recent analysis performed in our lab suggest that CP are the main player in epidermis maintenance during homeostasis and that SCs only divide slowly and reside in specific regions of the mouse tail epidermis, the interscale [102,103]. However, nothing is known about this hierarchy during postnatal growth and whether it is already present at birth or not.

In this study, we used *K14-CreER/Rosa-Confetti* mice, clonal lineage tracing, proliferation experiments and single cell RNA-sequencing (RNA-seq) to unravel the cellular dynamics taking place in skin epidermis during postnatal growth *in vivo*.

4.2.2 Methods and results

To evaluate the amount of tissue generated during postnatal growth, we measured the general expansion of the tail epidermis and the expansion of a HF unit delimitated by HF triplets during postnatal growth, from birth (P1) to adulthood (P60). Both measurement showed that the tissue increases its surface 15x in a linear manner from P1 to P30 and then reach a plateau until P60 (Figure 1, page 96). In order to study the cellular dynamics taking place during the tail epidermis post-natal growth we induced *K14-CreER/Rosa-Confetti* newborn mice at clonal dose (Figure 2, page 98). Using confocal microscopy, we quantified the number of basal and total cells per clone at P4, P7, P15, P30 and P60 in scale and interscale regions, as well as the number of clone per hair follicle area. Our data show that the

proportion of clones remaining in the tissue during postnatal growth was globally stable overtime while the average clone size was increasing and expands around 15x, which fully recapitulate the tissue expansion. We also noticed that the average size of the clones was bigger in the scale compared to interscale, suggesting either different cell fate decisions or different proliferation rate between the two regions. Finally, cumulative proportion of interscale and scale clones at each time point both fit with a single exponential, a hallmark of a single population of progenitors (Figure 2, page 98).

To study the proliferation rate of basal cells in the tail epidermis we first treated *K5tTa/tetoH2BGFP* mice (TetOFF system) with doxycycline at different ages and analyzed the decrease in H2BGFP signal in basal cells by FACS. Our data showed that proliferation rate was decreasing overtime. Second, using Edu/BrdU double pulses, we quantified the proportion of double labeled cells specifically in scale and interscale regions and showed that scale basal cells have a higher proliferation rate compared to interscale basal cells. Altogether, these data show that the proliferation rate of basal cells decreases overtime and that scale basal cells divide more rapidly than interscale (Figure 3 and Figure S2, pages 100 and 112).

We then used a previously validated statistical framework to decipher mathematically the cellular dynamics taking place during tail epidermis growth[102,103]. Our data fit with a simple model where a single population of Developmental Progenitors (DPs) undergoes stochastic cell fate decisions leading to 60% of asymmetrical division and 40% of symmetrical division (either self-renewal or differentiation) (Figure 4, page 102). The increase in basal clone size and the stable persistence of the clones is consistent with a model where basal cells display a constant imbalance of 24% in favor of self-renewal, meaning that cells achieve self-renewal decision in 32% of the cases (17% in homeostasis) against 8% for symmetric differentiation (21% in homeostasis) along the growing phase[103]. Taking into account the different proliferation rate in each region, this model recapitulates basal clonal growth and persistence in both scale and interscale from P1 to P30. An independent tracing started at P15 confirmed the clone size and persistence predicted by the model, strengthening our confidence in this constant imbalance model (Figure 4, page 102). By contrast, only the homeostatic model could recapitulate clones size

and persistence for a tracing initiated at P30 (Figure S5, page 118). Similar results were obtained from clonal analysis performed in the hindpaw epidermis and suggested that the constant imbalance model is a general strategy for epidermal expansion (Figure S3, page 114). Importantly, the constant imbalance model implies that a constant density of DPs and suprabasal cells is maintained along the growth. Our data confirmed a stable ratio between suprabasal and basal cells along the post-natal growth both in tail and paw epidermis (Figure 5, page 104). These data suggest that the constant imbalance model, coupled with an ever decreasing proliferation rate and leading to a linear growth of the tissue, is a general mechanisms to expand stratified epithelium *in vivo*. The results also suggest that the maintenance of an appropriate number of suprabasal cells is guaranteed by an optimality criterion that ensure the barrier properties along the growth process.

To assess the molecular differences between post-natal and adult epidermis we performed single cell RNA-seq on FACS sorted basal cells and compared young (P7) and adult (P60) tail epidermis using the 10X Genomics technology[130]. Unsupervised clustering subdivided the G0 basal cells of the young sample in two populations (DP G0 I and II) and adult G0 SC/CPs in three populations (SC/CP G0 I, II and III), supporting a higher heterogeneity in the adult basal stem/progenitors (Figure 6, page 106). Using SCENIC analysis[131] we identified the TFs and their transcriptional network associated with these cell populations. Finally, lineage trajectory using Slingshot[132] revealed a single lineage from the homogeneous population of DPs to differentiated cells in young sample and 3 lineage trajectories leading to scale and interscale differentiated cells as well as one lineage toward SC/CP III (Figure 6, page 106). Finally, single cell RNA-seq performed at P30 showed that, while they still cluster in 2 populations, basal cells already show signs of heterogeneity (Figure S6, p120). These data show that young epidermis display a more homogeneous population of basal progenitors compared to adult, and confirm the existence of equipotent DPs proposed by the mathematical modelling.

Interestingly, the majority of the clones generated during post-natal development were anisotropic and displayed a specific orientation depending on their location in the tail epidermis. Two-photon microscopy on clarified tissues highlighted specific alignment of collagen fibers with similar orientation compared

to the clones. We cultured primary keratinocytes on micro-patterning devices coated with aligned versus non-aligned collagen and showed that cells plated on aligned collagen divide along the collagen fibers while cells plated on non-aligned collagen have a random cell division orientation. These data show that cell division orientation is locally controlled by collagen fibers present in the underlying dermis (Figure 7, p108).

4.2.3 Conclusion

In this study, using lineage tracing, clonal analysis, proliferation experiments and single-cell transcriptional analysis, we demonstrated that, postnatal skin epidermis is composed of a homogeneous population of equipotent DPs that keep a constant imbalance toward self-renewal, coupled with an ever decreasing proliferation rate, to achieve tissue growth. Finally, using *in vivo* measurement and *in vitro* micro-patterning experiments, we show that DPs cell division orientation is locally influenced by the collagen fibers alignment in the underlying dermis.

Defining the design principles of skin epidermis postnatal growth

Sophie Dekoninck[1*], Edouard Hannezo[2,3*], Alejandro Sifrim[4,5], Yekaterina A. Miroshnikova[6,7,8], Mariaceleste Aragona[1], Milan Malfait[1], Souhir Gargouri[1], Charlotte de Neunheuser[1], Christine Dubois[1], Thierry Voet[4,5], Sara A. Wickström[6,7,8], Benjamin D. Simons[3,9,10] and Cédric Blanpain[1,11,#]

[1] Université Libre de Bruxelles, Laboratory of Stem Cells and Cancer, Brussels B-1070, Belgium.

[2] Institute of Science and Technology Austria, Am Campus 1, 3400 Klosterneuburg, Austria.

[3] The Wellcome Trust/Cancer Research UK Gurdon Institute, University of Cambridge, Tennis Court Road, Cambridge CB2 1QN, UK.

[4] University of Leuven, KU Leuven, Department of Human Genetics, Leuven, Belgium

[5] Wellcome Sanger Institute, Sanger Institute – EBI Single-Cell Genomics Centre, Hinxton, UK

[6] Helsinki Institute of Life Science, University of Helsinki, Biomedicum, Haartmaninkatu 8, 00290 Helsinki, Finland

[7]Wihuri Research Institute, Biomedicum, Haartmaninkatu 8, 00290 Helsinki, Finland

[8]Max Planck Institute for Biology of Ageing, Joseph Stelzmann Str. 9b 50931 Cologne, Germany

[9] Cavendish Laboratory, Department of Physics, J. J. Thomson Avenue, Cambridge CB3 0HE, UK.

[10] Wellcome Trust-Medical Research Council Stem Cell Institute, University of Cambridge, UK.

[11] WELBIO, Université Libre de Bruxelles, Brussels B-1070, Belgium.

Corresponding author

*Co-first author

Running title: Postnatal tissue expansion

SUMMARY

During embryonic and postnatal development, organs and tissues grow steadily to achieve their final size at the end of puberty. However, little is known about the cellular dynamics that mediate postnatal growth. By combining *in vivo* clonal lineage tracing, proliferation kinetics, single-cell transcriptomics on skin epidermis and *in vitro* micro-pattern experiments, we resolved the cellular dynamics taking place during postnatal tissue expansion. Our data revealed that harmonious growth is engineered by a single population of developmental progenitors presenting a fixed fate imbalance of self-renewing divisions, with an ever-decreasing proliferation rate. Single-cell RNA sequencing revealed that epidermal developmental progenitors form a more uniform population compared to adult stem/progenitor cells. Finally, we found that the spatial pattern of cell division orientation is dictated locally by the underlying collagen fiber orientation. Our results uncover a simple design principle of organ growth where both progenitors and differentiated cells expand in harmony with their surrounding tissues.

INTRODUCTION

Organism growth is a key process that needs to be orchestrated harmoniously throughout development. Animal development starts from a single cell to form a multicellular organism composed of tissues containing different cell types. Once the different cell types have been specified during embryonic development, the organs and tissues have to grow during postnatal life to achieve their final size at the end of puberty. In adult animals, cells lost by differentiation and cell death must be compensated by cell division in a process called tissue homeostasis. This last decade, great efforts have been made to understand the mechanisms controlling tissue homeostasis in adulthood. Lineage tracing and clonal analyses have been instrumental in defining the clonal dynamics ensuring asymmetric renewal at the population level, maintaining the balance between proliferation and differentiation (Blanpain and Simons, 2013). In contrast, very little is known about the mechanisms that ensure postnatal growth, from birth until animals reach their final size at the end of puberty. During postnatal growth, an imbalance between proliferation and differentiation is required to generate the excess of cells that fuel tissue expansion. How this imbalance is controlled and achieved is largely unknown.

The skin is the first barrier that protects animals against their microenvironment. The epidermis is composed of hair follicles (HFs) and their surrounding interfollicular epidermis (IFE). The IFE contains a single proliferative layer of basal cells (BCs) expressing keratin 14 and 5 (K14/K5), and several suprabasal layers of terminally differentiated cells expressing K1 and K10 that progressively become enucleated and are shed as squames at the skin surface (Blanpain and Fuchs, 2006). To compensate for the loss of terminally differentiated cells, the IFE is constantly renewed by the proliferation of stem cells (SCs) and progenitors (Blanpain and Simons, 2013). The

tail epidermis is a well-described tissue, composed of two distinct regions (the scale and interscale) in which the clonal dynamics mediating adult tissue homeostasis has been studied extensively. The mouse tail IFE homeostasis is ensured by SCs and committed progenitors (CPs), which together balance self-renewal and differentiation in a stochastic manner at the population level (Clayton et al., 2007; Mascre et al., 2012; Sanchez-Danes et al., 2016). In contrast, during postnatal growth, and the concomitant expansion of the skin, the SCs and/or progenitors need to adjust the balance between renewal and differentiation to expand the number of both basal and suprabasal cells. The mechanisms responsible for controlling the imbalance of self-renewal over differentiation, which mediates skin expansion, are currently unknown.

Here, we used the murine tail and paw epidermis to unravel the mechanisms that mediate postnatal skin expansion. Using a multidisciplinary approach, we define the pattern of cell fate decisions during tissue growth. We show that postnatal tail and paw skin expansion is mediated by a single population of equipotent developmental progenitors (DPs) that present a fixed fate imbalance of renewing divisions, coupled with an ever-decreasing proliferation rate. We show that this strategy is optimal to ensure the expansion of the basal progenitor cell pool while maintaining a constant suprabasal thickness. We validate the model via clonal analysis performed at different time points during postnatal development. Finally, we demonstrate that the direction of clonal growth does not follow large-scale cues from anisotropic tail growth, but local cues from the underlying collagen fiber orientation.

RESULTS

The IFE expands linearly during postnatal development

The mouse tail epidermis is composed of two regions that follow distinct differentiation programs: the interscale surrounds triplets of HFs and is characterized by suprabasal cells expressing K1/K10, and the scale is characterized by the expression of the keratin 31 (K31), keratin 36 (K36) and Keratin 84 (K84) in differentiated cells (Didierjean et al., 1983; Tobiasch et al., 1992). In adult mice, these two regions behave as independent compartments that are sustained by their own pool of stem and progenitor cells (Gomez et al., 2013; Sanchez-Danes et al., 2016). However, how and when these SC and progenitors and their compartmentalization are specified during development remains unclear.

To address these questions, we first assessed macroscopic tail expansion by measuring the length, width and total area of the tail from P1 to P60. The results showed that the tail surface grew in linearly from P1 to P30 by about 12-fold, and then slowly reached a plateau. Most of the expansion was due to the tail elongation (7-fold from P1 to P60), whereas its diameter increased only by 2.5-fold during the same period (Figure 1A-E). Altogether, our data shows that the tail surface increases 17-fold in a highly anisotropic fashion during neonatal growth.

We then defined postnatal tail expansion at the microscopic level. Using hair follicle triplets as a reference frame, we measured the area of IFE covered by the scale and half of the two adjacent interscale regions, which we defined as the “hair follicle area” (HF area) (Figure 1A-B and Figure S1A-D). As *de novo* HF formation does not occur after birth, the length and width of HF areas can be used as a proxy to measure local tissue expansion. We found that the distance between two hair follicle lines along the antero-posterior (AP) axis increased more (7-fold from P1 to P60) than the

distance between two adjacent HF follicle triplets along the left-right (LR) axis (2.3-fold from P1 to P60) (Figure 1F-H). Altogether, the HF area expands around 16-fold from P1 to P60. Thus, both macroscopic and microscopic measurements give statistically similar results, showing that the IFE surface expands uniformly from P1 to P60, with a linear increase from P1 to P30 (Figure 1I).

Lineage tracing of developmental progenitors recapitulate tissue growth

To define the spatio-temporal dynamics of IFE expansion at single-cell resolution, we performed clonal analysis using a multicolor lineage-tracing approach (Figure 2A, B). Tamoxifen (TAM) was administrated to *K14-CreER/Rosa-Confetti* mice at P1 at a dose that leads to fluorescent reporter expression in BCs sufficiently isolated from each other to be able to follow the fate and expansion of targeted individual cells. The number of basal and suprabasal cells per clone were quantified at different time points in the scale and interscale (Figure 2C, D). In both compartments, clones grew rapidly from P1 to P30, and then more slowly from P30 to P60 (Figure 2E-F), mirroring the tail surface, with clone survival (or persistence) being globally stable from P7 to P60 in both scale and interscale (Figure 2G), a hallmark of unbalanced clonal expansion via self-renewing divisions of BCs. Importantly, the overall increase in clone size matched well the overall tissue expansion (Figure 2H) and the BCs size did not change overtime (Figure S1D), demonstrating that the cells we targeted in our lineage-tracing experiments are representative of those that drive whole tissue expansion.

Interestingly, we found that scale clones were consistently larger than interscale clones at all time points (21-fold vs. 10-fold expansion from P1 to P30, P7: $P=0.007$, P15: $P<0.0001$, P30: $P<0.0001$, Mann-Whitney test), which could not be attributed to differential clone loss (Figure 2G). Moreover, the cumulative basal clone size distributions of interscale and scale clones fitted well

with a single exponential dependence at all time points (Figure 2I, J) which arises as a hallmark of stochastic cell fate choices from single populations of DPs, which mediate post-natal growth reliant (Klein and Simons, 2011).

Ever decreasing proliferation rate of DPs during postnatal growth

To ensure the quasi-linear growth of tissue supported by a single population of DPs, these cells must either progressively decrease the proportion of self-renewing division over commitment to terminal differentiation, or smoothly adjust their proliferation rate and transit time from the basal layer to the cornified layer (or potentially both). To discriminate between these possibilities, we performed quantitative label-dilution experiments using *K5tetOFF/Tet-O-H2BGFP* mice (Mascre et al., 2012; Sada et al., 2016; Tumbar et al., 2004; Zhang et al., 2009) at different time points during postnatal development. In the absence of Doxycycline (Dox), H2B-GFP was homogenously expressed at high level in all BCs (Figure S2A-C). H2B-GFP expression was chased by administrating Dox starting at P1, P7, P21 or P30 and the level of H2B-GFP label-dilution in BCs, representing the number of cell divisions accomplished during the chase period, was quantified by FACS at different time points (Figure S2D-G). These data showed that the rate of cell division decreased during postnatal development, with an average cell cycle time estimated to be around 1.2 days between P1 and P7, 1.9 days between P7 and P15, 4.1 days between P21 and P28 (Figure S2H,I), and 6.5 days at P60 (Mascre et al., 2012). Of note, we did not observe a significant slow-cycling population of BCs during post-natal tissue expansion (Figure S2D, E), in support of the idea of a single population of DPs.

Although the H2B-GFP label-dilution data shows that the rate of DP cell division decreases over time, the FACS quantification cannot discriminate whether the differential expansion of

clones in the scale and interscale regions is mediated by a difference in the rate of cell proliferation, or a different imbalance towards symmetrical division**.** To discriminate between these two possibilities, we turned to cell proliferation kinetics measurements using EdU/BrdU double labeling experiments allowing us to define whether cell cycle time is regulated in a region-specific manner during postnatal development. EdU was administrated first at P4, P7, P15, P30 and P60, and then BrdU was given continuously for measuring the proportion of double-labeled cells (and the proportion of suprabasal Edu+ cells), at different time points in the scale and in interscale (Figure 3A-O and Figure S2J), which fitted well with a single population of dividing cell with refractory period in each region. These results confirmed that the rate of cell cycle re-entry decreases over time, and demonstrated that DPs consistently cycle faster in the scale than in the interscale (Figure 3N-P), similar to their differential proliferation rate during adult homeostasis (Gomez et al., 2013; Mascre et al., 2012; Sada et al., 2016; Sanchez-Danes et al., 2016; Spearman and Garretts, 1966). Indeed, we reasoned that the progressive and constant decrease in the DP proliferation rate during postnatal growth could explain the linear, rather than an exponential, growth of the tail epidermis, and the differential scale-interscale growth.

To determine whether a cell autonomous or a non-autonomous mechanism controls the ever-decreasing rate of proliferation observed during postnatal development, we assessed the proliferation rate of primary keratinocytes freshly isolated from mice of different ages and cultured *in vitro* for 48h on fibronectin/collagen coated plates. Quantification of BrdU incorporation by FACS analysis showed that the proliferation of cultured keratinocytes decreased with the age of the mice similarly to what we found *in vivo* (Figure 3Q and Figure S2K,L). These data suggest that the decrease in proliferation of keratinocytes is not the consequence of a higher level of growth hormones in the serum of young mice but the consequence of keratinocyte autonomous

mechanisms. These results do not rule out the possibility that growth hormones modify the epigenetic and transcriptional landscape of the keratinocytes, rendering them more responsive to growth factors.

A constant excess of symmetric renewing division mediates postnatal development

The increase in the number of BCs per clone combined with a stable clonal persistence can only be achieved if DPs increase their number of symmetric renewing divisions at the expense of symmetric differentiation, creating an imbalance in favor of self-renewal. To test whether the adjustment of the proliferation rate over time is sufficient to quantitatively explain the spatio-temporal dynamics of postnatal growth, we turned to quantitative modeling of the lineage tracing data (see Methods). Taking the experimentally measured proliferation rate as inputs to the model and considering the observation that rescaled clone size distributions are consistently well-fitted by a single exponential, we explored whether the average clone size and clonal persistence could be explained by a minimal model consisting of a single equipotent DP population characterized by stochastic fate behavior.

In an out-of-homeostasis setting, clonal dynamics are only weakly dependent on the probability of asymmetric division (1-2r) and pre-dominantly dependent on the product of $\Delta\,\lambda$, where Δ is the degree of imbalance between symmetric divisions, here self-renewing and differentiation divisions, and λ the cell division rate (see Methods). One should note that the results of these models are also largely insensitive to the nature of fate regulation (for instance intrinsic vs. extrinsic fate choices or whether differentiation feedbacks on, or is mediated by, cellular proliferation events). Interestingly, based on the measured cell division rate, we found that a constant fate imbalance of Δ=24%+-4% (best fit +- 95% confidence interval) provided a very good

fit for the quasi-linear P1 to P30 growth dynamics of interscale clones (Figure 4A and B). Moreover, the model also provided a good prediction for the clonal persistence, showing an initial decrease followed by a plateau (Figure 4C), characteristic of imbalanced cell fates (see Methods). Even more surprisingly, the modelling of scale clones showed that the same constant fate imbalance, Δ=24%+-2% (best fit +- 95% confidence interval), provided a very good fit for the clone size across the course of postnatal growth (Figure 4D-F). This means that the two-fold enhancement of clonal growth in scale could be explained by the observed faster proliferation rate compared to interscale. These data suggest that scale and interscale compartments are each sustained by a single population of DPs, which undergo an excess of symmetric renewing divisions and acquire different proliferation rates during post-natal development depending on their localization.

To experimentally challenge this simple constant fate imbalance model, we then performed an additional lineage tracing experiment at P15, chasing clones for 4 and 14 days (Figure 4G-U). In interscale, clones increased their average basal size by a factor of 1.9 and their average total size by a factor of 4.1 in 2 weeks (Figure 4 J,L, N and O). Interestingly, this average clone size expansion, together with the persistence evolution from P4 to P15, fitted well with the model prediction (Figure 4R-T). Similarly, scale clones increased their basal content by a factor of 2.9 and their total content by a factor of 6.2, which also fitted well with the model prediction, both in terms of average clone size and persistence (Figure 4 K, M, P, Q, S and U). These data confirm that epidermal cells do not change their cell fate imbalance during the growth process.

We then assessed whether this mechanism of tissue growth (fixed imbalance for self-renewal combined with a progressively decreasing proliferation rate) uncovered in the tail epidermis is a general strategy of stratified epithelial postnatal expansion. To this end, we studied

at single cell resolution the cellular mechanisms that mediate postnatal growth in the paw epidermis. We performed clonal analysis using *K14-CreER/Rosa-Confetti* mice induced at P1 and assessed the clonal behavior of individual BCs at P4, P7, P15, P30 and P60 in relation with the length and width of the paw area. The paw area expands by a factor of 6,1 from P1 to P60 and in a more isotropic manner compared to the tail (2.7x in length; 2.4x in width) (Figure S3A-D). Most of the paw expansion occurred in a nearly linear manner although it reached its plateau earlier than in the tail (Figure 1I). We performed a single BrdU pulse and quantified the proportion of labelled cells after 4h, which can be used to approximate the proliferation rate (Figure S3E and Methods). Interestingly, the proportion of BrdU labelled cells decreased from P1 to P15, going from 29.8 ± 2.3% of labeled cells at P1 to 12.0 ± 1.9% at P15 and then remain stable from P15 to P60 (Figure S3F). Clonal analysis in the paw epidermis showed that the basal content of the clones expand 5.8x from P1 to P15 (Figure S3G-K), mirroring the paw tissue expansion, and that clone size distributions were well fitted at all time points by a single exponential, a hallmark of a single population of DPs being responsible for the skin expansion (Figure S3L). Implementing a similar theoretical model as before (with the proliferation rates measured in paw) showed that the clone size and persistence time-course data was well-fitted by the same constant imbalance model proposed for the tail, with an imbalance of 20% from P1 to P15 (see Methods and Figure S3M-O), demonstrating that the design principles uncovered in tail epidermis also account for the skin expansion in the paw epidermis.

A constant imbalance mediates harmonious tissue expansion

Our data and modelling approach suggest that DPs adjust only their division rate to match the spatio-temporally varying patterns of tissue growth, while keeping their imbalance in fate choices approximately constant. Why would such a strategy be implemented and selected in several

epidermal compartments? One possibility would be that such a state of constant imbalance towards symmetric renewal represents a stable, cell-intrinsic ground state for DPs (Mojtahedi et al., 2016). However, we postulated that the observed growth strategy could also be explained mechanistically by considering a simple optimality criterion for epidermal growth.

We reasoned that, if the only constraint in the system was the expansion of the basal layer at a prescribed speed, this could be achieved in many ways (Figure 5A-D and Methods). For instance, DPs could retain balanced cell fate choices throughout development, similarily to homeostasis but with a higher division rate, producing only differentiated cells that would accumulate both in the basal and suprabasal layer, and thus lead to the dilution of the basal DP pool, as observed in *Drosophila* intestinal regeneration (Jin et al., 2017)(Figure 5A). However, our H2B-GFP dilution experiments do not show such accumulation of differentiated cells (Figure S2). A second possibility would be that DPs first undergo a phase of purely symmetric divisions, to rapidly expand the DP pool, and then switch to a second phase of asymmetrical divisions to generate differentiated cells. This so-called "bang-bang" mechanism has been proposed to be optimal for the rapid formation of mouse intestinal crypts after birth (Itzkovitz et al., 2012) (Figure 5B). However, our clonal data initiated at P1 show that differentiated cells are produced early after birth (Figure 2E and F). Finally, while our proliferation experiments rule out this hypothesis, a constant division rate similar to homeostasis (one division every 4-5 days) would be sufficient to give rise to the observed linear growth, if the imbalance was close to 100% around birth and subsequently continuously decreasing (Figure 5C). Interestingly, all these scenario would lead either to the dilution of the DP (Figure 5A) or to a phase in which very few suprabasal cells would be produced, leading to skin thinning during expansion and potentially compromising skin barrier function (Figure 5B,C) (See more explanations in Methods). We thus explored the consequences

of a very simple design principle of epidermal growth; that basal area must grow (in response to the growth of the underlying tissue) by a prescribed amount, but also that the ratio of suprabasal to BCs must remain constant (to ensure sufficient epidermal thickness throughout the expansion phase). Strikingly, imposing these two constraints was only compatible with a single theoretical growth scenario, characterized by (i) near-constant fate imbalance, and (ii) continually decreasing division rates to adjust to growth characteristics (Figure 5D and Methods). This design principle thus provides a simple and robust explanation for the experimentally observed clonal dynamics, which we explored quantitatively.

Before going further towards a quantitative comparison of this optimality criterion against the data, we sought to verify whether its assumptions apply. For this we measured the ratio of suprabasal to BCs at all time points, both in tail scale and interscale as well as in the paw. Importantly, we found that this ratio was approximately constant across the growth phase (Figure 5E-F), validating the key assumption of the model. Moreover, in the tail, the ratio was equivalent in tail scale and interscale, although both regions display a two-fold difference in the degree of growth (Figure 2E, F and H). We then sought to test the hypothesis of constant imbalance by fitting the clonal data piece-wise to infer different values of imbalance (See Methods). Interestingly, we found that the inferred imbalance at each time point was close to its globally fitted value (Figure 5G, H). Finally, in order to see whether the other possible scenario could also fit our experimental data, we performed a sensitivity analysis to predict the time evolution of the basal cell density and suprabasal/basal ratio for each scenario (Figure S4A-D). Strikingly, this analysis confirmed that our constant imbalance model was the best fitting scenario (See Methods).

With a single fitting parameter (suprabasal loss rate, which we set as constant across compartment, but which has only weak effects on the resulting dynamics), our design principle

could then quantitatively predict the following data: (i) the experimentally inferred imbalance at each time point, i.e. the fact that it should be constant in time, and identical both in scale and interscale despite their differential growth rate; and (ii) the experimentally measured evolution of the division rate in both scale and interscale, as well as the observed enhanced division rate in scale throughout the growth phase (Figure 5 G,H, and Figure S4). This argues that the evolution of the proliferation kinetics and fate choices of DPs throughout growth can be predicted from simple principles, and suggests that they are optimized for harmonious and coordinated basal and suprabasal expansion.

Transition between postnatal expansion and adult homeostasis

As mentioned above, the global growth kinetics of the tail slows down drastically after P30, a feature reflected in the clone size evolution. Indeed, turning to a modelling approach for the P30-P60 clone size evolution, first in scale regions, we found that this was consistent with the homeostatic model that we previously proposed (Sanchez-Danes et al., 2016), characterized by perfectly balanced fate choices of a single CP population (Figure S5A, right). This argues for a transition from imbalanced to balanced cellular behavior occurring around or soon after P30. Turning to interscale regions, although P1 inductions do not provide the resolution to detect the appearance of the SC/CP hierarchy, the P30-P60 clone size evolution was also consistent with a sharp transition towards homeostatic, balanced cell fate around P30, as using the homeostatic SC/CP model provided a good fit for the data, albeit with an increased fate imbalance towards differentiation from CP compared to homeostasis (Figure S5A, left).

To further test these findings, we performed an additional lineage tracing experiment at P30, chasing clones for 4 days and 4 weeks (Figure S5B-P). Consistent with their lower

proliferation rate, interscale clones only increased their average basal size by 2 fold and their average total size by 5.3 fold in 4 weeks (Figure S5E, G, I and J). The homeostatic model accurately predicted both the average clone size and clone persistence (Figures S5M-N). Likewise, scale clones increased 2.4x their basal content and 6.2x their total content in 4 weeks (Figures S5F, H, K and L). Again, scale clone sizes/persistence were consistently well-fitted by the model (Figures S5O-P). These data suggest a transition from imbalanced to balanced cell fate occurring around P30 in both scale and interscale, and that the clonal dynamic of SC in the interscale (Sanchez-Danes et al., 2016) arises late in development, presumably during the transition phase towards homeostasis.

Single cell RNA sequencing of post-natal and adult tail epidermis

To define the molecular features associated with DPs and compare with adult SC/CP in homeostasis, we performed single cell RNA sequencing of FACS isolated basal tail keratinocytes depleted from HF cells (see Methods) of young (P7, n=9.389 after QC) an adult (P60, n=10.447 after QC) mice using 10X Genomics technology (Zheng et al., 2017). We performed unsupervised clustering and excluded the cell clusters of the infundibulum (*Sox9*^{high}, *Krt17*^{high}, and *Krt79*^{high}), sebaceous gland cells (*Scd1*^{high}, *Mgst1*^{high} and *Elovl6*^{high}) as well as cells containing a high content of mitochondrial genes, such as *mt-Co1* (dying cells) and performed further bioinformatics analysis on the IFE cells (Joost et al., 2016). After processing, 6102 and 7551 cells for P7 and P60 respectively were further analyzed (See Methods). We performed unsupervised clustering on individual samples using Seurat (Butler et al., 2018) and assessed the better level of resolution based on biological criteria (Figure 6A and B, left panels, see Methods). To better compare the young and adult epidermis, we also combined the two datasets using Harmony (Korsunsky et al., 2019; Tran et al., 2020), a method for batch integration suited for datasets containing continuous

transitioning between cell types/states, and annotated the clusters according to the individual clustering (Figure 6A and B, right panels). Interestingly, consistent with the modeling of the clonal fate data, individual clustering analysis revealed that the young IFE cells were more homogenous as compared to the adult IFE cells (Figure 6A and B). At P7, BCs, defined by their high expression for *Krt5* (Figure 6C), could be subclustered according to their different stages of the cell cycle (G1/S: cluster 3, S/G2/M : cluster 2, late G2/M: cluster 4 (Figures 6A-F, Figure S6A and Methods) and to their higher expression of known basal stem cells markers such as *Ccnd2*, *Col17a1* and *Sparc* which highlighted two populations in G0 (DP G0 : on main cluster 0 and one smaller cluster 5, Figure 6G-I) (Joost et al., 2016; Liu et al., 2019). More committed cells were defined by their expression for differentiated markers such as *Sbsn* (Committed and differentiated cells : cluster 1, Figure 6J). Similarly, adult tail epidermis clustering displayed BCs cell cycle related clusters (G1/S: cluster 3, G2/M : cluster 4) (Figures 6B-F and Figure S6B) as well as committed BCs expressing both *Krt5* and *Krt1* (Cluster 0) (Figures 6B,C and K). Two clusters of differentiated cells were found, corresponding to the interscale regions enriched for *Krt1/10* expression (cluster 5) and scale region (cluster 7) expressing higher level of scale markers *Krt36* and *Krt84* (Figure 6B, K,L and S6B), not expressed in the young sample, as predicted by the progressive appearance of scale markers during postnatal growth (Gomez et al., 2013; Tobiasch et al., 1992). In contrast, clustering of the adult tail epidermis uncovered that BCs in G0 could be subdivided into 3 distinct clusters (1, 2 and 6) associated with distinct signatures. G0 cluster 1 called SC/CP G0 (I), similar to what we found in P7, expressed higher level of *Sostdc1*, *Postn* or *Ifitm3* (Figure 6M and Figure S6B). The second G0 cluster (cluster 2, SC/CP G0 II) expressed higher levels of *Mt1/2* , *Tsc22d1* or *Dcn* (Figure 6N and Figure S6B) and the third cluster (cluster 6, SC/P G0 III) expressed higher level of *Wnt* related genes such as *Wnt3/Wnt4/Wnt10a/Wls*, as well as *Igfbp2/3/7, Il1r2* and *Tgm3* (Figure 6O and Figure S6B). Interestingly, the genes of these two last specific clusters were

expressed by the DP G0 II in P7 sample suggesting a higher molecular segregation or heterogeneity of BCs in adult (Figure 6N and O, and S6A). Some small clusters (6, 7 and 8, Figures 6A and B) were still high for *Krt17*, *Sox9* or expressed high level of *Krt6* and were considered as infundibulum cells in G2/M, and companion layer cells (Figure S6A-B). SCENIC analysis (Aibar et al., 2017), which allows the prediction of active Transcription Factors (TFs) and their putative target genes that control the identity of these stem and progenitor populations as well as their differentiated cells, showed that the DPs are enriched for regulons associated with *Jun*, *Fos* or *Trp63* (Figures S6C-E) whereas the committed and differentiated cells are enriched for *Klf4/5*and *Hes1* (Figures S6F and G), consistent with the well-established role of the Notch pathways and these TFs in promoting skin stratification (Blanpain and Fuchs, 2006). Finally, lineage trajectory analysis using Slingshot (Street et al., 2018) revealed one differentiation path at P7 and 2 differentiation paths (scale and interscale) in adult and allowed to separate the different cell clusters according to their commitment, and showed on path from the SC/CP G0 (I) to the SC/CP G0 (III) subpopulations (Figure 6P). Altogether, these single cell RNA sequencing data further support the existence of a more homogeneous population of DPs during postnatal skin expansion and the increase in cellular heterogeneity during the transition to adult IFE homeostasis. To define when this cellular heterogeneity emerges, we performed single cell RNA sequencing on the tail epidermis of a young adult mouse, at P30, when the clonal dynamic changes from growth to homeostasis. After quality control filtering, we analyzed the expression of all the markers identified in the adult SC/CP populations and compared them with the basal populations of P7 and P30 samples (Figure S6H). As expected, the differences between the two BC populations at P7 were minor, supporting a higher molecular homogeneity within the basal compartment as compared to adult. Markers of adult SC/CP G0 I, such as *Sostdc1* and *Ifitm3*, were more highly expressed in a fraction of BCs in all three samples, defining the BC populations I in all 3 datasets (see Figure S6H). As previously

mentioned, some markers from the adult SC/CP G0 II and III (such as *Dcn, Igfbp2* and *Wnt4*) were co-expressed within the second population of DP at P7 (DP G0 II), while most of the remaining markers were only weakly expressed. At P30, a larger amount of the SC/CP G0 II markers (*Dcn, Mt1, Mt2, Gpha2* and *S100a6*) were highly expressed in the P30 SC/CP G0 II population, but were still co-expressed with SC/CP G0 III markers (*Igfbp2, Igfbp7* and *Wnt4*) (Figure S6H). Finally, the tree SC/CP G0 populations were molecularly distinct at P60 (Figure S6H). To better visualize the difference in the cellular heterogeneity of basal epidermal cells between the 3 time points, BCs were plotted according to their Area Under the Curve (AUC) values for the markers specific for Adult SC/CP G0 II (x axis) and III (y axis) (Figure S6I-K, see Methods). While all BCs showed a linear correlation between the two AUC values in the young sample, some BCs, by contrast, start to deviate from the trend already at P30, and even more strongly in the adult sample (Figure S6I-K). Altogether, these data show that BCs of the tail epidermis are more homogeneous during early postnatal development and that cellular heterogeneity begins around P30, at the time of the transition from a growing to a homeostatic mode of division, and further increased until mice reach their final size. These data provide important molecular insights about the genes that control stem and progenitor heterogeneity, and their differentiation during postnatal development and adult homeostasis.

The local collagen pattern in the dermis determines clone orientation and cell division

Our constant imbalance model helps to understand the principles behind the regulation of cell fate decisions, both in terms of fate outcomes and division rate, for a globally expanding tissue. However, it does not take into account the geometry of these choices, such as the regulation of the cell division axis. While our clonal analysis data showed that DPs undergo a high proportion of

symmetric self-renewal, a closer observation of our clones suggest that the spatial localization of two DPs after division is not random. In a simple anisotropic growing epithelium, one could expect clones to all be oriented in the direction of net growth. However, the clones within the tail epidermis revealed a more complex geometrical pattern. During postnatal expansion, a fraction of clones were isotropic and grew equally in every direction (Figure S7A), whereas other clones were anisotropic, growing preferentially in one direction, either parallel to the antero-posterior (AP) axis or to the left-right (LR) axis of the tail. This prompted us to divide the interscale in two regions (the interscale AP and the interscale LR) and quantify the proportion and the orientation of clones in each region. At P30, around 70% of the clones were located in scale, 23% in interscale AP and 7% in interscale LR (Figure 7A). In each region, around 70% of the clones were anisotropic (Figure 7B). Measuring the orientation of the anisotropic clones revealed a striking and complex pattern of clonal orientation with interscale LR clones oriented perpendicularly to the long axis of the tail (Figure 7C), interscale AP clones elongated parallel to the long axis of the tail (Figure 7D), and scale clones with average angles between 40° and 80° (Figure 7E). Surprisingly, although the tail grows anisotropically in the AP direction, we found that the average orientation of all clones displayed little net anisotropic bias. This argued that the direction of cell division was decoupled with the direction of tissue growth in tail epidermis and raised the question of which local factor could influence cell division orientation

Previous studies highlighted the importance of the extracellular matrix and external forces on the orientation of cell division *in vitro* (Fink et al., 2011; Thery et al., 2005). To assess whether the collagen networks of the dermis could impose directional cues to clonal growth, we used bi-photon microscopy and second harmonic generation and analyzed the orientation of the fibrillar collagen within the upper dermis, in each IFE unit. At P30, a large-scale pattern in collagen was

clearly visible, oriented in the AP direction in the AP interscale, the LR direction in the LR interscale, and at nearly 45° in the scale (Figure 7F-H). Quantification of the orientation of the clones and orientation of collagen fibers revealed a strong correlation between the two (Figure 7 I-K). This spatial pattern thus matched perfectly the observed clonal orientation map, suggesting a functional link between the two. The strong correlation between collagen and clonal orientation was also found at earlier time points (Figure S7B-C).

To test whether the orientation of collagen fibers controls cell division orientation, we used photolithography-based micro-patterning to engineer adhesive surfaces surface with either aligned collagen fibers versus non-aligned collagen network both with 2µm spacing (Figure 7L and Methods). We cultured primary keratinocytes on the two surfaces and scored orientation of cell divisions in both conditions (Figure 7M). Interestingly, orientation of cell division correlated strongly with collagen fiber alignment while the cell division plane was randomized on the non-aligned collagen network pattern (Figure 7N). Altogether, these data suggest that the spatial organization of the orientation of DP is regulated by the local pattern of collagen fibers within the upper dermis during development.

DISCUSSION

In this study, we have unraveled the clonal dynamics and the underlying mechanisms that mediate postnatal skin expansion using mouse tail and paw epidermis as models. By combining proliferation kinetics, quantitative clonal analysis, mathematical modelling and single-cell RNA sequencing, we propose that the postnatal expansion of the skin is mediated by single populations of DPs in the different skin regions, which make stochastic fate choices at the single-cell level between division and differentiation, but which are robustly imbalanced at the population level

towards self-renewal. Our mathematical model reveals a surprising simplicity in the process of epidermal expansion. In particular, we find that quasi-linear epidermis growth is blueprinted via a combination of (i) steadily decreasing cell division rate over time, and (ii) an intermediary level of imbalance between self-renewal and differentiation, which is nearly constant over time and even across tail scale and interscale regions.

We propose that the optimality during postnatal epidermal growth requires that the epithelium maintains both a constant density of BCs throughout expansion, and that the ratio of basal to suprabasal cells is kept constant to ensure the barrier function of the skin, essential for animal survival. These two simple assumptions, which we validate experimentally, can only be fulfilled by a near-constant imbalance and ever-decreasing division rate, explaining qualitatively and quantitatively the design principles observed throughout the epidermal postnatal growth. This suggests a model where cells regulate their fate choices not only to in-plane tissue expansion, but also to constantly adjust the proportion of suprabasal cell produced to maintain the epidermal thickness.

Our current model proposing a single population of DPs mediating the tail growth in each scale and interscale regions contrasts with the homeostatic model previously proposed where a more heterogeneous cell populations consisting of SCs and CPs have been proposed to co-exist in the interscale (Mascre et al., 2012; Sanchez-Danes et al., 2016). Different hypotheses can be advanced to explain this difference. The first would be that the IFE is only composed of DPs during postnatal development and that SCs and CPs derive from DPs after puberty. A second possible hypothesis would be that SCs are already present at birth but have similar dynamics to the CPs and only acquire their slow cycling dynamics later, between P30 and P60. Our single cell RNA sequencing data suggest that IFE BCs are more homogeneous as compared to the adult BCs, which

present increase in heterogeneity with the appearance of an additional basal SC/CP population, starting to appear around P30, and two differentiated states corresponding to the scale and interscale differentiation program. The increase in basal cell heterogeneity coincided with the change in the clonal dynamic switching from an imbalance to a balance between renewal and differentiation, demonstrating that the clonal dynamic changes around P30 at the end of postnatal growth.

Interestingly, the strong imbalance observed during postnatal development is highly similar to the one found during tumor initiation after oncogenic Hedgehog (HH) signaling (Sanchez-Danes et al., 2016), but strongly contrasts with the clonal dynamics reported upon wound healing (Aragona et al., 2017). Interestingly, similar to our results in postnatal development, the strong imbalance induced by the oncogene is constant over time and accompanied by a decreasing proliferation rate leading to the linear growth of the lesions over several weeks/months (Sanchez-Danes et al., 2016). In contrast, upon wounding, a strong increase in IFE basal cell proliferation occurs shortly after damage, but the basal clone size expands linearly, suggesting that wound healing is a much more rapid process that does not trigger an imbalance for self-renewal, instead relying on the production of progenitors from activated SC populations (Aragona et al., 2017). Further experiments will be necessary to investigate the role of specific signaling pathways implicated in the control of cell fate decision.

Although we find epidermal expansion at the clonal level to be robustly coupled to the expansion of the underlying tissue, analysis of clonal orientations demonstrated a more complex picture. Indeed, we found that the local orientation of cell division (and consequently clonal orientation) does not follow the axis of tail growth (which is overwhelmingly in the antero-posterior) direction. Instead, clonal expansion is highly coupled to the local orientation of collagen

fibers in the dermis, which display well-defined long-ranged patterns throughout tail expansion. Using *in vitro* micro-pattern of orientated or non-aligned collagen, we further demonstrated that the clonal orientation is dictated by the local pattern of collagen fibers. Interestingly, the observed patterns of collagen/clonal orientation (Figure 7) closely mirror those observed in *Drosophila* wing disc morphogenesis (Mao et al., 2013). In both systems, a central epithelial region (scale in our case) divides faster than its surroundings and displays radially oriented clones, while the surrounding regions (interscale in our case) display orthoradially oriented clones. Given that this pattern of orientation can be fully recapitulated *in silico* by a vertex model, where the enhanced proliferation of the central region mechanically compresses its surroundings (Mao et al., 2013), this suggests that similar mechanical competition could occur in our system between scale and interscale regions, and provide a local orientation mechanism for clones. Further studies will be needed to understand how such intercalation events could be regulated, as well as how global tissue expansion can scale with clone size while being uncoupled to local clonal orientation.

Altogether, our results suggest that postnatal epidermal expansion relies on the tight and local regulation of three key parameters: cell fate imbalance, cell division rate and orientation of cell division. Although some of these parameters could be partially determined by cell-intrinsic factors (where imbalance for instance could be programmed to match the expected tissue growth, or division rate decaying autonomously in time), an alternative regulatory candidate would be cell-extrinsic cues such growth of the underlying dermis, epidermal thickness, cell density and other mechanical constraints arising from the other epidermal cells and the external microenvironment (Andersen et al., 2019). This is consistent with recent findings on the role of nearest-neighbor interactions to couple basal division and differentiation during epidermal homeostasis (Mesa et al., 2018; Miroshnikova et al., 2018; Rompolas et al., 2016), which provide a natural mechanism of

basal cell density regulation. Such extrinsic mechanisms would be expected to increase the robustness of the model with respect to fluctuations, which is key given that division rates and imbalances need to be tightly controlled in this system to achieve the correct size. Further experiments will be necessary to understand whether and how such feedbacks (from tissue size, local density, thickness to division rate and/or imbalance) are implemented mechanistically. Whether suprabasal density and/or tissue thickness are similarily regulated in other settings during development and homeostasis remains an intriguing possibility that will need to be explored in the future, as is the nature of the cross-talk between epidermis and dermis that couples dermal and epidermal growth.

ACKNOWLEDGMENTS

The authors acknowledge the animal house facility, the LiMiF microscopy platform and the Flow cytometry platform from ULB (Erasme campus). Sequencing was performed at the Brussels Interuniversity Genomics High Throughput core (www.brightcore.be) and the Genomics Core Leuven. The authors thank colleagues who provided reagents mentioned in the text, and J.-M. Vanderwinden and Michiel Martens for help with confocal imaging. S.D. is supported by a TELEVIE fellowship, M.A. is supported by a long-term fellowship of the HFSPO and a FNRS fellowhsip, A.S. and T.V. are supported by KULeuven (SymBioSys - C14/18/092), Foundation Against Cancer (2015-143), FWO (postdoctoral fellowship #12W7318N; I001818N). S.A.W. is supported by the Helsinki Institute of Life Science, Wihuri Research Institute, and Deutsche Forschungsgemeinschaft (DFG; project number 73111208 - SFB 829) and Y.A.M. has a Human Frontier Science Program fellowship LT000861/2018. B.D.S. is supported by the Royal Society (EP Abraham Research Professorship, RP\R1\180165) and the Wellcome Trust (098357/Z/12/Z). C.B. is an investigator with WELBIO and is supported by Fondation Contre le Cancer, the ULB

fondation, the Fond Gaston Ithier, the Télévie, the foundation Bettencourt Schueller, the foundation Baillet Latour, and the European Research Council (EXPAND : ERC-2013-CoG n°616333).

AUTHOR CONTRIBUTIONS

S.D., E.H., B.D.S and C.B. designed the experiments, performed data analysis and wrote the manuscript; S.D., E.H., B.D.S., M.A., and C.B. discussed the data and their interpretation. S.D. performed most of the experiments; A.S., M.M. and T.V. performed single-cell RNA sequencing data analysis; Y.A.M. and S.A.W. performed micro-patterning experiments and data analysis; S.L., C.dN, S.G. and C.D. provided technical support; E.H. and B.D.S. performed the mathematical modelling and statistical analysis of the clonal data.

DECLARATION OF INTERESTS

The authors declare no competing interests

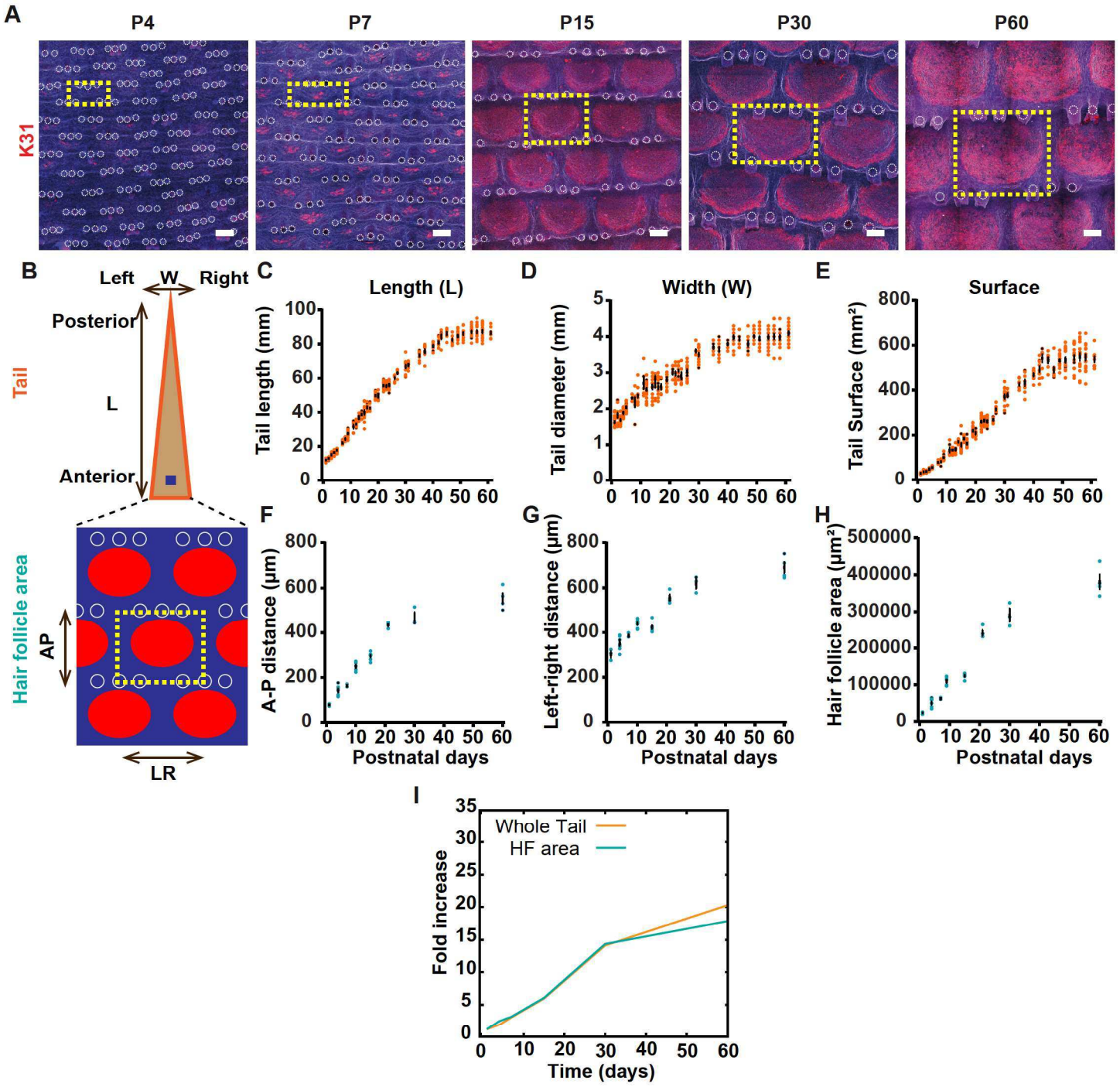

Dekoninck et al., Figure 1

FIGURE TITLES AND LEGENDS

Figure 1. The IFE expands linearly during postnatal development. (A) Representative immunostaining of K31 in whole mount tail epidermis showing the scale (K31+) and interscale (K31-) regions at the given time points (Maximum intensity projection of confocal images). Yellow dotted line : HF area, white circles :hair follicles. Nuclei are stained with Hoechst. Scale bar = 100µm. (B) Diagram of the tail epidermis showing its antero-posterior axis. Below a scheme representing the scale (red) and interscale (blue) regions. Yellow rectangle : HF area, L: length, W : width, white circles : hair follicles. (C-E) Measurement of the length (C), width (D) and calculated total surface of the tail (E) from P1 to P60 (n≥5 mice per time point). (F-H) Measurement of the AP (F), LR (G) distances and the calculated surface of the hair follicle area from P1 to P60 (n≥3 mice per time point). (I) Calculated fold increase of the tail surface (orange) and the hair follicle area (cyan) from P1 to P60. Data are represented as mean ± SEM. See also Figure S1.

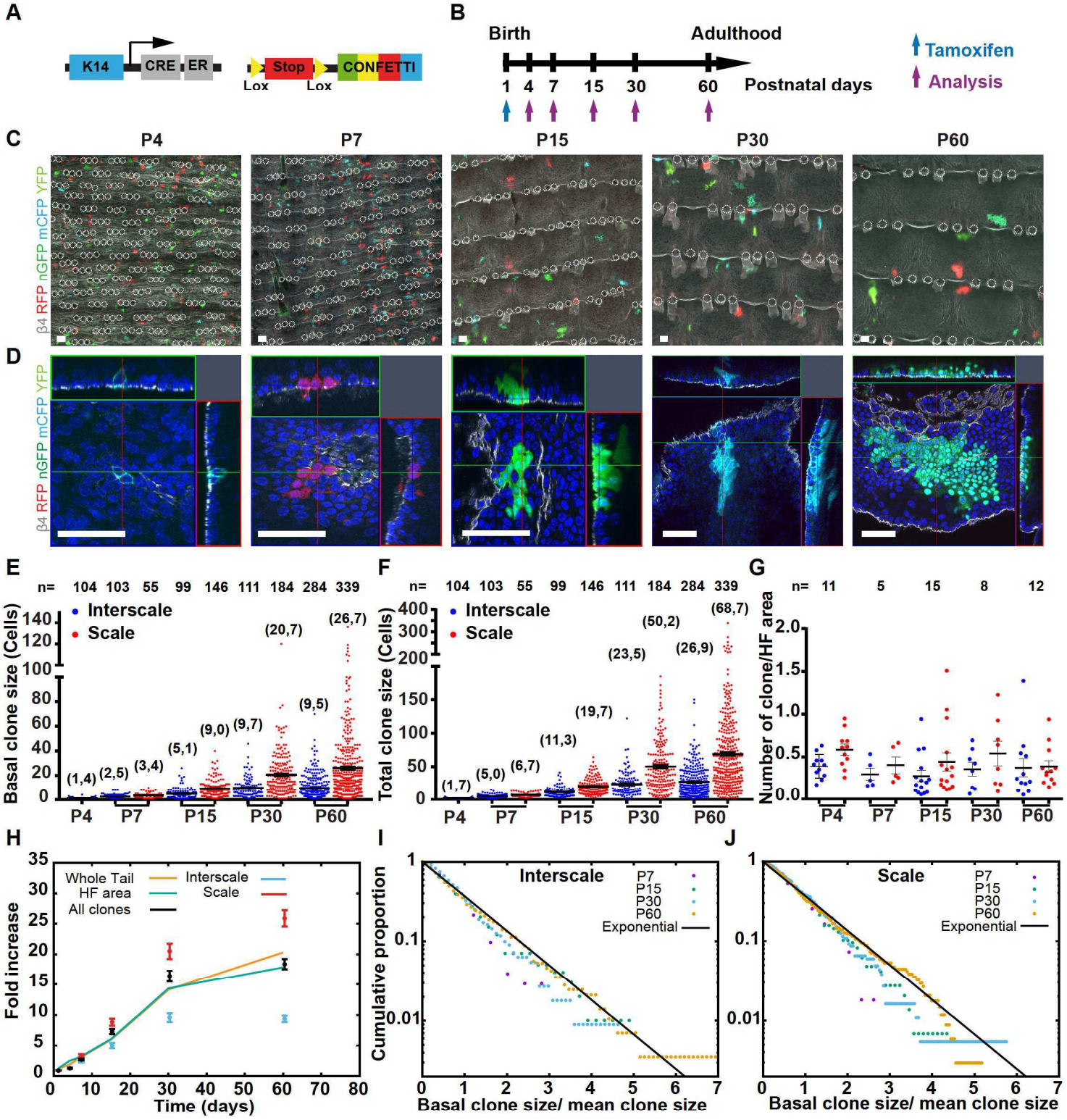
A
K14
CRE
ER
Stop
CONFETTI
Lox
Lox
B
Birth
Adulthood
1 4 7 15 30 60
Postnatal days
Tamoxifen
Analysis
C
P4
P7
P15
P30
P60
β4 RFP nGFP mCFP YFP
D
E
n= 104 103 55 99 146 111 184 284 339
Interscale
Scale
Basal clone size (Cells)
(1,4) (2,5) (3,4) (5,1) (9,0) (9,7) (20,7) (9,5) (26,7)
P4 P7 P15 P30 P60
F
n= 104 103 55 99 146 111 184 284 339
Total clone size (Cells)
(1,7) (5,0) (6,7) (11,3) (19,7) (23,5) (50,2) (26,9) (68,7)
G
n= 11 5 15 8 12
Number of clone/HF area
H
Whole Tail
HF area
All clones
Interscale
Scale
Fold increase
Time (days)
I
Interscale
P7
P15
P30
P60
Exponential
Cumulative proportion
Basal clone size/ mean clone size
J
Scale
Basal clone size/ mean clone size

Figure 2. Lineage tracing of developmental progenitors recapitulates tissue growth. (A) Genetic strategy used to target multicolor Confetti expression in K14-expressing BCs. (B) Protocol used to study the fate of BCs targeted at birth (P1). (C) Representative *K14-CreER/Rosa-Confetti* whole-mount tail epidermis collected at the given time points, induced clonally at P1 (Maximum intensity projection of confocal images). Scale bar = 50µm. (D) Confocal images showing Confetti clones from P4 to P60. Scale bar = 50µm. (E-F) Quantification of the number of basal (E) and total (F) cells per clone in interscale and scale. N= number of analyzed clones, brackets : average clone size . (G) Quantification of the number of clones per HF area in interscale and scale. N=number of mice. (H) Graph showing the basal clone size from scale, interscale and all clones normalized to their relative surface area, the expansion of the whole tail surface and HF area. (I,J) Cumulative distributions of interscale (I) and scale (J) basal clone size, rescaled by average clone size at all time points and well-described by a simple exponential distribution (black line). Data are represented as mean ± SEM.

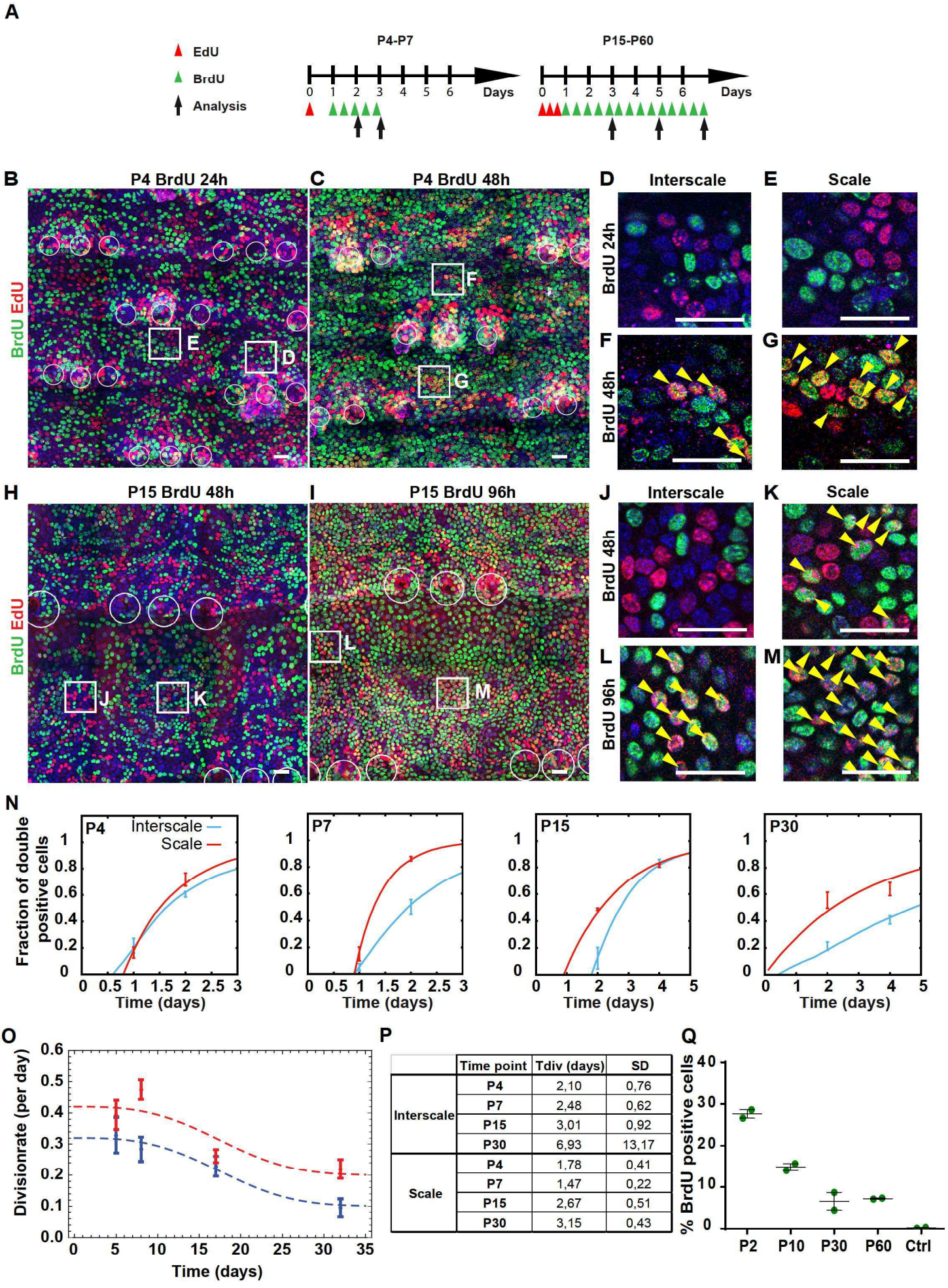

	Time point	Tdiv (days)	SD
Interscale	P4	2,10	0,76
	P7	2,48	0,62
	P15	3,01	0,92
	P30	6,93	13,17
Scale	P4	1,78	0,41
	P7	1,47	0,22
	P15	2,67	0,51
	P30	3,15	0,43

Figure 3. Ever-decreasing proliferation rate of DPs during postnatal growth. (A) Protocol of the EdU/BrdU double-labeling experiments. (B-G) Representative P4 whole-mount tail epidermis at the given time points (B and C) (Maximum intensity projection of confocal images) and higher magnification of BCs in interscale (D, F) and scale (E, G) at the same time points. (H-M) Representative P15 whole-mount tail epidermis at the given time points (H and I) (Maximum intensity projection of confocal images) and higher magnification of BCs in interscale (J, L) and scale (K, M) at the same time points. Yellow arrowheads : EdU/BrdU double-labeled cells. White circles : hair follicles. Nuclei are stained with Hoechst. Scale bar = 50µm. (N) Quantification of EdU/BrdU double positive BCs in scale and interscale. ($n \geq 3$ mice). Lines : theoretical fits from a model of stochastic division after a refractory phase. Data are represented as mean ± SEM. (O) Time evolution of the division rate in both scale (red) and interscale (blue) BCs from P1 to P30.Thin lines : fit of the decrease in division rate over time, used for subsequent clonal modelling. Error bars: mean and SD. (P) Average division time (TDiv) of epidermal BCs in interscale and scale calculated from EdU/BrdU analysis. (Q) Quantification of BrdU+ primary keratinocytes isolated from P2, P10, P30 and P60 mice, cultured for 48h and incubated for 2h with BrdU (n=2 experiments). See also Figure S2.

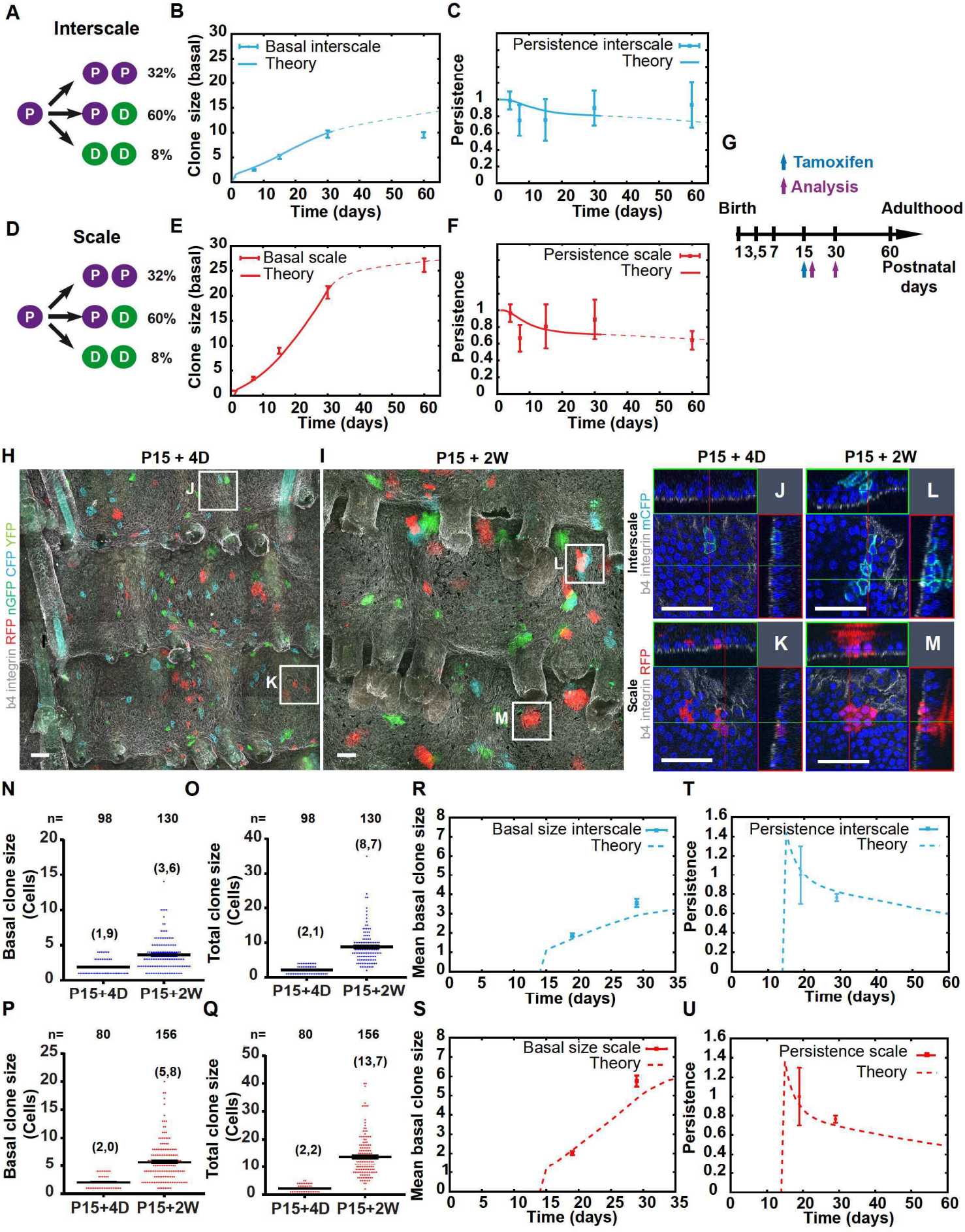
A
Interscale
P P 32%
P P D 60%
D D 8%
B
Basal interscale
Theory
Clone size (basal)
Time (days)
C
Persistence interscale
Theory
Persistence
Time (days)
D
Scale
P P 32%
P P D 60%
D D 8%
E
Basal scale
Theory
Clone size (basal)
Time (days)
F
Persistence scale
Theory
Persistence
Time (days)
G
Tamoxifen
Analysis
Birth
Adulthood
13,5 7
15
30
60
Postnatal days
H
P15 + 4D
I
P15 + 2W
b4 integrin RFP nGFP CFP YFP
J
K
L
M
P15 + 4D
P15 + 2W
Interscale
b4 integrin mCFP
Scale
b4 integrin RFP
N
Basal clone size (Cells)
n= 98 130
(1,9)
(3,6)
P15+4D P15+2W
O
Total clone size (Cells)
n= 98 130
(2,1)
(8,7)
P15+4D P15+2W
R
Mean basal clone size
Basal size interscale
Theory
Time (days)
T
Persistence
Persistence interscale
Theory
Time (days)
P
Basal clone size (Cells)
n= 80 156
(2,0)
(5,8)
P15+4D P15+2W
Q
Total clone size (Cells)
n= 80 156
(2,2)
(13,7)
P15+4D P15+2W
S
Mean basal clone size
Basal size scale
Theory
Time (days)
U
Persistence
Persistence scale
Theory
Time (days)

Figure 4. A constant excess of symmetric renewing division mediates postnatal development. (A-F) Theoretical modeling of the *K14-CreER/Rosa-Confetti* clonal data. A single population of DPs undergo stochastic fate choices with a constant imbalance of Δ=24% in favor of self-renewing division (PP) compared to differentiation (DD), together with an ever-decreasing proliferation rate between P1 and P30, in both interscale (A) and scale (D). This model fits well with the measured expansion of basal clone size (B and E) and clonal persistence (C and F) in each region. Symbols : experimental data, lines : model prediction (thick line : P1-P30 model, thin dashed line : P30-P60 homeostatic model). (G) Experimental design used to challenge the theoretical model. (H-I) Representative *K14-CreER/Rosa-Confetti* epidermis analyzed 4 days (H) and 2 weeks (I) after TAM injection at P15 (Maximum intensity projection of confocal images). (J-M) Confocal images of representative clones in interscale (J, L) and scale (K, M) 4 days and 2 weeks after TAM injection. Scale bar = 50µm. (N-Q) Quantification of interscale (N, O) and scale (P,Q) basal (N, P) and total (O, Q) clone size over time (n=5 mice). N=number of analyzed clones, brackets : average clone size . (R-U) The theoretical model predicts well the experimental measures of the basal clone size expansion (R,S) and the clonal persistence (T,U) in the interscale (R,T) and the scale (S,U) 4 days and 2 weeks after TAM administration to P15 mice. Symbols : experimental data, dashed lines : model predictions. Data are represented as mean ± SEM. See also Figure S3 and S5.

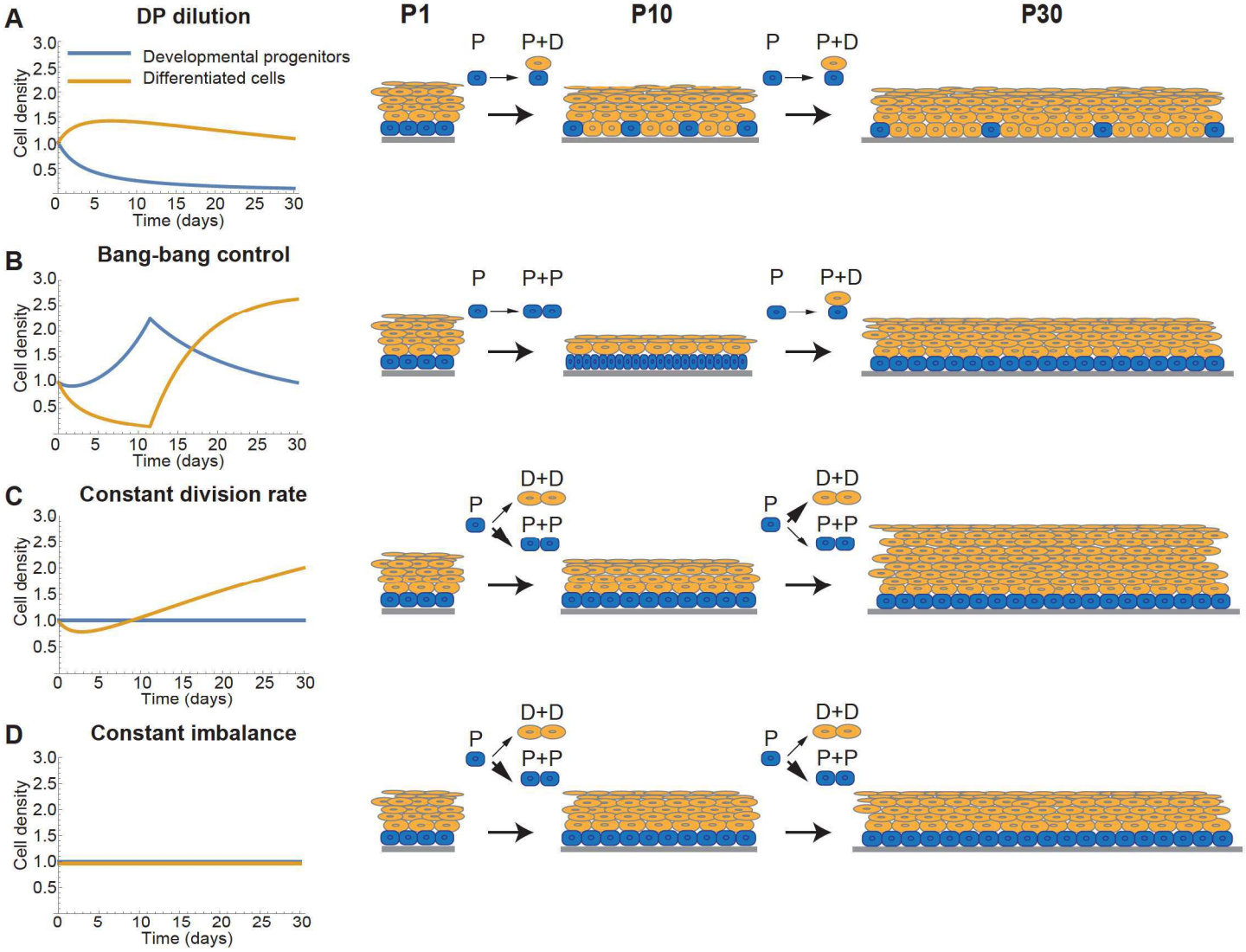

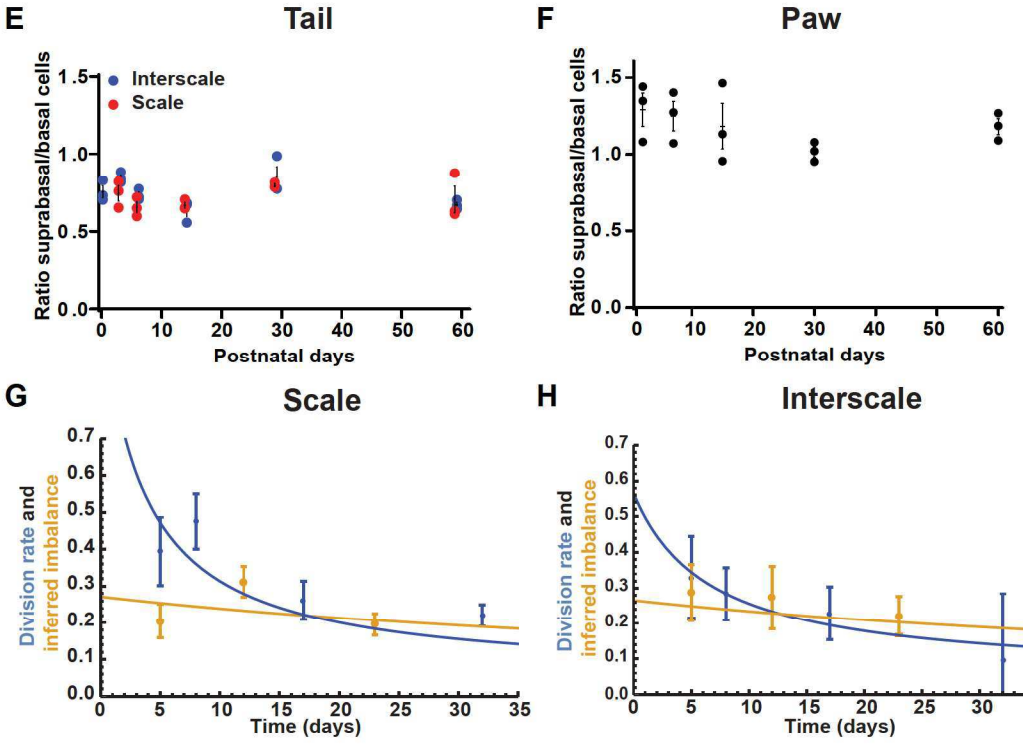

Dekoninck et al, Figure 5

Figure 5. A constant imbalance mediates harmonious tissue expansion. (A-D) Schematics of possible design principles underlying epidermal expansion (imposed by the growth of the tail)(See Method). Epidermis could grow following balanced cell fates and a higher proliferation rate (A) which would lead to the accumulation of non-dividing differentiated cells in the basal layer and DP dilution. In the case of Bang-Bang control mechanism (B) DPs would achieve only symmetrical renewal during a first period and produce an overshoot of DPs without any new suprabasal cells produced. In a second period, DPs would achieve only asymmetrical divisions to re-establish the suprabasal layers. In a constant division rate scenario (C), DPs would keep a constant division rate but always change their cell fate outcome. By contrast with the other scenarios, a constant imbalance (D) accompanied by a decreasing proliferation rate would enable to produce new DPs and sustain the suprabasal cell density along the growth. (E-F) Quantification of the number of suprabasal cells compared to the number of BCs in tail (E) and paw (F) epidermis(n=3 mice per time point). (G-H) Time evolution of the measured division rate (blue dots, from Figure 3O) and piece-wise inferred imbalance (orange dots, from clonal data) compared to the theory prediction (thick lines) in scale (G) and interscale (H), after inputting the overall growth rates of the two regions (from Figure 1) in the model. Theory of tissue expansion with the constraints of maintaining basal and suprabasal density constant predicts a nearly constant imbalance rate (orange line), and a constantly decaying division rate (blue line). Error bars: mean and SD. See also Figure S4 and STAR Method.

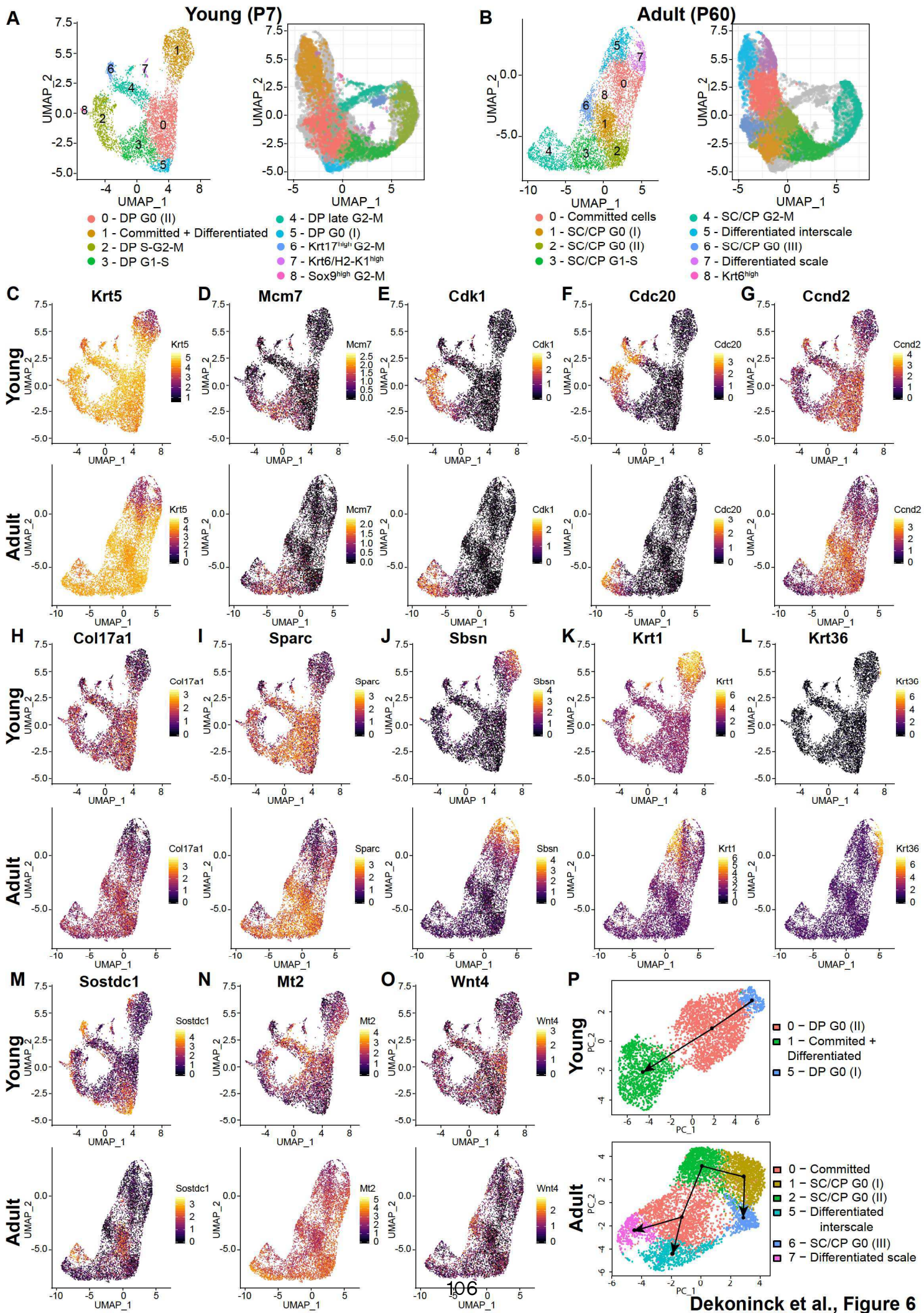

Dekoninck et al., Figure 6

Figure 6. Single cell RNA sequencing of BCs in young and adult tail epidermis.

(A-B) UMAP dimensionality reduction plots for the individual (left) P7 (A) and P60 (B) samples using Seurat and the integrated dataset (right) using Harmony. Colors represent cluster identities computed on the individual samples. (C-O) Normalized expression of genes expressed in young (upper panels) and adult (lower panels). *Krt5* (C) highlight basal cells. *Mcm7* (D), *Cdk1* (E) and *Cdc20* (F) are cell cycle genes revealing BCs in G1-S, S-G2-M and late G2-M respectively. *Ccnd2* (G), *Col17a1* (H) and *Sparc* (I) are three markers associated with Stem/progenitors cells. *Sbsn* (J), *Krt1* (K) and *Krt36* (L) highlight all differentiated cells, differentiated cells in adult interscale and in scale respectively. *Sostdc1* (M) is highly expressed in population SC/CP G0 I in adult and DP G0 I in young samples, *Mt2* (N) and *Wnt4* (O) appear in DP G0 II together but in separated populations in adult sample. (P) Slingshot lineage trajectories for non-cycling cells showing a unique direction toward differentiated cells in young sample (upper panel) and multiple directions toward interscale, scale and SC/CP III cell populations (lower panel). See also Figure S6.

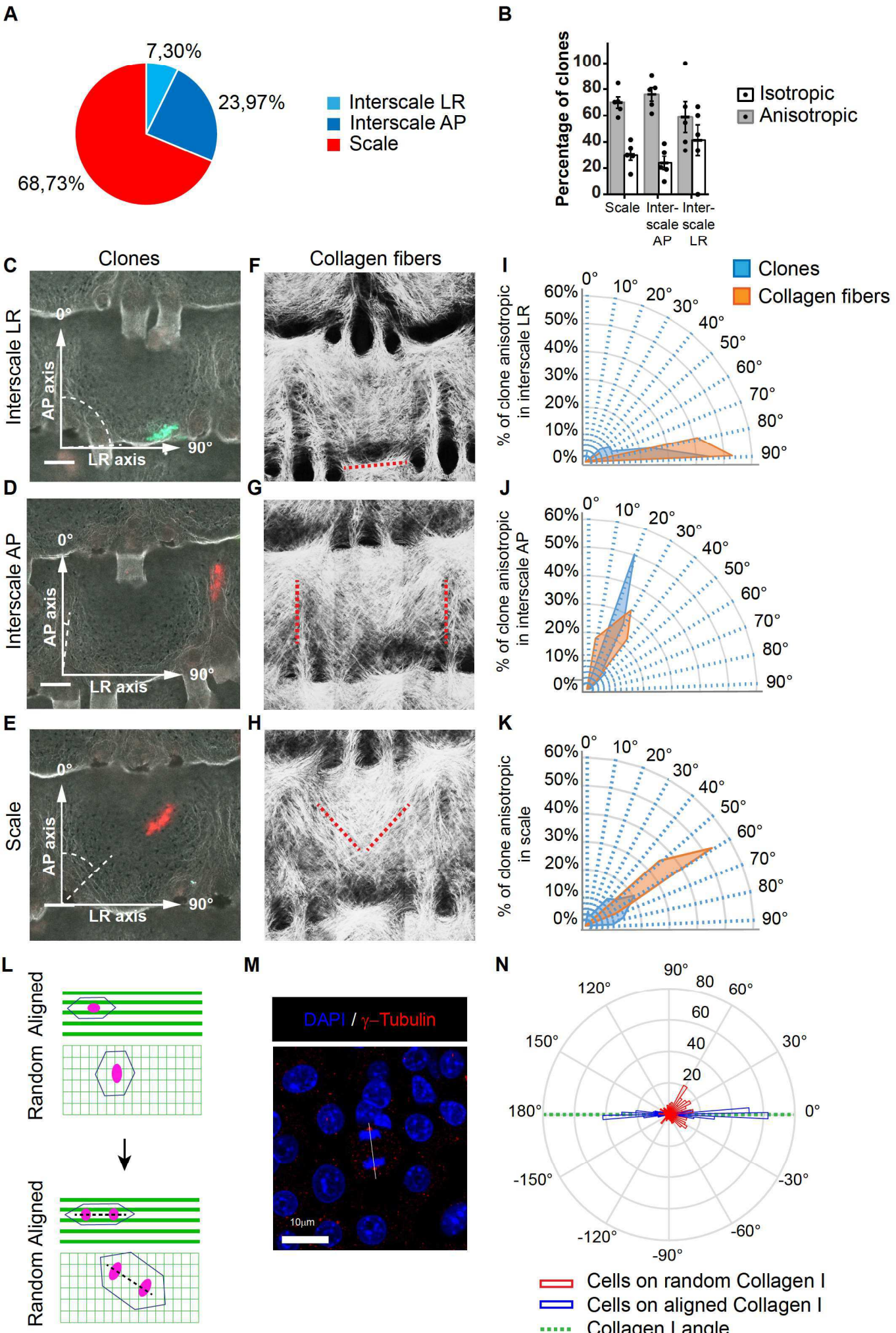

Dekoninck et al., Figure 7

Figure 7. The orientation of the collagen fibers correlates with clone anisotropy and tissue expansion. (A-B) Quantification of the clones repartition (A) and the proportion of anisotropic and isotropic clones (B) counted on *K14-CreER/Rosa-Confetti* mice induced at P1 and analyzed at P30. (n=726 clones, from 5 mice). (C-K) Maximum intensity projection of confocal images showing representative anisotropic clones in interscale LR (C), interscale AP (D) and scale (E) as well as second harmonic signal highlighting fibrillary collagen in the upper dermis of the tail (F-H), red dotted lines show fibers orientation, Scale bar = 100µm. (I-K) Quantification of the anisotropic clone orientation and collagen fibers orientation relative to the AP axis in interscale LR (I), interscale AP (J) and scale (K). (L-N) Schematic illustration (L) and quantification (M, N) of cell division orientation in primary keratinocyte 2D culture plated on collagen-coated micro-patterned surfaces, 24 hours post seeding. Roseplot shows orientation angle respect to aligned collagen fibers (0°). (n> 300 mitoses/condition from 3 independent experiments; $p<0.0001$*, Mann Whitney). See also Figure S7.

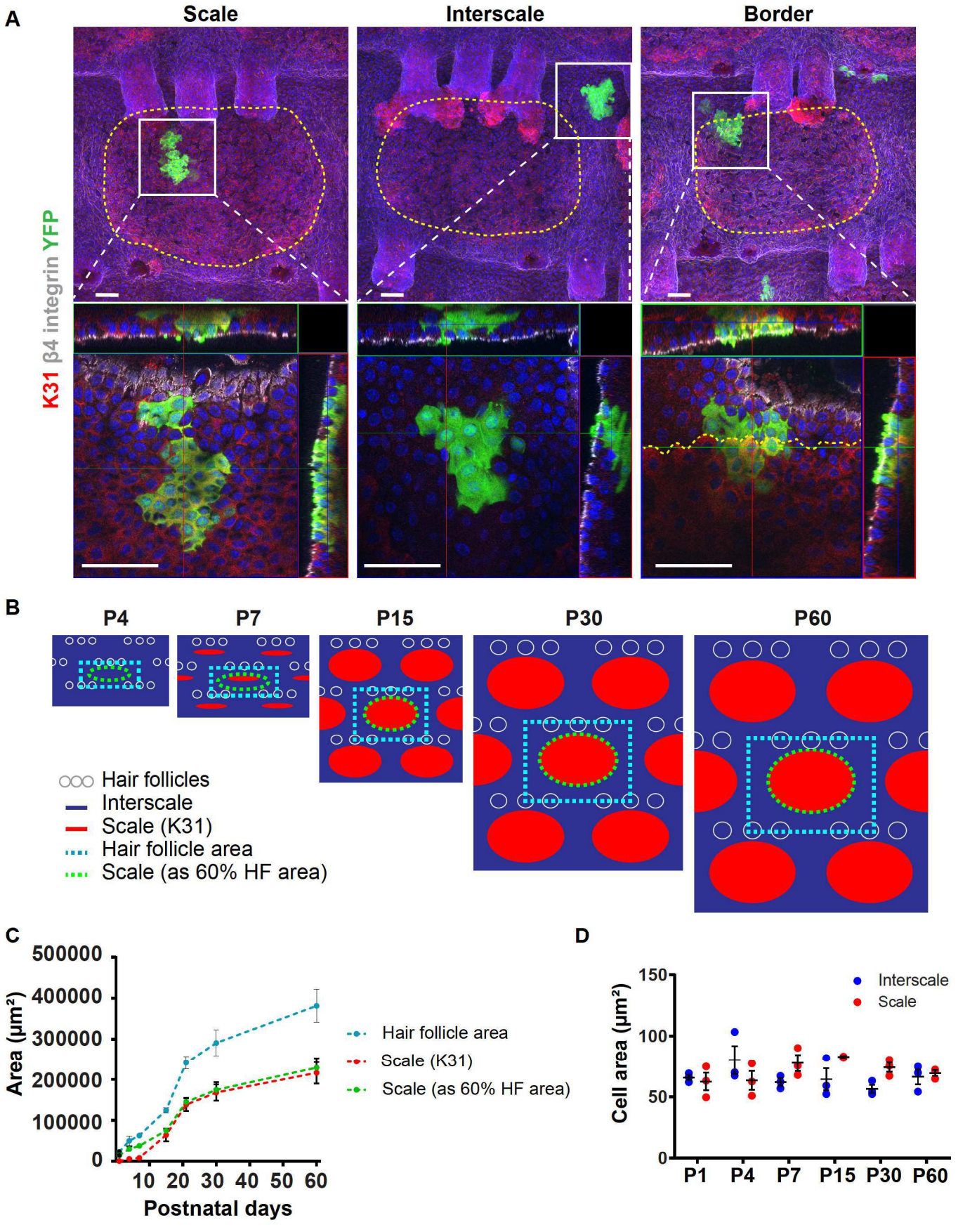

Dekoninck et al, Figure S1

SUPPLEMENTAL FIGURES TITLES AND LEGENDS

Figure S1. The hair follicle area expands linearly during postnatal development, related to Figure 1. (A) Maximum intensity projection (upper panels) and confocal images (lower panels) of *K14-CreER/Rosa-YFP* clones induced at P1 showing that clones appear in the scale (left), interscale (middle) and also at the border of the two regions (right) at P30. These data show that scale and interscale compartments are not yet defined at the time of the tracing induction. Yellow dotted line surround scale region. Nuclei are stained with Hoechst. Scale bar = 50µm. (B-C) Schematic (B) and measurement (C) of the surface area occupied by suprabasal cells expressing K31 compared to the hair follicle area measured by the HF coordinates as 60% of the HF area. Our measures show that the HF area grows 2-fold from P7 to P15 while K31 staining expands 8-fold, suggesting that a change in K31 expression occurs in the suprabasal cells that is not the reflection of cell division as no particular increased cell division in the scale region reflects this expansion. The expansion of K31 area correlates well with the overall tissue growth only after P15, when scale/interscale differentiation is complete. Data are represented as mean ± SEM (n≥3 mice per time point). (D) Surface area of the scale and interscale BCs at different time points, measured on confocal pictures, showing no difference of cell size during postnatal development (See Methods). Data are represented as mean ± SEM (n= 3 mice per time point).

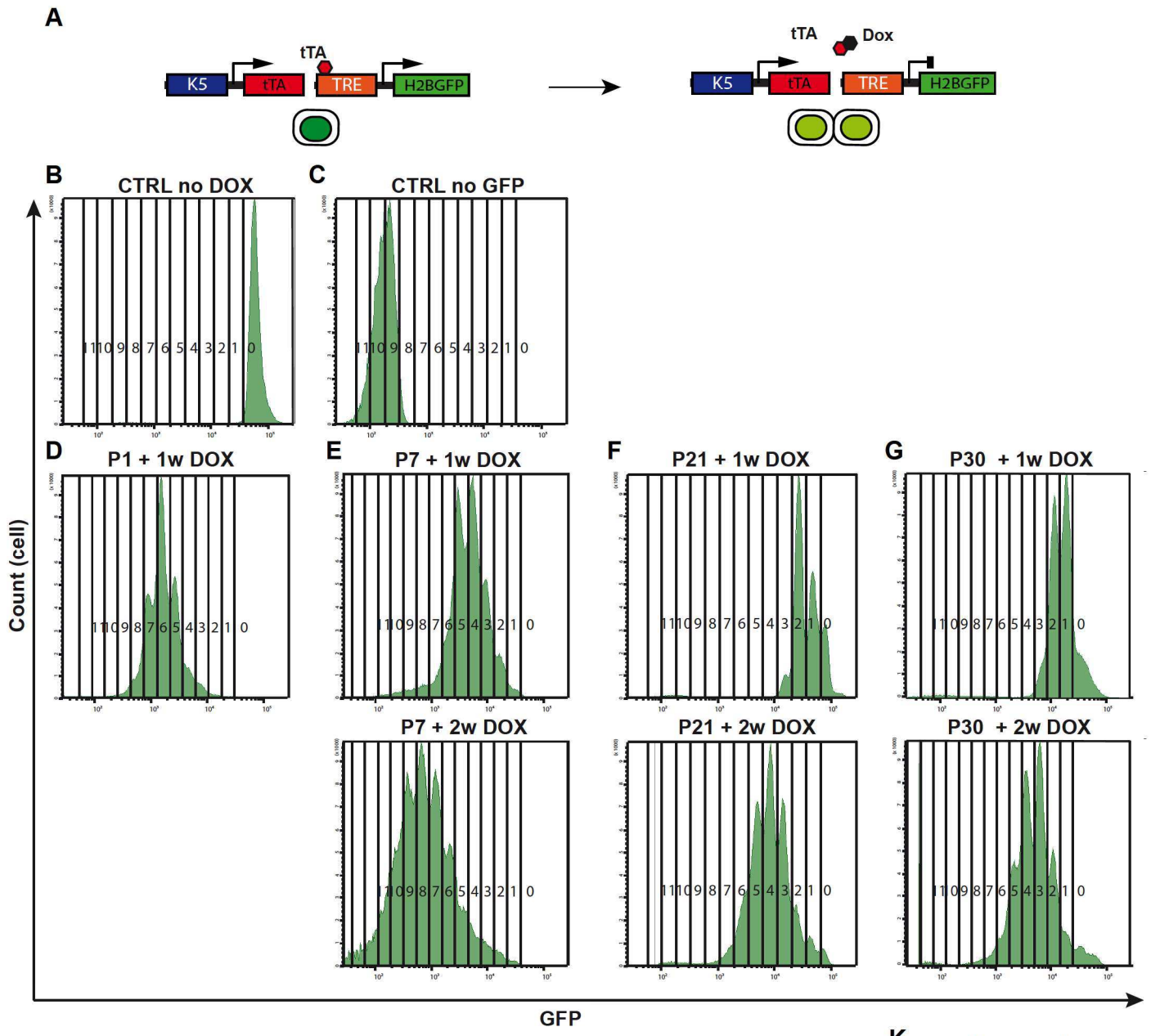

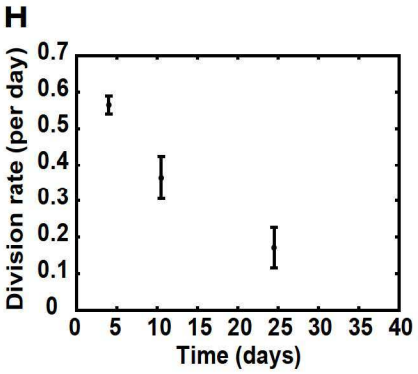

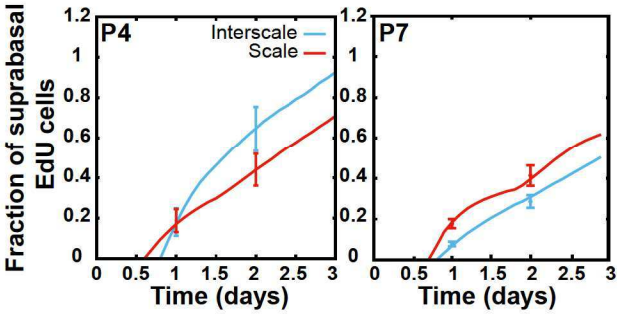

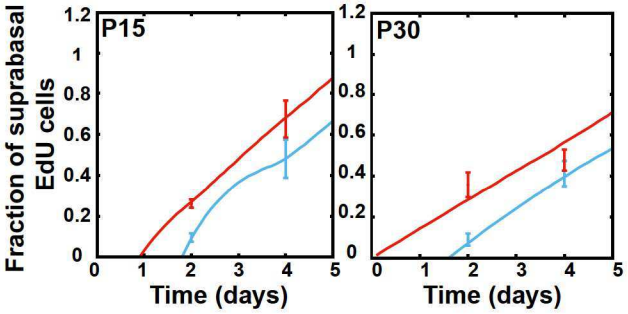

I

Time point	Tdiv (days)	SD
P1-P7	1,23	0,05
P7-P15	1,90	0,31
P21-P28	4,05	1,30

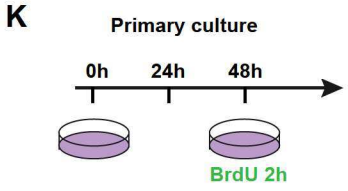

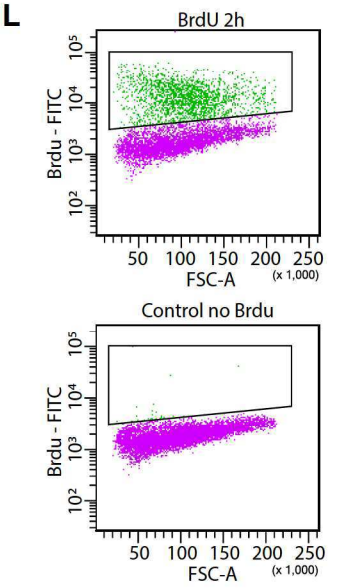

Dekoninck et al, Figure S2

Figure S2. Ever-decreasing proliferation rate of DPs during postnatal growth, related to Figure 3. (A) Genetic strategy used to induce H2B-GFP pulse chase experiments in epidermal BCs and monitor the number of basal cell division overtime. In the absence of doxycycline (Dox) in *K5tTA/TetO-H2B-GFP* mice, H2B-GFP is expressed at a uniform and high level in all BCs. Upon Dox addition, the transcription of H2BGFP is blocked and H2B-GFP fluorescence is diluted by 2 at each cell division, which can be quantitatively monitored by FACS. (B-G) Examples of H2B-GFP fluorescence peak patterns observed in Itga6^{high} CD34^{negative} by FACS analysis in unchased mice having a high intensity of H2B-GFP (B), control CD1 mouse without any GFP signal (C), P1 mice after one week of chase (D), P7 (E), P21 (F) and P30 (G) mice with different chase periods, n=3 mice per time point. (H-I) Calculated division rate of BCs over time from the distribution of the H2B-GFP dilution after 1 week (H) and average division time (Tdiv) of epidermal BCs for each mouse age inferred from H2B-GFP analysis (I). (J) Fraction of suprabasal EdU+ cells over basal EdU+ cells in scale and interscale in EdU/BrdU double labeling experiments at different time points (see Methods). n≥3 mice per time point. (K-L) Scheme (K) and representative FACS plot (L) of primary culture experiment used to asses the proliferation rate of freshly isolated keratinocytes. Primary cells isolated from tail mice aged of P2,P10, P30 and P60 were cultured for 48h, treated for 2h with BrdU and collected for FACS analysis. Untreated cells were used as negative control.

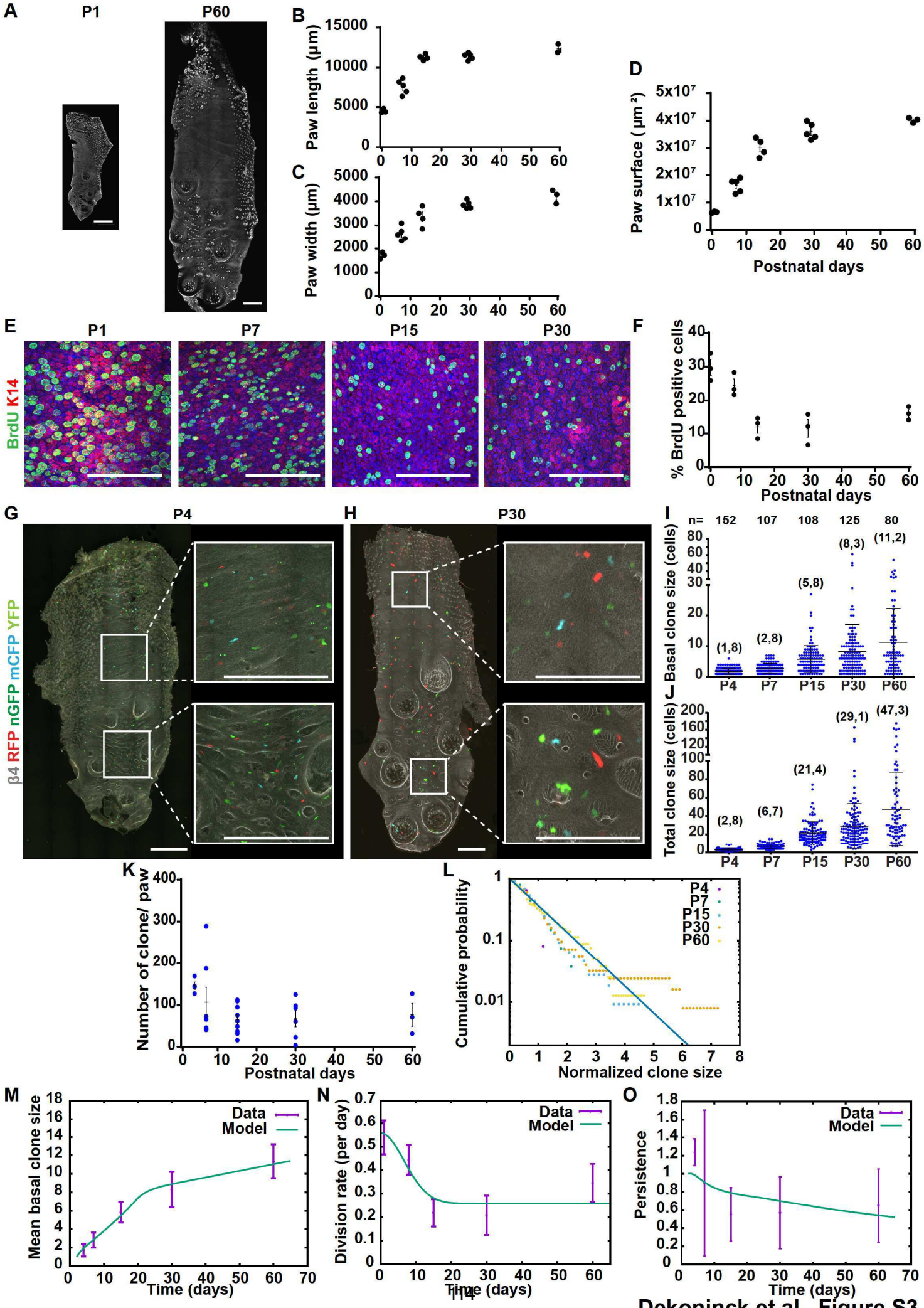

Dekoninck et al., Figure S3

Figure S3. Lineage tracing of developmental progenitors in the paw epidermis also recapitulate tissue expansion, related to Figure 4. (A) Whole-mount paw epidermis from newborn (P1) and adult (P60) mice. (B) Measurement of the length of the paw from P1 to P60 (n≥5 mice). (C) Measurement of the paw width from P1 to P60 (n≥5 mice). (E) Calculated total paw surface showing a linear increase from P1 to P15 reaching a plateau after P21 (n≥5 mice). (E-F) Whole-mount paw epidermis (E) and quantification of BrdU positive BCs (F) analysed in P1, P7, P15 and P30 epidermis 4h after a pulse of BrdU. (G-H) Representative pictures of whole-mount paw epidermis from *K14-CreER/Rosa-Confetti* mice induced with 10µg of Tamoxifen at P1 and collected at P4 (G) and P30 (H). Scale bar = 1mm. (I-J) Quantification of the number of basal (I) and total (J) cells per clone in paw epidermis counted on confocal pictures from P4 to P60 and showing the expansion of the clones over time. N: number of analyzed clones , brackets : average clone size . (K) Quantification of the number of clone per paw epidermis overtime. (L) Cumulative distributions of paw basal clone size, rescaled by average clone size at all time points (purple, green, blue, orange and yellow dots resp. for P4, P7, P15, P30 and P60). In all cases, the rescaled distributions are well-described by a simple exponential distribution (black line). Data are represented as mean ± SEM. (M-O) The theoretical model predicts well the experimental measures of the basal clone size expansion (M), the decreasing proliferation rate (N) and the clonal persistence (O) in the paw epidermis. Symbols : experimental data, green lines : model predictions. Data are represented as mean ± SEM.

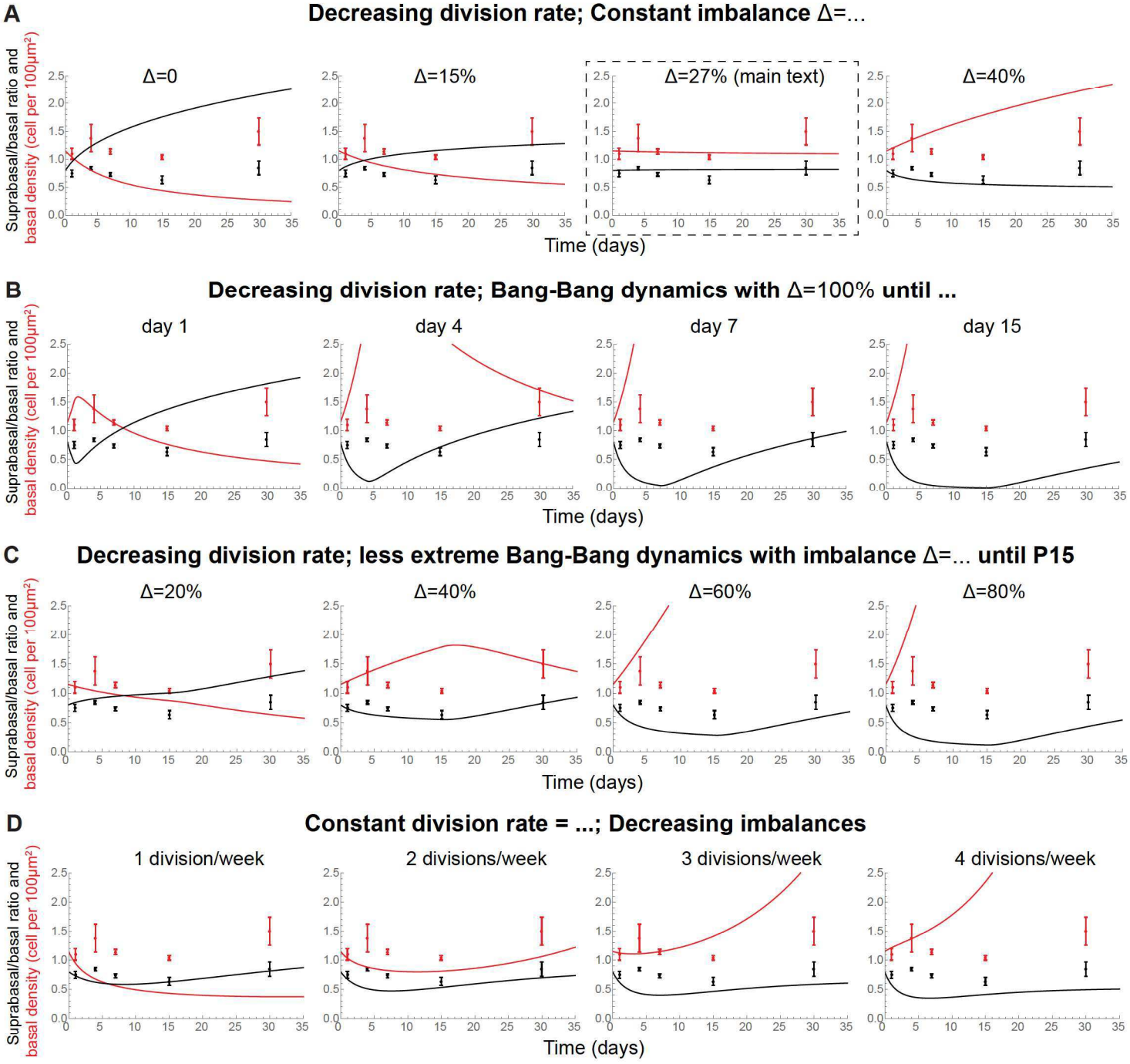
A
Decreasing division rate; Constant imbalance Δ=...
Δ=0
Δ=15%
Δ=27% (main text)
Δ=40%
B
Decreasing division rate; Bang-Bang dynamics with Δ=100% until ...
day 1
day 4
day 7
day 15
C
Decreasing division rate; less extreme Bang-Bang dynamics with imbalance Δ=... until P15
Δ=20%
Δ=40%
Δ=60%
Δ=80%
D
Constant division rate = ...; Decreasing imbalances
1 division/week
2 divisions/week
3 divisions/week
4 divisions/week
Suprabasal/basal ratio and
basal density (cell per 100µm²)
Time (days)

Figure S4. Simulation of basal cell density and basal to suprabasal ratio according to the different theoretical models, related to Figure 5. Comparison between model prediction and data (both shown for interscale). Black : suprabasal/basal ratio, red : basal density in cell per μm^2. (A) Influence of the value of constant imbalance $\Delta = 0, 15, 27, 40\%$ (with continually adjusting division rate as in main text), showing for instance that imbalances of 15% or 40% produce highly different predictions, while an imbalance of 27% produces harmonious growth with constant basal and suprabasal densities (B) Predictions of bang-bang dynamics (transition from Δ=100% to 0% imbalance at varying time points: P1, P4, P7 and P15) together with a continually decreasing division rate (as in main text), producing a vast excess of BCs. (C) Prediction of a "soft" bang-bang dynamics (transition from varying, partial imbalance values $\Delta = 20,40,60,80\%$ to Δ =0% at P15), which again provides poor fits to the data, in particular as it predict a drop of basal density post P15, not observed in the data. (D) Predictions for a continually adjusting/decreasing imbalance, together with a constant division rate, not observed in the data (resp. 1,2,3 and 4 divisions per week). Error bars: mean and SD.

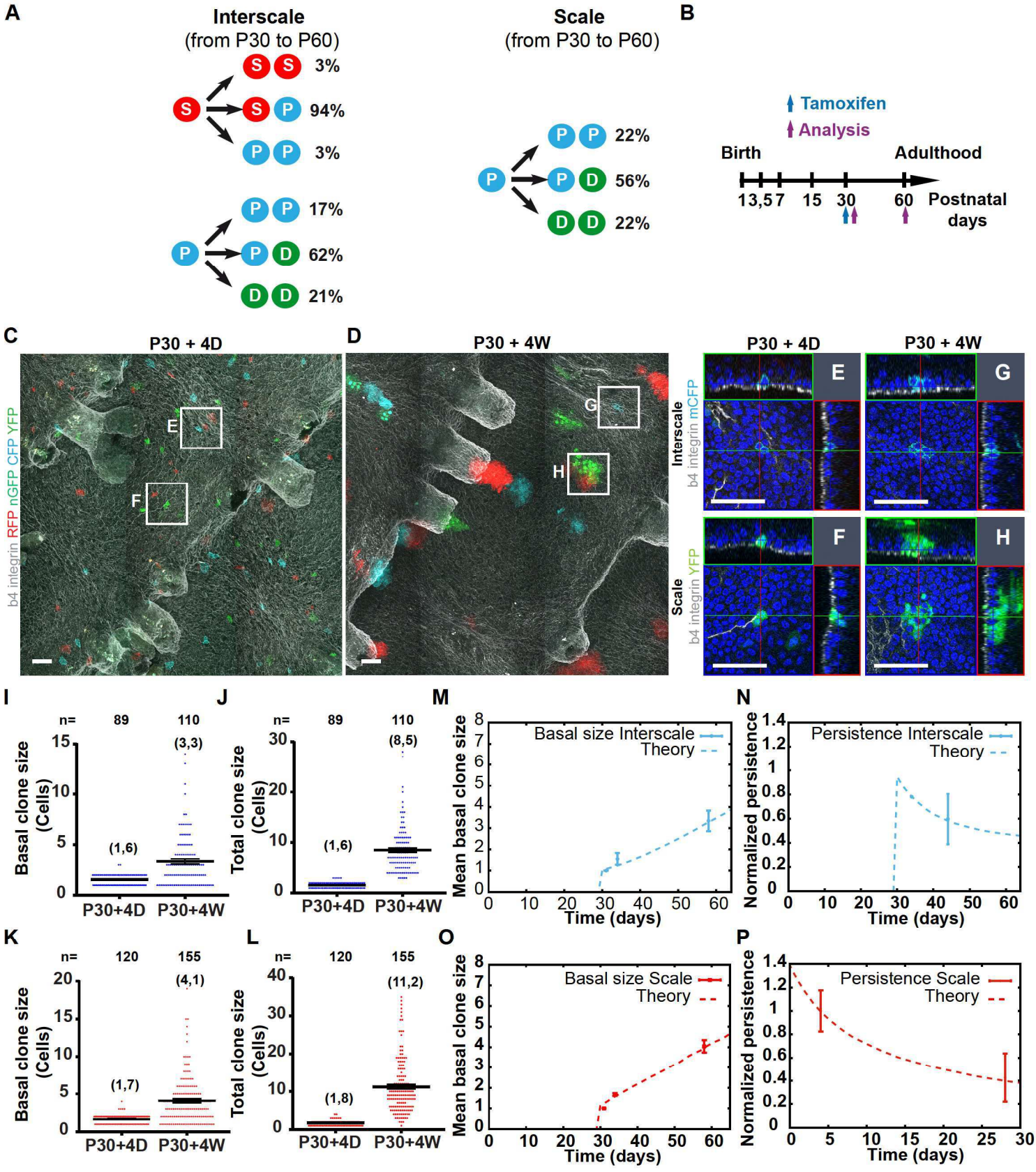
A
Interscale
(from P30 to P60)
S S 3%
S S P 94%
P P 3%
P P 17%
P P D 62%
D D 21%
Scale
(from P30 to P60)
P P 22%
P P D 56%
D D 22%
B
Tamoxifen
Analysis
Birth
Adulthood
13,5 7 15 30 60 Postnatal days
C
P30 + 4D
D
P30 + 4W
b4 integrin RFP nGFP CFP YFP
E
F
G
H
P30 + 4D
P30 + 4W
Interscale
b4 integrin mCFP
Scale
b4 integrin YFP
I
Basal clone size (Cells)
n= 89 110
(1,6)
(3,3)
P30+4D P30+4W
J
Total clone size (Cells)
n= 89 110
(1,6)
(8,5)
P30+4D P30+4W
M
Mean basal clone size
Basal size Interscale
Theory
Time (days)
N
Normalized persistence
Persistence Interscale
Theory
Time (days)
K
Basal clone size (Cells)
n= 120 155
(1,7)
(4,1)
P30+4D P30+4W
L
Total clone size (Cells)
n= 120 155
(1,8)
(11,2)
P30+4D P30+4W
O
Mean basal clone size
Basal size Scale
Theory
Time (days)
P
Normalized persistence
Persistence Scale
Theory
Time (days)

Figure S5. Transition between postnatal expansion and adult homeostasis, related to Figure 4. (A) Model of the clonal dynamics governing scale and interscale homeostasis (Sanchez-Danes et al., 2016). (B) Experimental scheme of the clonal analysis performed at the time of the transition between the postnatal growth and adult homeostasis to challenge the theoretical model. (C-D) Representative *K14-CreER/Rosa-Confetti* whole-mount epidermis analyzed 4 days (C) and 4 weeks (D) after TAM injection at P30 (Maximum intensity projection of confocal images). (E-H) Confocal images of representative clones in interscale (E, G) and scale (F, H) 4 days and 4 weeks after TAM injection. Scale bar = 50µm. (I-L) Quantification of interscale (I, J) and scale (K, L) basal (I, K) and total (J, L) clone size over time at P30. N: number of clones analyzed from 5 mice, brackets : average clone size. (M-P) The model predicts well the basal clone size expansion (M, O) and the clonal persistence (N, P) in interscale and the scale at the different time points. Symbols :experimental data, dashed lines ; model prediction. Data are represented as mean ± SEM.

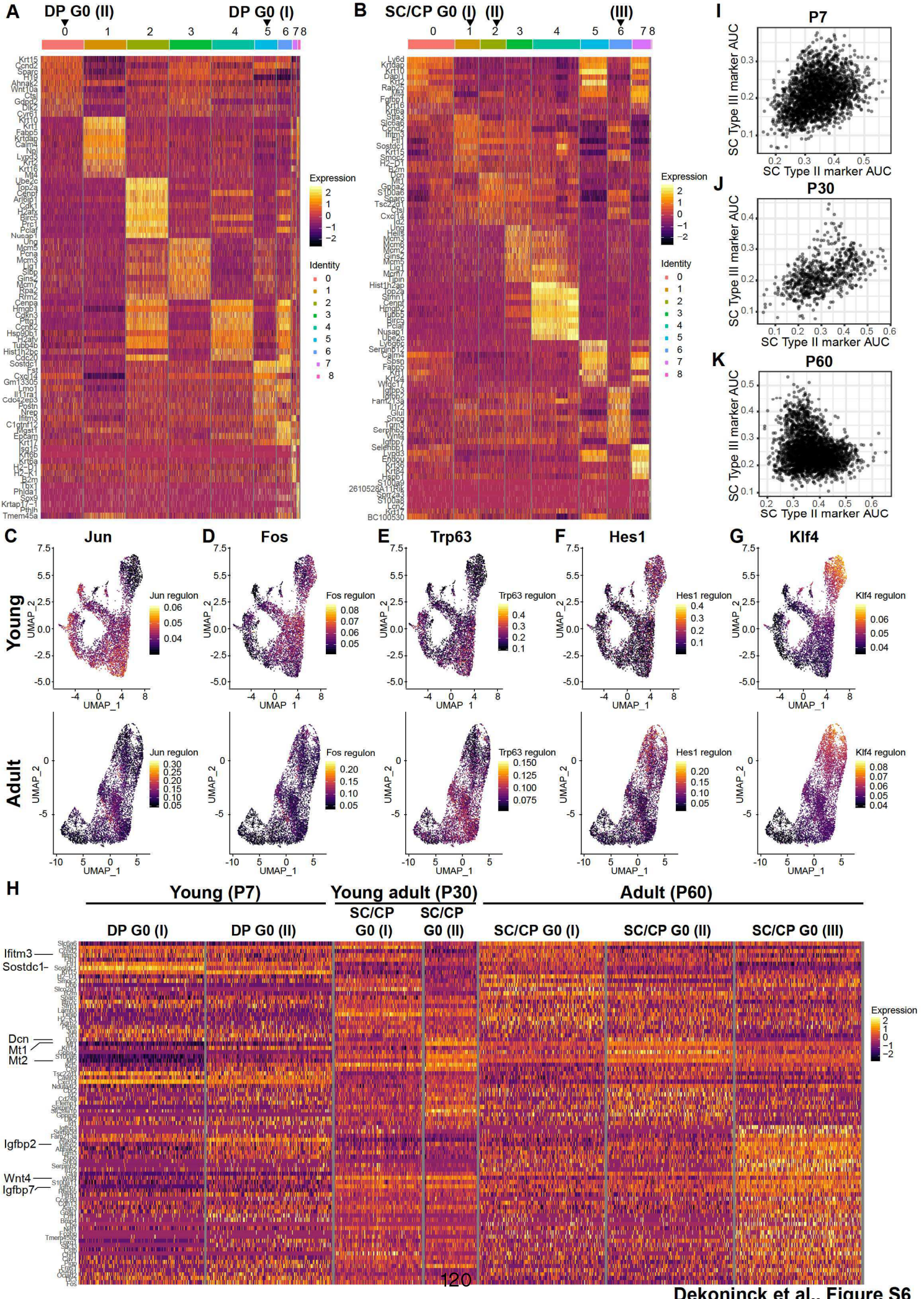

Dekoninck et al., Figure S6

Figure S6. Single-cell RNA sequencing of Developmental Progenitors in young and Stem/progenitors in adult, related to Figure 6. (A-B) Heatmap showing the relative expression of the genes defining the different populations in young (A) and adult (B) samples. DP G0 and SC/CP G0 populations are shown with arrows. (C-G) UMAP dimensionality reduction plots colored by the degree of regulon activation for transcription factors differentially activated (AUC rank-sum test FDR corrected p-value < 0.05) in DP G0 I (C) and DP G0 II (D) or both (E) and in differentiated cells (F,G) in young (upper panel) and adult (lower panel). Color scaling :AUC value of target genes in the regulon being expressed as computed by SCENIC. (H) Heatmap showing the relative expression of the genes identified in adult SC/CP populations in non-cycling BCs at P7, P30 and P60. Rows represent marker genes for P60 SC/CP subpopulations with a log-fold change in expression greater than 0.3. Columns represent cells belonging to DP clusters at P7 and SC/CP clusters at P30 and P60. The colour of the cells represent normalized expression values for each gene-cell combination. P7 and P60 samples were subsampled to 200 cells each respectively. (I-K) Scatter plots of marker gene set enrichment. Dots represent individual cells in DP clusters at P7 (I) and SC/CP clusters at P30 (J) and P60 (K). The x-axis represents the AUC values computed for each cell using the AUCell package and describe how high they express the P60 SC/CP G0 II marker genes whereas the y-axis represents AUC values for the SC/CP G0 III marker genes. Linear correlations between the two AUC values is linked to sensitivity of detection and is correlated with the number of detected genes. Cells following a diagonal trend represent cells that homogeneously express the two sets of markers while cells deviating from the trend represent cells expressing distinct transcriptional marker gene signatures.

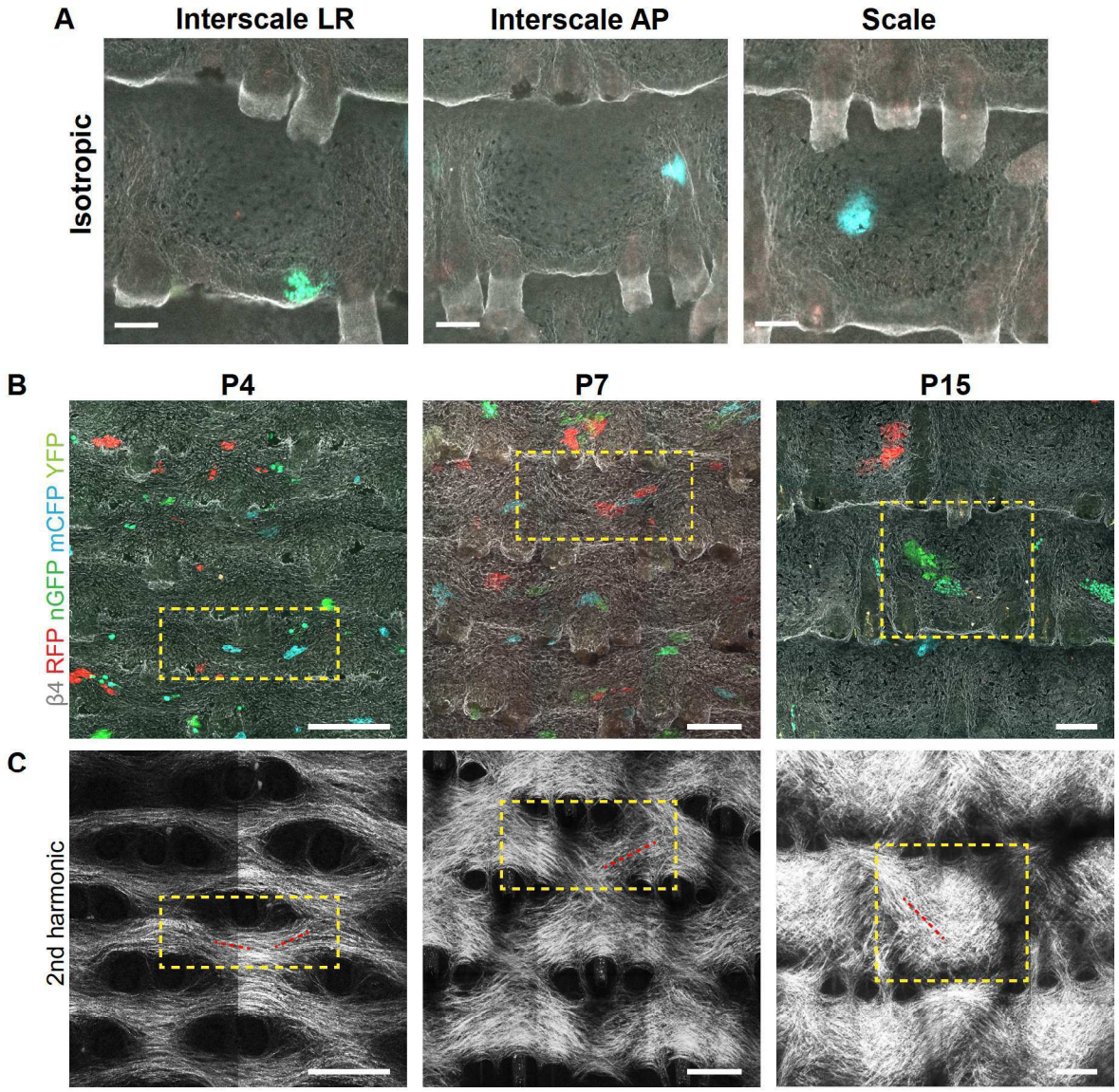

Dekoninck et al., Figure S7

Figure S7. Clone shape and mechanical constraints during postnatal skin expansion, related to Figure 7. (A) Whole-mount tail skin epidermis showing isotropic clones in the different regions of the tail IFE at P30 in a *K14-CreER/Rosa-Confetti* mouse induced at P1 (Maximum intensity projection of confocal pictures). (B-C) Whole-mount epidermis (B) and second harmonic signal highlighting fibrillary collagen in similar area (C) collected from mice aged of P4, P7 and P15. Yellow dotted square : hair follicle area with the scale in the center, red dotted lines : orientation of the collagen fibers. Note the preferential orientation of the clone along the collagen fibers. Scale bar = 100µm.

STAR METHODS

CONTACT FOR REAGENT AND RESOURCE SHARING.

Further information and request for resources and reagent should be directed to the Lead Contact, Cedric Blanpain (cedric.blanpain@ulb.ac.be).

EXPERIMENTAL MODEL AND SUBJECT DETAILS

Experimental model and subjects details

Mice. *K14-CreER (Vasioukhin et al., 1999)* and *TRE-mCMV-H2B-GFP* (Tumbar et al., 2004) transgenic mice were provided by E. Fuchs. *K5tTA* (Diamond et al., 2000) mice were a kind gift from Glick. *Rosa-Confetti* (or *Brainbow-2.1*) mice (Livet et al., 2007) were provided by H. Clevers. *Rosa-YFP* (Srinivas et al., 2001) mice were purchased from Jackson Laboratory (USA). *Lgr5*$^{DTR\text{-}EGFP}$ (used to exclude bulge *Lgr5+* cells) mice (Tian et al., 2011) were kindly provided by Genentech (San Fransisco, USA). CD1 mice were purchased from Charles River (France). Mice used in this study were composed of males and females with mixed genetic background. The single-cell RNA sequencing was performed on males. No statistical methods were used to predetermine sample size. The experiments were not randomized. The investigators were not blinded to allocation during experiments and outcome assessment. Mice colonies were maintained in a certified animal facility in accordance with European guidelines. The experiments were approved by the local ethical committee (CEBEA) (#446N; #604N).

Method details

Monitoring epidermis growth. For the tail epidermis analysis (Figure 1), 3 mouse litters were used to measure the length (L) and width (W) (at the proximal part) of the tail every 1 to 3 day from P1 to P60 using a precision calliper. The surface (S) of the tail was calculated as a triangle

with the formula S = (W x π x L)/2. For the hindpaw epidermis, pictures of whole-mount hindpaw were acquired entirely and the length (L) and the width (W) of the tissue were measured using the Zen software (n = 4 hinpaws per time point). The paw surface was calculated as a rectangular shape with the formula S= L x W.

Quantification of Hair follicle, K31 and basal cell areas. For Hair follicle and scale K31+ areas, measures were performed on maximum intensity projection of confocal pictures (10x objective) from whole-mount tissues stained with K31, β4 integrin and Hoechst. These data show that the epidermal region undergoing scale differentiation (K31+) arises around P7 at the center of the future scale region and is spreading rapidly until P14. After P14, the relative surface of the scale and interscale regions remains constant during the course of postnatal growth until adult homeostasis (Figure S1C-D). For K31+ area, a drawing line surrounding the surface was performed manually and the area was calculated using the ZEN2012 software. The HF area is defined as a rectangle surrounding the scale in which the width corresponds to the distance between two hair follicle lines in the antero-posterior axis (=Antero-Posterior (AP) distance) and the length corresponds to the distance between two central hair follicles located in adjacent triplets (= Left-Right (LR) distance). These distances were measured using the ZEN2012 software (Zeiss). The hair follicle (HF) area was calculated with this formula : HF= AP x LR. The average of four hair follicle units was calculated for each mouse for each time point (n≥3 mice per time point). To measure basal cell area, whole-mount tissues were stained with β4 integrin, phalloidin and Hoechst and pictures were acquired with the confocal microscope (40x objective, z=1 µm). BCs were identified based on the orthogonal view and the expression of β4 integrin in their basal side. Cell area was measured manually by drawing the contour of each cell revealed by phalloidin signal in the x-y plan using the ZEN2012 software (Zeiss). The average area of 10 cells in scale and 10 cells in interscale was calculated per mouse (n=3 mice per time point).

***Rosa-Confetti* and *Rosa-YFP* clones induced in mice.** For lineage tracing experiment, *K14-CreER/Rosa-Confetti* mice were induced at postnatal day 1 (P1),P15 or P30 with Tamoxifen (0,01 mg/g diluted in 5-10%vol/vol Ethanol and sunflower seed oil, Sigma cat. n° T5648) by intra-peritoneal (IP) injection. The same dose of tamoxifen was used to induce clones in both tail and paw epidermis. *K14-CreER/Rosa-YFP* mice were injected IP at P1 with Tamoxifen (0,001 mg/g). Mice were then sacrificed at the appropriate time points following injections.

Antibodies. The following primary antibodies were used: anti-Integrin β4/CD104 (rat, 1:200, BD Biosciences, 553745), anti-K14 (chicken, 1: 2000, custom batch, Thermo Fisher), anti-K31 (guinea pig, 1:400, Progen, GP-hHa1), anti-BrdU (rat, 1:200, Abcam), Alexa 647-coupled BrdU antibody (mouse, 1:200, BD Biosciences, 560209), anti-α6-integrin PE-conjugated (clone GoH3; 1:200, ebioscience) and biotinylated CD34 (clone RAM34; 1:50, BD Biosciences). The following secondary antibodies were used: anti-rat conjugated to Cy5 (Jackson Immuno Research) or to A488 (Molecular Probes), anti-chicken conjugated to Rhodamine Red-X (Jackson Immuno Research), anti-guinea pig conjugated to Rhodamine Red-X (Jackson Immuno Research) or to Alexa488 (Molecular Probes) and Streptavidin conjugated to APC (1:400, BD Biosciences). Alexa488 conjugated phalloidin (Life Technologies) was used 1:200 in blocking buffer to visualize F-actin microfilaments and highlight cell membranes. Nuclei were stained with Hoechst (1:2000).

Epidermal whole-mount and immunostaining. Pieces of skin from tail or hindpaw were incubated in PBS /EDTA (20mM) on a rocking plate at 37°C for 30 min (P1-P7 tail skin), 45 min (P15 tail skin) or 1 hour (P30, P60 tail skin and all hindpaw skin). Epidermis was separated from the dermis using forceps as an intact sheet and washed 3 times with PBS. Pieces of epidermis were pre-fixed in 4% paraformaldehyde for 30 min to 1 hour at room temperature. Epidermis were rinsed

3 times with PBS for 5 min and conserved in PBS with 0.2% azide at 4°C. For immunofluorescence staining the entire pieces of epidermis were incubated in blocking buffer (1% BSA, 5% horse serum, 0.8% Triton in PBS) for 3 hours at room temperature on a rocking plate (100 rpm). The samples were incubated in primary antibodies overnight at room temperature, on the rocking plate (100rpm). Samples were then washed 3 times in PBS with 0.2% tween during 1 hour and incubated in appropriate secondary antibodies diluted 1:400 and Hoechst solution diluted 1:2000 in blocking buffer for 1-2 hour at room temperature on the rocking plate (100rpm). Then the samples were washed 3 times in PBS 0,2% tween and mounted in DAKO mounting medium supplemented with 2.5% Dabco (Sigma). For EdU/BrdU staining, samples were first stained with the primary antibody, washed and stained with the secondary antibody, following the protocol described above. Edu staining was performed following the manufacturer's instructions (Invitrogen). Briefly, the samples were blocked with a solution of BSA3% for 5min, permeabilized with a solution of Triton 0,8% for 20 min, blocked again with BSA3% for 5min and incubated in Click-it reaction Cocktail for 40 min in dark. The cocktail was removed and the samples were again blocked with BSA 3% for 5min, washed 3 times in PBS, fixed in PFA 4% for 10min and washed 3 times in PBS and incubated in HCl 1M at 37°C for 45 min. After, they were washed with PBS 0,2% Tween and incubated overnight with BrdU antibody in blocking buffer. The next day, samples were washed in PBS 0,2% Tween, incubated in Hoechst solution diluted 1:2000 in PBS 0,2% tween for 30 min. Samples were washed 3 times in PBS 0,2% Tween and mounted as described above.

Whole skin clarification. Whole skin (dermis and epidermis) was removed from the tail bone and fixed overnight in 4% PFA at 4°C. Samples were washed 3x in PBS and cleared using the Clear, Unobstructed Brain Imaging Cocktails and Computational analysis (CUBIC) described by Susaki and colleagues (Susaki et al., 2014). Briefly, ScaleCUBIC-1 (reagent 1) was prepared as a mixture of 25 wt% urea (Nacalai Tesque Inc., 35904-45, Japan), 25 wt% N,N,N',N'-tetrakis(2-

hydroxypropyl) ethylenediamine (Tokyo Chemical Industry CO., LTD., T0781, Japan), and 15 wt% polyethylene glycol mono-p-isooctylphenyl ether/Triton X-100 (Nacalai Tesque Inc., 25987-85, Japan). ScaleCUBIC-2 (reagent 2) was prepared as a mixture of 50 wt% sucrose (Nacalai Tesque Inc., 30403-55, Japan), 25 wt% urea, 10 wt% 2,20,20'-nitrilotriethanol (Wako Pure Chemical Industries Ltd., 145-05605, Japan), and 0.1% (v/v) Triton X-100. Skin was cutted in pieces (1 to 2cm^2) and incubated in reagent 1 for 3 days on a rocking plate (100 rpm) at 37°C protected from the light, after which the solution was exchanged and the sample was washed with PBS several times at room temperature while gently shaking, immersed in 20% (w/v) sucrose (#107651, Merck) in PBS, degassed, and immersed in reagent 2 containing 7-AAD (1:1000, A9400, Sigma) for nuclei vizualisation, for 2 days at room temperature on a rocking plate. Each reagent were prepared freshly. Samples were acquired using 2-PE microscopy with the reagent 2 as immersion solution.

Microscope image acquisition and measurements. All confocal images from whole-mount epidermis were acquired at room temperature with a LSM780 confocal system fitted on an AxioExaminer Z1 upright microscope equipped with C-Apochromat 40x/1,1 water, Plan Apochromat 25x/0.8 water and C-Apochromat 10x/0.45 water immersion objectives (Zeiss, Iena, Germany). Optical sections (z = 2µm) 512 x 512 pixels were collected sequentially for each fluorochrome. Confetti colors were acquired using tracks (mCFP : Ex: 458 nm, Em : 464-518nm/ RFP : Ex: 543nm; Em: 570-625nm/ EYFP-nGFP: Ex: 488; Em: 508-571nm). For whole tissue representations of tail and paw, maximum intensity projections of confocal pictures were obtained with the ZEN2012 software. Second harmonic signal was acquired from cleared whole skin samples at room temperature with a LSM780 confocal system fitted on an AxioExaminer Z1 inverted microscope equipped with C-Apochromat 40x/1,1 immersion objective and a 2Photon laser Chameleon Vision II (690-1064nm) (Coherent) (Zeiss). Samples were excited at 920nm and

acquired as z-stacks (z=4 µm). The data sets generated were merged and displayed with the ZEN2012 software (Zeiss). Pictures representing second harmonic signal are maximum intensity projections of several pictures over 40µm in the upper dermis.

EdU/Brdu proliferation experiments. For the double pulse experiments in the tail epidermis, mice were first injected IP with EdU (12,5mg/kg in PBS, Invitrogen) and second with BrdU (50mg/kg in PBS, Sigma). P4 and P7 CD1 mice were injected with one single injection IP of EdU and several injections (continuous pulse, 3 injections/day) of BrdU, 12h after the last EdU injection. Mice were sacrificed 24h and 48h after the first BrdU injection. P15 CD1 mice were injected IP with EdU (3 injections/day) and then injected IP with BrdU (3 injections/day) 12h after the last EdU injection. Mice were sacrificed 48h and 96h after the first BrdU injection. P30 and P60 CD1 mice were injected IP with EdU (3 injections/day) and then injected with BrdU (1 injection/ day) and BrdU was added in drinking water (1mg/ml). P30 and P60 CD1 mice were sacrificed 48h-96h and 96h-144h respectively after the first BrdU injection. For the BrdU experiments in the hindpaw, mice were injected with a single dose of BrdU (50mg/kg in PBS, Sigma) intraperitoneally and sacrificed 4 hours after.

H2BGFP proliferation experiments. *K5tTA/TRE-mCMV-H2B-GFP* mice were first treated with doxycycline (Sigma, cat n° D9891) by intraperitoneal injection (26mg/kg) at P1, P7, P21 or P30. Mice were continuously fed with doxycycline in drinking water (2g/L) (through their feeding mother for mice younger than P21) during one, two and for weeks until animal euthanasia. Samples were collected and analysed by FACS.

FACS analysis of basal epidermal cells. The dermis and epidermis were removed from the tail bone using forceps. The samples were incubated in HBSS (Gibco) 0,25% trypsin (Gibco) at 4°C overnight. The next day, the epidermis was separated from the dermis. Epidermis was then incubated on a rocking plate (100 rpm) at room temperature for 5 min. BCs were mechanically

separated from the epidermis by flushing 10 times under the epidermis. Tissues were then cut in small pieces with a scalpel and trypsin was neutralized by adding DMEM medium (Gibco) supplemented with 2% Chelex Fetal Calf Serum (cFCS). Samples were filtrated on 70 and 40µm filter (Falcon). Cells were incubated in PBS 2% cFCS with primary antibodies for 30 min on ice, protected from the light, with shaking every 10 min. Basal IFE and upper hair follicle cells were stained using PE-conjugated anti-α6-integrin (clone GoH3; 1:200, ebioscience) and bulge cells were stained with biotinylated CD34 (clone RAM34; 1:50, BD Biosciences). Primary antibodies were washed with PBS 2% cFCS and cells incubated for 30 min in APC-conjugated streptavidin (BD Biosciences), on ice, with shaking every 10 min. Secondary antibody was washed with PBS 2% FCS and cells were incubated in Hoechst solution (1:4000 in PBS 2%cFCS) prior FACS analysis. Living epidermal cells were gated by forward scatter, side scatter and negative staining for Hoechst dye. For H2BGFP proliferation experiments, *K5tTA/TRE-mCMV-H2B-GFP* mice chased with doxycycline were used. BCs were targeted using CD34 negative and α6 integrin positive gating. For P7, P30 P60 basal epidermal cells sorting, *Lgr5*$^{DTR\text{-}EGFP}$ mice (Tian et al., 2011)(knockin mice containing an Enhanced Green Fluorescent Protein (EGFP) under the control of the *Lgr5* regulatory region, allowing to identify and exclude *Lgr5*-expressing cells of the bulge) were used and BCs of the interfollicular epidermis were enriched using EGFP negative, CD34 negative, α6 integrin positive gating. Analysis were performed on a FACS Fortessa (BD Bioscience) and using FACS Diva software. Cell sorting was performed using a BD Influx at KULeuven Core facility (Leuven, Belgium) (P7 and P60) or a FACS Aria I at the ULB Flow Cytometry platform (Brussels, Belgium) (P30).

Primary culture of keratinocytes. Primary tail keratinocytes were freshly isolated from mice aged of P2, P10, P30 and P60. Before isolation, the whole tail was washed 30sec in distilled water, 1min

in 70% ethanol, 30 sec in distilled water, 1 min in PBS and cleaned 5min in an antibiotic solution (Penicillin-Streptomycin diluted 200U in PBS). An incisional cut was performed along the long axis of the tail with a scalpel, the dermis and epidermis were separated from the tail bone and incubated (epidermis up) for 20min (P2) to 60 min (P60) in PBS 0,8% Trypsin (Gibco) at 37°C on rocking plate. The epidermis was separated from the dermis and flushed 10x with a Pasteur pipette on the dermal side. The epidermis was cut in small pieces and trypsin was neutralized by adding Keratinocyte Growth Medium (KGM). KGM is composed of Minimum essential medium eagle (MEM, M8167, Sigma) complemented with Insulin (5µg/ml, I5500, Sigma), EGF (10ng/ml, SRP3196, Sigma), Transferrin (10µg/ml, T8158, Sigma), Phosphoethanolamine (10µM, P0503 Sigma), Ethanolamine (10µM, E0135, Sigma), hydrocortisone (0,36µg/ml, cat no 386698, Calbiochem), Glutamine (2mM, Gibco), Penicillin (100U/ML), Streptomycin (100µg/ml, Gibco), chelated fetal calf serum (cFCS, 10%, Gibco) and CaCl2 (100µM). The cells were further dissociated with 5ml pipette up & down (15x). The cell solution was filtered through 70µm filter, centrifuged at 250xg for 10 min and resuspend in KGM. Viability was assessed by manual counting and Trypan blue. $1{,}5x10^5$ living cells were plated in 12 wells plates pre-coated with human fibronectin (10µg/ml) and rat tail collagen I (30µg/ml). The medium was changed after 24h to remove non-adhering cells.

Quantification of EdU/BrdU experiments. The quantification was made manually with the ZEN2012 software (Zeiss), using z-stack acquisitions (z=1-2µm, 40x objective) of wholemount tissues stained for K31, EdU and BrdU for the tail epidermis and for BrdU and K14 for the hindpaw epidermis. Nuclei were colored with Hoechst. For the tail epidermis analysis, a minimum of 300 basal EdU+ cells were counted per mouse for each time point in at least 4 HF units ($n \geq 3$ mice per time point). Given the slowing down of the division rate in time, we adapted the duration of the BrdU chase with developmental time (24h/48h for P4 and P7, 48h/96h for P15 and P30) in order

to capture better dynamically the evolution of double labelling in time. For the hindpaw epidermis analysis, a minimum of 185 basal BrdU+ cells were counted per mouse for each time point (n = 3 mice per time point).

Quantification and proliferation experiments on primary keratinocytes. After 48h of culture, half of the medium was removed from each well containing primary keratinocytes and replaced by medium containing either BrdU (10µM final concentration) or fresh medium (control) for 2h. Cells were washed 3 times with PBS and incubated with Trypsin 0,25% and 0,5mM EDTA (Gibco) for 20min at 37°C. Trypsin was neutralized with KGM containing serum, cells centrifuged (10min at 250 x g) and resuspend in PBS 2% cFCS for counting. 10^6 cells were stained for BrdU following the manufacturer's protocol (BD Bioscience). Briefly, cells were incubated with PE-conjugated anti-α6-integrin (clone GoH3; 1:200, ebioscience) diluted in PBS 2% cFCS for 30min on ice, with shaking every 10min. Cells were then washed with PBS 2% cFCS, centrifuged and the pellet was resuspended in Cytofix/Cytoperm. After an incubation of 15min at room temperature, cells were washed with Perm/Wash and centrifuged. Cells were then resuspended in Cytoperm Plus, incubated for 10 min on ice then washed with Perm/Wash and centrifuged. Cells were re-fixed with Cytofix/Cytoperm for 5 min at room temperature, washed with Permwash and centrifuged. Cells were then treated with DNAse for 1h at 37°C, then washed with Perm/Wash and centrifuged. Finally, cells were resuspended in FITC-conjugated anti-BrdU (clone B44; 1:50, BD Biosciences) diluted in Perm/Wash and incubated 30 min at room temperature, then wash with Perm/Wash and centrifuged. Cells were finally resuspended in PBS 2% cFCS for FACS analysis. FITC positive cells were quantified using the FACS Diva Software among the α6-integrin^{high} in two biological samples. At least 6000 living cells were analysed for each experiment.

Quantification of clone size and persistence. For the tail epidermis analysis, regarding the absence of correlation between K31 staining and hair follicle area surface increase at early time points, we decided to not use the K31 staining to score the clones in scale but rather consider an elliptical surface covering 60% of the HF area at each time point (Figure S1A-C). Whole-mounts obtained from *K14-CreER/Rosa-Confetti* induced at P1,P15 or P30 and stained for β4 integrin were analysed by confocal microscopy. Orthogonal view was used to see in 3 dimensions RFP, YFP, mCFP or nGFP positive cells and quantify the number of basal and total cells per clone. Cells were considered as basal when their basal side was positive for β4 integrin. For the tracing induced in the tail epidermis at P1, 104 clones at P4 (n= 3 mice), 158 clones at P7 (n= 4 mice), 245 clones at P15 (n=5 mice), 295 clones at P30 (n=5 mice) and 623 clones at P60 (n=9 mice) were analysed. For the tracing induced at P15, 178 clones at 4 days post-induction (n=5 mice) and 286 clones at 2 weeks post-induction (n=5mice) were analysed. For the tracing induced at P30, 209 clones at 4 days (n=5 mice) and 265 clones at 4 weeks (n=5 mice) post induction were analysed. For clonal persistence, large areas of tissue (at least 100 hair follicle triplets/mouse for P1 tracing, and 4 to 10 hair follicle triplets/mouse for P15 and P30 tracing) were scanned using the 10x or 25x objectives. The number of basally attached clones was divided by the number of hair follicle triplets counted in the same area (n≥5 mice per time point). For the hindpaw epidermis, clones were induced at P1 and were analysed in the portion of the paw devoided of hair follicles and pads. 152 clones at P1 (n=3 mice), 107 clones at P7 (n= 2 mice), 108 clones at P15 (n=3 mice), 125 clones at P30 (n= 3 mice) and 80 clones at P60 (n= 3 mice) were analysed. For the clonal persistence, the surface of the paw without hair follicles and pads was calculated on wholemount using the Zen software and the total number of clones present within this area was counted.

Quantification of the ratio suprabasal/ BCs and basal cell density in tail and paw epidermis. Whole-mount tissues stained for β4 integrin, phalloidin and hoechst were acquired with confocal microscope (40x objective). BCs were positive for β4 integrin on their basal side. For the ratio of suprabasal/ BCs, the number of basal and suprabasal nuclei within a surface delimited in tail scale, tail interscale or paw were counted manually using the ZEN21012 software (Zeiss) for each time point. Suprabasal cells in the stratum corneum were not included. At least 230 BCs were counted per region per animal (n= 3 mice per time point).

Quantification of clones and collagen fibers orientation. To quantify clone orientation, whole-mount tissues stained with β4 integrin were acquired with confocal microscope (10x objective), files were processed with the ZEN2012 software (Zeiss) to obtain maximum intensity projection and were saved as *tiff.* files. 726 clones were manually scored as isotropic or anisotropic in *K14-CreER/Rosa-Confetti* (WT) (n=5mice). Clone orientation was measured using Axiovision LE64 software (Zeiss) using the *Angle 3* measure tool, setting the 0° parallel to the antero-posterior direction of the Hair follicles. A total of 348, 131 and 29 anisotropic clones were measured in scale, interscale AP and interscale LR respectively, in *K14-CreER/Rosa-Confetti* (WT) mice (n=5 mice). To quantify collagen fibers orientation, clarified whole pieces of skin from tail were acquired using 2-PE confocal microscopy. Z-stack pictures representing second harmonic signal were merged as maximum intensity projections over 40µm in the upper dermis. Pictures were saved as *.tiff* files and quantification of the collagen fibers was made using the Fibriltool ImageJ plugin (see (Boudaoud et al., 2014) for details). In brief, boxes were manually defined on large-scale 2D projections of the dermis, in each LR interscale, AP interscale and scale regions, and an average angle of orientation was extracted for each (defined as shown in Figure 7).

***In vitro* collagen I micro-patterning and quantification.** Nikon TI-E inverted microscope (Nikon Instruments) equipped with a Super Plan FLuor 20x ELWD lens (Nikon) lens and a DMD-based

UV (375nm) patterned PRIMO illumination device (Alveole) was used for all micropatterning experiments. PRIMO was controlled by the associated Leonardo plugin (V3.3, Alveole) on a micromanager platform (Fiji). In order to generate non-aligned mesh-like and aligned micropatterns, 2µm-spaced grids of either perpendicularly-intersecting or parallel lines, respectively, were projected onto plasma-treated (Corona Treater, ETP), PLLgPEG-passivated (SUSOS) 35mm glass-bottom dishes (Ibidi). Patterned areas were then conjugated with a uniform coating of collagen I by polymerizing 0.5mg/mL solution of rat tail collagen I (BS Bioscience) in 0.02N acetic acid over night at 4 degrees centigrade. The substrates were then washed with PBS, sterilized with 70% ethanol solution, and equilibrated with DMEM (Gibco) prior to seeding 500K of freshly isolated E15.5 mouse keratinocytes onto each 35mm dish. Keratinocyte monolayers were allowed to proliferate on the patterns for 24 hours, at which time they were fixed and processed for immunofluorescence and quantification analyses. Division angles were quantified with respect to the directions of aligned collagen grids (set to 0 degrees) using γ-tubulin to mark the division axis. MATLAB software (vR2010a Student, Mathworks) was used to generate rose plots of angle distributions.

Single cell RNA library preparation and sequencing. After sorting, 6000 cells were loaded onto each channel of the Chromium Single Cell 3' microfluidic chips (V2-chemistry, PN-120232, 10X Genomics) and individually barcoded with a 10X Chromium controller according to the manufacturer's recommendations (10X Genomics). RNA from the barcoded cells was reverse transcribed, followed by amplification, shearing 5′ adaptor and sample index attachment. The libraries were prepared using the Chromium Single Cell 3' Library Kit (V2-chemistry, PN-120233, 10X Genomics), quantified using a low coverage Illumina NextSeq 550 run and sequenced on an Illumina NovaSeq generating 343M, 245M and 336M reads for the P7, P30 and P60 libraries respectively. 10.338, 948 and 10.920 cells were detected, with a mean number

of 33.179, 245.972 and 30.857 reads per cell, detecting a median of 2.290, 5.050 and 2.309 of genes per cell.

Single cell bio-informatic analysis. Sequencing reads were aligned and annotated with the mm10-1.2.0 reference data set as provided by *10X Genomics* and demultiplexed using CellRanger (version 3.0.2) with default parameters. Cell-cycle assignment was performed using the *scran* R package (version 1.10.1). Expression value scaling and normalization, PCA and UMAP dimensionality reductions and clustering were performed using the Seurat (Butler et al., 2018) R package (version 3.0.1). After filtering contaminant cells belonging to the infundibulum (*Sox9*^{high}, *Krt17*^{high}, *Krt79*^{high}) and sebaceous gland (*Scd1*^{high}, *Mgst1*^{high} and *Elovl6*^{high}) as well as cells containing a high content of mitochondrial genes, such as *mt-Co1* (dying cells) and filtering for cells with fewer than 2.500 UMI counts, 6.102, 673 and 7.551 cells were further analyzed in P7, P30 and P60 samples respectively. After filtering, expression values were renormalized, rescaled and reclustered and cells were manually annotated based on their expression of differentiation related genes. A subset of clusters expressed cell-cycle related genes and were manually annotated considering the higher expression of known cell-cycle stage genes. Genes controlling DNA replication licensing (*Mcm2, Mcm3, Mcm7*) and DNA replication forks (*Lig1, Rpa2*) were used to define G1-S cluster (cluster 3 at P7 and P60). Genes controlling the entry in mitosis (*Top2a, Cdk1, Cenpf, Birc5, Cenpa, Ccnb2, Hmgb1*) were used to define the S-G2-M cluster (cluster 2 at P7 and cluster 4 at P60) which also had low expression of genes of the G1-S cluster (*Mcm2, Mcm3, Mcm7*). The Late G2-M cluster (cluster 4 at P7) harbored well known genes controlling mitosis (*Cenpa, Ccnb2, Hmgb1*) without the genes controlling G1-S (*Mcm2, Mcm3, Mcm7*) and lower expression of the genes controlling the entry of mitosis (*Top2a, Cdk1, Cenpf, Birc5*). Clusters were defined using Seurat at multiple resolutions (0.3, 0.5, 0.7, 0.9) and marker gene discovery was performed using the FindAllMarkers function of the Seurat package using the Wilcoxon Ranked Sum test. A

clustering resolution of 0.5 was chosen as it resulted in the clearest set of transcriptional signatures and revealed clusters with biological significances, such as the differentiated cells in scale and interscale at P60. Markers were then selected by setting the threshold to all genes with an adjusted *p-value* lower than 0.05. Pseudotime ordering of the IFE population was performed using the Slingshot R package (version (1.3.1) on the PCA embedding and the trajectories were visualized on the first 2 UMAP Components. Trajectory inference was performed on the datasets filtering out automatically annotated cycling cells and manually annotated cell-cycle related clusters.Gene regulatory network analysis was performed using pySCENIC (commit 0.9.9+2.gcaded79) (Aibar et al., 2017) with default parameters. AUC values for gene set enrichment were computed using the AUCell R package (version 1.6.1). Batch integration was performed using Harmony (version 1.0) after scaling expression values for each sample independently using Seurat.

Theoretical modelling

Theoretical basis for interpreting lineage tracing experiments

The theoretical basis of the lineage tracing data analysis in the mouse epidermis have been reviewed extensively in (Mascre et al., 2012; Sanchez-Danes et al., 2016), particularly in the context of homeostatic renewal and oncogenic activation. These studies have revealed that scale and interscale regions in the mouse tail epidermis consist of independent, stochastically renewing, populations: (i) a single population of progenitors in scale with perfectly balanced fate (dividing every 4-5 days); and (ii) a hierarchy of nearly-balanced, long-lived progenitors (also dividing every 4-5 days, and preferentially labelled in *Inv-CreER* mice), renewed infrequently by a rare population of stem cells (preferentially labelled in *K14-CreER* mice), undergoing stochastic fate choice, in

the interscale. In order to clarify whether this hierarchy and spatial compartmentalization holds during postnatal development, a strategy of quantitative lineage tracing was implemented via the *K14-CreER* mouse tracing from P1 to P4, P7, P15, P30 and P60, to follow the dynamics of tail growth at the clonal level.

At all time points, clone size distributions, both for basal and suprabasal cells (resp. n_b and n_s), were found to be highly heterogeneous, and growing by a similar amount to the tail as a whole, arguing for clonal representativeness. We also found that scale clones were larger than interscale clones at all time points (see the "Quantification and Statistical analysis" section). Strikingly, we found that basal clone size distributions at all time points converged towards a simple scaling form when rescaled by their average clone size $< n_b(t) >$, such that $P_{n_b}(t) = \frac{1}{<n_b(t)>} f\left(\frac{n_b}{<n_b(t)>}\right)$, and that this scaling form was consistent with a simple exponential size dependence, $f(n) = \exp(-n)$. Such an exponential scaling is expected to arise in the case of stochastic fate choices (i.e. a birth-death process) made by a single progenitor population. For instance, in the presence of a hierarchy of SCs and CPs both contributing significantly to the dynamics, clonal distributions should adopt more complex shapes which wouldn't show such scaling, as is observed upon oncogenic activation in mouse tail epidermis (Sanchez-Danes et al., 2016). We thus denote λ_s and λ_i respectively as the division rate of the progenitor population in scale and interscale. Upon each division, a progenitor P can give rise to three possible fate outcomes:

- $P \rightarrow P + P$ with probability $r + \Delta/2$
- $P \rightarrow P + D_b$ with probability 1-2 r
- $P \rightarrow D_b + D_b$ with probability $r - \Delta/2$

where r denotes the rate of symmetric over asymmetrical outcomes, and Δ the degree of imbalance between renewal and differentiation, which can be non-zero in a non-homeostatic condition. For reasons that will become clear, in the following sections, we take into account a differentiated basal intermediary D_b, which does not divide further and is committed to differentiation, with suprabasal stratification $D_b \rightarrow D_s$ taking place at rate Γ_1. Suprabasal cells do not divide and are shed at a rate Γ_2. Importantly, in the case of $\Delta = 0$, the theory predicts that, although the total labelled cell fraction should stay constant, the surviving clone size should increase linearly due to neutral drift (with a slope proportional to $r\lambda$), being compensated by a converse decrease in clonal persistence. The parameter r thus becomes crucial for the resulting dynamics. In contrast, in the presence of any amount of imbalance Δ, the persistence rapidly plateaus (Harris, 2002) while the clone size increases exponentially as $n_s(t) \propto \exp(\Delta\lambda t)$. Thus, the parameter r quickly becomes irrelevant to the resulting dynamics, and cannot be meaningfully constrained by our model fits. Indeed, as detailed below, Δ is large enough here to erase from the earliest time points the influence of r on clonal dynamics. We therefore concentrated on the imbalance Δ in this manuscript. We further note that, as in a developmental setting, all of the aforementioned parameters can be in principle time-dependent, drastically increasing the size of the parameter-space.

Theoretical basis for interpreting proliferation kinetics experiments.

Because of the breadth of parameter space, we thus sought to constrain some parameters; in particular, the rates of division and differentiation over time. We thus turned to double-pulse EdU/BrdU experiments at all time points studied in the lineage tracing experiments, to both measure experimentally the rate of cell division in scale and interscale (by monitoring how quickly a cell that incorporated EdU will incorporate BrdU again), as well as the rate of basal to suprabasal transfer (by monitoring how quickly a cell that incorporated EdU will move to the suprabasal

layers). The theoretical model used to fit the data was the same as that described in the section above, with three cell types considered (basal progenitor, basal differentiated and suprabasal differentiated). However, a small addition had to be made to the model, as we consistently observed that the processes of division and differentiation were not Poissonian: Instead, we found a refractory period after division, where a cell could neither divide again nor differentiate. This is consistent with findings from live-imaging studies of mouse epidermal homeostasis (Rompolas et al., 2016). We thus amended the model by considering that, for each process of division and differentiation, there was a latency period (respectively τ_{div} and τ_{diff}), followed by conventional stochastic (Poissonian) events. Such a two-phase model provided very good fits at all time points for both the fraction of double-labelled cells (Figure 3N) and the ratio of EdU suprabasal to BCs (Figure S2J) over time. We note, however, that such short-time correlations induced by refractory periods become quickly erased from the clonal data and, thus, for the lineage tracing experiments we used as inputs compound Poissonian rates defined by adding the two time scales (refractory and stochastic phases). These are shown as effective division rates in Figure 3O. Interestingly, we noted that the time scales of divison λ and suprabasal stratification Γ_1 were very similar in both compartments and across all time points. This is consistent with the basal layer being composed of a mixture of dividing progenitors and cells awaiting suprabasal stratification (in a roughly 1:1 ratio), matching with older observations (Potten, 1975). This is thus consistent with an extrinsic regulation of cell fate via near-neighbor couplings, as reported in homeostasis (Rompolas et al., 2016). The analysis also revealed consistently higher division and differentiation rates in scale throughout development, consistent with the increased clone size we observed in this region.

Fitting procedure and model validation

Once the division rate has been fixed by our proliferation kinetics experiments, we performed stochastic simulations of the model described in the subsection "*Theoretical basis for interpreting lineage-tracing experiments".* The initial condition for the numerical simulation is $n_b(0) = 1$ and $n_s(0) = 0$, mirroring the P1 clonal induction of single BCs. We perform at least 10,000 simulations for both scale and interscale, and calculate persistence, surviving clone sizes, and clone size distributions at all time points from these simulations (until P30, as growth drastically slows down after this time point). The only fitting parameters are Δ and r. We then performed a least-squares fitting procedure on the evolution of the mean basal clone size up to P30, to obtain optimal values of Δ and r in scale and interscale, as well as bootstrapping to build 95% confidence intervals on these parameters, following the same procedure as detailed in (Mascre et al., 2012; Sanchez-Danes et al., 2016). However, as mentioned above, r cannot be reliably fitted, given its low level of impact on the clonal dynamics. Indeed, trying to fit both Δ and r parameters from the basal clone size evolution yielded extremely large confidence intervals: $\Delta = 20\%^{+8\%}_{-8\%}$ and $r = 33\%^{+17\%}_{-20\%}$ in scale, and $\Delta = 24\%^{+4\%}_{-8\%}$ and $r = 21\%^{+15\%}_{-7\%}$ in interscale. Moreover, persistence could not be used either to meaningfully constrain the value of r, given its low effect on the dynamics, and the error bar involved in the measurements. As the values of r in both scale and interscale during development cannot be distinguished within these confidence intervals from its homeostatic values, we used these homeostatic values of $r \approx 0.2$ in the simulations.

In the following, we thus resorted to fitting procedure where Δ was the only fitting parameter. Importantly, we found that we could obtain very good fits to the mean basal clone size distribution with a single value of the fate imbalance (Figure 4A and 4D). As expected, the model reproduced well the exponential clone size distributions observed in the data at all time points (Figure 4B and 4E). We also found that the model could accurately predict the time evolution of

the clonal persistence in both scale and interscale, characterized by an initial drop in persistence during the first week, followed by a near-plateauing behavior (Figure 4C and 4F). To probe further whether fate imbalance Δ could truly be considered as constant throughout development, we performed the same simulations and fitting procedure as before, but defining the imbalance Δ as a piece-wise function, which could take different inferred values Δ_1 (between P1 and P7), Δ_2 (between P7 and P15) and Δ_3 (between P15 and P30). This enabled us to test whether the fitting could be improved by inferring different values of imbalance over time, and thus test further the hypothesis of a near-constant inferred imbalance. Importantly, this analysis confirmed that imbalance does not show a strongly varying temporal trend (neither in scale nor interscale), as shown on Figure 5G and H, although we cannot exclude small variations around the average imbalance, which would give rise to small variations of suprabasa/basal ratio.

Finally, to challenge the model further, we tested whether it could predict a fully independent set of data, performing clonal lineage tracing in the same mouse system, but inducing at P15 (and tracing for 4 days and 2 weeks). Importantly, we found that the model, as calibrated above (and thus in the absence of remaining free-parameters), provided a good prediction in scale and interscale, for both the time evolution of the surviving clone sizes (Figure 4R-S) and the clonal persistence (Figure 4T-U). This provided further support to the model, as well as to the assumption of a single progenitor population with near-constant imbalance in fate choice. After P30, the data on local and global tail expansion displays a transition phase towards a growth plateau, consistent with our observations at the clonal level (Figure 4B,E). We thus assumed that the system was abruptly transitioning towards homeostasis (Sanchez-Danes et al., 2016) after P30 (note that given the large clone size at P30, neither the evolution of clone sizes nor clonal persistence provided very strong constraints on the detailed dynamics), and used this as a guide for the eye (dashed lines in

Figure 4B,C,E,F). This assumption was further supported by our P30 tracing (Figure S5), which displayed results close to homeostasis (Sanchez-Danes et al., 2016).

Design principles of epidermal growth

As analysis of the lineage tracing data revealed a surprising degree of simplicity in the rules underlying tail epidermis expansion (nearly constant imbalance over time and across scale/interscale regions, while the division rate decreased steadily), we sought to understand the design principles underlying this phenomenology. To answer such a question, we resorted to a mean-field description of growth, forgetting about the stochasticity of cell fate choices, and writing conservation equations for the number of basal and suprabasal cells (*b* and *s* respectively):

$$\begin{cases} b'(t) = \lambda(t)\Delta(t)b(t) \\ s'(t) = \lambda(t)(1-\Delta(t))b(t) - \Gamma_2 b(t) \end{cases}$$

Here, we choose a loss rate for suprabasal cells proportional to basal cell number. This choice is rooted in the fact that suprabasal cells are not lost in "bulk", but instead are shed at the outer-most surface of the skin (which is thus proportional to the area of the skin surface). Note that because basal progenitors and basal differentiated cells have similar kinetics throughout development, we do not include at first the latter to give generic qualitative insights into the dynamics (although we will include it for quantitative matching to the results). As detailed below, as we impose the condition that basal cell number follows the growth of the underlying tissue, this results in this equation.

For mouse tail expansion, the epithelium is mechanically coupled to the growth of the underlying conjunctive tissue, which likely imposes its overall growth. A simple design principle for epidermal growth is thus, for BCs to maintain a constant density, so that their number evolution

as a function of time is prescribed: $b(t) = b_0(t)$ a function which is imposed by the growth of underlying tissues. However, there are two unknown in the equation above, the division rate $\lambda(t)$ and the imbalance $\Delta(t)$, so that $b(t) = b_0(t)$ only imposes a relationship between the two.Thus, this could be both achieved via constant imbalance and varying division rate, or vice versa. A second design/principle must thus be enforced, and we review several possibilities below (Figure 5 A-D):

- Maintaining a constant number of progenitors ($\Delta = 0$) (Figure 5A). This case would correspond to settings where the stem cell/progenitor pool is fixed and non-plastic (as observed for instance in experiments depleting the stem cell pool in *Drosophila* midgut (Jin et al., 2017). In this case, a third species (basal differentiated cells) must be taken into account to increase basal cell numbers, and the concentration of basal progenitors would get depleted in time as more and more differentiated BCs populate the basal layer to keep up with the growth of the underlying tissue. This is not what is observed in our data, and is also inconsistent with adult homeostasis of the tail epidermis (Mascre et al., 2012; Sanchez-Danes et al., 2016).
- Minimizing the total number of basal divisions (for instance to minimize the time to build up a population), corresponding to a so-called "bang-bang" dynamics as studied for the growth of intestinal crypts (Itzkovitz et al., 2012) (Figure 5B). In this case, the solution is a phase of purely symmetric division ($\Delta = 100\%$) to build-up progenitor cell numbers, followed by differentiated cell production. However, this results in a depletion of the density of suprabasal cells during the primary phase (not observed *in vivo*, see Figure 5E), and is not consistent with our lineage tracing data set either showing that suprabasal cells

are produced after birth (Compare the average number of basal and total cells at P4 in Figure 2E and F).

- Maintaining a constant division rate λ_p (Figure 5C).In this case, the imbalance must constantly adapt to fuel basal expansion, and can be expressed simply as $\Delta(t) = b_0'(t)/\lambda_p/b_0(t)$. One should note that this puts some constraints on growth (or division), as the imbalance can never be larger than 1; although this can be implemented in the realistic growth coefficients measured here. However, this scenario (which is not supported by our cell proliferation kinetics) would then predict a changing (and typically non-monotonous) evolution of suprabasal clones sizes (as the imbalance is too high initially to produce enough suprabasal cells, and too large afterwards).
- Finally, a fourth possibility is that the epithelium needs to maintain a given suprabasal cell number as well $s(t) = s_0(t)$ (which means that even in the absence of suprabasal loss, a precise number of suprabasal cell must be produced to keep up with area expansion) (Figure 5D). We measured the time evolution of basal and suprabasal cell concentrations in both scale and interscale, and found that this assumption was well-supported by the data. We thus explore its consequences for the regulation of division rate and imbalance during post-natal growth.

In the general case, this fourth constraint (prescribed evolution of basal and suprabasal densities) leads to

$$\begin{cases} \Delta(t) = \dfrac{1}{1 + \lambda b'/b + s'/b'} \\ \lambda(t) = \Gamma_2 + \dfrac{b' + s'}{b} \end{cases}$$

where the division rate needs to match the loss rate, in addition to a part of the growth burden. Furthermore, in the case where the epithelium seeks to maintain an identical ratio of basal to suprabasal cell $s_0(t)/b_0(t) = K$, (which is also supported by our data, see Figure 5E), the equation simplifies to

$$\begin{cases} \Delta(t) = \dfrac{1}{1 + K + \Gamma_2\, b'/b} \\ \lambda(t) = \Gamma_2 + \dfrac{b' + s'}{b} \end{cases}$$

In the limit of negligible suprabasal cell loss Γ_2, the imbalance Δ generically becomes a time-independent constant, for any temporal evolution of tail growth $b_0(t)$. This fitted well our findings, where we found the imbalance not only to be almost constant in time, but also constant in scale and interscale, even though both compartments grow at different rates.

To go beyond such qualitative arguments, we then incorporated the fact that tail growth is nearly linear ($b(t) = 1 + \alpha t$, where $\alpha \approx 0.3d^{-1}$ for interscale and $\alpha \approx 0.6d^{-1}$ for scale, based on Figure 1), used the experimentally measured ratio of basal to suprabasal cells, $K = 0.8$, and included differentiated BCs in the descriptions (with the constraint of 1:1 ratios with BCs throughout development). This yields a modified, but qualitatively similar expression:

$$\begin{cases} \Delta(t) = \dfrac{1/2}{1 + K + \Gamma_2/(1/\alpha + t)} \\ \lambda(t) = 2\dfrac{(1+K)\alpha + \Gamma_2(1+\alpha t)}{2 + \alpha t} \end{cases}$$

where, again, in the limit of negligible suprabasal loss, one predicts a constant imbalance and time-varying division rate. Quantitatively, applying this simple theory with the measured *K* ratio predicts $\Delta = 27\%$ in close agreement to the experimentally inferred value from lineage

tracing ($\Delta = 24\%$). More quantitatively, we found that performing a joint fitting for $\Delta(t)$ and $\lambda(t)$ revealed that a loss rate of $\Gamma_2 \approx 0.04d^{-1}$ provided good fits for the time evolution of the division rates and imbalance. In Figure 5G-H, we show this, plotting the inferred imbalance when fitted as piece-wise function (see section "*Fitting procedure and model validation"*), to emphasize the lack of strong temporal variation in imbalance compared to division. Strikingly, the model predicted that the twice-faster growth of the scale region should dominantly translate into a consistently higher division rate in scale, in qualitative and quantitative agreement with the data (Figure 3O,P). This argues that the evolution of both the division rate and the fate choices of DPs can be predicted quantitatively via the simple design principle of uniform basal and suprabasal growth (and is, in fact, the only scenario consistent with this principle).

To further demonstrate how large deviations from our paradigm would produce different predictions on observable data such as the evolution of the basal density and suprabasal/basal ratio, we also performed a sensitivity analysis (Figure S4A-D). We explored in particular: i) the influence of the value of constant imbalance Δ (with continually adjusting division rate), showing for instance that imbalances of 15% or 40% produce highly different predictions, poorly fitting the data (which is due to the fact that unbalanced dynamics constitutes an exponential process, highly sensitive to variations in growth rate, Figure S4A), ii) the predictions of bang-bang dynamics (transition from Δ=100% to 0% imbalance at varying time points) together with a continually decreasing division rate, showing a very poor fit to the data, in particular as it produces a vast excess of BCs (Figure S4B), iii) the prediction of a "soft" bang-bang dynamics (transition from varying, partial imbalance values Δ to 0% imbalance at P15), which again provides poor fits to the data, in particular as it predict a drop of basal density post P15, not observed in the data (Figure S4C), and iv) a continually adjusting/decreasing imbalance, together with a constant division rate, although we show with

independent proliferation experiments that this is not the case in the mouse epidermis (shown in Figure S4D for 1,2,3 and 4 divisions per week).

Extension to the morphogenesis of the neonatal paw epidermis

Finally, we sought to test whether a similar paradigm could be found in other tissues, such as the paw epidermis. Neonatal paw epidermis expanded 6-fold between P1 and P60, with most of the growth occurring between P1 and P15 (4.5-fold, Figure S3D). Rescaled clone size distributions at all time points fitted well with a single exponential (Figure S3L), as in scale and interscale of the tail epidermis, so we fitted the clonal data to the same model of a single population undergoing stochastic fate choices as described in the above paragraphs. Proliferation kinetics were inferred via short pulses of Brdu and measuring the fraction of Brdu+ cells in the basal layer at P4, P7, P15, P30 and P60 (Figure S3E,F). To convert this information into division rate, we used the live-imaging data of Rompolas et al, 2016 in paw homeostasis to estimate the division rate of BCs at P60, and used this calibration to proportionately estimate the division rates at the other time points (shown in Figure S3N). Then, we estimated as before the fate choice parameters of BCs between P1 and P15 as $\Delta = 20\%$, which provided good fits for the time evolution of the basal clone size (Figure S3M) and clonal persistence (Figure S3O). Based on the overall dynamics of paw growth, we assumed that imbalance was zero around P18 (sharp transition to homeostasis), which fitted well the subsequent P30 and P60 time points (Figure S3M), although our time resolution cannot distinguish sharp vs. smooth transitions to homeostasis. As this provided a good fit to the data, this argues again that neonatal growth in paw is well described by a model of near-constant fate

imbalance towards symmetric division, with a constantly decreasing division rate. Based on our optimality theory, and given the measurements in paw of growth speed of $\alpha \approx 0.3\, d^{-1}$ (very similar to the growth speed of the interscale in tail epidermis) and suprabasal to basal ratio of $K \approx 1.2$ (slightly highly than in tail epidermis), we would predict (in the simplified case without loss) that $\Delta = 24\%$ which is thus again in good agreement with the experimental findings.

QUANTIFICATION AND STATISTICAL ANALYSIS

Quantification of clone sizes were performed on whole-mount tissue acquired by confocal microscopy and counted manually using the ZEN2012 software.

To test whether scale and interscale clone size distributions were significantly different, we compared the basal clone sizes of each of them, using the Mann-Whitney non-parametric test (as distributions were exponential and didn't pass a normality test). We found significant differences at all time points (P7: P=0.007, P15: P<0.0001, P30: P<0.0001, P60: P<0.0001), with interscale clones being consistently smaller. This could not be explained by a conversely higher suprabasal clone size in interscale, as scale suprabasal clones were also consistently and significantly larger, again assessed via a Mann-Whitney test (P7: P=0.028, P15: P<0.0001, P30: P<0.0001, P60: P<0.0001).

DATA AND SOFTWARE AVAILABILITY

The single-cell RNA sequencing data discussed in this publication have been deposited in NCBI's Gene Expression Omnibus (Edgar et al., 2002) and are accessible through GEO Series accession number GSE146122 (https://www.ncbi.nlm.nih.gov/geo/query/acc.cgi?acc=GSE146122).

REFERENCES

Aibar, S., Gonzalez-Blas, C.B., Moerman, T., Huynh-Thu, V.A., Imrichova, H., Hulselmans, G., Rambow, F., Marine, J.C., Geurts, P., Aerts, J.*, et al.* (2017). SCENIC: single-cell regulatory network inference and clustering. Nature methods *14*, 1083-1086.

Andersen, M.S., Hannezo, E., Ulyanchenko, S., Estrach, S., Antoku, Y., Pisano, S., Boonekamp, K.E., Sendrup, S., Maimets, M., Pedersen, M.T.*, et al.* (2019). Tracing the cellular dynamics of sebaceous gland development in normal and perturbed states. Nature cell biology *21*, 924-932.

Aragona, M., Dekoninck, S., Rulands, S., Lenglez, S., Mascre, G., Simons, B.D., and Blanpain, C. (2017). Defining stem cell dynamics and migration during wound healing in mouse skin epidermis. Nature communications *8*, 14684.

Blanpain, C., and Fuchs, E. (2006). Epidermal stem cells of the skin. Annual review of cell and developmental biology *22*, 339-373.

Blanpain, C., and Simons, B.D. (2013). Unravelling stem cell dynamics by lineage tracing. Nature reviews Molecular cell biology *14*, 489-502.

Boudaoud, A., Burian, A., Borowska-Wykret, D., Uyttewaal, M., Wrzalik, R., Kwiatkowska, D., and Hamant, O. (2014). FibrilTool, an ImageJ plug-in to quantify fibrillar structures in raw microscopy images. Nature Protocols *9*, 457-463.

Butler, A., Hoffman, P., Smibert, P., Papalexi, E., and Satija, R. (2018). Integrating single-cell transcriptomic data across different conditions, technologies, and species. Nature biotechnology *36*, 411-420.

Clayton, E., Doupe, D.P., Klein, A.M., Winton, D.J., Simons, B.D., and Jones, P.H. (2007). A single type of progenitor cell maintains normal epidermis. Nature *446*, 185-189.

Diamond, I., Owolabi, T., Marco, M., Lam, C., and Glick, A. (2000). Conditional gene expression in the epidermis of transgenic mice using the tetracycline-regulated transactivators tTA and rTA linked to the keratin 5 promoter. The Journal of investigative dermatology *115*, 788-794.

Didierjean, L., Wrench, R., and Saurat, J.H. (1983). Expression of cytoplasmic antigens linked to orthokeratosis during the development of parakeratosis in newborn mouse tail epidermis. Differentiation; research in biological diversity *23*, 250-255.

Edgar, R., Domrachev, M., and Lash, A.E. (2002). Gene Expression Omnibus: NCBI gene expression and hybridization array data repository. Nucleic acids research 30, 207-210.

Fink, J., Carpi, N., Betz, T., Betard, A., Chebah, M., Azioune, A., Bornens, M., Sykes, C., Fetler, L., Cuvelier, D.*, et al.* (2011). External forces control mitotic spindle positioning. Nature cell biology *13*, 771-778.

Gomez, C., Chua, W., Miremadi, A., Quist, S., Headon, D.J., and Watt, F.M. (2013). The interfollicular epidermis of adult mouse tail comprises two distinct cell lineages that are differentially regulated by Wnt, Edaradd, and Lrig1. Stem cell reports *1*, 19-27.

Harris, T. (2002). The theory of branching processes. Courier Corporation.

Itzkovitz, S., Blat, I.C., Jacks, T., Clevers, H., and van Oudenaarden, A. (2012). Optimality in the development of intestinal crypts. Cell *148*, 608-619.

Jin, Y., Patel, P.H., Kohlmaier, A., Pavlovic, B., Zhang, C., and Edgar, B.A. (2017). Intestinal Stem Cell Pool Regulation in Drosophila. Stem cell reports *8*, 1479-1487.

Joost, S., Zeisel, A., Jacob, T., Sun, X., La Manno, G., Lonnerberg, P., Linnarsson, S., and Kasper, M. (2016). Single-Cell Transcriptomics Reveals that Differentiation and Spatial Signatures Shape Epidermal and Hair Follicle Heterogeneity. Cell systems *3*, 221-237.

Klein, A.M., and Simons, B.D. (2011). Universal patterns of stem cell fate in cycling adult tissues. Development (Cambridge, England) *138*, 3103-3111.

Korsunsky, I., Millard, N., Fan, J., Slowikowski, K., Zhang, F., Wei, K., Baglaenko, Y., Brenner, M., Loh, B., and Raychaudhuri, S. (2019). Fast, sensitive and accurate integration of single-cell data with Harmony. Nature methods *16*, 1289-1296.

Liu, N., Matsumura, H., Kato, T., Ichinose, S., Takada, A., Namiki, T., Asakawa, K., Morinaga, H., Mohri, Y., De Arcangelis, A., *et al.* (2019). Stem cell competition orchestrates skin homeostasis and ageing. Nature *568*, 344-350.
Livet, J., Weissman, T.A., Kang, H., Draft, R.W., Lu, J., Bennis, R.A., Sanes, J.R., and Lichtman, J.W. (2007). Transgenic strategies for combinatorial expression of fluorescent proteins in the nervous system. Nature *450*, 56-62.
Mao, Y., Tournier, A.L., Hoppe, A., Kester, L., Thompson, B.J., and Tapon, N. (2013). Differential proliferation rates generate patterns of mechanical tension that orient tissue growth. The EMBO journal *32*, 2790-2803.
Mascre, G., Dekoninck, S., Drogat, B., Youssef, K.K., Brohee, S., Sotiropoulou, P.A., Simons, B.D., and Blanpain, C. (2012). Distinct contribution of stem and progenitor cells to epidermal maintenance. Nature *489*, 257-262.
Mesa, K.R., Kawaguchi, K., Cockburn, K., Gonzalez, D., Boucher, J., Xin, T., Klein, A.M., and Greco, V. (2018). Homeostatic Epidermal Stem Cell Self-Renewal Is Driven by Local Differentiation. Cell stem cell *23*, 677-686.
Miroshnikova, Y.A., Le, H.Q., Schneider, D., Thalheim, T., Rubsam, M., Bremicker, N., Polleux, J., Kamprad, N., Tarantola, M., Wang, I., *et al.* (2018). Adhesion forces and cortical tension couple cell proliferation and differentiation to drive epidermal stratification. Nature cell biology *20*, 69-80.
Mojtahedi, M., Skupin, A., Zhou, J., Castano, I.G., Leong-Quong, R.Y., Chang, H., Trachana, K., Giuliani, A., and Huang, S. (2016). Cell Fate Decision as High-Dimensional Critical State Transition. PLoS biology *14*, e2000640.
Potten, C.S. (1975). Epidermal transit times. The British journal of dermatology *93*, 649-658.
Rompolas, P., Mesa, K.R., Kawaguchi, K., Park, S., Gonzalez, D., Brown, S., Boucher, J., Klein, A.M., and Greco, V. (2016). Spatiotemporal coordination of stem cell commitment during epidermal homeostasis. Science (New York, NY) *352*, 1471-1474.
Sada, A., Jacob, F., Leung, E., Wang, S., and White, B.S. (2016). Defining the cellular lineage hierarchy in the interfollicular epidermis of adult skin. Nature cell biology *18*, 619-631.
Sanchez-Danes, A., Hannezo, E., Larsimont, J.C., Liagre, M., Youssef, K.K., Simons, B.D., and Blanpain, C. (2016). Defining the clonal dynamics leading to mouse skin tumour initiation. Nature *536*, 298-303.
Spearman, R.I., and Garretts, M. (1966). The effects of subcutaneous saline injections on growth and keratinization of mouse tail epidermis. The Journal of investigative dermatology *46*, 245-250.
Srinivas, S., Watanabe, T., Lin, C.S., William, C.M., Tanabe, Y., Jessell, T.M., and Costantini, F. (2001). Cre reporter strains produced by targeted insertion of EYFP and ECFP into the ROSA26 locus. BMC developmental biology *1*, 4.
Street, K., Risso, D., Fletcher, R.B., Das, D., Ngai, J., Yosef, N., Purdom, E., and Dudoit, S. (2018). Slingshot: cell lineage and pseudotime inference for single-cell transcriptomics. BMC genomics *19*, 477.
Susaki, E.A., Tainaka, K., Perrin, D., Kishino, F., Tawara, T., Watanabe, T.M., Yokoyama, C., Onoe, H., Eguchi, M., Yamaguchi, S., *et al.* (2014). Whole-brain imaging with single-cell resolution using chemical cocktails and computational analysis. Cell *157*, 726-739.
Thery, M., Racine, V., Pepin, A., Piel, M., Chen, Y., Sibarita, J.B., and Bornens, M. (2005). The extracellular matrix guides the orientation of the cell division axis. Nature cell biology *7*, 947-953.
Tian, H., Biehs, B., Warming, S., Leong, K.G., Rangell, L., Klein, O.D., and de Sauvage, F.J. (2011). A reserve stem cell population in small intestine renders Lgr5-positive cells dispensable. Nature *478*, 255-259.

Tobiasch, E., Winter, H., and Schweizer, J. (1992). Structural features and sites of expression of a new murine 65 kD and 48 kD hair-related keratin pair, associated with a special type of parakeratotic epithelial differentiation. Differentiation; research in biological diversity *50*, 163-178.
Tran, H.T.N., Ang, K.S., Chevrier, M., Zhang, X., Lee, N.Y.S., Goh, M., and Chen, J. (2020). A benchmark of batch-effect correction methods for single-cell RNA sequencing data. Genome biology *21*, 12.
Tumbar, T., Guasch, G., Greco, V., Blanpain, C., Lowry, W.E., Rendl, M., and Fuchs, E. (2004). Defining the epithelial stem cell niche in skin. Science (New York, NY) *303*, 359-363.
Vasioukhin, V., Degenstein, L., Wise, B., and Fuchs, E. (1999). The magical touch: genome targeting in epidermal stem cells induced by tamoxifen application to mouse skin. Proceedings of the National Academy of Sciences of the United States of America *96*, 8551-8556.
Zhang, Y.V., Cheong, J., Ciapurin, N., McDermitt, D.J., and Tumbar, T. (2009). Distinct self-renewal and differentiation phases in the niche of infrequently dividing hair follicle stem cells. Cell stem cell *5*, 267-278.
Zheng, G.X., Terry, J.M., Belgrader, P., Ryvkin, P., Bent, Z.W., Wilson, R., Ziraldo, S.B., Wheeler, T.D., McDermott, G.P., Zhu, J., *et al.* (2017). Massively parallel digital transcriptional profiling of single cells. Nature communications *8*, 14049.

5 DISCUSSION

5.1 DEFINING STEM CELL DYNAMICS AND MIGRATION DURING WOUND HEALING IN MOUSE SKIN EPIDERMIS

5.1.1 Compartmentalization during wound healing

Wound healing is a complex mechanism through which different cell populations need to spatially and temporally orchestrate rapid tissue repair to avoid infection and reform the barrier. Using punch biopsy we performed full thickness wound on the mouse tail and analysed whole-mount epidermis 0, 2 ,4, 7, 10 and 14 days after wound after a short pulse of BrdU (Figure 1, page 36). Our data show that BrdU incorporation did not change the first hours after wound (day 0), but start to increase 2 days post wound, being multiplied by 5 fold until 7 days post wound. Proliferation occurs in a ring of around 1mm large, the proliferative hub, at a distance of 0,5 mm from the wound edge, delimitating a quiescent leading edge (LE) around the wound. These transient compartments are maintained until around 10 days post-wound (Figure 1, page 36). The epidermal wound was totally closed after 14 days. Although the existence of a quiescent LE was already described in human and mammals based on skin sections in the 1970s, our short term BrdU pulse experiments observed on 3D whole-mount tail epidermis at different time point after wound healing enable to confirm and better appreciate the dynamics and the spatial compartments occurring within the epidermis[133-135]. Using phalloidin staining to label the actin cytoskeleton of the cells and confocal images, we show that the first rows of LE basal cells were elongated toward the wound 1 day after the damage, suggesting that they actively migrate. By contrast, 2 days after wound basal cells were oriented perpendicularly to the wound direction, suggesting that they were compressed. This orientation was still obvious 4 days after wound, but disappeared at 7, 10 and 14 days post wound. Strikingly, we also observed that the cell density was increased in the proliferative hub, 4 days post wound, reflecting the massive increase of proliferation already observed at this stage. Treating mice with 5-FU to block cell proliferation prevented proper wound closure and also partially rescued the cell elongation toward the wound. These data suggest that the massive

proliferation induce the compression of the LE cells around 2 and 4 days post-wound. Interestingly, the same compartments (proliferative hub and LE), were also recently observed by *in vivo* live imaging on mouse ear using 1mm punch biopsy[136]. Following cells over 12h, 3 days after wound, Park and colleagues showed that the fastest cells to migrate are the cells located within a distance of 0,5 mm around the wound and that cell proliferation is the highest at a distance of 0,5 to 1,5mm away from the wound[136]. Altogether, these data obtained in different tissues (tail versus ear) with different size of wound (3mm versus 1mm) support the idea that this compartmentalization is a general mechanism for epidermis healing independent of the wound size[135]. Moreover, our microarray analysis performed specifically on the LE and proliferative hub cells show that they are molecularly different (see below). We show that specific markers of the LE are expressed in the leading cells all along the healing process and disappear when the two sides of the wound reach each other and close the wound. Further experiments would be necessary to understand how these compartments are initiated and resolved and what is the molecular mechanisms for their spatial confinements.

5.1.2 Wound healing signature

Knowing the reproducibility and the precise localization of the two compartments around the wound we aimed to decipher their molecular signature and micro dissected the two regions using 4 mm punch biopsy (to target the LE) and 6 mm punch biopsy (to target the proliferative hub) and compare them with cells located far from the wound, 4 and 7 days after the wound. We performed bulk microarray and identified genes upregulated in the two regions. This generic wound signature included genes coding for cell cytoskeleton proteins such as *Krt6b or* the actin-bundling protein Fascin1 (*Fscn1),* important for cell rigidity and cell migration[137,138], the desmosome protein Desmocollin 2 (*Dsc2*) to resist against tissue shearing, and membrane permeability proteins (*Sprr1b, Sprr2h*) (Supplementary figure 2a, page 37). Genes implicated in cell signaling such as the gene coding for the epidermal growth factor Amphiregulin (*Areg)* important for keratinocyte proliferation[139,140] or the transmembrane glycoprotein Embigin *(Emb*) which may play a role in cell adhesion were also upregulated in both regions[141]. We also observed upregulation of genes implicated in inflammatory signals such as the gene coding

for the interleukin 24 (*Il24)* which have been shown to promote wound healing in a diabetic mouse model after topical application[142] or the S100 calcium binding protein A8 and 9 *(S100a8, S100a9*) which can act as cytokines and were shown to stimulate keratinocyte proliferation and migration *in vitro*[143]. Finally, the wound signature encompasses genes regulating cell cycle proteins such as the cell division cycle associated 2 and 8 (*Cdca2, Cdca8)* or the cyclin A2 and B1 *(Ccna2, Ccnb1*) upregulated in both compartments.

Our first microarray analysis identified Itgα5 as marker for LE cells (Figure 3b, page 38 and supplementary figure 2e, page 49). This marker was already described at the LE of human epithelial wound[144,145] and in migrating cells during eyelid closure[146]. We used Itgα5 as a marker to isolate pure population of LE cells by FACS and performed, on this pure population, a second microarray analysis highlighting for the first time a spatial molecular signature of the LE and proliferative cells during wound healing (Figure 3 d-j, page 38). This LE signature showed the upregulation of Ephrin-B1 (*Efnb1*) and its receptor (*Ephb2*), which have been recently shown to promote wound healing[147]. It also encompasses several matrix metalloproteinases (MMPs) (*Mmp1b*, *Mmp9*, *Mmp13*), important for the breakdown of ECM and cell migration during healing (Figure 3d, page 38)[148-152]. Consistent with this finding, the inhibitor of MMPs, *Timp3*, was highly down regulated in the LE cells (Supplementary figure 2f, page 37). LE cells upregulate genes with important role in inflammation such as chemokines (*Cxcl2*, *Cxcl3*), described as pro-angiogenic chemoattractant, and chemokine receptors such as *Cxcr4,* implicated in neutrophils recruitment and neo-vascularization[153,154]. Interestingly, the local expression of Cxcr4 on keratinocytes is consistent with the local expression of its ligand by dermal cells, Cxcl12/Sdf-1, as observed at the wound margins of human skin after incision wound[155]. LE cells also up-regulate complement receptor genes (*C5ar1*) as well as Plasminogen Activator urokinase and its receptor implicated in the degradation of fibrin clot (*Plau*, *Plaur*)[156]. The Protein C Receptor (*Procr*), was also highly upregulated in the LE (Figure 3e, page 38). Interestingly, topical application of its ligand, the Activated Protein C (APC), has been shown to promote anti-coagulation and angiogenesis[157,158]. *Procr* was also upregulated in the proliferative hub and may also have a role in the mitotic activity of the cells in this compartment as APC application has been shown to induce

keratinocytes proliferation[158]. All these genes support the important role of LE cells in the degradation of the fibrin clot, the recruitment of neutrophils and macrophages to remove cellular debris, the blocking of coagulation and the attraction of neo-vessels in the wound site, four key steps important to ensure the progression of the wound repair from the inflammation to the proliferative phase. LE cells also specifically upregulate genes coding for integrins (*Itga5*, *Itga6*), protocadherins (*Pcdh7*, *Pcdhb19*, *Pcdhga1*), desmosomes (*Cdsn*) and Gap junction proteins (*Gjb6/Cx30*, *Gjb2/Cx26*), all essential for cell adhesion and cell-cell communication. We also noticed an upregulation of *Gjb2* in the proliferative hub (figure 3f, page 38). *Gjb2* expression is known to be higher in psoriatic epidermis or in hyper-proliferative epidermis after tape-stripping in human[159,160] and overexpression of *Gjb2* in mouse lead to a thicker and higher proliferating epidermis, suggesting a role of Gjb2 in the establishment of the proliferative hub[160,161]. Interestingly, we identified a fibronectin leucine rich transmembrane protein (*Flrt2*) which was not previously described in wound healing but has been known to be important for neuronal guidance[162]. Extracellular matrix ligands found in the basement membrane such as laminin-332 genes (*Lama3*, *Lamb3*, *Lamc2*) or fibronectin (*Fn1*) are also more specifically upregulated by the LE keratinocytes, showing that this transient structure controls the re-establishment of the BM (Figure 3f and h, page 38). Several cytoskeleton proteins such as Myosin (*Myh9, Myo1b,Myo5b*), Tropomyosin (*Tpm1*, *Tpm2*) and Tubulin (*Tubb2a, Tubb2b, Tubb3, Tubb6*), as well as actin regulators (*Cald1*, *Fscn1*, *Fmnl2*, *Nav2*), which are critical for cell movement, are also upregulated in the LE cells and support the migrating behavior of this LE (Figure 3i, page 38). Specific TFs not previously described in wound healing but associated with migration and invasion in cancer in other tissues (*Elk3*, *Hmga2*)[163-165] or repressor of proliferation (*E2f7*)[166,167] were also part of this LE signature (Figure 3g, page 38). These TFs may therefore be important for the migrating and quiescent behavior of the LE cells. Finally, several ligands of different cell signaling pathways associated with migration or wound healing were highly induced in the LE (Figure 3j, page 38). Among them, *Inhibin-βa* codes for a subunit of Activin A, a ligand from the TGF-b family, and which overexpression increases wound healing in mice[168-171]. Its upregulation in the leading edge also confirmed previous in-situ hybridization on mice samples[172]. Epiregulin (*Ereg*), a ligand for

Epithelial Growth Factor Receptor (EGFR) and ErbB tyrosine kinase receptors, which was associated with enhanced wound healing, was also specifically upregulated in the LE cells (Figure 3j, page 38)[173]. Other genes coding for secreted proteins (such as *Fgf18*, *Tgfa*, *Wnt5a*) upregulated in the LE cells were associated with proliferation, migration or invasion in other tissues and in cancer[173-177]. These secreted ligands specifically upregulated in the LE cells support the importance of this structure to create a gradient of growth factors around the wound and attract other cells into the wound. Interestingly, *Gprc5a*, an orphan G protein coupled receptor, was not previously described in wound healing but is a tumor-suppressor gene in lung tissue acting on EGFR and STAT3 signaling (Figure 3j, page 38)[178-180]. In addition, more recently, experiments using *Gprc5a* KO cancer cell lines show a decrease in cell adhesion on collagen I substrates and reduced activation of Rac1 and RhoA GTPase which suggest a role of *Gprc5a* in cell matrix adhesion[181]. Altogether, this LE signature support the idea that, more than being a quiescent and migrating edge, this transient structure is key to degrade the provisional matrix, regenerate a new BM, attract inflammatory cells to remove cell debris and endothelial cells to form neo-vessels in close proximity to the wound. We propose that this structure act as a scaffold to protect proliferative cells behind from the wound and help to progress into the repair.

In order to understand if the proliferation could be decoupled from the LE signature, mice were treated with 5-FU topically (Figure 5a, page 41). 5-FU treatment decreased the proliferation within the epidermis, but did not change the expression of the leading edge markers, suggesting that these markers were induced independently of cell division (Figure 5b-c, page 41). As inflammation is well known to play a role in wound healing[116,118,182] we tested whether blocking inflammation could have an impact on the formation of the LE and proliferative hub. Interestingly, wounded mice treated with dexamethasone, an anti-inflammatory drug of the GC family, partially re-established proliferation in the LE cells but did not impair the expression of the LE markers (Figure 5 d-g, page 41). These data suggest that an inhibitor of proliferation, which can be blocked by GC treatment, act locally on LE cells. This inhibitor could be expressed by keratinocytes or secreted by inflammatory cells recruited upon wound. Altogether, these experiments show that the quiescent

status of the LE cells can be functionally and molecularly uncoupled from the expression of the specific markers.

5.1.3 Proliferation and migration during wound healing

Our close observation of the migrating LE edge cells, revealed by phalloidin staining, showed that the first rows of cells were elongated toward the wound, 1 day after wound. By contrast, at day 2 post-wound, LE cells drastically change their axis of elongation and become elongated perpendicular to the wound edge, both in basal and suprabasal layers, suggesting that they are compressed (Figure 2a, page 37). Strikingly, this observation was concomitant with the increase in proliferation observed in the proliferative hub. These observations raised the question whether the proliferation could be a major driver for cell migration. In order to decipher the importance of proliferation versus migration in the repair process, we aimed to block specifically proliferation using pharmacological treatment. The strong delay in wound healing following 5FU treatment suggest that proliferation is indispensable for proper healing (Figure 2e, page 37). Interestingly, blocking proliferation also partially restore the elongation of LE cells toward the wound (Figure 2f, page 37). These data show that the burst of proliferation may lead to the compression of the LE cells and suggest that proliferation is important for wound closure not only to produce new cells for the repair but may also push migrating LE edge cells toward the center of the wound, at least in the tail epidermis. Similar conclusions can be drawn from Park and colleagues' data on ear epidermis regarding the importance of proliferation in repair. Indeed, although blocking proliferation with Mitomycin C, a DNA cross linker, does not prevent cell migration in mouse ear epithelium it does have an impact on wound repair as cells acquire compensatory features and become bigger (as shown by a reduced cell density in the LE zone)[136]. Interestingly, depleting proliferation also extend the zone of migration further around the wound suggesting that if cells are not replaced through proliferation, the new cells are recruited further away[136]. Altogether, these data show that proliferation and migration are independent phenomenon but strongly support the importance of cell proliferation in proper wound repair to replenish the pool of cells that migrate and also suggest that the proliferation hub serve as boundaries to constrain cell migration within the wound zone.

Importantly, while GC administration are known to block inflammation and delay wound healing[116], our dexamethasone treatments experiments showed that it lead to a partial restoration of proliferation in the LE. GC may act directly on keratinocytes. Overexpression of the GC receptor on K5+ basal keratinocytes induces a similar delay in wound closure and a similar decrease in pro-inflammatory cytokines than dexamethasone treatment, suggesting that part of the delay observed in wound healing under GC treatment may be due to a direct action of GC on keratinocytes[183]. K5+ cells overexpressing the GC receptor show a strong decrease in BrdU incorporation *in vivo* suggesting that GC treatment decreases keratinocyte proliferation[183]. Consistent with this, we see a decrease in proliferation of keratinocytes located within the proliferative hub (Figure 5e, page 41). However, our data also show that LE cells reacquire a proliferative status under GC treatment. These results suggest that GC partially block keratinocytes proliferation directly but also re-activate proliferation, likely indirectly, by preventing a quiescent signal to reach keratinocytes at the LE. It is possible that this quiescent state of the LE edge cells is dictated by some factors secreted by immune cells recruited inside the wound clot. In line with this hypothesis, previous studies using 3D-organotypic culture of human keratinocytes and fibroblasts did not observe the quiescent LE *in vitro*[184]. The first immune cells activated at the wound site may potentially be the DETCs that reside within the epidermis[185]. After activation by damaged keratinocytes, DETCs partially loose their dendritic shape around the wound edge[186]. However it is unclear whether the zone of DETC activation corresponds to the LE or to the proliferative hub. Activated DETCs are known to stimulate keratinocyte proliferation and express specific chemokines and cytokines to attract macrophages[185]. Mice lacking DETCs display a delay in wound closure and a decrease in keratinocyte proliferation[186]. It is likely that these cells are responsible for the increased proliferation observed within the proliferative hub and their pro-proliferative signal may be counteract, at the LE, by other recruited immune cells present within the wound clot. The immune cells recruited at the wound site are neutrophils and macrophages[116]. Conditional depletion of macrophage before wound delays healing in the early phases but do not drastically impact the timing of wound closure[187,188]. However, the impact of their depletion was not assessed in the LE specifically. Finally, γδ T cells present within the dermis are also important for

wound healing but they were shown to only be recruited after 10 days post-wound and therefore unlikely play a role in the LE quiescence[189]. Further experiments would be necessary to understand the origin and the nature of the signals that regulate the quiescence in the LE cells and understand its role in wound healing (See Perspectives).

While our study was performed on fixed samples, lineage tracing performed at clonal density showed that cell progeny within a clone were oriented toward the wound in both basal and suprabasal layers and therefore enable to, somehow, capture cell movement. These data suggest that migration but also oriented cell division takes place in order to send cell progeny toward the center of the wound (Figure 6j-l, page 42). These oriented division in the basal layer of the epidermis were also observed in live imaging[136]. Interestingly, oriented cell division seem to strongly rely on the Rho GTPase, Rac1, as cell division orientation is randomized in *Rac1*$^{-/-}$ mice[136]. These data support the important role of cytoskeleton machinery to sense the microenvironment[190]. Finally, our study performed during post-natal development showed that cell division orientation is dictated by the orientation of collagen fibers. It would therefore be interesting to analyze whether collagen fibers or other ECM components also orient cell division in wound healing.

Finally, our lineage tracing showed that both suprabasal and basal cells migrate toward the wound at different velocity and suggest that differentiation and upward movement of differentiated cells is still ongoing during wound repair. Moreover the *Inv-CreER* tracing initiated before wound suggest that there is no reversion of suprabasal cells during wound repair. This is supported by live imaging data in mouse ear epithelium showing an exclusive upward movement of cells [136]. However recent lineage tracing experiments suggest that a small populations of Gata6+ cells, normally restricted within the sebaceous duct, can migrate out of the SG and refuel the suprabasal compartment of IFE upon wound healing. More surprisingly, while most of the labelled cells are suprabasal in the early days after wound, a fraction of the Gata6 progeny can be found within the basal compartment at later stage (12 days after wound), suggesting that reversion from suprabasal to basal fate is possible [191]. However, the presence of a small fraction of Gata6+ basal cells at every time points precludes any strong conclusion. More experiments are

necessary to understand whether this reversion really occurs and the importance of this phenomenon in wound repair (See Perspectives).

5.1.4 Clonal dynamics during wound healing

During homeostasis, IFE SC and CP divide asymmetrically and balance their self-renewal and differentiation at the population level to maintain the number of cell constant and produce sufficient amount of cells to replenish the loss of the others. This equilibrium is maintained through a stable cell division rate in both populations, with CPs dividing more frequently and ensuring the majority of the maintenance, and SCs dividing less frequently to replenish the CP compartment[102,103]. Interestingly, recent studies performed on human primary keratinocytes show that these cell fate decisions probabilities can also be observed *in vitro* and that upon scratch wound assay, CP increase their self-renewal and switch to an "expanding" mode of division, switching from 38±3% of symmetrical renewal to 88±2% [110]. Our major aim was to understand whether this switch also occur *in vivo* upon wound healing. It is important to note that, regarding the burst of proliferation observed at 4 days post wound, if the clones had switched to an "expanding" mode of division, they would remain in the tissue and the basal content of each clone would increase dramatically and exponentially. Surprisingly, several observations coming from our clonal analysis show that progenitors do not increase their self-renewal division upon wound healing. First, the proportion of *K14-CreER/Rosa-Confetti* attached clones dropped dramatically from day 0 to day 4 post wound, consistent with a scenario where, at each round of cell division, basal cells achieve 21±11% of symmetric differentiation (similar to the homeostatic model) leading to the loss of the clone, but here in an accelerated way due to the burst of proliferation (Figure 6h, page 42) [103]. Second, our clonal analysis performed on remaining clones 4 and 7 days after wound do not show a dramatic increase in the basal cell content, despite the burst of proliferation. Instead, we observed an increase in the production of suprabasal cells, also reflected by the increased thickness of the epidermis observed at 7 days post-wound (Figure 8b and 6i, pages 44 and 42). Third, over the time course, K14 remaining clones increase their average basal cell content in a linear manner (Figure 8c, page 44). These three elements strongly support the idea that the homeostatic mode is maintained in the first days following wound, and that CP are

unable to switch toward more symmetrical self-renewal *in vivo*. Interestingly, our mathematical modelling suggest that the growth of the remaining clones can not be explained by the activation of CPs only, as it would necessitate a cell cycle time of around 6h, which is unreasonably fast. Instead, the linear increase of basal content after 4 days post wound can be explained by the reactivation a more slow cycling population, the SCs, dividing asymmetrically to replenish the CPs (Supplementary Theory). The existence of a SC population proliferating and remaining in the basal layer and a CP population balancing symmetrical renewal and symmetrical differentiation to produce differentiated cells is highly consistent with the increased thickness of the IFE and the fragmentation of the streaks. Similarily, the *Lrig1-CreER/Rosa-Confetti* tracing showed that, once in the IFE, progenitors coming from the infundibulum also increase their basal content in a linear manner and produce a majority of suprabasal cells. Again, this is consistent with the idea that they follow a homeostatic mode of division, with a majority of division giving rise to one basal and one suprabasal cell (Figure 8c, page 44). Strikingly however, the Lrig1 clones are growing faster than K14 clones. Our mathematical modeling suggest that this can be explained by the same model as proposed for K14 (keeping the balance between self-renewal and differentiation), but with a first division being a symmetrical self-renewal decision in the SC population. Altogether, our data suggest that *in vivo* IFE SCs and CPs are unable to switch to an "expanding" mode of division, such as the one described *in vitro* [110], and instead increase their proliferation while keeping their homeostatic cell fate decision to repair tissue.

It is interesting to note that few attempts were made in the past to understand the relative contribution of each population in tissue repair. Using mathematical modelling, we estimate that 2054±254 clonal stripes would be necessary to cover the entire wound. However, we estimate that K14 SC only contribute to 343±120 stripes, meaning that they only represent around 15% of the total area (Supplementary Theory). The recruitment of HF cells during wound healing are probably the source of the other cells required to close the wound. As described by others using lineage tracing experiments, SC arising from bulge (*Lgr5+*), isthmus (*Lgr6+*) or upper isthmus (*Lrig1+*) rapidly migrate out of the HF to the center of the wound upon wound healing[125].

If SC/CP are unable to switch to an “expanding” mode *in vivo*, it is tempting to speculate that some external signals constrain them in their decision. It has been shown that human keratinocytes are more prone to differentiate when cultured on small ECM-rich island compared to large island[192]. Importantly, this process is highly dependent on the shape of the island rather than its surface or the type of ECM and is called shape-induced differentiation[192]. This mechanism has been linked to actin cytoskeleton and FA. Keratinocytes cultured on large island display high number of FA and F-actin stress fibers while they show few and small FA as well as F-actin arranged in dense shell around the cell cortex when cultured on small island[192]. Connelly and colleagues propose that spread cells are less prone to differentiate than compacted cells. Mechanistically, cell spreading increases actin depolymerisation, which increases the amount of G-actin and prevent Serum Response Factor (SRF) TF to bind its cofactor MAL. This prevent JunB expression and blocks keratinocyte differentiation. By contrast, in small island, the cell is more compact, actin filaments are numerous, G-actin is less abundant and SRF-MAL can activate JunB expression and trigger differentiation[192]. Consistent with this, activation of ROCK2, a kinase which also triggers actin polymerization, increases keratinocyte differentiation, *in vitro* [193]. All these data suggest that the change in cell shape plays a key role in keratinocytes differentiation. Interestingly, ROCK2 also seems to have a role in cell fate decision. *In vitro*, cells in “expanding” mode of division switch to “balanced” mode at the center of a colony, where cells are confluent. ROCK2 inhibition does not have any impact on “balanced” mode of division but prevents “expanding” colonies to switch to “balanced” mode, suggesting an important role for ROCK2 and the actin cytoskeleton to “sense” cell confluence in this process[110]. These data suggest that the confluence may change the shape of cells in the center of a colony and be responsible for the switch from the “expanding” to the “balanced” mode of division[110]. *In vivo*, epidermal cells migrate altogether as a uniform sheet, and may maintain a certain level of confluence all along the process. This may possibly explain why cells do not switch to an “expanding” mode of division upon wound healing, *in vivo*. The only cells that could be out of this constraint, and therefore could potentially switch to an “expanding” mode, would be the LE cells, but these cells are quiescent. More experiments must be performed

to better understand the role of the confluence on cell fate decision *in vivo* (See Perspectives).

Many lineage tracing experiments have shown the plasticity of epidermal cells during wound healing[119,123,125,194,195]. However, none of these studies interrogates the cellular dynamics underlying this process. Our clonal analysis and mathematical modelling suggest that Lrig1 upper isthmus cells achieve initially one self-renewing division, but rapidly acquire the same fate decision dynamics as observed for the IFE cells : they balance symmetric self-renewal and differentiation. These data suggest that, as soon as they arrive in the IFE, Lrig1 derived progeny are under the same constraint that the one operated on IFE cells and therefore suggest a role for the microenvironment in the regulation of cell fate decision. Today, the progress made in transcriptional sequencing and epigenetic modifications analysis on low amount of cells enable to study with more accuracy the molecular differences between bulge, upper isthmus and IFE SC populations. The progressive acquisition of IFE gene signature and the loss of upper hair follicle or bulge signature has been recently characterized in Lgr6 and Lgr5 progeny respectively at the single cell level using RNA sequencing[196]. Interestingly, they show that while Lgr5 bulge cells take 3 days to move out of the HF and reach the wound, their molecular identity is already changing as soon as 1 day after wound, as highlighted by the increased expression of receptor for wound ECM ligands[196]. By contrast, Lgr6 upper HF cells already expressed receptors for wound ECM ligands, providing a possible explanation for the rapid mobilization of these cells into the IFE upond wound. The upregulation of these receptors for ECM-ligands again support the importance of the microenvironment in this plasticity. However, only few cells where identified as “wound cells” (106 cells) in this study[196]. Using the same analysis background, coupled with lineage tracing and single cell RNA-seq from the 10X Genomics technology[130], it could be interesting to interrogate the molecular changes taking place in the Lrig1 population and see which receptors for ECM ligands they express before and after wound.

In another study, using the Assay for Transposase Accessible Chromatin with high-throughpout sequencing (ATAC-seq), Ge and colleagues looked for the epigenetic modifications within keratinocytes taking place during wound.

Combining these data with transcriptional profiling and Chromatin ImmunoPrecipitation followed by sequencing (Chip-seq), they showed that IFE SC have similar and different regions of accessible chromatin (ATAC peaks) compared to HF SCs during homeostasis. Among the peaks unique for IFE SC, they show motifs for TF such as Klf5, Gata, Grhl or AP2[197]. By contrast, Sox9 or Tcf motifs were only present in HF SCs. These data were further confirmed with immunostaining using Sox9 and Klf5 antibodies showing the exclusive expression of Klf5 in IFE and Sox9 in HF SC. By contrast, 3 days after wound, Sox9+ cells start to express Klf5, even if they are still residing within the HF, suggesting they acquire an IFE identity before migration, a process called lineage infidelity[197]. Ablation of *Sox9* or *Klf5* with CRISPR/Cas9 prevented the recruitment of HF SC to repair epidermis after its removal on neonatal P3 mice. Importantly, upregulation of *Klf5* decreases *Sox9* expression, a key step to resolve lineage infidelity after repair. Interestingly, this resolution do not occur in cancer due to chromatin regions (epicenters) that are maintained open, and keratinocytes remain in a lineage infidelity that never resolve[197]. These results support the importance of Klf5 and Sox9 in lineage plasticity of bulge SCs and pave the way toward a better understanding of the molecular mechanisms underlying this phenomenon during wound healing. Further experiments would be needed to understand which TF control lineage infidelity in the other SCs populations, such as Lrig1 SCs (See Perspectives).

Clonal analysis using a genetically induced fluorescent reporter is not possible to perform in human. However, somatic mutations can be used as a genetic tracer within human samples. Using deep-sequencing on biological samples and bio-informatic algorithm, it is possible to evaluate clonal evolution within human tissue[198,199]. Recently, a study reported how a patient suffering from Junctional Epidermolysis Bullosa (JEB), a severe a lethal genetic skin disease, has been cured by autologous grafting of genetically engineered skin[200]. A retrovirus was used to re-introduce the missing full length *LAMB3*-cDNA into autologous keratinocytes isolated from a 4 cm^2 biopsy from an healthy part of the patient's skin. The genetically corrected keratinocytes were expanded *in vitro* as transgenic epidermal sheets able to cover 0.85 m^2 in surface. Around 80% of the patient's skin was replaced by the transgenic skin. Ten punch biopsies were taken randomly 4, 8 and

21 months after grafting. The newly formed skin was mainly composed of transgenic keratinocytes which successfully re-express Lamb3, as shown by immunostaining[200]. Sequencing of the integration site of the retrovirus was used to trace the different clones that constitute the new skin. Pre-graft and post-graft samples shared some similar integration sites. Sequencing of integration site were also performed on holoclones (clones with high colony forming potential), paraclones and meroclones (clones with limited colony forming potential) derived form pre-graft and post-graft cultures. Strikingly, while 91% of paraclones and meroclones display different integration sites compared to holoclones in pre-graft culture, this percentage has decreased to 37% in 4 month post-graft derived culture and to nearly 0% in 8 month post-graft derived culture in which all paraclones and meroclones display similar integration site as holoclones. These results support the idea that holoclones contains SCs which gave rise to the para- and merclones in the newly regenerated epidermis[200]. It therefore suggest that the SC-CP model developed in mouse epidermis can be applied to human skin. Importantly, this study show that future improvement may be achieved in clinics concerning the use of cell therapy to cure chronic wounds.

5.2 Defining the design principles of Skin epidermis postnatal growth

5.2.1 Clonal dynamics during postnatal development

The purpose of this study was to define the cellular mechanism underlying epidermis post-natal growth. In theory, the expansion of a stratified epithelium could occur in many different ways, playing on the cell fate decision, the proliferation rate or both. A first possible model would be that cells achieve a majority of asymmetrical cell fate decisions and perfectly balance self-renewal and differentiation (homeostatic model) but reduce the shedding at the skin surface (Figure 5A, p104). In this case, the tissue would increase through an accumulation of non-dividing differentiated cells in the basal layer which would dilute the number of DPs (Figure 5A, page 104). In our case, the proliferation experiments performed

with the *K5-Tet-OFF* system and the Edu/Brdu pulses show that all basal cells divide overtime meaning that no differentiated cells accumulate in the basal layer (Figure 3 and Figure S2, pages 100 and 112). A second scenario is called the "bang-bang" control and proposed to be optimal for fast intestinal crypt expansion[201]. This model implies that DPs would undergo 100% of self-renewal to increase the pool of DP during a certain time, and then achieve 100% of asymmetrical divisions to ensure the production of suprabasal cells. This would lead to a short period during which the suprabasal cells would not be produced and the density of basal cells would increase, potentially jeopardizing skin barrier function. However, histological characterization show that the ratio between differentiated suprabasal cells and basal cells remains constant from P1 to P60 (Figure 5 E,F, page 104). A third possible scenario would be that DPs would adapt their cell fate decision overtime while keeping a constant and high proliferation rate until P30 (Figure 5C, page 104). DP would for example have a slight imbalance for self-renewal in the beginning to increase its pool and then switch to an imbalance for symmetric differentiation, which would give a different ratio between suprabasal and basal cells at different time point. But once again, this scenario is not consistent with our data. First, we show that the ratio suprabasal to basal is constant from P1 to P60. Second, two independent proliferation experiments (Tet-OFF system and EdU/BrdU pulses) showed that to the DPs decrease their proliferation rate from P1 to P30 (Figure 3 and Figure S2, pages 100 and 112). Third, when we performed a second clonal tracing initiated at P15, the imbalance found with the tracing at P1 could accurately predict the clone size and persistence of our second P15 tracing (Figure 4, page 102). These data show that the imbalance calculated at P1 is maintained throughout the post-natal growth, ruling out the possibility that DP adapt their cell fate decision. Interestingly, all these tree theoretical scenarios would imply either a decrease in the DPs density or a decrease in suprabasal cells density for a short period of time, which would potentially compromise the skin barrier. Finally, we looked whether a constant fate bias toward self-renewing division coupled with a decreasing cell division rate over time, could predict the clonal dynamics during postnatal development (Figure 5D, page 104). Strikingly, we found that the range of clonal fate data obtained in both the scale and interscale regions of epidermis could be predicted by such a constant imbalance model, with an imbalance of 24% in favor of

symmetrical self-renewal (32% of symmetrical self-renewal versus 8% of symmetrical differentiation). Interestingly, this imbalance is identical between the two compartments and the larger clone size observed in the scale can be explained by the higher proliferation rate observed in scale compared to interscale at all time points. If the proliferation rate was constant, this imbalance toward self-renewal would lead to an exponential growth of the tissue. By contrast, the gradual decrease in proliferation that we observe can explain the linear increase of the tissue measured experimentally (Figure 1,2 and S3, pages 96, 98 and 114). Importantly, as proliferation was measured independently, the degree of fate imbalance was the only fitting parameter in the model. This single parameter could be fitted based on the time evolution of clone sizes alone, so that multiple independent features of our dataset could then be predicted. These included the evolution of clonal persistence, the conserved exponential shape of clone size distributions, both over time and across tail interscale, tail scale and paw epidermis, and the clonal induction at other time points. All these features were experimentally measured and could be accurately predicted by the model, strengthening our confidence in the constant imbalance hypothesis. In order to see whether this model could be applied to another type of epidermis, we also performed clonal analysis in the hindpaw. Our data show that paw epidermis also followed a linear increase from P1 to P15 and a decreasing proliferation rate overtime. Clonal analysis in the paw epidermis also fit with a constant imbalance model where an equipotent population of DPs have an imbalance of 20% toward self-renewal over symmetrical differentiation (Figure S3, page 114). Finally, the constant imbalance model ensures a constant density of DPs and suprabasal cells along the growth, contrasting with the other scenarii. Very interestingly, our histological charachterization fit perfectly with this prediction and show that the ratio between suprabasal and basal cell density is indeed constant overtime both in the tail and the paw epidermis (Figure 5 E, F, page 104). Altogether, these data strongly support the concept where an equipotent population of DPs sustain the post-natal growth of the epidermis through a constant imbalance for self-renewal compensated by an attenuated proliferation rate overtime, in tail scale and interscale as well as in paw.

This strong imbalance observed during post-natal growth contrasts with our observations performed in adult during wound healing but are highly similar to the cellular dynamics ongoing during tumor initiation after the constitutive activation of the Hedgehog (Hh) signaling pathway[103]. Indeed, using a mouse model to study skin Basal Cell Carcinoma (BCC) where the Smoothened receptor (Smo) is constitutively active in K14+ cells, our group recently performed clonal analysis in the mouse tail in oncogenic context. Interestingly, these data show that shortly after the activation of the Hh pathway, SC and CPs switch their proliferation dynamics and show a strong imbalance (17%) toward self-renewal over differentiation (34±10% of symmetrical self-renewal versus 17±12%% of symmetrical differentiation). Very similarly to the post-natal development, SC and CP decrease their proliferation rate overtime so that the net effect is a linear growth of the tumor. These results suggest that oncogenic context and postnatal development present similar fate imbalance. In the wound, basal cells do not change the proportion of self-renewal and differentiation division but rather increase their proliferation rate. The absence of cell fate change and the fact that SC and CP are continuously achieving a majority of asymmetrical cell division in damaged tissue suggest that specific signals may constrain these decisions in healthy homeostatic and renewing tissue. Interestingly, the paw epidermis seem to be relieved from such a constraint, at least during homeostasis. Initial static clonal analysis showed a similar proliferation dynamics as decribed for the tail IFE (20% of symmetrical self-renewal; 60% of asymmetrical division ; 20% of symmetrical differentiation)[45]. However, mother and daughters cells fate decision were recently tracked by live imaging and a total of 101 cell divisions were scored in the paw epidermis in homeostasis. The data show that symmetrical self-renewal actually occur in 34±5% of the cases, asymmetrical division in 35±5% and symmetrical differentiation in 32±5% of the cases[107]. These probabilities are more close to random decision and therefore suggest that different signals impact on cell fate decision in tail and paw epidermis. These signals could come from differences in the microenvironment or from cell-intrinsic properties. More attention should be paid on paw tissue to better understand the mechanisms regulating this decision. Transcriptional analysis of paw epidermal basal cells at single cell level and comparison of these data with tail IFE cells could be useful to identify the molecular mechanisms responsible for this constraint.

5.2.2 Transcriptional profiling of epidermal progenitors

The rescaled cumulative distribution of our clones traced from P1 to P60 in both scale and interscale fit with a linear trend when displayed in a logarithmic scale, a hallmark of a system where one population of equipotent progenitors are responsible for the maintenance of each epidermis region[101] (Figure 2I,J, page 98). While the presence of a single population of equipotent progenitors has also been described in the scale adult tissue, these results strongly contrast with the SC-CP hierarchy we recently described in the adult interscale[102,103]. In fact, the cumulative distribution of the interscale clones size analysed during homeostasis in the last time point (24 weeks of tracing), clearly show a large proportion of bigger clones which do not fit with the linear trend[103]. These "outliners" appeared exclusively in the *K14-CreER* tracing obtained in the interscale and indicate the presence of clones that were anchored by long lived SC. Such fraction of clone is not observed in our interscale tracing performed during post-natal development. Two hypothesis can explain this discrepancy. One could be that SC and CP are already present and molecularly different at birth but that SC are "hidden" in the clonal analysis because they have a similar dynamics to the CPs and only acquire their slow cycling dynamics later, between P30 and P60. The other hypothesis is that SC and CP status are not fixed from the beginning in the epidermis but rather are specified later from DPs at a transition stage between post-natal development and adult, possibly by the action of the microenvironment. Interestingly, our single cell RNA-seq data seem to favor the second hypothesis. Indeed, these data confirm the higher homogeneity within basal cells during post-natal development compared to adult tissue. Unsupervised clustering performed at 0.5 resolution show two populations of $K14^{high}$ DPs in G0 in the young sample (cluster 0 and 5, Figure 6A, page 106) while tree populations of SC/CPs were identified in adult (clusters 1, 2 and 6, Figure 6B, page 106). These populations, observed in young and adult samples, expressed Stem/progenitors markers already described in epidermis such as the proliferative gene coding for the Cyclin D2 which trigger G1-S transition (*Ccnd2)*, the gene coding for the alpha chain of collagen XVII *(Col17a1),* a key component of hemidesmosomes, or the Secreted Protein Acidic and Cysteine Rich *(Sparc* or *BM-40)* important for extracellular matrix synthesis[202-204] (Figure 6G-I, page 106). Interestingly, the role of *Col17a1* in division orientation and SC maintenance was recently shown in the epidermis[203]. *Col17a1,*

(also called *BPAG2* or *BP180*) codes for a structural component of the hemidesmosomes, is critical for cell adhesion, and mutation in this gene as been found in patient suffering from JEB[7,205]. Conditional KO of *Col17a1* coupled with clonal analysis show a higher proportion of detaching clones in the mouse tail epidermis. Analysis of cell division orientation show that wild type basal cells divide always parallel to the BM while cells depleted for *Col17a1* show an increased proportion of perpendicular (40%) or oblique (20%) cell division, providing an explanation for the rapid clone loss[203]. These data suggest that *Col17a1* is critical to maintain SC and CP within the basal layer and is a good marker for basal cells.

As mentioned, the unsupervised clustering identified two basal populations in the young sample (called DP G0 I and II) (Figure 6A, page 106) and three populations in adult SC/CPs (called SC/CP G0 I, II and III) (Figure 6B, page 106), supporting a higher heterogeneity in adult basal stem/progenitors. Interestingly, 3 populations of basal epidermal cells were also described by Joost and colleagues in the mouse backskin[204]. One of our adult population is characterized by a higher level of expression of *Fst*, *Postn*, *Iftm3* and the Wnt inhibitor *Sostdc1* (SC/CP G0 I) (Figure 6M and Figure S6B, pages 106 and 120). These 4 markers, together with the *Krt79*, have been described to be expressed by the infundibulum cells in adult mouse backskin[204]. While our cluster does not express *Krt79*, it is likely that this population corresponds to basal cells at the junction between HF and IFE. Interestingly, lineage tracing in the mouse backskin suggest that the proliferative status of the IFE cells located within this region could be influenced by the HF cycle[206]. Although this difference in proliferation has not been observed in the tail epidermis, it suggest that cells located at the junction between infundibulum and IFE could be influenced by different external signals compared to IFE cells, and therefore be transcriptionally different. This population is also present in the young sample (DP G0 I) (Figure S6A, page 120). The two remaining populations observed in adult express either high level of *Wnt4*, *Wnt10a, Il1r2* and *Igfbp2/3/7* (SC/CP G0 III) or *Mt1/Mt2*, *Tsc22d1* and *Dcn* (SC/CP G0 II) (Figure 6N-O and Figure S6B, pages 106 and 120). In the young sample, by contrast, only one homogeneous population of cells (DP G0 II) expressing *Mt2, Wnt4, Wnt10a* and *Igfbp2/7* is present while other markers were only weakly expressed (Figure 6A and Figure S6A, pages 106 and 120). Interestingly, a larger

amount of the SC/CP G0 II markers (*Dcn, Mt1, Mt2, Gpha2* and *S100a6*) were highly expressed in the young adult sample (at P30) but still co-expressed SC/CP G0 III markers (*Igfbp2, Igfbp7* and *Wnt4*) (Figure S6H, page 120). To better visualize the difference in the cellular heterogeneity of basal epidermal cells between the 3 time points, basal cells were plotted according to their Area Under the Curve (AUC) values for the markers specific for Adult SC/CP G0 II (x axis) and III (y axis) (Figure S6I-K, page 120). In the young sample, all basal cells showed a linear correlation between the two AUC values (Figure S6I, page 120). By contrast, at P30, some basal cells, start to deviate from the trend (P30, figure S6J, page 120). Interestingly, this deviation is even more strong at P60, in the adult sample (Figure S6K, page 120). Altogether, these data show that basal cells of the tail epidermis are relatively homogeneous during early post-natal development and the cellular heterogeneity begins around P30, at the time of the transition from a growing to a homeostatic mode of division.

Igfbp2 was initially described as an inhibitor of the Igf-induced proliferation, but its role on cell proliferation is conflicting and can be either positive either negative, depending on the context and cell lines[207]. In the skin, Igfbp2 seem to be associated with higher proliferation as it is overexpressed in BCC in *K14-Cre/Patch1$^{f/f}$* transgenic mice and in some human BCC biopsies[208]. Treating *K14-Cre/Patch1$^{f/f}$* skin explants with anti-Igfbp2 decreased K15 and p63 expression suggesting that Igfbp2 is important to promote a progenitor state[208]. Further experiments will be needed to understand the role of Igfbp2 in epidermis and whether it could be a potential SC marker. Interestingly, two studies highlighted the importance of Wnt signaling as an autocrine positive signal for SC maintenance within the IFE and showed that blocking this signaling in epidermal cells lead to a decrease in basal cell proliferation and a premature differentiation[38,45]. Recently, patients harboring a *Wnt10a* mutation have been shown to suffer from dental abnormalities and palmoplantar scaling. Further analysis using mouse lines demonstrated the important role for *Wnt10a* in epithelial appendages formation and IFE maintenance and differentiation[209]. Could the SC/CP population that express these Wnt ligands be the SC while the other would be the CPs on their way for differentiation ? Further experiments would be necessary to answer to this question.

Finally, we used SCENIC analysis to predict active TFs and their putative target genes, or regulon, in our single cell RNA-seq data[131]. This analysis showed an active transcriptional network for known TF such as AP-1 (*Jun, Fos*) and *Trp63* in basal DPs and SC/CPs, consistent with their important role in promoting proliferation and SC maintenance in epidermis[47,48,51-56,58,76] (Figure S6C-E, page 120). SCENIC analysis also showed that differentiated cells expressed TFs and their regulons known to promote epidermis barrier function such as *Klf4* and the Notch effector *Hes1* (Figure S6F,G, page 120)[26-29,31,83]. Other TF and their regulons (data not shown), such as *Klf5*, *Cebpa/Cebpb*, *Gata3*, *Grhl3*, *Pou3f1* and *Pou2f3* were also active in the cells commited to suprabasal layers, consistent with their important role in promoting differentiation in epidermis[69-72,84,86-89,92,93]. Adult SC/CP and young DP populations also express TF such as *Sox4, Nfib/c* or *Mef2a*. A recent study showed that, although specific depletion of *Sox4* in the epidermis does not have a major phenotype on tissue development, double conditional ablation of *Sox4* and *Sox11* leads to premature barrier function acquisition in the epidermis during embryogenesis and delays wound healing in adult, suggesting that these TF together repress differentiation and promote migration[210]. Chip-seq analysis confirmed that *Sox4* and *Sox11* directly regulate the expression of genes implicated in differentiation as well as cell migration and extracellular matrix organization[210]. TF from the Nuclear Factor I family (NFI), such as *Nfib* and *Nfic*, are known to regulate cell proliferation and differentiation during development in osteoblasts and hematopoietic cells, in central nervous system, mammary gland and lung and are also associated with different kind of cancers such as glioblastoma or lung carcinoma[211]. In epidermis, *Nfib* is upregulated in quiescent bulge stem cells[43]. Specific conditional knock out of *Nfib* in bulge stem cells, using *Sox9-CreER* mice, increases cells proliferation in the bulge and promote the expression of the secreted factor endothelin 2, which induce a premature differentiation of melanocytes and accumulation of melanin pigments[212]. Altough *Nfib* cKO does not have any impact on hair pigmentation or formation, these data suggest an important role for *Nfib* in the control of stem cells niche[212]. Its role in IFE is currently unknown. The Myocyte Enhancer factor 2a (*Mef2a)* has been shown to bind and regulate upstream region of the Glucose transporter GLUT4 in adipose tissues, heart and muscles and to be important for the maintenance of mitochondria in cardiomyocytes[213,214]. However, its role in the epidermis is currently unknown.

Further experiments will be needed to assess the specific role of these TF in the IFE (See Perspectives).

SCENIC analysis also highlighted specific TFs and their regulons associated with SC/CP G0 III population such as *Cebpb, Ets1/2, Pparg, Klf10* or *Pou2f3*. Interestingly, *Cebpb* and *Pou2f3* are also expressed by differentiated cells in the interscale and scale clusters, consistent with their role in promoting epidermal differentiation[69,70]. Using siRNA and Chip-seq analysis, *in vitro* studies showed that *Cebpb* and *Pou2f3* inhibit the activity of the enhancer that controls *p63* expression leading to *p63* repression and promoting differentiation in cultured keratinocytes[215]. PPARγ is known to regulate genes implicated in inflammation, lipid homeostasis and differentiation in the skin[216]. In human skin, PPARγ localization is mainly cytoplasmic in basal cells and nuclear in suprabasal cells consistent with its expression correlating with differentiation markers[217,218]. Mice harboring a specific deletion of PPARγ in HF cells, using *K15-Cre* promoter, start to display progressive scratching behavior, hair follicle loss and inflammatory cells infiltration in the dermis after 3 months of age showing a role for PPARγ in skin homeostasis[219]. Moreover, specific deletion of PPARγ in basal cells using *K14-Cre* or *K15-Cre/PPARγ$^{f/f}$* mice lead to an increase in cell proliferation and hyperkeratosis suggesting a role of PPARγ to repress proliferation[219,220]. The upregulation of these three TF and their regulons in SC/CP G0 III may suggest that this population is on its way for differentiation and therefore potentially represent a CP population. On the other hand, *Ets1* expression is, by contrast, associated with basal cell maintenance[77]. Ets1 protein is predominantly expressed in the nuclei of basal cells in mouse and human epidermis[77,221]. Forced expression of *Ets1* in suprabasal cells of adult mice, using *Inv-tTA/TetO-Ets1* transgenic animals, leads to hyperplasia and pronounced invasion of the epidermis and increased angiogenesis in the dermis[77,222]. Histologically, *Inv-tTA/TetO-Ets1* epidermis show ectopic expression of p63 and K14 in suprabasal cells and their co-expression with spinous marker such as K10 as well as reduced expression of cornified envelope markers[77,222]. *Ets1* also control the expression of several MMP genes, more particularly *Mmp13*, consistent with the invasive phenotype[77,222]. These results suggest an important role for *Ets1* in the control of basal cell identity and proliferation, the repression of late differentiation markers

and possibly the remodeling of the BM. It is possible that the co-expression of these TF implicated either in differentiation (*PPARγ, Cebp* and *Pou2f3*) either in basal maintenance (*Ets1*) may confer a specific behavior to these SC/CP GO III group. More experiments will be necessary to determine whether these TF play a role in SC and CP identity in skin epidermis. Finally, lineage trajectory analysis using Slingshot revealed a single lineage from the homogeneous population of DPs to differentiated cells in young sample and 3 lineage trajectories leading to scale and interscale differentiated cells as well as one lineage toward SC/CP III, again higligthing the heterogeneity within the basal cells in adult epidermis[132].

Our clonal analysis combined with the single cell RNA seq all point toward the possibility that a single and homogeneous population of DPs give rise later to a hierarchy of SC and CPs leading to a higher heterogeneity within the basal compartment. Interestingly, this scenario has recently been described for the intestine. While many studies identified Lgr5 as a marker of adult SC residing in the intestinal crypt[127,223,224], it has been shown that SC can arise from any of the equipotent precursors cells that constitute the intestine during embryonic development[225]. These results suggest the possibility that SC are not intrinsically programmed since early stage of embryonic development to act as SC but rather acquire their SC properties along the way. In adult epidermis, our group demonstrated that SCs were localized within the interscale compartment[103]. Could the two adult SC/CP populations (SC/CP G0 II and III) correspond to scale and interscale specific basal cells ? Or do they highlight different cell state ? Interestingly, the fetal intestine initially does not contain any crypt which appear late during embryonic development, just before birth[225,226 146]. Similarly, the tail epidermis is highly uniform at birth and the pattern interscale-scale is not yet present. The progressive acquisition of scale markers around P7 may suggest a change within the skin epidermis after that time point. Could the scale-interscale patterning be responsible for the establishment of a niche during the post-natal development as it is suggested for the crypt within the intestine[225] ? In the past, many attempts were made to understand whether IFE SCs where depending on a specific niche. Some studies showed that skin denervation had an impact on HFSCs and IFE SCs maintenance and argued that signals coming from the nerve could be a niche signal for epidermal

SC[194,227]. Other recent lineage tracing experiments showed that blood vessels branching point where located preferentially under the scale where the cells are fast cycling and therefore suggest that dermal vasculature could influence the proliferative status of the epidermal basal cells[228]. Further experiments will be necessary to validate these hypothesis and identify the signals responsible for the SC specification (See Perspectives).

5.2.3 Cell division orientation and collagen fibers

Our clonal tracing revealed unexpected clone shape in the tail epidermis and clearly show that beside fate decision, cells do not divide randomly in the plane of the tissue but seem to be constrained. Clones were not necessarily elongated toward the length of the tail, as we could expect if a global tension was present in the sense of the growth. Rather our data show strong correlation between clone orientation and collagen fiber orientation *in vivo* (Figure 7C-K, page 122). In addition, our micro-pattern experiments in which collagen fibers are coated aligned in one direction versus non-aligned show that collagen fibers orient cell division (Figure 7L-N, page 122). Another study showed that collagen fibers also dictate directionality and branching in the mammary epithelium, suggesting that this process could be conserved across different tissues[229].

Other factors could potentially explain the anisotropy of the clones. Our data showed that basal cells within the scale proliferate faster than the interscale cells. In drosophila imaginal wing disc, live-imaging and mathematical *in silico* models showed that spatial differences in proliferation rate can lead to anisotropy within the tissue. Clones having a higher proliferation rate influence neighbors clones which then grow anisotropically around them[230]. It is therefore tempting to speculate that scale “fast” dividing cells exert a certain pressure on interscale “low” dividing cells. It is also interesting to notice that on average 30% of the clones observed in the tail are isotropic in both compartments. Could these isotropic clones be “more” proliferative clones and also influence their neighbor clones within the scale compartment ? Further experiments will be necessary to understand the different mechanisms that governs clone anisotropy within the tail epidermis.

6 PERSPECTIVES

6.1 WOUND REPAIR

Cell fate regulation. The switch from a "balanced" to an "expanding" mode of proliferation observed by others on primary epidermal human cells suggest that keratinocytes are intrinsically able to change their cell fate decision *in vitro* [110]. However our clonal analysis show that basal CPs cannot switch to a proliferative/self-renewing mode *in vivo.* One possible parameter controlling this switch is cell confluence [110]. *In vivo*, the only cells that could be out of this confluence are the LE cells. We showed that the quiescence of the LE can be released under dexamethasone treatment. It could be interesting to see, using live imaging and single cell clonal analysis, whether this switch to an "expanding" mode could happen *in vivo* when proliferation is rescued at the leading edge or whether we observe a change on cell fate dynamics when the LE fronts touch each other, at the end of the wound repair. Likewise, it could be interesting to perform clonal analysis on stratified reconstructed skin *in vitro* to see whether the switch from "balanced" to "expanding" occurs or not at the LE of a confluent reconstructed epidermis.

Compartmentalization. The compartmentalization of the skin epidermis upon wound healing is clearly defined locally, which raised further question : What are the molecular mechanisms regulating the temporal and spatial appearance (and resolution) of the LE and the proliferative hub ? To answer to these questions, it would be interesting to sort LE versus Proliferative hub cells on the basis of their Itgα5 expression and perform ATAC-seq to understand the epigenetic modifications associated with these compartments. Focusing on the promoter regions of the LE genes, one could identify the TFs responsible for these upregulation. It has been shown that an inflammatory memory exist within the keratinocytes after tissue damage which enables keratinocytes to be re-activated faster in a second damage[188]. Performing ATAC-seq at the end of the healing process, when the LE gene expression is resolved, would also bring important informations to understand what control the LE signature and whether this kind of memory also exist in LE cells. To validate

candidate TF, GOF and LOF experiments should be performed *in vivo* upon wound and using the expression of the LE genes signatures as a read out. Another important question arising from our wound experiments is the specific role of some new molecules identifies in the LE, such as *Gprc5a* or *Flrt2* and *3*. Are these genes important for the migration, the attachment of the cell over the providential matrix or the quiescence ? GOF and LOF experiments should be performed *in vitro* using scratch wound assay on epidermal cell lines to understand their function and why they are specifically upregulated at the LE.

Role of the inflammation. Our data showed that blocking inflammation using dexamethasone releases LE cells from their quiescence, suggesting that some inflammatory cells may secrete signals or directly block epidermal proliferation. What is the impact of this quiescence in healing ? Which are these inflammatory cells and through which mechanisms they block epidermal proliferation ? The first immune cells recruited on the wound site are neutrophils and monocytes [116]. First, FACS analysis has to be performed on wound skin treated and untreated with dexamethasone in order to identify which cell population is decreased. A recent FACS protocol has been proposed to accurately identify all types of lymphoid immune cells (B cells, T cells, NK cells) and myeloid immune cells (neutrophils, monocytes, macrophages, dendritic cells) based on their expression for specific markers (CD45, Ly6G, CD11c, Cd11b, IA/IE, CD64 and CD24)[231]. An alternative method would be to perform 10X Genomics on all cells isolated form dermis and epidermis at different time point after wound and, based on the expression of these specific markers, identify which population is missing or show a change in their gene expression, in particular the genes regulating proliferation in a paracrine manner, after dexamethasone treatment. Using this strategy, one could assess the change in the proportion of these cell populations after dexamethasone treatment and perform further experiment on mice deficient for this cell population to see whether the quiescence of the LE cells is maintained and whether it improves healing or not. Intraperitoneal injection of Clodronate liposomes [188] or anti-Csfr1 [232] have been shown to successfully deplete macrophages in mice. However the best depletion experiments would be to combine the Cre-inducible Diphteria Toxin Receptor (iDTR) mouse line with lineage specific Cre[233]. *CD4-Cre/iDTR* mice can be used to delete

CD4+ CD8+ T lymphocytes [234], *Foxp3-DTR-eGFP* to deplete specifically Treg [235], *CD19-Cre*[236] or *Mb1-Cre*[237]*/iDTR* to delete B lymphocytes. *MRP8-Cre* could be used to deplete neutrophils and *Cx3cr1-Cre* to deplete macrophages specifically[238]. Although it is well known that depletion of neutrophils and macrophages with the *LysMCre/iDTR* mice show a delay in wound healing when the ablation is performed early after wound, their contribution to the quiescence of the LE were not assessed[187]. It would therefore be interesting to check the effect of these different lineage depletion on the quiescent status of the LE cells using BrdU incorporation.

Role of the ECM. Wound healing is characterized by the local disruption of the ECM and the accumulation of a hemostatic fibrin clots which serve as a provisional matrix for keratinocytes, fibroblasts and inflammatory cells migration[116]. This provisional matrix may have a different stiffness compared to normal ECM. Matrix stiffness have been shown to regulate proliferation status of cells in many tissues by a mechanism called mechanotransduction[239]. This is mediated by the activation and the translocation of the Yes Associated Protein (YAP) and TAZ into the nucleus, two transcriptional co-regulators, which, under increased matrix stiffness or cell spreading, activate cell proliferation[239]. As a consequence, decreased matrix stiffness and cell shape area are known to decrease cell proliferation, due to the inactivation of YAP and TAZ[239]. It is therefore intriguing to know whether the quiescence of the LE is dictated by mechanical signals such as a decreased stiffness. Mice deficient for YAP and TAZ in their epidermis harbor a delay in wound healing, suggesting a role for these mechanotransducers in repair[240]. However, nothing is known about the potential role of YAP and TAZ in the LE. Wound healing should be performed on *K14-CreER/YAP*$^{f/f}$*TAZ*$^{f/f}$ mice, combined with BrdU incorporation to assess whether the ablation of YAP and TAZ have an impact on the quiescence or the molecular profile of the LE cells. In order to know whether the provisional matrix harbor a decreased stiffness compared to normal ECM, Atomic force microscopy (AFM) should be performed on thick section at the LE and in the proliferative hub, at different time point after wound. If this is the case, a better characterization of the composition of the provisional matrix should be performed using mass spectrometry. Artificial ECM harboring a similar composition and/or fiber

orientation could be engineered and used to see whether the LE and proliferative hub could be recapitulated *in vitro* with reconstructed skin epidermis.

Plasticity during wound healing. Using single cell RNA-seq, clonal analysis and ATAC-seq, recent studies, shed lights on the molecular mechanisms regulating plasticity and memory during wound healing[188,196,197]. Ge and colleagues showed that IFE SC have similar and unique regions of accessible chromatin compared to HF SC and highlighted the key role of TF such as Sox9 and Klf5 to regulate HF SC and IFE SC identity respectively[197]. Joost and colleagues showed that Lgr5 bulge cells already change their molecular identity before their migrate out of the HF, and more specifically increase the expression of receptor for wound ECM ligands, suggesting a key role for the microenvironment in this plasticity[196]. By contrast, Lgr6 upper HF cells already expressed receptors for wound ECM ligands, providing a possible explanation for the rapid mobilization of these cells into the IFE upond wound[196]. Naik and colleagues showed that IFE SC have an inflammatory memory and conserve a chromatin configuration after inflammation that enable to react faster during a second inflammation[188]. These discoveries, in parallel with our results showing a similar clonal dynamics of infundibulum and IFE cells upon wound healing, raise a lot of new questions. What are the genes responsible for lineage infidelity of isthmus and upper isthmus SC populations ? Is their an inflammatory memory in the HF bulge and upper isthmus SC populations ? What are the transcriptional transition states followed by Lrig1 derived cells upon wound ? Are they similar to Lgr5 and Lgr6 derived cells[196] ? In order to answer to these questions, ATAC-seq and single cell RNA-seq using 10X Genomics technology[130] should be performed on *Lgr5-CreER*, *Lgr6-CreER* and *Lrig1-CreER* lineage traced cells before and at different time point after wound. By comparing the list of genes upregulated (or downregulated) upon wound at the transcriptional level and the new ATAC peaks acquired during wound, it would be possible to identify candidate genes responsible for the establishment of the natural lineage barrier and understand what is the temporality of the molecules breaking this barrier. The specificity and relevance of these genes in plasticity should then be assessed through LOF and GOF experiments, during homeostasis and repair, by checking the ability of each SC population to migrate out of their niche and invade IFE.

In addition, one could wonder whether the regulation of these genes could be mechanical and influenced by cell shape or ECM rigidity. Key mediators of mechano-transduction are YAP and TAZ, two transcriptional co-regulators, which transduce mechanical signals into biological effects such as cell proliferation or differentiation[239]. While ablation of YAP and TAZ in K5+ basal IFE cells have been shown to delay wound closure in mice, the role of these mechanotransducers in specific SC populations is currently unknown[240]. To test whether mechanotransduction could play a role in the lineage infidelity of specific SC populations, we should use *Lgr6-*, *Lgr5-* or *Lrig1-CreER/Rosa-Confetti/YAP$^{f/f}$ TAZ$^{f/f}$* mice and perform lineage tracing and 10X Genomics at different time point before and after wound. Combining the clonal analysis and the transcriptional profiling of each cell population, we should be able to assess the consequence of the specific deletion of YAP and TAZ on the molecular profile of these cells and on their ability to migrate out of the HF upon wound repair. Similarly, to test whether sensing via actin cytoskeleton is important for lineage infidelity, we could use *Lgr6-*, *Lgr5-* or *Lrig1-CreER/Rosa-Confetti/Rac1$^{fl/fl}$* mice and see the impact of *Rac1* deletion specifically on the transcription profile and the recruitment of these SC population during wound healing.

Finally, uncertainty remains concerning the reversion. Are suprabasal cells able to revert and establish as *bona fide* SC after wound ? The way to answer this question is complex as most of the *CreER* mouse line under the control of a suprabasal promoter (*Gata6, Inv, K10*) also target basal cells. In this case, the use of photo-activatable construct such as the PAmCherry placed under the control of *K10* promoter could be usefull[107,241]. This new mouse line should be crossed with a constitutive fluorescent membrane reporter such as the *K14-GFP-actin* mouse line[242]. Using 2-photon live imaging, it would be possible to activate the PAmCherry with light specifically in a large number of isolated suprabasal cells at different time point after wound and follow their fate overtime.

6.2 POST-NATAL DEVELOPMENT

Niche and SC specification. Our clonal analysis and single cell RNA seq data suggest that an homogeneous population of DPs exist during post-natal development and that the SC/CP populations are therefore specified later on. In addition, recent lineage tracing data obtained in the laboratory on adult tail epidermis suggest that interscale contains SC and CP while scale only contains CPs[103]. Do the two SC/CP populations identified in our single cell RNA seq data corresponds to scale and interscale specific populations ? In order to answer to this question, further immunostaining or in situ hybridization should be performed to see whether these markers have a restricted spatial expression corresponding to scale and interscale regions. If it is not the case, it could also be that these two SC/CP populations represent different cellular states. Using different markers in combination, we should check whether basal cells express markers from different populations at the same time. In order to understand the dynamics of their expression, we could also engineer new knockin mouse lines where different fluorescent reporters, such as the nGFP, RFP and mCFP, are placed under the endogenous promoter of specific genes identified in our SC/CP G0 population I, II and III. Specific markers would be for example the Wnt antagonist *Sostdc1* (SC/CP G0 I), the extracellular matrix protein *Decorin* (Dcn ; SC/CP G0 II) and *Wnt4* (SC/CP G0 III). Each promoter being associated with a specific color, it should be possible, using live imaging to see whether a unique cell expresses these three markers simultaneously or not and potentially identify a temporal pattern of expression for these factors.

The late specification of the SC/CP hierarchy suggest that niche signals may appear during post-natal development. These niche signals can be of different type. A first possible scenario would be a paracrine secretion form the underlying fibroblast, such as the one described for HF placode specification[3], or other cell types such as blood vessels, nerves or resident inflammatory cells, as previously suggested[194,227,228]. In order to identify these signals, single cell RNA sequencing using 10X Genomics technology[130] could be performed on whole skin, including the dermis, in P1, P7, P21 and adult mice. Using unsupervised clustering and public database to identify the different cell types, we should be able to check whether dermal

fibroblasts, endothelial cells, neurons or Langerhans cells express different signaling molecules during post-natal development and adult. Then, using specific database for receptor-ligand combined with the transcriptional profile of IFE cells at each specific time point, it is now possible to screen for the more promising interactions. The most promising interactions should first be validated by immunostaining or in situ hybridization (RNA scope) on skin samples. Then, the receptor-ligand functionality should be confirmed through the use of blocking antibodies or lineage specific GOF/LOF experiments *in vivo* and the relevance of this pathway for SC maintenance should be assessed by clonal analysis and wound experiments.

A second possible signal could be local mechanical signals due to epidermal cell crowding or different ECM stiffness within the dermis. Recent studies highlighted the importance of tissue mechanics on gene expression through chromatin remodeling[17,190]. It would be interesting to measure the stiffness of the dermis within scale and interscale regions by AFM and see whether this is correlated with the proliferative status of the cells. Then, in order to check whether specific markers, such as *Sparc, Tsc22d1, Dcn, Igfbp2, Wnt4,* or *Wnt10a*, are regulated by ECM stiffness or cell crowding, we could create new cell lines using CRISPR/CAS9 technology where the promoter sequence of these markers control a fluorescent reporter. Using *in vitro* micro-patterning with different stiffness or overcrowding and scratch wound assay we should be able to identify whether tissue mechanics can influence the expression of these factors.

Finally, the niche signal could also come from the SC themselves or the CPs. Our data show that one SC/CP express high levels of *Wnt4* and *Wnt10a*. Blocking Wnt secretion in basal IFE cells decrease their proliferation and induce their premature differentiation *in vivo* suggesting that Wnt signaling could be an autocrine niche signal[45,243]. Could the expression of Wnt ligands reflect the SC or CP status of the basal cells ? Are the Wnt ligands all equivalent to maintain SC ? In order to assess the role of a specific Wnt ligand on SC maintenance we could use the induced, fluorescent and genetic Mosaic (ifgMosaic) construct[244]. This construct was specifically designed to insert easily the coding sequence of up to three genes of interest and couple their expression with a fluorescent Histone 2B protein, highlighting the nucleus of modified cells with a specific color (ichrMosaic)[244]. By

inserting Wnt ligand sequence and Wnt ligand sequence harboring a point mutation in the genetic construct, we could generate a ichr-Wnt-Mosaic mouse line. Crossing this mouse line with *K14-CreER* would enable, upon TAM administration, to induce in a mosaic manner H2B-Cherry colored wild type clones, H2B-GFP colored cells with LOF of Wnt ligand and H2B-cerulean colored cells with GOF for the Wnt ligand. Following the proliferation dynamics and clonal persistence overtime of each type of clone, we should be able to see whether this specific Wnt ligand is important for an autocrine SC maintenance. If specific clones display a decrease in proliferation, analysis of the clone shape (isotropic versus anisotropic) should also be made to check whether a correlation exist between proliferation and isotropy. The same approach could be used for the other markers highlighted in this study.

Cell fate decision regulation. In this project we studied cell fate decision upon two processes where skin has to expand : wound repair and post-natal growth. As the results show, while both situations lead to new tissue generation, the mechanisms underlying each type of expansion are different. Another situation where skin has to expand is currently used in esthetic surgery for mammary reconstruction or before skin graft covering burn defect : the forced mediated skin expansion. This technique implies the use of a inflatable prosthesis place subcutaneously and inflated progressively through physiological liquid injection. The inflation of the device under the skin forces the tissue to expand and the surplus can then be used to cover a neighbor area[245]. Is the force-mediated expansion able to induce an imbalance toward self-renewal ? Our recent unpublished data suggest that it does. Using subcutaneous hydrogel placed on the back of *K14-CreER/Rosa-Confetti* mice we saw that basal clones follow the amount of expansion but nevertheless have a stable persistence compared to homeostasis, suggesting that they increased their self-renewal during forced mediated expansion (Unpublished data). Strikingly, oncogenic hit such as the constitutive activation of the Shh pathway also induce an imbalance toward self-renewal in *K14-CreER/Rosa-SmoM2* transgenic mice[103]. These results suggest that several conditions of epidermis expansion lead to an imbalance in favor of self-renewal.

To understand which epigenetic modifications are necessary to induce self-renewal, we should perform ATAC-seq on basal cells coming from *K14-CreER/Rosa-*

SmoM2 GFP+ clones at different time point in the first days following TAM administration and compare with TAM treated control mice. Combining these data with RNA sequencing data will allow to analyse the dynamics taking place during increased self-renewal and decipher the chromatin modifications associated with this phenomenon. Motif discovery analysis will highlight the TF implicated in this process. As our results show that an imbalance for self-renewal also takes place during post-natal development, we should also perform ATAC-seq on P7 young mice and compare the TF which display active regulon and open chromatin in tumor formation and P7 young mice growth and see which are common. TF of interest can then be deleted (alone or in combination) using the ifgMosaic cells[244] construct in oncogenic mouse model. Clonal analysis should be performed to trace the cells *in vivo* and see whether the LOF prevents the self-renewal advantage in the *K14-CreER/Rosa-SmoM2* mutant clones. By contrast, gain of function experiments can be performed on adult homeostatic tail epidermis to see whether the TF can confer an advantage for self-renewal. Similarily, the role of TF associated with adult homeostasis such as *Nfib, Mef2a, PPARγ or Ets1* should be analysed more precisely by specific GOF and LOF to understand their specific role in the adult tissue. By combining *Nfib*$^{f/f}$ [212] or PPARγ$^{f/f}$ [246] mice with *K14-CreER/Rosa-Confetti* mice or by using ifgMosaic construct to engineer new transgenic mice, one could assess whether the loss of these genes, alone or in combination, changes the proliferation dynamics of the adult IFE cells and whether their gain or loss function confer an advantage for self-renewal.

7 CONCLUSION

In this thesis, we analysed two conditions in which the epidermal tissue has to increase in size : the re-epithelialization after wound healing and the tissue expansion during post-natal growth. Using the mouse epidermis as a model, clonal analysis and mathematical modelling, we showed that these two physiological phenomena are achieved through different cellular mechanisms. Our data show that wound healing is achieved through an increase in proliferation and SC reactivation while basal cells retain their homeostatic mode of division and keep balancing self-renewal and differentiation. In addition, while Infundibulum and IFE SCs reside in different regions in the skin, they acquire the same dynamics upon wound healing. By contrast, during post-natal growth, basal cells display a constant imbalance for self-renewal, at the expense of symmetric differentiation, with an ever decreasing proliferation rate, leading to an harmonious growth.

Moreover, we provide new insights in the molecular identity of basal epidermal cells. Transcriptional profile of the epidermis during wound healing highlighted two molecularly distinct and transient compartments : a quiescent LE and a proliferative hub. Our results show that LE cells have a specific transcriptional signature that can be uncoupled from their quiescent state and we uncover new markers not previously described in wound healing. Using single-cell transcriptional analysis we show that postnatal skin epidermis is composed of a homogeneous population of equipotent developmental progenitors (DPs) and that tissue heterogeneity is acquired at the transition between young and adult mouse. Finally, *in vivo* measurement and *in vitro* micro-patterning experiments show that DPs cell division orientation is locally influenced by the collagen fibers alignment in the underlying dermis. These data suggest that the SC specification occurs late during development and that division orientation is influenced by extrinsic factors. Further experiments will be necessary to understand which factors are essential for SC/CP specification, which external and internal factors can promote self-renewal, and through which molecular pathway they are connected. Resolving these key questions would help to find new

targets for treatment of chronic ulcers or severe burns and is an important medical and societal challenge.

8 REFERENCES

1 Hsu, Y. C., Li, L. & Fuchs, E. Emerging interactions between skin stem cells and their niches. *Nature medicine* **20**, 847-856, doi:10.1038/nm.3643 (2014).

2 Driskell, R. R. *et al.* Distinct fibroblast lineages determine dermal architecture in skin development and repair. *Nature* **504**, 277-281, doi:10.1038/nature12783 (2013).

3 Blanpain, C. & Fuchs, E. Epidermal stem cells of the skin. *Annual review of cell and developmental biology* **22**, 339-373, doi:10.1146/annurev.cellbio.22.010305.104357 (2006).

4 Lynch, M. D. & Watt, F. M. Fibroblast heterogeneity: implications for human disease. *The Journal of clinical investigation* **128**, 26-35, doi:10.1172/jci93555 (2018).

5 Driskell, R. R., Jahoda, C. A., Chuong, C. M., Watt, F. M. & Horsley, V. Defining dermal adipose tissue. *Experimental dermatology* **23**, 629-631, doi:10.1111/exd.12450 (2014).

6 Coulombe, P. A., Kerns, M. L. & Fuchs, E. Epidermolysis bullosa simplex: a paradigm for disorders of tissue fragility. *The Journal of clinical investigation* **119**, 1784-1793, doi:10.1172/jci38177 (2009).

7 Tsuruta, D., Hashimoto, T., Hamill, K. J. & Jones, J. C. Hemidesmosomes and focal contact proteins: functions and cross-talk in keratinocytes, bullous diseases and wound healing. *Journal of dermatological science* **62**, 1-7, doi:10.1016/j.jdermsci.2011.01.005 (2011).

8 Garcia, M. A., Nelson, W. J. & Chavez, N. Cell-Cell Junctions Organize Structural and Signaling Networks. *Cold Spring Harbor perspectives in biology* **10**, doi:10.1101/cshperspect.a029181 (2018).

9 Niessen, C. M. Tight junctions/adherens junctions: basic structure and function. *The Journal of investigative dermatology* **127**, 2525-2532, doi:10.1038/sj.jid.5700865 (2007).

10 Goodenough, D. A. & Paul, D. L. Gap junctions. *Cold Spring Harbor perspectives in biology* **1**, a002576, doi:10.1101/cshperspect.a002576 (2009).

11 Koster, M. I. & Roop, D. R. Mechanisms regulating epithelial stratification. *Annual review of cell and developmental biology* **23**, 93-113, doi:10.1146/annurev.cellbio.23.090506.123357 (2007).

12 Roshan, A. & Jones, P. H. Act your age: tuning cell behavior to tissue requirements in interfollicular epidermis. *Seminars in cell & developmental biology* **23**, 884-889, doi:10.1016/j.semcdb.2012.08.013 (2012).

13 Lechler, T. & Fuchs, E. Asymmetric cell divisions promote stratification and differentiation of mammalian skin. *Nature* **437**, 275-280, doi:10.1038/nature03922 (2005).

14 Smart, I. H. Variation in the plane of cell cleavage during the process of stratification in the mouse epidermis. *The British journal of dermatology* **82**, 276-282 (1970).

15 Kulukian, A. & Fuchs, E. Spindle orientation and epidermal morphogenesis. *Philosophical transactions of the Royal Society of London. Series B, Biological sciences* **368**, 20130016, doi:10.1098/rstb.2013.0016 (2013).

16 Williams, S. E., Beronja, S., Pasolli, H. A. & Fuchs, E. Asymmetric cell divisions promote Notch-dependent epidermal differentiation. *Nature* **470**, 353-358, doi:10.1038/nature09793 (2011).

17 Miroshnikova, Y. A. *et al.* Adhesion forces and cortical tension couple cell proliferation and differentiation to drive epidermal stratification. *Nature cell biology* **20**, 69-80, doi:10.1038/s41556-017-0005-z (2018).

18 Muroyama, A. & Lechler, T. Polarity and stratification of the epidermis. *Seminars in cell & developmental biology* **23**, 890-896, doi:10.1016/j.semcdb.2012.08.008 (2012).

19 Rubsam, M. *et al.* Adherens Junctions and Desmosomes Coordinate Mechanics and Signaling to Orchestrate Tissue Morphogenesis and Function: An Evolutionary Perspective. *Cold Spring Harbor perspectives in biology* **10**, doi:10.3390/ijms19051354

10.1101/cshperspect.a029207 (2018).
20 Mesa, K. R. *et al.* Homeostatic Epidermal Stem Cell Self-Renewal Is Driven by Local Differentiation. *Cell stem cell* **23**, 677-686.e674, doi:10.1016/j.stem.2018.09.005 (2018).
21 Artavanis-Tsakonas, S., Rand, M. D. & Lake, R. J. Notch signaling: cell fate control and signal integration in development. *Science (New York, N.Y.)* **284**, 770-776 (1999).
22 Lai, E. C. Notch signaling: control of cell communication and cell fate. *Development (Cambridge, England)* **131**, 965-973, doi:10.1242/dev.01074 (2004).
23 Hori, K., Sen, A. & Artavanis-Tsakonas, S. Notch signaling at a glance. *Journal of cell science* **126**, 2135-2140, doi:10.1242/jcs.127308 (2013).
24 Luo, B., Aster, J. C., Hasserjian, R. P., Kuo, F. & Sklar, J. Isolation and functional analysis of a cDNA for human Jagged2, a gene encoding a ligand for the Notch1 receptor. *Molecular and cellular biology* **17**, 6057-6067 (1997).
25 Powell, B. C., Passmore, E. A., Nesci, A. & Dunn, S. M. The Notch signalling pathway in hair growth. *Mechanisms of development* **78**, 189-192 (1998).
26 Rangarajan, A. *et al.* Notch signaling is a direct determinant of keratinocyte growth arrest and entry into differentiation. *The EMBO journal* **20**, 3427-3436, doi:10.1093/emboj/20.13.3427 (2001).
27 Blanpain, C., Lowry, W. E., Pasolli, H. A. & Fuchs, E. Canonical notch signaling functions as a commitment switch in the epidermal lineage. *Genes & development* **20**, 3022-3035, doi:10.1101/gad.1477606 (2006).
28 Yamamoto, N., Tanigaki, K., Han, H., Hiai, H. & Honjo, T. Notch/RBP-J signaling regulates epidermis/hair fate determination of hair follicular stem cells. *Current biology : CB* **13**, 333-338 (2003).
29 Pan, Y. *et al.* gamma-secretase functions through Notch signaling to maintain skin appendages but is not required for their patterning or initial morphogenesis. *Developmental cell* **7**, 731-743, doi:10.1016/j.devcel.2004.09.014 (2004).
30 Mammucari, C. *et al.* Integration of Notch 1 and calcineurin/NFAT signaling pathways in keratinocyte growth and differentiation control. *Developmental cell* **8**, 665-676, doi:10.1016/j.devcel.2005.02.016 (2005).
31 Moriyama, M. *et al.* Multiple roles of Notch signaling in the regulation of epidermal development. *Developmental cell* **14**, 594-604, doi:10.1016/j.devcel.2008.01.017 (2008).
32 Kretzschmar, K. & Clevers, H. Wnt/beta-catenin signaling in adult mammalian epithelial stem cells. *Dev Biol* **428**, 273-282, doi:10.1016/j.ydbio.2017.05.015 (2017).
33 Hao, H. X. *et al.* ZNRF3 promotes Wnt receptor turnover in an R-spondin-sensitive manner. *Nature* **485**, 195-200, doi:10.1038/nature11019 (2012).
34 Koo, B. K. *et al.* Tumour suppressor RNF43 is a stem-cell E3 ligase that induces endocytosis of Wnt receptors. *Nature* **488**, 665-669, doi:10.1038/nature11308 (2012).
35 Huelsken, J., Vogel, R., Erdmann, B., Cotsarelis, G. & Birchmeier, W. beta-Catenin controls hair follicle morphogenesis and stem cell differentiation in the skin. *Cell* **105**, 533-545 (2001).
36 van Genderen, C. *et al.* Development of several organs that require inductive epithelial-mesenchymal interactions is impaired in LEF-1-deficient mice. *Genes & development* **8**, 2691-2703, doi:10.1101/gad.8.22.2691 (1994).
37 Andl, T., Reddy, S. T., Gaddapara, T. & Millar, S. E. WNT signals are required for the initiation of hair follicle development. *Developmental cell* **2**, 643-653 (2002).

38 Choi, Y. S. *et al.* Distinct functions for Wnt/beta-catenin in hair follicle stem cell proliferation and survival and interfollicular epidermal homeostasis. *Cell stem cell* **13**, 720-733, doi:10.1016/j.stem.2013.10.003 (2013).
39 Lowry, W. E. *et al.* Defining the impact of beta-catenin/Tcf transactivation on epithelial stem cells. *Genes & development* **19**, 1596-1611, doi:10.1101/gad.1324905 (2005).
40 Gat, U., DasGupta, R., Degenstein, L. & Fuchs, E. De Novo hair follicle morphogenesis and hair tumors in mice expressing a truncated beta-catenin in skin. *Cell* **95**, 605-614, doi:10.1016/s0092-8674(00)81631-1 (1998).
41 Zhou, P., Byrne, C., Jacobs, J. & Fuchs, E. Lymphoid enhancer factor 1 directs hair follicle patterning and epithelial cell fate. *Genes & development* **9**, 700-713, doi:10.1101/gad.9.6.700 (1995).
42 DasGupta, R. & Fuchs, E. Multiple roles for activated LEF/TCF transcription complexes during hair follicle development and differentiation. *Development (Cambridge, England)* **126**, 4557-4568 (1999).
43 Tumbar, T. *et al.* Defining the epithelial stem cell niche in skin. *Science (New York, N.Y.)* **303**, 359-363, doi:10.1126/science.1092436 (2004).
44 Jaks, V. *et al.* Lgr5 marks cycling, yet long-lived, hair follicle stem cells. *Nature genetics* **40**, 1291-1299, doi:10.1038/ng.239 (2008).
45 Lim, X. *et al.* Interfollicular epidermal stem cells self-renew via autocrine Wnt signaling. *Science (New York, N.Y.)* **342**, 1226-1230, doi:10.1126/science.1239730 (2013).
46 Dai, X. & Segre, J. A. Transcriptional control of epidermal specification and differentiation. *Current opinion in genetics & development* **14**, 485-491, doi:10.1016/j.gde.2004.07.002 (2004).
47 Mills, A. A. *et al.* p63 is a p53 homologue required for limb and epidermal morphogenesis. *Nature* **398**, 708-713, doi:10.1038/19531 (1999).
48 Yang, A. *et al.* p63 is essential for regenerative proliferation in limb, craniofacial and epithelial development. *Nature* **398**, 714-718, doi:10.1038/19539 (1999).
49 Yang, A. *et al.* p63, a p53 homolog at 3q27-29, encodes multiple products with transactivating, death-inducing, and dominant-negative activities. *Molecular cell* **2**, 305-316 (1998).
50 Rinne, T., Brunner, H. G. & van Bokhoven, H. p63-associated disorders. *Cell cycle (Georgetown, Tex.)* **6**, 262-268, doi:10.4161/cc.6.3.3796 (2007).
51 Senoo, M., Pinto, F., Crum, C. P. & McKeon, F. p63 Is essential for the proliferative potential of stem cells in stratified epithelia. *Cell* **129**, 523-536, doi:10.1016/j.cell.2007.02.045 (2007).
52 Koster, M. I., Kim, S., Mills, A. A., DeMayo, F. J. & Roop, D. R. p63 is the molecular switch for initiation of an epithelial stratification program. *Genes & development* **18**, 126-131, doi:10.1101/gad.1165104 (2004).
53 Romano, R. A., Birkaya, B. & Sinha, S. A functional enhancer of keratin14 is a direct transcriptional target of deltaNp63. *The Journal of investigative dermatology* **127**, 1175-1186, doi:10.1038/sj.jid.5700652 (2007).
54 Romano, R. A., Ortt, K., Birkaya, B., Smalley, K. & Sinha, S. An active role of the DeltaN isoform of p63 in regulating basal keratin genes K5 and K14 and directing epidermal cell fate. *PloS one* **4**, e5623, doi:10.1371/journal.pone.0005623 (2009).
55 Truong, A. B., Kretz, M., Ridky, T. W., Kimmel, R. & Khavari, P. A. p63 regulates proliferation and differentiation of developmentally mature keratinocytes. *Genes & development* **20**, 3185-3197, doi:10.1101/gad.1463206 (2006).
56 Romano, R. A. *et al.* DeltaNp63 knockout mice reveal its indispensable role as a master regulator of epithelial development and differentiation. *Development (Cambridge, England)* **139**, 772-782, doi:10.1242/dev.071191 (2012).

57 Suh, E. K. *et al.* p63 protects the female germ line during meiotic arrest. *Nature* **444**, 624-628, doi:10.1038/nature05337 (2006).
58 Candi, E. *et al.* Differential roles of p63 isoforms in epidermal development: selective genetic complementation in p63 null mice. *Cell death and differentiation* **13**, 1037-1047, doi:10.1038/sj.cdd.4401926 (2006).
59 Tadeu, A. M. & Horsley, V. Notch signaling represses p63 expression in the developing surface ectoderm. *Development (Cambridge, England)* **140**, 3777-3786, doi:10.1242/dev.093948 (2013).
60 Kouwenhoven, E. N. *et al.* Transcription factor p63 bookmarks and regulates dynamic enhancers during epidermal differentiation. *EMBO reports* **16**, 863-878, doi:10.15252/embr.201439941 (2015).
61 Bao, X. *et al.* A novel ATAC-seq approach reveals lineage-specific reinforcement of the open chromatin landscape via cooperation between BAF and p63. *Genome biology* **16**, 284, doi:10.1186/s13059-015-0840-9 (2015).
62 Soares, E. & Zhou, H. Master regulatory role of p63 in epidermal development and disease. **75**, 1179-1190, doi:10.1007/s00018-017-2701-z (2018).
63 Nguyen, B. C. *et al.* Cross-regulation between Notch and p63 in keratinocyte commitment to differentiation. *Genes & development* **20**, 1028-1042 (2006).
64 Nerlov, C. The C/EBP family of transcription factors: a paradigm for interaction between gene expression and proliferation control. *Trends in cell biology* **17**, 318-324, doi:10.1016/j.tcb.2007.07.004 (2007).
65 Oh, H. S. & Smart, R. C. Expression of CCAAT/enhancer binding proteins (C/EBP) is associated with squamous differentiation in epidermis and isolated primary keratinocytes and is altered in skin neoplasms. *The Journal of investigative dermatology* **110**, 939-945, doi:10.1046/j.1523-1747.1998.00199.x (1998).
66 Maytin, E. V. & Habener, J. F. Transcription factors C/EBP alpha, C/EBP beta, and CHOP (Gadd153) expressed during the differentiation program of keratinocytes in vitro and in vivo. *The Journal of investigative dermatology* **110**, 238-246, doi:10.1046/j.1523-1747.1998.00123.x (1998).
67 Loomis, K. D., Zhu, S., Yoon, K., Johnson, P. F. & Smart, R. C. Genetic ablation of CCAAT/enhancer binding protein alpha in epidermis reveals its role in suppression of epithelial tumorigenesis. *Cancer research* **67**, 6768-6776, doi:10.1158/0008-5472.can-07-0139 (2007).
68 Zhu, S. *et al.* C/EBPbeta modulates the early events of keratinocyte differentiation involving growth arrest and keratin 1 and keratin 10 expression. *Molecular and cellular biology* **19**, 7181-7190, doi:10.1128/mcb.19.10.7181 (1999).
69 Lopez, R. G. *et al.* C/EBPalpha and beta couple interfollicular keratinocyte proliferation arrest to commitment and terminal differentiation. *Nature cell biology* **11**, 1181-1190, doi:10.1038/ncb1960 (2009).
70 Andersen, B. *et al.* Functions of the POU domain genes Skn-1a/i and Tst-1/Oct-6/SCIP in epidermal differentiation. *Genes & development* **11**, 1873-1884, doi:10.1101/gad.11.14.1873 (1997).
71 Faus, I., Hsu, H. J. & Fuchs, E. Oct-6: a regulator of keratinocyte gene expression in stratified squamous epithelia. *Molecular and cellular biology* **14**, 3263-3275, doi:10.1128/mcb.14.5.3263 (1994).
72 Sugihara, T. M., Kudryavtseva, E. I., Kumar, V., Horridge, J. J. & Andersen, B. The POU domain factor Skin-1a represses the keratin 14 promoter independent of DNA binding. A possible role for interactions between Skn-1a and CREB-binding protein/p300. *The Journal of biological chemistry* **276**, 33036-33044, doi:10.1074/jbc.M103000200 (2001).
73 Zenz, R. & Wagner, E. F. Jun signalling in the epidermis: From developmental defects to psoriasis and skin tumors. *The international journal of biochemistry & cell biology* **38**, 1043-1049, doi:10.1016/j.biocel.2005.11.011 (2006).

74 Li, G. *et al.* c-Jun is essential for organization of the epidermal leading edge. *Developmental cell* **4**, 865-877 (2003).
75 Zenz, R. *et al.* c-Jun regulates eyelid closure and skin tumor development through EGFR signaling. *Developmental cell* **4**, 879-889 (2003).
76 Zenz, R. *et al.* Psoriasis-like skin disease and arthritis caused by inducible epidermal deletion of Jun proteins. *Nature* **437**, 369-375, doi:10.1038/nature03963 (2005).
77 Nagarajan, P., Romano, R. A. & Sinha, S. Transcriptional control of the differentiation program of interfollicular epidermal keratinocytes. *Critical reviews in eukaryotic gene expression* **18**, 57-79 (2008).
78 Leask, A., Rosenberg, M., Vassar, R. & Fuchs, E. Regulation of a human epidermal keratin gene: sequences and nuclear factors involved in keratinocyte-specific transcription. *Genes & development* **4**, 1985-1998, doi:10.1101/gad.4.11.1985 (1990).
79 Leask, A., Byrne, C. & Fuchs, E. Transcription factor AP2 and its role in epidermal-specific gene expression. *Proceedings of the National Academy of Sciences of the United States of America* **88**, 7948-7952, doi:10.1073/pnas.88.18.7948 (1991).
80 Maytin, E. V. *et al.* Keratin 10 gene expression during differentiation of mouse epidermis requires transcription factors C/EBP and AP-2. *Dev Biol* **216**, 164-181, doi:10.1006/dbio.1999.9460 (1999).
81 Wang, X. *et al.* AP-2alpha: a regulator of EGF receptor signaling and proliferation in skin epidermis. *The Journal of cell biology* **172**, 409-421, doi:10.1083/jcb.200510002 (2006).
82 Wang, X., Pasolli, H. A., Williams, T. & Fuchs, E. AP-2 factors act in concert with Notch to orchestrate terminal differentiation in skin epidermis. *The Journal of cell biology* **183**, 37-48, doi:10.1083/jcb.200804030 (2008).
83 Segre, J. A., Bauer, C. & Fuchs, E. Klf4 is a transcription factor required for establishing the barrier function of the skin. *Nature genetics* **22**, 356-360, doi:10.1038/11926 (1999).
84 Sur, I., Unden, A. B. & Toftgard, R. Human Kruppel-like factor5/KLF5: synergy with NF-kappaB/Rel factors and expression in human skin and hair follicles. *European journal of cell biology* **81**, 323-334, doi:10.1078/0171-9335-00257 (2002).
85 Ohnishi, S. *et al.* Developmental expression of the mouse gene coding for the Kruppel-like transcription factor KLF5. *Developmental dynamics : an official publication of the American Association of Anatomists* **217**, 421-429, doi:10.1002/(sici)1097-0177(200004)217:4<421::aid-dvdy9>3.0.co;2-1 (2000).
86 Sur, I., Rozell, B., Jaks, V., Bergstrom, A. & Toftgard, R. Epidermal and craniofacial defects in mice overexpressing Klf5 in the basal layer of the epidermis. *Journal of cell science* **119**, 3593-3601, doi:10.1242/jcs.03070 (2006).
87 Kaufman, C. K. *et al.* GATA-3: an unexpected regulator of cell lineage determination in skin. *Genes & development* **17**, 2108-2122, doi:10.1101/gad.1115203 (2003).
88 de Guzman Strong, C. *et al.* Lipid defect underlies selective skin barrier impairment of an epidermal-specific deletion of Gata-3. *The Journal of cell biology* **175**, 661-670, doi:10.1083/jcb.200605057 (2006).
89 Kurek, D., Garinis, G. A., van Doorninck, J. H., van der Wees, J. & Grosveld, F. G. Transcriptome and phenotypic analysis reveals Gata3-dependent signalling pathways in murine hair follicles. *Development (Cambridge, England)* **134**, 261-272, doi:10.1242/dev.02721 (2007).
90 Auden, A. *et al.* Spatial and temporal expression of the Grainyhead-like transcription factor family during murine development. *Gene expression patterns : GEP* **6**, 964-970, doi:10.1016/j.modgep.2006.03.011 (2006).
91 Kudryavtseva, E. I. *et al.* Identification and characterization of Grainyhead-like epithelial transactivator (GET-1), a novel mammalian Grainyhead-like factor. *Developmental dynamics : an official publication of the American Association of Anatomists* **226**, 604-617, doi:10.1002/dvdy.10255 (2003).

92 Ting, S. B. *et al.* A homolog of Drosophila grainy head is essential for epidermal integrity in mice. *Science (New York, N.Y.)* **308**, 411-413, doi:10.1126/science.1107511 (2005).
93 Yu, Z. *et al.* The Grainyhead-like epithelial transactivator Get-1/Grhl3 regulates epidermal terminal differentiation and interacts functionally with LMO4. *Dev Biol* **299**, 122-136, doi:10.1016/j.ydbio.2006.07.015 (2006).
94 Potten, C. S. The epidermal proliferative unit: the possible role of the central basal cell. *Cell and tissue kinetics* **7**, 77-88 (1974).
95 Potten, C. S. Cell replacement in epidermis (keratopoiesis) via discrete units of proliferation. *International review of cytology* **69**, 271-318 (1981).
96 Mackenzie, I. C. Relationship between mitosis and the ordered structure of the stratum corneum in mouse epidermis. *Nature* **226**, 653-655 (1970).
97 Potten, C. S. Epidermal cell production rates. *The Journal of investigative dermatology* **65**, 488-500 (1975).
98 Ghazizadeh, S. & Taichman, L. B. Multiple classes of stem cells in cutaneous epithelium: a lineage analysis of adult mouse skin. *The EMBO journal* **20**, 1215-1222, doi:10.1093/emboj/20.6.1215 (2001).
99 Ro, S. & Rannala, B. A stop-EGFP transgenic mouse to detect clonal cell lineages generated by mutation. *EMBO reports* **5**, 914-920, doi:10.1038/sj.embor.7400218 (2004).
100 Clayton, E. *et al.* A single type of progenitor cell maintains normal epidermis. *Nature* **446**, 185-189, doi:10.1038/nature05574 (2007).
101 Klein, A. M. & Simons, B. D. Universal patterns of stem cell fate in cycling adult tissues. *Development (Cambridge, England)* **138**, 3103-3111, doi:10.1242/dev.060103 (2011).
102 Mascre, G. *et al.* Distinct contribution of stem and progenitor cells to epidermal maintenance. *Nature* **489**, 257-262, doi:10.1038/nature11393 (2012).
103 Sanchez-Danes, A. *et al.* Defining the clonal dynamics leading to mouse skin tumour initiation. *Nature* **536**, 298-303, doi:10.1038/nature19069 (2016).
104 Didierjean, L., Wrench, R. & Saurat, J. H. Expression of cytoplasmic antigens linked to orthokeratosis during the development of parakeratosis in newborn mouse tail epidermis. *Differentiation; research in biological diversity* **23**, 250-255 (1983).
105 Gomez, C. *et al.* The interfollicular epidermis of adult mouse tail comprises two distinct cell lineages that are differentially regulated by Wnt, Edaradd, and Lrig1. *Stem cell reports* **1**, 19-27, doi:10.1016/j.stemcr.2013.04.001 (2013).
106 Spearman, R. I. & Garretts, M. The effects of subcutaneous saline injections on growth and keratinization of mouse tail epidermis. *The Journal of investigative dermatology* **46**, 245-250 (1966).
107 Rompolas, P. *et al.* Spatiotemporal coordination of stem cell commitment during epidermal homeostasis. *Science (New York, N.Y.)* **352**, 1471-1474, doi:10.1126/science.aaf7012 (2016).
108 Doupe, D. P., Klein, A. M., Simons, B. D. & Jones, P. H. The ordered architecture of murine ear epidermis is maintained by progenitor cells with random fate. *Developmental cell* **18**, 317-323, doi:10.1016/j.devcel.2009.12.016 (2010).
109 Doupe, D. P. *et al.* A single progenitor population switches behavior to maintain and repair esophageal epithelium. *Science (New York, N.Y.)* **337**, 1091-1093, doi:10.1126/science.1218835 (2012).
110 Roshan, A. *et al.* Human keratinocytes have two interconvertible modes of proliferation. *Nature cell biology* **18**, 145-156, doi:10.1038/ncb3282 (2016).
111 Lin, S., Li, C., Li, C. & Zhang, X. Growth Hormone Receptor Mutations Related to Individual Dwarfism. *International journal of molecular sciences* **19**, doi:10.3390/ijms19051433 (2018).

112 Edmondson, S. R., Thumiger, S. P., Werther, G. A. & Wraight, C. J. Epidermal homeostasis: the role of the growth hormone and insulin-like growth factor systems. *Endocrine reviews* **24**, 737-764, doi:10.1210/er.2002-0021 (2003).
113 Zhou, Y. *et al.* A mammalian model for Laron syndrome produced by targeted disruption of the mouse growth hormone receptor/binding protein gene (the Laron mouse). *Proceedings of the National Academy of Sciences of the United States of America* **94**, 13215-13220, doi:10.1073/pnas.94.24.13215 (1997).
114 Lupu, F., Terwilliger, J. D., Lee, K., Segre, G. V. & Efstratiadis, A. Roles of growth hormone and insulin-like growth factor 1 in mouse postnatal growth. *Dev Biol* **229**, 141-162, doi:10.1006/dbio.2000.9975 (2001).
115 DiGiovanni, J. *et al.* Constitutive expression of insulin-like growth factor-1 in epidermal basal cells of transgenic mice leads to spontaneous tumor promotion. *Cancer research* **60**, 1561-1570 (2000).
116 Sun, B. K., Siprashvili, Z. & Khavari, P. A. Advances in skin grafting and treatment of cutaneous wounds. *Science (New York, N.Y.)* **346**, 941-945, doi:10.1126/science.1253836 (2014).
117 Fuchs, E. Epithelial Skin Biology: Three Decades of Developmental Biology, a Hundred Questions Answered and a Thousand New Ones to Address. *The Journal of cell biology* **116**, 357-374, doi:10.1083/jcb.201708099

10.1016/bs.ctdb.2015.11.033 (2016).
118 Gurtner, G. C., Werner, S., Barrandon, Y. & Longaker, M. T. Wound repair and regeneration. *Nature* **453**, 314-321, doi:10.1038/nature07039 (2008).
119 Ito, M. *et al.* Stem cells in the hair follicle bulge contribute to wound repair but not to homeostasis of the epidermis. *Nature medicine* **11**, 1351-1354, doi:10.1038/nm1328 (2005).
120 Jensen, K. B. *et al.* Lrig1 expression defines a distinct multipotent stem cell population in mammalian epidermis. *Cell stem cell* **4**, 427-439, doi:10.1016/j.stem.2009.04.014 (2009).
121 Levy, V., Lindon, C., Harfe, B. D. & Morgan, B. A. Distinct stem cell populations regenerate the follicle and interfollicular epidermis. *Developmental cell* **9**, 855-861, doi:10.1016/j.devcel.2005.11.003 (2005).
122 Levy, V., Lindon, C., Zheng, Y., Harfe, B. D. & Morgan, B. A. Epidermal stem cells arise from the hair follicle after wounding. *FASEB journal : official publication of the Federation of American Societies for Experimental Biology* **21**, 1358-1366, doi:10.1096/fj.06-6926com (2007).
123 Snippert, H. J. *et al.* Lgr6 marks stem cells in the hair follicle that generate all cell lineages of the skin. *Science (New York, N.Y.)* **327**, 1385-1389, doi:10.1126/science.1184733 (2010).
124 Vasioukhin, V., Degenstein, L., Wise, B. & Fuchs, E. The magical touch: genome targeting in epidermal stem cells induced by tamoxifen application to mouse skin. *Proceedings of the National Academy of Sciences of the United States of America* **96**, 8551-8556 (1999).
125 Page, M. E., Lombard, P., Ng, F., Gottgens, B. & Jensen, K. B. The epidermis comprises autonomous compartments maintained by distinct stem cell populations. *Cell stem cell* **13**, 471-482, doi:10.1016/j.stem.2013.07.010 (2013).
126 Livet, J. *et al.* Transgenic strategies for combinatorial expression of fluorescent proteins in the nervous system. *Nature* **450**, 56-62, doi:10.1038/nature06293 (2007).
127 Snippert, H. J. *et al.* Intestinal crypt homeostasis results from neutral competition between symmetrically dividing Lgr5 stem cells. *Cell* **143**, 134-144, doi:10.1016/j.cell.2010.09.016 (2010).
128 Lapouge, G. *et al.* Identifying the cellular origin of squamous skin tumors. *Proceedings of the National Academy of Sciences of the United States of America* **108**, 7431-7436, doi:10.1073/pnas.1012720108 (2011).

129 Srinivas, S. *et al.* Cre reporter strains produced by targeted insertion of EYFP and ECFP into the ROSA26 locus. *BMC developmental biology* **1**, 4 (2001).
130 Zheng, G. X. *et al.* Massively parallel digital transcriptional profiling of single cells. *Nature communications* **8**, 14049, doi:10.1038/ncomms14049 (2017).
131 Aibar, S. *et al.* SCENIC: single-cell regulatory network inference and clustering. *Nature methods* **14**, 1083-1086, doi:10.1038/nmeth.4463 (2017).
132 Street, K. *et al.* Slingshot: cell lineage and pseudotime inference for single-cell transcriptomics. *BMC genomics* **19**, 477, doi:10.1186/s12864-018-4772-0 (2018).
133 Bereiter-Hahn, J. *Biology of the Integument*. Springler-Verlag, edn, Vol. Vol. 2 443-471 (1986).
134 Stenn, K. S., DePalma, L. *Re-epithelialization*. Plenum Press, New York edn, 321-335 (1988).
135 Coulombe, P. A. Wound epithelialization: accelerating the pace of discovery. *The Journal of investigative dermatology* **121**, 219-230, doi:10.1046/j.1523-1747.2003.12387.x (2003).
136 Park, S. *et al.* Tissue-scale coordination of cellular behaviour promotes epidermal wound repair in live mice. *Nature cell biology* **19**, 155-163, doi:10.1038/ncb3472 (2017).
137 Vignjevic, D. *et al.* Role of fascin in filopodial protrusion. *The Journal of cell biology* **174**, 863-875, doi:10.1083/jcb.200603013 (2006).
138 Wong, P. & Coulombe, P. A. Loss of keratin 6 (K6) proteins reveals a function for intermediate filaments during wound repair. *The Journal of cell biology* **163**, 327-337, doi:10.1083/jcb.200305032 (2003).
139 Plowman, G. D. *et al.* The amphiregulin gene encodes a novel epidermal growth factor-related protein with tumor-inhibitory activity. *Molecular and cellular biology* **10**, 1969-1981, doi:10.1128/mcb.10.5.1969 (1990).
140 Cook, P. W. *et al.* Transgenic expression of the human amphiregulin gene induces a psoriasis-like phenotype. *The Journal of clinical investigation* **100**, 2286-2294, doi:10.1038/s41467-019-11880-9

10.1172/jci119766 (1997).
141 Huang, R. P., Ozawa, M., Kadomatsu, K. & Muramatsu, T. Embigin, a member of the immunoglobulin superfamily expressed in embryonic cells, enhances cell-substratum adhesion. *Dev Biol* **155**, 307-314, doi:10.1006/dbio.1993.1030 (1993).
142 Kolumam, G. *et al.* IL-22R Ligands IL-20, IL-22, and IL-24 Promote Wound Healing in Diabetic db/db Mice. *PloS one* **12**, e0170639, doi:10.1371/journal.pone.0170639 (2017).
143 Iotzova-Weiss, G. *et al.* S100A8/A9 stimulates keratinocyte proliferation in the development of squamous cell carcinoma of the skin via the receptor for advanced glycation-end products. *PloS one* **10**, e0120971, doi:10.1371/journal.pone.0120971 (2015).
144 Larjava, H., Salo, T., Haapasalmi, K., Kramer, R. H. & Heino, J. Expression of integrins and basement membrane components by wound keratinocytes. *The Journal of clinical investigation* **92**, 1425-1435, doi:10.1172/jci116719 (1993).
145 Hertle, M. D., Kubler, M. D., Leigh, I. M. & Watt, F. M. Aberrant integrin expression during epidermal wound healing and in psoriatic epidermis. *The Journal of clinical investigation* **89**, 1892-1901, doi:10.1172/jci115794 (1992).
146 Heller, E., Kumar, K. V., Grill, S. W. & Fuchs, E. Forces generated by cell intercalation tow epidermal sheets in mammalian tissue morphogenesis. *Developmental cell* **28**, 617-632, doi:10.1016/j.devcel.2014.02.011 (2014).
147 Nunan, R. *et al.* Ephrin-Bs Drive Junctional Downregulation and Actin Stress Fiber Disassembly to Enable Wound Re-epithelialization. *Cell reports* **13**, 1380-1395, doi:10.1016/j.celrep.2015.09.085 (2015).

148 Stevens, L. J. & Page-McCaw, A. A secreted MMP is required for reepithelialization during wound healing. *Molecular biology of the cell* **23**, 1068-1079, doi:10.1091/mbc.E11-09-0745 (2012).
149 Hattori, N. *et al.* MMP-13 plays a role in keratinocyte migration, angiogenesis, and contraction in mouse skin wound healing. *The American journal of pathology* **175**, 533-546, doi:10.2353/ajpath.2009.081080 (2009).
150 Hartenstein, B. *et al.* Epidermal development and wound healing in matrix metalloproteinase 13-deficient mice. *The Journal of investigative dermatology* **126**, 486-496, doi:10.1038/sj.jid.5700084 (2006).
151 Madlener, M., Parks, W. C. & Werner, S. Matrix metalloproteinases (MMPs) and their physiological inhibitors (TIMPs) are differentially expressed during excisional skin wound repair. *Experimental cell research* **242**, 201-210, doi:10.1006/excr.1998.4049 (1998).
152 Okada, A. *et al.* Expression of matrix metalloproteinases during rat skin wound healing: evidence that membrane type-1 matrix metalloproteinase is a stromal activator of pro-gelatinase A. *The Journal of cell biology* **137**, 67-77 (1997).
153 Avniel, S. *et al.* Involvement of the CXCL12/CXCR4 pathway in the recovery of skin following burns. *The Journal of investigative dermatology* **126**, 468-476, doi:10.3390/ijms19103217

10.1038/sj.jid.5700069 (2006).
154 Ridiandries, A., Tan, J. T. M. & Bursill, C. A. The Role of Chemokines in Wound Healing. *International journal of molecular sciences* **19**, doi:10.3390/ijms19103217 (2018).
155 Toksoy, A., Muller, V., Gillitzer, R. & Goebeler, M. Biphasic expression of stromal cell-derived factor-1 during human wound healing. *The British journal of dermatology* **157**, 1148-1154, doi:10.1111/j.1365-2133.2007.08240.x (2007).
156 Lund, I. K. *et al.* Concomitant lack of MMP9 and uPA disturbs physiological tissue remodeling. *Dev Biol* **358**, 56-67, doi:10.1016/j.ydbio.2011.07.021 (2011).
157 Xue, M., Campbell, D., Sambrook, P. N., Fukudome, K. & Jackson, C. J. Endothelial protein C receptor and protease-activated receptor-1 mediate induction of a wound-healing phenotype in human keratinocytes by activated protein C. *The Journal of investigative dermatology* **125**, 1279-1285, doi:10.1111/j.0022-202X.2005.23952.x (2005).
158 Jackson, C. J. *et al.* Activated protein C prevents inflammation yet stimulates angiogenesis to promote cutaneous wound healing. *Wound repair and regeneration : official publication of the Wound Healing Society [and] the European Tissue Repair Society* **13**, 284-294, doi:10.1111/j.1067-1927.2005.00130311.x (2005).
159 Rivas, M. V. *et al.* Identification of aberrantly regulated genes in diseased skin using the cDNA differential display technique. *The Journal of investigative dermatology* **108**, 188-194, doi:10.1111/1523-1747.ep12334217 (1997).
160 Chanson, M., Watanabe, M., O'Shaughnessy, E. M., Zoso, A. & Martin, P. E. Connexin Communication Compartments and Wound Repair in Epithelial Tissue. *International journal of molecular sciences* **19**, doi:10.3390/ijms19051354 (2018).
161 Djalilian, A. R. *et al.* Connexin 26 regulates epidermal barrier and wound remodeling and promotes psoriasiform response. *The Journal of clinical investigation* **116**, 1243-1253, doi:10.1172/jci27186 (2006).
162 Yamagishi, S. *et al.* FLRT2 and FLRT3 act as repulsive guidance cues for Unc5-positive neurons. *The EMBO journal* **30**, 2920-2933, doi:10.1038/ncomms11184

10.1038/emboj.2011.189 (2011).
163 Lee, J. H. *et al.* ELK3 promotes the migration and invasion of liver cancer stem cells by targeting HIF-1alpha. *Oncology reports* **37**, 813-822, doi:10.3892/or.2016.5293 (2017).

164 Kong, S. Y. *et al.* The ELK3-GATA3 axis orchestrates invasion and metastasis of breast cancer cells in vitro and in vivo. *Oncotarget* **7**, 65137-65146, doi:10.18632/oncotarget.11427 (2016).
165 Shi, Z. *et al.* Silencing of HMGA2 promotes apoptosis and inhibits migration and invasion of prostate cancer cells. *Journal of biosciences* **41**, 229-236 (2016).
166 Endo-Munoz, L. *et al.* E2F7 can regulate proliferation, differentiation, and apoptotic responses in human keratinocytes: implications for cutaneous squamous cell carcinoma formation. *Cancer research* **69**, 1800-1808, doi:10.1158/0008-5472.can-08-2725 (2009).
167 Thurlings, I. *et al.* Synergistic functions of E2F7 and E2F8 are critical to suppress stress-induced skin cancer. *Oncogene* **36**, 829-839, doi:10.1038/onc.2016.251 (2017).
168 Munz, B. *et al.* Overexpression of activin A in the skin of transgenic mice reveals new activities of activin in epidermal morphogenesis, dermal fibrosis and wound repair. *European journal of immunology* **18**, 5205-5215, doi:10.1002/eji.201747395

10.1093/emboj/18.19.5205 (1999).
169 Wankell, M. *et al.* Impaired wound healing in transgenic mice overexpressing the activin antagonist follistatin in the epidermis. *The EMBO journal* **20**, 5361-5372, doi:10.1093/emboj/20.19.5361 (2001).
170 Bamberger, C. *et al.* Activin controls skin morphogenesis and wound repair predominantly via stromal cells and in a concentration-dependent manner via keratinocytes. *The American journal of pathology* **167**, 733-747, doi:10.1016/s0002-9440(10)62047-0 (2005).
171 Antsiferova, M. *et al.* Keratinocyte-derived follistatin regulates epidermal homeostasis and wound repair. *Laboratory investigation; a journal of technical methods and pathology* **89**, 131-141, doi:10.1038/labinvest.2008.120 (2009).
172 Hubner, G., Hu, Q., Smola, H. & Werner, S. Strong induction of activin expression after injury suggests an important role of activin in wound repair. *Dev Biol* **173**, 490-498, doi:10.1006/dbio.1996.0042 (1996).
173 Draper, B. K., Komurasaki, T., Davidson, M. K. & Nanney, L. B. Topical epiregulin enhances repair of murine excisional wounds. *Wound repair and regeneration : official publication of the Wound Healing Society [and] the European Tissue Repair Society* **11**, 188-197 (2003).
174 Antoine, M. *et al.* Fibroblast growth factor 16 and 18 are expressed in human cardiovascular tissues and induce on endothelial cells migration but not proliferation. *Biochemical and biophysical research communications* **346**, 224-233, doi:10.1016/j.bbrc.2006.05.105 (2006).
175 Song, N. *et al.* FGF18 Enhances Migration and the Epithelial-Mesenchymal Transition in Breast Cancer by Regulating Akt/GSK3beta/Beta-Catenin Signaling. *Cellular physiology and biochemistry : international journal of experimental cellular physiology, biochemistry, and pharmacology* **49**, 1019-1032, doi:10.1159/000493286 (2018).
176 Luetteke, N. C. *et al.* TGF alpha deficiency results in hair follicle and eye abnormalities in targeted and waved-1 mice. *Cell* **73**, 263-278 (1993).
177 Pourreyron, C. *et al.* Wnt5a is strongly expressed at the leading edge in non-melanoma skin cancer, forming active gradients, while canonical Wnt signalling is repressed. *PloS one* **7**, e31827, doi:10.1371/journal.pone.0031827 (2012).
178 Tao, Q. *et al.* Identification of the retinoic acid-inducible Gprc5a as a new lung tumor suppressor gene. *Journal of the National Cancer Institute* **99**, 1668-1682, doi:10.1093/jnci/djm208 (2007).
179 Zhong, S. *et al.* Lung Tumor Suppressor GPRC5A Binds EGFR and Restrains Its Effector Signaling. *Cancer research* **75**, 1801-1814, doi:10.1158/0008-5472.can-14-2005 (2015).

180 Chen, Y. *et al.* Gprc5a deletion enhances the transformed phenotype in normal and malignant lung epithelial cells by eliciting persistent Stat3 signaling induced by autocrine leukemia inhibitory factor. *Cancer research* **70**, 8917-8926, doi:10.1158/0008-5472.can-10-0518 (2010).
181 Bulanova, D. R. *et al.* Orphan G protein-coupled receptor GPRC5A modulates integrin beta1-mediated epithelial cell adhesion. *BioMed research international* **11**, 434-446, doi:10.1080/19336918.2016.1245264 (2017).
182 Arwert, E. N., Hoste, E. & Watt, F. M. Epithelial stem cells, wound healing and cancer. *Nature reviews. Cancer* **12**, 170-180, doi:10.1038/nrc3217 (2012).
183 Sanchis, A., Alba, L., Latorre, V., Sevilla, L. M. & Perez, P. Keratinocyte-targeted overexpression of the glucocorticoid receptor delays cutaneous wound healing. *PloS one* **7**, e29701, doi:10.1371/journal.pone.0029701 (2012).
184 Safferling, K. *et al.* Wound healing revised: a novel reepithelialization mechanism revealed by in vitro and in silico models. *The Journal of cell biology* **203**, 691-709, doi:10.1083/jcb.201212020 (2013).
185 Macleod, A. S. & Havran, W. L. Functions of skin-resident gammadelta T cells. *Cellular and molecular life sciences : CMLS* **68**, 2399-2408, doi:10.1007/s00018-011-0702-x (2011).
186 Jameson, J. *et al.* A role for skin gammadelta T cells in wound repair. *Science (New York, N.Y.)* **296**, 747-749, doi:10.1126/science.1069639 (2002).
187 Lucas, T. *et al.* Differential roles of macrophages in diverse phases of skin repair. *Journal of immunology (Baltimore, Md. : 1950)* **184**, 3964-3977, doi:10.4049/jimmunol.0903356 (2010).
188 Naik, S. *et al.* Inflammatory memory sensitizes skin epithelial stem cells to tissue damage. *Nature* **550**, 475-480, doi:10.1038/nature24271 (2017).
189 Gay, D. *et al.* Fgf9 from dermal gammadelta T cells induces hair follicle neogenesis after wounding. *Nature medicine* **19**, 916-923, doi:10.1038/nm.3181 (2013).
190 Wickstrom, S. A. & Niessen, C. M. Cell adhesion and mechanics as drivers of tissue organization and differentiation: local cues for large scale organization. *Current opinion in cell biology* **54**, 89-97, doi:10.1016/j.ceb.2018.05.003 (2018).
191 Donati, G., Rognoni, E., Hiratsuka, T., Liakath-Ali, K. & Hoste, E. Wounding induces dedifferentiation of epidermal Gata6(+) cells and acquisition of stem cell properties. *Nature cell biology* **19**, 603-613, doi:10.1038/ncb3532 (2017).
192 Connelly, J. T. *et al.* Actin and serum response factor transduce physical cues from the microenvironment to regulate epidermal stem cell fate decisions. *Nature cell biology* **12**, 711-718, doi:10.1038/ncb2074 (2010).
193 McMullan, R. *et al.* Keratinocyte differentiation is regulated by the Rho and ROCK signaling pathway. *Current biology : CB* **13**, 2185-2189, doi:10.1016/j.cub.2003.11.050 (2003).
194 Brownell, I., Guevara, E., Bai, C. B., Loomis, C. A. & Joyner, A. L. Nerve-derived sonic hedgehog defines a niche for hair follicle stem cells capable of becoming epidermal stem cells. *Cell stem cell* **8**, 552-565, doi:10.1016/j.stem.2011.02.021 (2011).
195 Fullgrabe, A. *et al.* Dynamics of Lgr6(+) Progenitor Cells in the Hair Follicle, Sebaceous Gland, and Interfollicular Epidermis. *Stem cell reports* **5**, 843-855, doi:10.1016/j.stemcr.2015.09.013 (2015).
196 Joost, S. *et al.* Single-Cell Transcriptomics of Traced Epidermal and Hair Follicle Stem Cells Reveals Rapid Adaptations during Wound Healing. *Cell reports* **25**, 585-597.e587, doi:10.1016/j.celrep.2018.09.059 (2018).
197 Ge, Y. *et al.* Stem Cell Lineage Infidelity Drives Wound Repair and Cancer. *Cell* **169**, 636-650.e614, doi:10.1016/j.cell.2017.03.042 (2017).
198 Martincorena, I. *et al.* Tumor evolution. High burden and pervasive positive selection of somatic mutations in normal human skin. *Science (New York, N.Y.)* **348**, 880-886, doi:10.1126/science.aau3879

10.1126/science.aaa6806 (2015).
199 Martincorena, I. *et al.* Somatic mutant clones colonize the human esophagus with age. *Science (New York, N.Y.)* **362**, 911-917, doi:10.1126/science.aau3879 (2018).
200 Hirsch, T. *et al.* Regeneration of the entire human epidermis using transgenic stem cells. *Nature* **551**, 327-332, doi:10.1038/nature24487 (2017).
201 Itzkovitz, S., Blat, I. C., Jacks, T., Clevers, H. & van Oudenaarden, A. Optimality in the development of intestinal crypts. *Cell* **148**, 608-619, doi:10.1016/j.cell.2011.12.025 (2012).
202 Hunzelmann, N., Hafner, M., Anders, S., Krieg, T. & Nischt, R. BM-40 (osteonectin, SPARC) is expressed both in the epidermal and in the dermal compartment of adult human skin. *The Journal of investigative dermatology* **110**, 122-126, doi:10.1046/j.1523-1747.1998.00094.x (1998).
203 Liu, N. *et al.* Stem cell competition orchestrates skin homeostasis and ageing. *Nature* **568**, 344-350, doi:10.1038/s41586-019-1085-7 (2019).
204 Joost, S. *et al.* Single-Cell Transcriptomics Reveals that Differentiation and Spatial Signatures Shape Epidermal and Hair Follicle Heterogeneity. *Cell systems* **3**, 221-237.e229, doi:10.1016/j.cels.2016.08.010 (2016).
205 McGrath, J. A. *et al.* Mutations in the 180-kD bullous pemphigoid antigen (BPAG2), a hemidesmosomal transmembrane collagen (COL17A1), in generalized atrophic benign epidermolysis bullosa. *Nature genetics* **11**, 83-86, doi:10.1038/ng0995-83 (1995).
206 Roy, E. *et al.* Bimodal behaviour of interfollicular epidermal progenitors regulated by hair follicle position and cycling. *The EMBO journal* **35**, 2658-2670, doi:10.15252/embj.201693806 (2016).
207 Hoeflich, A. *et al.* Insulin-like growth factor-binding protein 2 in tumorigenesis: protector or promoter? *Cancer research* **61**, 8601-8610 (2001).
208 Villani, R. M., Adolphe, C., Palmer, J., Waters, M. J. & Wainwright, B. J. Patched1 inhibits epidermal progenitor cell expansion and basal cell carcinoma formation by limiting Igfbp2 activity. *Cancer prevention research (Philadelphia, Pa.)* **3**, 1222-1234, doi:10.1158/1940-6207.capr-10-0082 (2010).
209 Xu, M. *et al.* WNT10A mutation causes ectodermal dysplasia by impairing progenitor cell proliferation and KLF4-mediated differentiation. *Nature communications* **8**, 15397, doi:10.1038/ncomms15397 (2017).
210 Miao, Q. *et al.* SOX11 and SOX4 drive the reactivation of an embryonic gene program during murine wound repair. *Nature communications* **10**, 4042, doi:10.1038/s41467-019-11880-9 (2019).
211 Chen, K. S., Lim, J. W. C., Richards, L. J. & Bunt, J. The convergent roles of the nuclear factor I transcription factors in development and cancer. *Cancer letters* **410**, 124-138, doi:10.1016/j.canlet.2017.09.015 (2017).
212 Chang, C. Y. *et al.* NFIB is a governor of epithelial-melanocyte stem cell behaviour in a shared niche. *Nature* **495**, 98-102, doi:10.1038/nature11847 (2013).
213 Thai, M. V., Guruswamy, S., Cao, K. T., Pessin, J. E. & Olson, A. L. Myocyte enhancer factor 2 (MEF2)-binding site is required for GLUT4 gene expression in transgenic mice. Regulation of MEF2 DNA binding activity in insulin-deficient diabetes. *The Journal of biological chemistry* **273**, 14285-14292, doi:10.1074/jbc.273.23.14285 (1998).
214 Naya, F. J. *et al.* Mitochondrial deficiency and cardiac sudden death in mice lacking the MEF2A transcription factor. *Nature medicine* **8**, 1303-1309, doi:10.1038/nm789 (2002).
215 Antonini, D. *et al.* A composite enhancer regulates p63 gene expression in epidermal morphogenesis and in keratinocyte differentiation by multiple mechanisms. *Nucleic acids research* **43**, 862-874, doi:10.1093/nar/gku1396 (2015).

216 Ramot, Y. *et al.* The role of PPARgamma-mediated signalling in skin biology and pathology: new targets and opportunities for clinical dermatology. *Experimental dermatology* **24**, 245-251, doi:10.1111/exd.12647 (2015).
217 Rivier, M. *et al.* Differential expression of peroxisome proliferator-activated receptor subtypes during the differentiation of human keratinocytes. *The Journal of investigative dermatology* **111**, 1116-1121, doi:10.1046/j.1523-1747.1998.00439.x (1998).
218 Westergaard, M. *et al.* Expression and localization of peroxisome proliferator-activated receptors and nuclear factor kappaB in normal and lesional psoriatic skin. *The Journal of investigative dermatology* **121**, 1104-1117, doi:10.1046/j.1523-1747.2003.12536.x (2003).
219 Karnik, P. *et al.* Hair follicle stem cell-specific PPARgamma deletion causes scarring alopecia. *The Journal of investigative dermatology* **129**, 1243-1257, doi:10.1038/jid.2008.369 (2009).
220 Mao-Qiang, M. *et al.* Peroxisome-proliferator-activated receptor (PPAR)-gamma activation stimulates keratinocyte differentiation. *The Journal of investigative dermatology* **123**, 305-312, doi:10.1111/j.0022-202X.2004.23235.x (2004).
221 Keehn, C. A., Smoller, B. R. & Morgan, M. B. Ets-1 immunohistochemical expression in non-melanoma skin carcinoma. *Journal of cutaneous pathology* **31**, 8-13, doi:10.1046/j.0303-6987.2004.0158.x (2004).
222 Nagarajan, P. *et al.* Ets1 blocks terminal differentiation of keratinocytes and induces expression of matrix metalloproteases and innate immune mediators. *Journal of cell science* **123**, 3566-3575, doi:10.1242/jcs.062240 (2010).
223 Barker, N. *et al.* Identification of stem cells in small intestine and colon by marker gene Lgr5. *Nature* **449**, 1003-1007, doi:10.1038/nature06196 (2007).
224 Sato, T. *et al.* Single Lgr5 stem cells build crypt-villus structures in vitro without a mesenchymal niche. *Nature* **459**, 262-265, doi:10.1038/nature07935 (2009).
225 Guiu, J. *et al.* Tracing the origin of adult intestinal stem cells. *Nature* **570**, 107-111, doi:10.1038/s41586-019-1212-5 (2019).
226 Guiu, J. & Jensen, K. B. From Definitive Endoderm to Gut-a Process of Growth and Maturation. *Stem cells and development* **24**, 1972-1983, doi:10.1089/scd.2015.0017 (2015).
227 Liao, X. H. & Nguyen, H. Epidermal expression of Lgr6 is dependent on nerve endings and Schwann cells. *Experimental dermatology* **23**, 195-198, doi:10.1111/exd.12340 (2014).
228 Sada, A., Jacob, F., Leung, E., Wang, S. & White, B. S. Defining the cellular lineage hierarchy in the interfollicular epidermis of adult skin. *Nature cell biology* **18**, 619-631, doi:10.1038/ncb3359 (2016).
229 Brownfield, D. G. *et al.* Patterned collagen fibers orient branching mammary epithelium through distinct signaling modules. *Current biology : CB* **23**, 703-709, doi:10.1016/j.cub.2013.03.032 (2013).
230 Mao, Y. *et al.* Differential proliferation rates generate patterns of mechanical tension that orient tissue growth. *The EMBO journal* **32**, 2790-2803, doi:10.1038/emboj.2013.197 (2013).
231 Yu, Y. R. *et al.* A Protocol for the Comprehensive Flow Cytometric Analysis of Immune Cells in Normal and Inflamed Murine Non-Lymphoid Tissues. *PloS one* **11**, e0150606, doi:10.1371/journal.pone.0150606 (2016).
232 Uderhardt, S., Martins, A. J., Tsang, J. S., Lammermann, T. & Germain, R. N. Resident Macrophages Cloak Tissue Microlesions to Prevent Neutrophil-Driven Inflammatory Damage. *Cell* **177**, 541-555.e517, doi:10.1016/j.cell.2019.02.028 (2019).
233 Buch, T. *et al.* A Cre-inducible diphtheria toxin receptor mediates cell lineage ablation after toxin administration. *Nature methods* **2**, 419-426, doi:10.1038/nmeth762 (2005).

234 Lee, P. P. *et al.* A critical role for Dnmt1 and DNA methylation in T cell development, function, and survival. *Immunity* **15**, 763-774, doi:10.1016/s1074-7613(01)00227-8 (2001).
235 Haertel, E., Joshi, N., Hiebert, P., Kopf, M. & Werner, S. Regulatory T cells are required for normal and activin-promoted wound repair in mice. *European journal of immunology* **48**, 1001-1013, doi:10.1016/j.cell.2016.10.052

10.1002/eji.201747395 (2018).
236 Rickert, R. C., Roes, J. & Rajewsky, K. B lymphocyte-specific, Cre-mediated mutagenesis in mice. *Nucleic acids research* **25**, 1317-1318, doi:10.1093/nar/25.6.1317 (1997).
237 Hobeika, E. *et al.* Testing gene function early in the B cell lineage in mb1-cre mice. *Proceedings of the National Academy of Sciences of the United States of America* **103**, 13789-13794, doi:10.1073/pnas.0605944103 (2006).
238 Abram, C. L., Roberge, G. L., Hu, Y. & Lowell, C. A. Comparative analysis of the efficiency and specificity of myeloid-Cre deleting strains using ROSA-EYFP reporter mice. *Journal of immunological methods* **408**, 89-100, doi:10.1016/j.jim.2014.05.009 (2014).
239 Panciera, T., Azzolin, L., Cordenonsi, M. & Piccolo, S. Mechanobiology of YAP and TAZ in physiology and disease. *Nature reviews. Molecular cell biology* **18**, 758-770, doi:10.1038/nrm.2017.87 (2017).
240 Elbediwy, A. *et al.* Integrin signalling regulates YAP and TAZ to control skin homeostasis. *Development (Cambridge, England)* **143**, 1674-1687, doi:10.1242/dev.133728 (2016).
241 Subach, F. V. *et al.* Photoactivatable mCherry for high-resolution two-color fluorescence microscopy. *Nature methods* **6**, 153-159, doi:10.1038/nmeth.1298 (2009).
242 Vaezi, A., Bauer, C., Vasioukhin, V. & Fuchs, E. Actin cable dynamics and Rho/Rock orchestrate a polarized cytoskeletal architecture in the early steps of assembling a stratified epithelium. *Developmental cell* **3**, 367-381 (2002).
243 Chacon-Martinez, C. A., Koester, J. & Wickstrom, S. A. Signaling in the stem cell niche: regulating cell fate, function and plasticity. *Development (Cambridge, England)* **145**, doi:10.1242/dev.165399 (2018).
244 Pontes-Quero, S. *et al.* Dual ifgMosaic: A Versatile Method for Multispectral and Combinatorial Mosaic Gene-Function Analysis. *Cell* **170**, 800-814.e818, doi:10.1016/j.cell.2017.07.031 (2017).
245 Bozkurt, A. *et al.* Retrospective analysis of tissue expansion in reconstructive burn surgery: evaluation of complication rates. *Burns : journal of the International Society for Burn Injuries* **34**, 1113-1118, doi:10.1016/j.burns.2008.05.008 (2008).
246 He, W. *et al.* Adipose-specific peroxisome proliferator-activated receptor gamma knockout causes insulin resistance in fat and liver but not in muscle. *Proceedings of the National Academy of Sciences of the United States of America* **100**, 15712-15717, doi:10.1073/pnas.2536828100 (2003).